REPORT DOCUMENTATION PAGE

Form Approved
OMB NO. 0704-0188

1. AGENCY USE ONLY (Leave Blank)	2. REPORT DATE	3. REPORT TYPE AND DATES COVERED
	20021	Final Progress Report

4. TITLE AND SUBTITLE
Pokeweed Antiviral Protein as an Universal Virus Neutralizer

5. FUNDING NUMBERS
(G) N65236-99-1-5422

6. AUTHOR(S)
Fatih M. Uckun, M.D., Ph.D.

7. PERFORMING ORGANIZATION NAME(S) AND ADDRESS(ES)
Parker Hughes Institute

8. PERFORMING ORGANIZATION REPORT NUMBER

9. SPONSORING / MONITORING AGENCY NAME(S) AND ADDRESS(ES)
U. S. Army Research Office
P.O. Box 12211
Research Triangle Park, NC 27709-2211

10. SPONSORING / MONITORING AGENCY REPORT NUMBER
43689.1-LS

11. SUPPLEMENTARY NOTES
The views, opinions and/or findings contained in this report are those of the author(s) and should not be construed as an official Department of the Army position, policy or decision, unless so designated by other documentation.

12 a. DISTRIBUTION / AVAILABILITY STATEMENT
Approved for public release; distribution unlimited.

12 b. DISTRIBUTION CODE

13. ABSTRACT (Maximum 200 words)

The objective of this project is to develop strategies which will allow the use of recombinant mutant pokeweed antiviral protein (PAP) as a potential countermeasure against biological warfare attempts employing pathogenic viruses. In order to increase the therapeutic index of the naturally occurring PAP, recombinant PAP mutants with superior antiviral activity and low toxicity will be constructed. The recombinant PAP mutants will be designed using the state-of-the-art technologies including X-ray crystallography, computer modeling, rational protein design and protein engineering.

14. SUBJECT TERMS
Antiviral
Viral
Pokeweed
Mutagenesis
Dianthin

15. NUMBER OF PAGES
6

16. PRICE CODE

17. SECURITY CLASSIFICATION OR REPORT	18. SECURITY CLASSIFICATION ON THIS PAGE	19. SECURITY CLASSIFICATION OF ABSTRACT	20. LIMITATION OF ABSTRACT
UNCLASSIFIED	UNCLASSIFIED	UNCLASSIFIED	UL

Unconventional Pathogen Countermeasures
FINAL REPORT

Project Title:

Pokeweed Antiviral Protein as an Universal Neutralizer

Principal Investigator Information:

Fatih M. Uckun, M.D., Ph.D.
Director, Parker Hughes Institute
2699 Patton Road
St. Paul, MN 55113
(651) 796-5400
Fatih_Uckun@ih.org

Contract/Grant Number: N65236-99-1-5422
Contract Start Date: 03/04/1999
Contract Projected End Date: 03/03/02
Total Contract Value: $5,260,391

List of Appendixes

I. List of all participating scientific personnel showing any advanced degrees earned by them while employed on the project

II. 10 Reprints as identified in body of report

II. 3 Manuscripts as identified in body of report

STATEMENT OF THE PROBLEM STUDIED

There is a need for a broad spectrum antiviral agent. Pokeweed Antiviral Protein (PAP) has broad spectrum antiviral activity. However, PAP cannot be obtained from natural sources in sufficient quantities. Furthermore, Pokeweed Antiviral Protein has toxic side effects. Therefore, for PAP be considered as an universal antiviral agent of practical potential, a need exists to have unlimited supplies of PAP and to develop nontoxic PAP species. Availability of a nontoxic Pokeweed Antiviral Protein as a broad spectrum antiviral agent would strengthen our capacity to counteract biological warfare efforts using pathogenic viruses.

SUMMARY OF THE MOST IMPORTANT RESULTS

The most important milestones that have been achieved and the most important results obtained through the research supported are as follows.

- The availability problem for PAP has been solved. We have cloned the gene for PAP and established large scale production and purification procedures of the cloned recombinant PAP.

- An E. Coli expression system has been published in the July 1999 issue of the peer-reviewed journal, Protein Expression and Purification (Vol. 16, pp 359-360). The yeast expression system has been reported in the March 2000 issue of *Protein Expression and Purification* (Vol. 18, pp 193-201)

- We have demonstrated that recombinant PAP is active. We have tested recombinant PAP in side-by-side comparison with native PAP. We discovered that recombinant PAP has potent antiviral activity and is capable of depurinating viral RNA. Two papers have been published in the July and September 1999 issues of the peer-reviewed journal *Biochemical and Biophysical Research Communications.*

- We have managed to crystalize PAP and elucidate the structural basis for the activity of PAP against viral RNA. A paper was published in the September 1999 issue of *Protein Science* regarding the structural basis of RNA deadenylation. Another paper was published in the November 1999 issue of *Protein Science* regarding the structural bases of the deguanylation of RNA by PAP. Subsequently, we have been able to crystallize another PAP species, namely PAP-II, and publish the results in the August 2000 issue of the peer-reviewed journal *Biochemical and Biophysical Research Communications.* This month we have completed the crystallization and structural analysis of a third species of PAP, namely, PAP-III and have submitted the manuscript for publication. Collectively, these papers provided novel insights into the structural basis for PAP-RNA interactions.

- We established a computer model as a guide for construction of nontoxic PAP mutants. We have used this model along with mitogenesis studies to identify the functional domains of PAP. There is also published in the February 2000 issue of the peer-reviewed journal, *Journal of Biological Chemistry.*

- We have determined the mode of interactions between PAP and ribosomes as well as RNA substrates. The results of these studies were published in the June 2001 issue of *Journal of Biological Chemistry* (Vol. 276, pp 24075-24081), and August 2001 issue of *Biochemistry* (Vol. 40, pp 9104-9114).

- We have constructed and produced several mutant recombinant pokeweed antiviral proteins and identified candidates with superior antiviral activity. Specifically, FLP 102 and FLP 105 have been identified as nontoxic PAP proteins with antiviral activity. A paper has been prepared detailing the findings and submitted for publication. A patent application has also been prepared and will be shortly filed. A licensing agreement is underway with Virochem, a biotech company, for further development of this technology.

- We have also prepared recombinant Dianthin as a highly active functional homolog of recombinant PAP. This protein is capable of not only depurinating viral RNA, but also inhibiting viral integrase.

In summary, we have cloned pokeweed antiviral protein, established large scale procedures for production and purification of the recombinant PAP, confirmed it as an active antiviral agent, crystallized and resolved the crystal structure of PAP, established a computer model for the structure based design and engineering of novel PAP mutants that lack toxicity but retain their antiviral activity and identified two lead engineered proteins for further development.

LISTING OF ALL PUBLICATIONS AND TECHNICAL REPORTS

PAPERS PUBLISHED IN PEER-REVIEWED JOURNALS

1: Rajamohan F, Ozer Z, Mao C, Uckun FM.
Active center cleft residues of pokeweed antiviral protein mediate its high-affinity binding to the ribosomal protein L3. Biochemistry. 2001 Aug 7;40(31):9104-14.

2: Rajamohan F, Mao C, Uckun FM.
Binding interactions between the active center cleft of recombinant pokeweed antiviral protein and the alpha-sarcin/ricin stem loop of ribosomal RNA. J Biol Chem. 2001 Jun 29;276(26):24075-81.

3: Rajamohan F, Doumbia SO, Engstrom CR, Pendergras SL, Maher DL, Uckun FM.
Expression of biologically active recombinant pokeweed antiviral protein in methylotrophic yeast Pichia pastoris. Protein Expr Purif. 2000 Mar;18(2):193-201.

4: Rajamohan F, Pugmire MJ, Kurinov IV, Uckun FM.
Modeling and alanine scanning mutagenesis studies of recombinant pokeweed antiviral protein. J Biol Chem. 2000 Feb 4;275(5):3382-90.

5: Kurinov IV, Rajamohan F, Venkatachalam TK, Uckun FM.
X-ray crystallographic analysis of the structural basis for the interaction of pokeweed antiviral protein with guanine residues of ribosomal RNA. Protein Sci. 1999 Nov;8(11):2399-405.

6: Rajamohan F, Kurinov IV, Venkatachalam TK, Uckun FM.
Deguanylation of human immunodeficiency virus (HIV-1) RNA by recombinant pokeweed antiviral protein. Biochem Biophys Res Commun. 1999 Sep 24;263(2):419-24.

7: Rajamohan F, Engstrom CR, Denton TJ, Engen LA, Kourinov I, Uckun FM.
High-level expression and purification of biologically active recombinant pokeweed antiviral protein. Protein Expr Purif. 1999 Jul;16(2):359-68.

8: Rajamohan F, Venkatachalam TK, Irvin JD, Uckun FM.
Pokeweed antiviral protein isoforms PAP-I, PAP-II, and PAP-III depurinate RNA of human immunodeficiency virus (HIV)-1. Biochem Biophys Res Commun. 1999 Jul 5;260(2):453-8.

9: Kurinov,IV, Mao,C, Irvin,JD, and Uckun,FM:
X-ray crystallographic analysis of pokeweed antiviral protein-2 after reductive methylation of lysine residues. Biochemical and Biophysical Research Communications, 2000, Aug. 28; 275 (2): 549-52

10: Kurinov,IV, Myers,DE, Irvin, JD, and Uckun,FM:

X-ray crystallographic analysis of the structural basis for the interactions of pokeweed antiviral protein with its active site inhibitor and ribosomal RNA substrate analogs. Protein Science 1999, Sep; 8(9): 1765-72

MANUSCRIPTS SUBMITTED, BUT NOT PUBLISHED

1: Kurinov, IV, Rajamohan,F, and Uckun,FM: High resolution x-ray structure and potent anti-HIV activity of recombinant Dianthin antiviral protein. 2002, submitted.
2: Kurinov, IV and Uckun,FM: High resolution x-ray structure of potent anti-HIV pokeweed antiviral protein-III. 2002, submitted.
3: Uckun,FM, Rajamohan,F, Pendergrass,S, Ozer,Z, Waurzyniak,B, Mao,C: Structure based design and engineering of a nontoxic recombinant pokeweed antiviral protein with potent anti-HIV activity, 2002 submitted.

LIST OF ALL PARTICIPATING SCIENTIFIC PERSONNEL SHOWING ANY ADVANCED DEGREES EARNED BY THEM WHILE EMPLOYED ON THE PROJECT

See attached

REPORT OF INVENTIONS, BY TITLE ONLY

Invention: Nontoxic recombinant pokeweed antiviral proteins with potent anti-HIV activity.

BIBLIOGRAPHY

See the bibliography of the papers and reprints in the appendices

APPENDICES:
10 reprints and copies
3 manuscripts and copies

PAP as an Universal Virus Neutralizer

List of Participating Scientific Personnel

Year 1

Aubrecht, Jiri
Beatty, Carolyn
Chen, Chun-Lin
Dahlke, Dawn
Denton, Tammy-Jo
Dibirdik, Ilker
Engen-Harmala, Lisa
Engstrom, Cherri
Gill, Patricia
Goodman, Patricia
Hibbs, Kathleen
Holm, Marlene
Kiey, Linda
Kurinov, Igor
LaRue, Rebecca
Li, Baolin
Maher, Danielle
Mao, Chen
Matzke, Brent
Myers, Dorothea
Navara, Christopher
Rajamohan, Francis
Rostovtsev, Alexander
Sun, Lei
Tuel-Ahlgren, Lisa
Uckun, Fatih
Vassilev, Alexei
Waurzyniak, Barbara
Wendorf, Heather

Year 2

Beatty, Carolyn
Chen, Chun-Lin
Czech, Jennifer
Dahlke, Dawn
Denton, Tammy-Jo
Dibirdik, Ilker
Dopkins, Andrea
Gill, Patricia
Henning, Michelle
Hibbs, Kathleen
Holm, Marlene
Kiey, Linda
Kurinov, Igor
LaRue, Rebecca
Maher, Danielle
Mao, Chen
Myers, Dorothea
Navara, Christopher
Rajamohan, Francis
Schaefer, David
Tuel-Ahlgren, Lisa
Uckun, Fatih
Vassilev, Alexei
Waurzyniak, Barbara
Wendorf, Heather

Year 3

Burkhardt, Nicole
Chen, Chun-Lin
Clemenson, Dina
Czech, Jennifer
Dibirdik, Ilker
Dopkins, Andrea
Dvorak, Nancy
Gill, Patricia
Hardenbrook, Jennifer
Henning, Michelle
Jin, Jizhong
Kiey, Linda
Kurinov, Igor
Lisowski, Elizabeth
Mahajan, Sandeep
Maher, Danielle
Mao, Chen
Myers, Dorothea
Ozer, Zahide
Pendergrass, Sharon
Rajamohan, Francis
Schaefer, David
Tibbles, Heather
Tong, Thuy
Tuel-Ahlgren, Lisa
Uckun, Fatih
Vassilev, Alexei
Waurzyniak, Barbara

Active Center Cleft Residues of Pokeweed Antiviral Protein Mediate Its High-Affinity Binding to the Ribosomal Protein L3[†]

Francis Rajamohan,[*,‡,§] Zahide Ozer,[||] Chen Mao,[⊥] and Fatih M. Uckun[*,‡,#]

Biotherapy Program, Parker Hughes Cancer Center, and Departments of Protein Engineering, Biochemistry, Structural Biology, and Virology, Parker Hughes Institute, St. Paul, Minnesota 55113

Received December 15, 2000; Revised Manuscript Received June 5, 2001

ABSTRACT: Pokeweed antiviral protein (PAP) is a ribosome-inactivating protein (RIP) which catalytically cleaves a specific adenine base from the highly conserved α-sarcin/ricin loop (SRL) of the large ribosomal RNA and thereby inhibits the protein synthesis. The ribosomal protein L3, a highly conserved protein located at the peptidyltransferase center of the ribosomes, is involved in binding of PAP to ribosomes and subsequent depurination of the SRL. We have recently discovered that recombinant PAP mutants with alanine substitution of the active center cleft residues ^{69}NN^{70} (FLP-4) and ^{90}FND^{92} (FLP-7) that are not directly involved in the catalytic depurination at the active site exhibit >150-fold reduced ribosome inhibitory activity [(2000) *J. Biol. Chem. 275, 3382−3390*]. We hypothesized that the partially exposed half of the active site cleft could be the potential docking site for the L3 molecule. Our modeling studies presented herein indicated that PAP residues 90−96, 69−70, and 118−120 potentially interact with L3. Therefore, mutations of these residues were predicted to result in destabilization of interactions with rRNA and lead to a lower binding affinity with L3. In the present structure−function relationship study, coimmunoprecipitation assays with an in vitro synthesized yeast ribosomal protein L3 suggested that these mutant PAP proteins poorly interact with L3. The binding affinities of the mutant PAP proteins for ribosomes and recombinant L3 protein were calculated from rate constants and analysis of binding using surface plasmon resonance biosensor technology. Here, we show that, compared to wild-type PAP, FLP-4/^{69}AA^{70} and FLP-7/^{90}AAA^{92} exhibit significantly impaired affinity for ribosomes and L3 protein, which may account for their inability to efficiently inactivate ribosomes. By comparison, recombinant PAP mutants with alanine substitutions of residues ^{28}KD^{29} and ^{111}SR^{112} that are distant from the active center cleft showed normal binding affinity to ribosomes and L3 protein. The single amino acid mutants of PAP with alanine substitution of the active center cleft residues N69 (FLP-20), F90 (FLP-21), N91 (FLP-22), or D92 (FLP-23) also showed reduced ribosome binding as well as reduced L3 binding, further confirming the importance of the active center cleft for the PAP−ribosome and PAP−L3 interactions. The experimental findings presented in this report provide unprecedented evidence that the active center cleft of PAP is important for its in vitro binding to ribosomes via the L3 protein.

Pokeweed antiviral protein (PAP)[1] is a naturally occurring type I ribosome-inactivating protein (RIP) isolated from the leaves of the pokeweed plant, *Phytolacca americana* (*1*, 2). The therapeutic potential of PAP as a ribosome inhibitory anticancer agent has gained considerable interest in recent years due to the clinical use of native PAP as the active moiety of immunoconjugates against cancer (*3*−*6*). PAP exhibits a highly specific RNA *N*-glycosidase activity that cleaves the glycosidic bond of a single adenine base (A^{4324} of the tetraloop sequence GAGA) that is located in the highly conserved "α-sarcin/ricin loop" (SRL) of the large ribosomal RNA (rRNA) species in eukaryotic (28S rRNA) and prokaryotic (23S rRNA) ribosomes (*7*, *8*). This catalytic depurination of the SRL by PAP results in irreversible inhibition of protein synthesis at the translocation step by impairing the elongation factor (EF) 1 dependent binding of aminoacyl-tRNA as well as the GTP-dependent binding of EF-2 to the affected ribosome (*3*, *9*−*11*).

Endo and Tsurugi (*8*) demonstrated that the ribosome inhibitory protein ricin-A chain is capable of deadenylating rat liver ribosomes with a K_{cat} value nearly 10^5-fold greater than that measured using naked 28S rRNA. The highly conserved catalytic site residues of the RIPs exhibit virtually the same level of depurinating activity for naked 28S rRNA derived from different species. However, these same RIPs differ in their depurinating activity against intact ribosomes isolated from different species (*7*, *12*). These observations imply an important role for ribosomal elements in RIP−rRNA interactions. A recent study by Hudak et al. (*13*)

[†] This work was supported by the Defense Advanced Research Projects Agency under Grant N65236-99-1-5422 (awarded to F.M.U.).

[*] To whom correspondence should be addressed: Parker Hughes Institute, 2657 Patton Road, Roseville, MN 55113. Phone: (651) 628-9988. Fax: (651) 697-1042. E-mail: frajamohan@ih.org; fatih_uckun@ih.org.

[‡] Biotherapy Program, Parker Hughes Cancer Center.

[§] Department of Protein Engineering, Parker Hughes Institute.

[||] Department of Biochemistry, Parker Hughes Institute.

[⊥] Department of Structural Biology, Parker Hughes Institute.

[#] Department of Virology, Parker Hughes Institute.

[1] Abbreviations: PAP, pokeweed antiviral protein; SRL, α-sarcin/ricin loop; EF, elongation factor; RIP, ribosome-inactivating protein; rRNA, ribosomal RNA; MBP, maltose binding protein; IPTG, isopropyl thiogalactoside; HM, *Haloarcula marismortui*.

10.1021/bi002851p CCC: $20.00
Published on Web 00/00/0000 PAGE EST: 10.7

indicated that the ribosomal protein L3, a highly conserved protein located at the peptidyltransferase center of the ribosomes, is involved in the binding of PAP to ribosomes and subsequent depurination of the SRL. Notably, PAP failed to depurinate ribosomes in yeast cells expressing a mutant L3 protein (*13*), prompting the hypothesis that the interaction of PAP with L3 is essential for its ability to bind to and inactivate ribosomes by depurination. Furthermore, footprinting studies of *Escherichia coli* 23S rRNA studies showed that L3, together with L6, has protected the SRL, suggesting that the protein L3 is located in close proximity to the SRL (*14*).

We have recently discovered that recombinant PAP mutants with alanine substitutions of the active center cleft residues ^{69}NN^{70} (FLP-4) and ^{90}FND^{92} (FLP-7) that are not directly involved in the catalytic depurination at the active site exhibit >150-fold reduced ribosome inhibitory activity (*15*). We hypothesized that the partially exposed half of the active site cleft could be the potential docking site for the L3 molecule. Our modeling studies indicated that PAP residues 90−96, 69−70, and 118−120 potentially interact with L3. The active center cleft residues Asn^{69}, Asn^{70}, and Asp^{92} as well as the active site residue Arg^{122}, which is not directly involved in the catalytic depurination of rRNA, promote specific interactions with the phosphate backbone of the target SRL of rRNA. On the other hand, these residues are on the protein surface, and all but residue 122 potentially interact with L3 in our model. Therefore, mutations of these residues were predicted to result in destabilization of interactions with rRNA and lead to a lower binding affinity with L3 (except 122). Coimmunoprecipitation assays with an in vitro synthesized yeast ribosomal protein L3 suggested that these active center cleft mutants of PAP poorly interact with L3. The binding affinities of the mutant PAP proteins for ribosomes and recombinant L3 protein were calculated from rate constants and analysis of binding using surface plasmon resonance (SPR) biosensor technology. Here, we show that, compared to wild-type PAP, FLP-4/^{69}AA^{70} and FLP-7/^{90}AAA^{92} exhibit significantly impaired affinity for ribosomes and L3 protein, providing a cogent explanation for their inability to efficiently inactivate ribosomes. The single amino acid mutants of PAP with alanine substitution of the active center cleft residues N69 (FLP-20), F90 (FLP-21), N91 (FLP-22), or D92 (FLP-23) also showed reduced L3 binding. By comparison, recombinant PAP mutants with alanine substitutions of residues ^{28}KD^{29} and ^{111}SR^{112} that are distant from the active center cleft showed normal binding affinity to ribosomes and L3 protein. The experimental findings presented herein provide unprecedented evidence that the active center cleft of PAP is important for its in vitro binding to ribosomes via the L3 protein.

EXPERIMENTAL PROCEDURES

Molecular Modeling. The molecular model of the PAP−rRNA stem loop complex was derived from the 2.4 Å crystal structure of a large ribosomal subunit from *Haloarcula marismortui* (HM) (Protein Data Bank access code 1FFK) (*16*) and the crystal structure of the PAP−nucleotide complex (access code 1pag). This model represents a refinement of our recently published model of the PAP−rRNA stem loop complex (*15*). First, we superimposed the HM ribosome structure with the stem loop structure in our previous PAP−RNA complex model. The conformation of rRNA was adjusted near the adenine A2697 (A2660 in *E. coli*) of the GAGA tetraloop, and the rest of the PAP molecule was left unchanged. The adenosine was manually adjusted by a 38° rotation at the C5′ position and a 5.4 Å translation of the adenine ring. The model was used to perform fixed docking using the Docking module in InsightII employing the CVFF and a Monte Carlo strategy in the Affinity program (InsightII User Guide 1991, MSI, San Diego, CA). The parameters used in this docking included searching for five unique structures, with 1000 minimization steps for each structure, energy range 10.0 kcal/mol, maximum translation of the ligand of 3.0 Å, maximum rotation of the ligand of 10°, and an energy tolerance of 1500 kcal/mol. During the minimization steps of the docking procedure, only the tetraloop and the active site residues of PAP were allowed to be flexible, whereas the rest of rRNA and PAP remained fixed. The best molecular position was chosen on the basis of the best Ludi score which included the contribution of the loss of translational and rotational entropy of the RNA fragment, the number of hydrogen bonds, the hydrogen bond geometry, and contributions from ionic and lipophilic interactions to the binding energy. The refined structure was then analyzed in CHAIN (*17*). Finally, we examined the potential docking site for the L3 molecule. On the basis of the HM crystal structure, a rational choice for a binding location for PAP would be on the outer surface near residues 65 and 350, in a region that does not interact with rRNA and is closest to the SRL region. Therefore, the rRNA region containing SRL between 2684 and 2704 (2647 and 2667, respectively, in *E. coli*) and the PAP molecule were docked as a rigid body near the aforementioned region of L3. This was accomplished using the Docking module within the InsightII program in a similar manner as for the docking of rRNA to PAP.

Construction of Mutants. The recombinant wild-type PAP construct (pBS-PAP) was obtained by subcloning the *PAP-I* gene (amino acids 22−313) at the *Bam*HI and *Hin*dIII sites of the *E. coli* expression vector, pBluescript SK$^-$ (Stratagene, La Jolla, CA). PAP mutants were constructed using site-directed mutagenesis techniques as described previously (*15*).

Expression and Purification of Mutants. Wild-type and mutant recombinant PAP proteins were expressed in *E. coli* MV1190 as inclusion bodies, isolated, solubilized, and refolded, as described previously (*18*). The refolded proteins were analyzed by SDS−12% polyacrylamide gel electrophoresis (PAGE). Protein concentrations were determined from the gel using bovine serum albumin (BSA) as a standard.

Immunoblot Analysis of PAP Mutants. One microgram of the protein samples was resolved on a SDS−12% PAGE gel and transferred onto a poly(vinylidene difluoride) (PVDF) membrane (Roche Molecular Biochemicals, Indianapolis, IN) using the Bio-Rad trans-blot apparatus, as described previously (*18*). The membrane was immunoblotted using rabbit anti-PAP serum (1:2000 dilution) and horseradish peroxidase conjugated goat anti-rabbit IgG (1:1000 dilution) as the primary and secondary antibodies, respectively. The blot was developed using 3,3′-diaminobenzidine (Sigma) as the colorimetric indicator for peroxidase activity.

In Vitro RNA Transcription and Radiolabeling of the L3 Protein. A plasmid containing the cDNA (pJD166.trp) that

encodes the *Saccharomycis cerevisiae* ribosomal protein L3, wild type, was a kind gift from Dr. Jonathan D. Dinman, University of Medicine and Dentistry of New Jersey. Radiolabeled L3 protein was synthesized by a linked transcription−translation system (TNT T3-coupled reticulocyte lysate system, Promega) according to the manufacturer's instructions (Promega). The translation products were resolved on SDS−10% PAGE; gels were dried and autoradiographed.

Coimmunoprecipitation. The mouse anti-L3 monoclonal antibody was a kind gift from Dr. Jonathan R. Warner, Department of Cell Biology, Albert Einstein College of Medicine, Bronx, NY. The in vitro synthesized L3 protein (8×10^4 cpm) was incubated with 1 mg of wild-type or mutant PAP proteins in 50 mL (final volume) of binding buffer (10 mM K_2HPO_4, 5 mM NaCl, pH 8.0) at 30 °C for 30 min. The PAP−L3 complex was coimmunoprecipitated by adding 5 μL of the mouse anti-L3 monoclonal antibody (1:500 dilution). After 60 min of incubation at 30 °C, the PAP−L3−antibody complex was precipitated by addition of 50 mL of protein A−Sepharose beads that had been pretreated with rabbit anti-mouse IgG (20 μL/mL beads) and the incubation continued for another 1 h at 4 °C. The beads were washed three times with phosphate-buffered saline containing 0.1% Triton X-100, and the proteins were eluted from the Sepharose beads with SDS sample buffer. The proteins were separated through SDS−12% PAGE, transferred to a PVDF membrane, and probed with the polyclonal rabbit anti-PAP antibody (1:2000 dilution) and horseradish peroxidase conjugated goat anti-rabbit IgG (1:1000 dilution) as the primary and secondary antibodies, respectively. The blot was developed using 3,3′-diaminobenzidine (Sigma) as the colorimetric indicator for peroxidase activity. The dried membrane was also exposed to autoradiography to estimate the amounts of L3 protein.

Preparation of Ribosomes and Binding to PAP Mutants. Ribosomes were isolated from rabbit reticulocyte-rich whole blood (Pel-Freez, Rogers, AR), as described previously (*19*). Ribosome binding assays were carried out by incubating 5 μg samples of ribosome isolates with 1 μg of wild-type or mutant PAP proteins in 50 μL of TKM buffer (25 mM Tris-HCl, pH 8.0, 25 mM KCl, 5 mM $MgCl_2$) for 30 min at 30 °C. The ribosome−PAP complexes were separated by ultracentrifugation (90 000 rpm for 30 min), and the pellet was washed three times with 100 μL of HEPES−T buffer (0.1% Tween-20, 10 mM HEPES, pH 8) in order to remove the unbound PAP. The proteins were solubilized with SDS sample buffer, separated by SDS−12% polyacrylamide gel electrophoresis (PAGE), transferred to a PVDF membrane, and probed with the polyclonal antibody to PAP.

Expression and Purification of Recombinant L3 Protein in E. coli. The plasmid containing the cDNA (pJD166.trp) that encodes the *S. cerevisiae* wild-type ribosomal protein L3 was subcloned into the fusion vector, pMAL-c2 (New England Biolabs Inc., Beverly, MA), downstream from the *malE* gene, which encodes the maltose binding protein (MBP). The resulting construct, pMAL-L3, was transformed into *E. coli* cells, and the expression of the MBP−L3 fusion protein was induced by the addition of IPTG (1 mM final concentration). The L3 fusion protein was purified by binding to an amylose affinity purification column according to the manufacturer's instructions (New England Biolabs). The purified MBP−L3 fusion protein was analyzed by SDS−10% PAGE.

Expression and Purification of Recombinant L3 Protein in a Baculovirus Expression System. The *L3* gene in plasmid pJD166.trp was amplified by polymerase chain reaction (PCR) using the *Nco*I site-containing 5′-primer, 5′-AATTATCCATGGCTCACAGAAAGTACG-3′, and the *Eco*RI site-containing 3′-primer, 5′-AATTATGAATTCTTATTACAAGTCCTTCTTCAAAGTACC-3′. PCR was performed in 25 cycles with a Ericomp, DeltaCycler II, DNA Thermocycler system using a Gene Amp kit (Takara Shuzo Co., Ltd.) according to the procedure recommended by the supplier. After digestion of the PCR fragment with *Nco*I and *Eco*RI, the 1170 base pair fragment product was cloned into the pFastBac HTb His-tagged vector. The final construct, pFas-L3, was expressed in SF9 cells using the Bac-To-Bac baculovirus expression system (Gibco Life Technologies) following the manufacturer's instructions (Gibco). The 6×His−L3 fusion protein was purified by using the nickel−NTA spin kit (Quiagen, Inc.), as described in Quiagen protocols.

Monitoring of Binding Interactions Using Surface Plasmon Resonance Technology. A BIAcore 2000 surface plasmon resonance-based biosensor system (Pharmacia Biosensor AB) was used to measure the kinetic parameters for the interactions between soluble recombinant PAP proteins (analytes) and the immobilized ribosomes or the ribosomal protein L3 (ligands). In ribosome binding assays, ribosomes were covalently linked to the dextran on the surface of research grade CM5 sensor chips via primary amino groups using the amine coupling kit from Pharmacia according to the manufacturer's instructions (Pharmacia). Thirty-five microliters of the ribosome isolate (10 μg/mL) in 10 mM sodium acetate, pH 5.5, was injected onto the surface at a flow rate of 5 μL/min. Typically, a 1200 RU resonance signal was obtained following this procedure. The protein samples were diluted in PBS buffer (1 mM KH_2PO_4, 10 mM Na_2HPO_4, 0.137 M NaCl, 2.7 mM KCl, 0.005% Tween P20, pH 7.4) to a final concentration of 50 nM before the injection. Samples were injected at 25 °C at a flow rate of 5 μL/min onto the sensor chip surface on which the ribosome had been immobilized or onto a control surface on which BSA had been immobilized. The binding surface was regenerated by washing with 2 M NaCl.

In binding assays using the MBP−L3 fusion protein, an anti-MBP antibody was covalently linked to the dextran on the surface of research grade CM5 sensor chips via primary amino groups using the amine coupling kit (Pharmacia). The CM5 chip was activated by injecting a mixture of *N*-hydroxysuccinimide and *N*-ethyl-*N*′-(3-dimethylaminopropyl)carbodiimide followed by 35 μL of the anti-MBP antibody (10 μg/mL) (New England Biolabs) in 10 mM sodium acetate, pH 5.0. Ethanolamine hydrochloride, pH 8.5, was injected to block unreacted *N*-hydroxysuccinimide esters (35 μL). The MBP−L3 fusion protein was captured by injecting 40 μL of the fusion protein (20 μg/mL) over the surface of the CM5 sensor chip, which was immobilized (amine coupling) with an anti-MBP antibody, at a flow rate of 5 μL/min in HBS−EP buffer (0.1 M HEPES, pH 7.4, 0.15 M NaCl, 3 mM EDTA, and 0.005% polysorbate 20). Typically, an average resonance (RU) signal of 1500 was obtained by following this procedure. Unoccupied sites were

blocked by injecting 30 μL of MBP (25 μg/mL) in HBS−EP buffer as above. The protein samples were diluted in HSEM buffer (10 mM HEPES, pH 8.0, 50 mM NaCl, 1 mM EDTA, 5 mM $MgCl_2$, and 0.005% polysorbate 20) to a final concentration of 50 nM before the injection. In a kinetic study, 30 μL of samples (150 nM) was injected at 25 °C at a flow rate of 8 μL/min onto the sensor chip surface on which the MBP−L3 fusion protein has been captured or onto a control surface on which MBP had been immobilized, using HBS−EP as the running buffer. Between samples, the binding surfaces were regenerated by a 3 min injection of 1 M NaCl and 50 mM NaOH solution at a flow rate of 10 μL/min. Each experiment was carried out at least twice on the same chip, and samples were injected in random order.

In binding assays using His-tagged recombinant L3 protein 6×His−L3 produced in the baculovirus expression system, the NTA sensor chip was saturated by injecting 20 μL of 500 mM $NiCl_2$ solution at a flow rate of 20 μL/min in NTA buffer (10 mM HEPES, 0.15 M NaCl, 50 mM EDTA, 0.005% Surfactant P20, pH 7.4). The 6×His−L3 protein was diluted in NTA buffer to a final concentration of 150 nM and was immobilized on the sensor chip by injecting 25 μL at a flow rate of 5 μL/min. Typically, an average resonance signal of 1000 RU was obtained by following this procedure. Between samples, the binding surface was regenerated by injecting 30 μL of regeneration buffer (10 mM HEPES, 0.15 M NaCl, 0.35 M EDTA, 0.005 Surfactant P20, pH 8.3) at a flow rate of 10 μL/min.

For the binding of L3 protein to the recombinant wild-type PAP, the N-terminus 6×His−PAP fusion protein was used. The 6×His−PAP protein was cloned, expressed, and purified from *E. coli* as described previously (*18*). The NTA sensor chip was activated by injecting 20 mL of 500 mM $NiCl_2$ in NTA buffer at a flow rate of 20 mL/min. The 6×His−PAP protein was diluted in NTA buffer to a final concentration of 150 nM and was immobilized on the sensor chip by injecting 20 μL at a flow rate of 5 μL/min, giving a change in RU value of 275. A 30 mL solution of MBP−L3 protein (25 nM) alone or after preincubation with 250 nM native or recombinant wild-type PAP in buffer (50 mM HEPES, 10 mM $MgCl_2$, 50 mM NaCl, pH 7.6) at room temperature for 1 h was then injected over immobilized 6×His−PAP at a flow rate of 8 μL/min. Between samples, the binding surface was regenerated by injecting 30 μL of regeneration buffer (10 mM HEPES, 0.15 M NaCl, 0.35 M EDTA, 0.005 Surfactant P20, pH 8.3) at a flow rate of 10 μL/min. As a control for nonspecific binding, a MBP−L3 sample solution was injected over the flow cell without the immobilized 6×His−PAP protein, and each control signal was subtracted to correct for a nonspecific binding.

The primary data were analyzed using the BIAevaluation software (Version 3.0) supplied with the instrument (Biacore, Inc.). To prepare the data for analysis, baselines were adjusted to zero for all curves, and injection start times were aligned. Background sensorgrams were then subtracted from the experimental sensorgrams to yield curves representing specific binding. All of the kinetic data were fit most adequately by assuming a simple bimolecular reaction model for interaction between soluble analyte and immobilized ligand, equivalent to the Langmuir isotherm for adsorption to a surface. For determination of k_{on} only the middle portion of the association curve was used for fitting. For determination of k_{off} only the initial portion of the curve encompassing the fast dissociation phase was used for fitting. The goodness of fit was assessed by inspecting the statistical value χ^2 and the residuals (observed−calculated). The χ^2 values were low (<2) and the residuals randomly distributed about zero. The accuracy of the quantitative measurements of the off rates for the PAP−L3 interactions may be compromised because of the very slow dissociation of the ligand from the protein immobilized on the biosensor chip.

RESULTS AND DISCUSSION

Molecular Model of the PAP−rRNA−L3 Complex and Structure-Based Design of Recombinant PAP Proteins with Altered L3 Binding Affinity. The precise molecular interaction between the ribosomal protein L3 and PAP has yet to be revealed by a crystal structure of the PAP−ribosome complex. However, on the basis of the crystal structure of a large subunit of the *H. marismortui* (HM) ribosome (Protein Data Bank access code 1FFK), the outer surface near residues 65 and 350, which does not interact with rRNA, is the closest region to the α-sarcin/ricin loop. Moreover, on the basis of our previously published molecular model of the PAP−RNA stem loop complex (*15*), half of the active site cleft of PAP is in contact with SRL but the other half which consists of four loop regions, including residues 40−44, 69−70, 91−96 and 120−122, is only partially in contact with SRL and partially exposed to the solvent environment. We reasoned that the partially exposed half of the active site cleft of PAP could be the potential docking site for the L3 molecule. We constructed a molecular model to show the proposed docking position of L3 relative to the active site cleft of PAP. This was accomplished with a docking procedure using a Monte Carlo simulation strategy combined with a docking score evaluation (see Experimental Procedures). Our refined molecular model of the PAP−RNA stem loop complexed with L3 is depicted in Figure 1.

It has been shown that C769T (causing a Pro to Ser change at residue 257) and G765C (causing a Trp to Cys change at residue 255), two adjacent missense mutations of the yeast RPL3 gene which are predicted to structurally alter the encoded L3 protein, significantly affect the programmed −1 ribosomal frame-shift efficiencies of yeast ribosomes (*20*). Interestingly, the mutant protein also showed poor binding to PAP, suggesting that the quaternary structure of a ribosome containing mak8−−1p may differ from a wild-type ribosome such that the binding site for PAP may be masked in the mutant ribosome (*13*). The yeast L3 residues W255 and P257 correspond to the L3 residues W241 and P243 in *H. marismortui* (HM). On the basis of the recently resolved crystal structure of a large ribosomal subunit from HM (Protein Data Bank access code 1FFK) (*16*), these two residues are situated on the nonglobular extension of L3, deeply buried inside the ribosome and interact closely with rRNA reaching toward the peptidyltransferase site (Figure 1A). Therefore, the notion that PAP might interact with these two residues is not consistent with the new structural information provided by the HM crystal structure upon which our model was based.

According to our model, PAP residues 43, 67 (paired with 97), 69, 70, 92, 206−210, 212−213, 217, 224−225, and 253−255 participate in its interaction with rRNA. Our

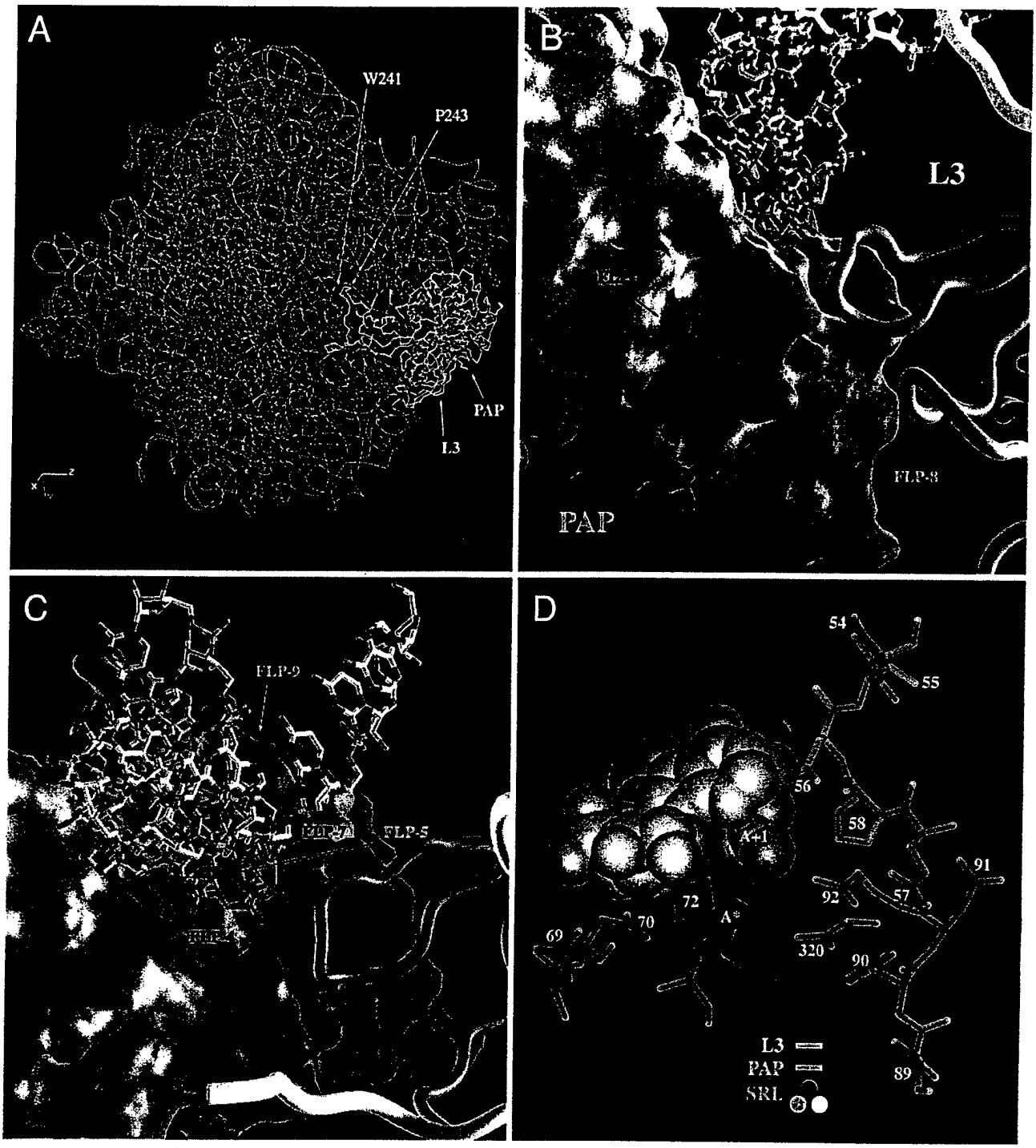

FIGURE 1: Molecular model of PAP interactions with the large ribosome of *Haloarcula marismortui* (HM) and ribosomal protein L3. (A) Model of PAP (green) interacting with the large ribosome unit with rRNA (blue), L3 (white), and the rest of ribosomal proteins (red). As illustrated, the yeast W255 and P257 equivalent residues, W241 and P243, are deeply buried inside the ribosome and interact closely with rRNA reaching toward the peptidyl transferase site. (B and C) PAP−rRNA−L3 model as viewed from two different angles: PAP molecule (blue), L3 (white ribbon), and rRNA (stick model, multicolor). The positions of the alanine-substituted residues of the recombinant PAP mutants FLP-1, FLP-4, FLP-5, FLP-7, and FLP-9 are indicated. The conformation of rRNA (shown in white; phosphate backbone in yellow) was adjusted around the adenine A2697 (A2660 in *E. coli*) of the GAGA tetraloop, and the rest of the PAP molecule remains unchanged. The adenosine was manually adjusted by a 38° rotation at the C5′ position and a 5.4 Å translation of the adenine ring. There are no steric collisions between PAP and nearby ribosomal proteins. L3 is shown as a white ribbon. The loop region around residues 65 and 350 (based on the amino acid sequence of yeast L3) is in close contact with PAP in the regions where mutations occur in FLP-4 and FLP-7 but not in the regions where mutations occur in FLP-1, FLP-5, and FLP-9. The image was created using GRASP software (*23*). (D) Detailed interaction of L3 (blue) with SRL (space-filling model) and PAP (pink and green).

modeling studies indicated that PAP residues 69−70, 90−96, and 118−120 potentially interact with L3. The active center cleft residues Asn^{69}, Asn^{70}, and Asp^{92} as well as the active site residue Arg^{122}, which are not directly involved in the catalytic depurination of rRNA, promote specific interactions with the phosphate backbone of the target SRL of rRNA. On the other hand, these residues are on the protein surface, and all but residue 122 potentially interact with L3 in our model. Therefore, mutations of these residues (except for residue 122) were predicted to result in destabilization

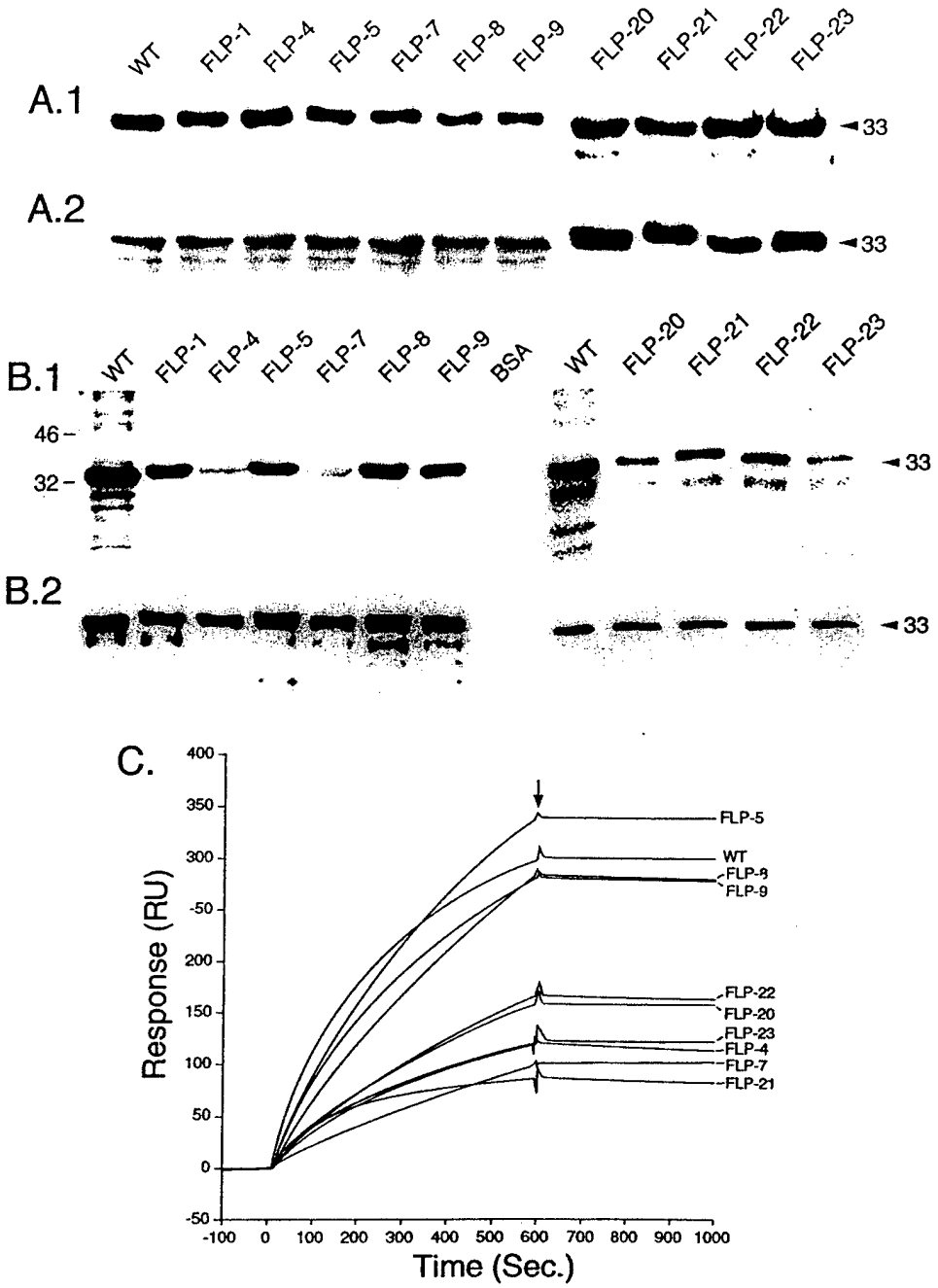

FIGURE 2: (A) Coomassie Blue-stained SDS−12% PAGE (A.1) and Western blot analysis (A.2) of wild-type (WT) and mutant recombinant PAP proteins. The mass of the protein (in kDa) is shown on the right. Each lane contained 5 μg of recombinant PAP protein. (B and C) Association of PAP mutants with ribosomes isolated from rabbit reticulocyte enriched blood. (B.1) Total ribosomal protein (5 μg) was incubated with 1 μg of PAP, and the ribosome−PAP complexes were isolated by ultracentrifugation. The ribosome−PAP complexes were separated through SDS−12% PAGE, electroblotted onto a poly(vinylidene difluoride) (PVDF) membrane, and immunoblotted with a polyclonal antibody to PAP. (B.2) A fraction (5 mL) of the reaction mixture, prior to separation of the PAP−ribosome complex, was removed, separated through SDS−12% PAGE, transferred to PVDF membrane, and immunoblotted with a polyclonal antibody to PAP. The results show that equal amounts of PAP proteins were added to the reaction mixture. (C) Representative sensorgram showing the binding of wild-type and mutant PAP to rabbit ribosomes immobilized on a CM5 sensor chip. Wild-type or mutant PAP proteins were injected onto the surface on which 1200 RU of the MBP−L3 fusion protein had been immobilized at a flow rate of 5 μL/min (40 μL total volume).

of interactions with rRNA and lead to a lower binding affinity with L3. The mutant PAP protein FLP-4 (^{69}AA^{70}) has been engineered by alanine substitution of the active center cleft residues N69 and N70. These residues are located on an antiparallel β turn and interact via hydrogen bonds with the backbone of rRNA from the A +1 position to the A +3 position. Both residues are in close contact with the region near residue 350 on L3 (Figure 1B,C). FLP-7 (^{90}AAA^{92}) has been engineered by alanine substitution of the active center cleft residues 90−92. These residues are positioned on the C-terminal end of the β7 strand and are predicted to contribute to the binding of PAP to the tetraloop structure of RNA. D92 interacts with the base of G(+1). F90 can have van der Waals interactions with four nearby hydrophobic residues. The side chain of residue N91 is located further away from SRL than D92 and has little contact with the tetraloop (Figure 1D). Mutation of F90 is anticipated to affect the local conformation of the β8 strand and the following

Table 1: Kinetic Rates and Dissociation Constants of the Binding Interactions between Recombinant PAP Proteins and Intact Rabbit Ribosomes

mutants	original residue numbered	substituted residue	k_{on} (M^{-1} s^{-1})[a]	k_{off} (M^{-1} s^{-1})[b]	K_D (nM)[c]	K_D/K_D of wild-type PAP
wild type			$8.0 \pm 0.3 \times 10^4$	$2.3 \pm 0.1 \times 10^{-5}$	0.3 ± 0.1	1
FLP-4	^{69}NN^{70}	^{69}AA^{70}	$3.4 \pm 0.1 \times 10^4$	$1.8 \pm 0.1 \times 10^{-4}$	4.7 ± 0.4	16
FLP-5	^{71}LY^{72}	^{71}AA^{72}	$4.8 \pm 0.1 \times 10^4$	$1.1 \pm 0.12 \times 10^{-5}$	0.2 ± 0.1	0.9
FLP-7	^{90}FND^{92}	^{90}AAA^{92}	$1.5 \pm 0.1 \times 10^4$	$1.2 \pm 0.12 \times 10^{-4}$	7.8 ± 0.5	28
FLP-8	^{111}SR^{112}	^{111}AA^{112}	$3.7 \pm 0.3 \times 10^4$	$3.3 \pm 0.13 \times 10^{-5}$	0.9 ± 0.1	3.0
FLP-9	^{122}RY^{123}	^{122}AA^{123}	$8.2 \pm 0.8 \times 10^4$	$6.2 \pm 0.5 \times 10^{-5}$	0.8 ± 0.2	2.7
FLP-20	N69	A69	$2.0 \pm 0.1 \times 10^4$	$1.8 \pm 0.2 \times 10^{-4}$	9.0 ± 0.3	30
FLP-21	F90	A90	$2.3 \pm 0.1 \times 10^4$	$1.2 \pm 0.1 \times 10^{-4}$	5.2 ± 0.4	17
FLP-22	N91	A91	$2.0 \pm 0.1 \times 10^4$	$1.7 \pm 0.1 \times 10^{-4}$	8.5 ± 0.5	28
FLP-23	D92	A92	$3.0 \pm 0.2 \times 10^4$	$2.0 \pm 0.1 \times 10^{-4}$	6.7 ± 0.6	22

[a] k_{on} is the average and SD of measurements from the association phase from two cycles, where 50 nM/150 nM samples were injected. [b] k_{off} is the average and SD of measurements from the dissociation phase from two cycles, where 50 nM/150 nM samples were injected. [c] $K_D = k_{off}/k_{on}$.

loop region which consists of residues 121−123. Mutation of N91 is predicted to have less effect on binding to SRL. Meanwhile, residues 91 and 92 are near residue 58 of a loop region on L3 (see Figure 1D). Residue N91, but not F90 and D92, may interact with this loop region on L3 near residue 65 (Figure 1B,C). Thus mutation of F90 is anticipated to affect the local conformation of the β8 strand and the following loop region which consists of residues 121−123. Taken together, both FLP-4 and FLP-7 were anticipated to show impaired binding of PAP to rRNA and disrupt binding to L3. The single amino acid substitution mutants of PAP, FLP-20 (N69A), FLP-21(F90A), FLP-22 (N91A), and FLP-23 (D92A), were engineered and tested in order to further confirm the importance of the PAP active center cleft residues N69, F90, N91, and D92 for the ability of PAP to bind L3. FLP-24 (N70A) which was also engineered could not be included in biochemical analyses because it was unstable under our solubilization and refolding conditions.

The 121−123 loop of PAP is close enough to interact with the sugar, base, and phosphate groups of the targeted adenosine but is too distant to affect L3 binding. Both Y72 (mutated in FLP-5) and Y123 (mutated in FLP-9) can interact by aromatic group stacking with the base ring of the target adenosine on the basis of the crystal structure of PAP−FMP complex (*21*) and our current model. The side chain of Y123 is partially exposed on the PAP surface, but the side chain of Y72 is mostly buried. Thus Y72 and Y123 are unlikely to interact with L3 although mutations of Y72 and Y123 are predicted to have a significant impact on substrate turnover. Due to the reasons mentioned previously, both FLP-5 (^{71}AA^{72}) and FLP-9 (^{122}AA^{123}) should have unimpaired binding to L3. The control mutants FLP-1 and FLP-8 with alanine substitutions of residues ^{28}KD^{29} and ^{111}SR^{112} that are distant from the active center cleft and are too distant to be interact with L3 on the basis of our model were predicted to exhibit normal L3 binding (Figure 1B,C).

The recombinant PAP mutants with alanine substitutions were constructed using site-directed mutagenesis, as previously described (*15*). These mutant proteins were expressed in the *E. coli* strain, MV1190, as inclusion bodies, purified, solubilized, refolded, and analyzed by SDS−PAGE (Figure 2A). Each of the mutant PAP proteins had an apparent molecular mass of 33 kDa, similar to that of the recombinant wild-type PAP (Figure 2A.1). The refolded recombinant wild-type and mutant proteins were highly immunoreactive with the anti-PAP serum (Figure 2A.2). In a recent study, we demonstrated that the translation inhibition IC_{50} values of the catalytic site mutants FLP-5 (^{71}LY^{72}) and FLP-9 (^{122}AA^{123}), as well as the active center cleft mutants FLP-4 (^{69}AA^{70}) and FLP-7(^{90}AAA^{92}) ,were much higher than those of wild-type PAP (*15*). Furthermore, using a sensitive HPLC method for measuring the amount of adenine released by these mutants from *E. coli* 23/16S rRNA, we determined that wild-yype PAP releases 396 pmol of adenine/μg of RNA, whereas FLP-4 releases only 46 pmol of adenine/μg of RNA and FLP-7 releases only 19 pmol of adenine/μg of RNA (*15*). The ribosome inhibitory activities of the recombinant PAP mutants with alanine substitutions of residues ^{28}KD^{29} and ^{111}SR^{112} that are distant from the catalytic site and active center cleft (FLP-1 and FLP-8), however, were comparable to that of the wild-type PAP (*15*).

Interaction of Wild-Type or Mutant Recombinant PAP Proteins with Rabbit Ribosomes. To evaluate the ability of recombinant PAP proteins to bind ribosomes, intact ribosomes from rabbit reticulocytes were treated with the various PAP proteins, the ribosome−PAP complexes were isolated, and the ribosome-bound PAP proteins were detected by immunoblot analysis using a rabbit anti-PAP antibody. As shown in Figure 2B.1, the active center cleft mutants FLP-4, FLP-7, FLP-20, FLP-21, FLP-22, and FLP-23 showed less binding to intact ribosomes than wild-type PAP. By contrast, all other recombinant PAP proteins, including the catalytic site mutants FLP-5 and FLP-9, bound to the ribosomes as much as wild-type PAP did (Figure 2B.1). Controls confirmed that similar amounts of PAP proteins were used in the respective incubations and immunoprecipitations (Figure 2B.2).

We next compared the binding affinity of recombinant PAP proteins for the intact ribosomes by surface plasmon resonance. The active center cleft mutants FLP-4 and FLP-7 had slower on rates and faster off rates than the wild-yype recombinant PAP protein (Figure 2C, Table 1). The affinities of FLP-4 (K_D = 4.7 nM) and FLP-7 (K_D = 7.8 nM) for the intact rabbit ribosomes were 16-fold and 28-fold lower, respectively, than the affinity of the wild-type PAP (K_D = 0.3 nM) protein (Table 1). The single amino acid mutants of PAP with alanine substitution of the active center cleft residues N69 (FLP-20), F90 (FLP-21), N91 (FLP-22), or D92 (FLP-23) also showed > 10-fold reduced ribosome binding, further confirming the importance of the active center cleft for the PAP−ribosome interactions (Table 1). By comparison, the affinity of the catalytic site mutant FLP-5 (K_D = 0.2 nM) was virtually identical to that of wild-type PAP, and the affinity of the other catalytic site mutant FLP-9 (K_D

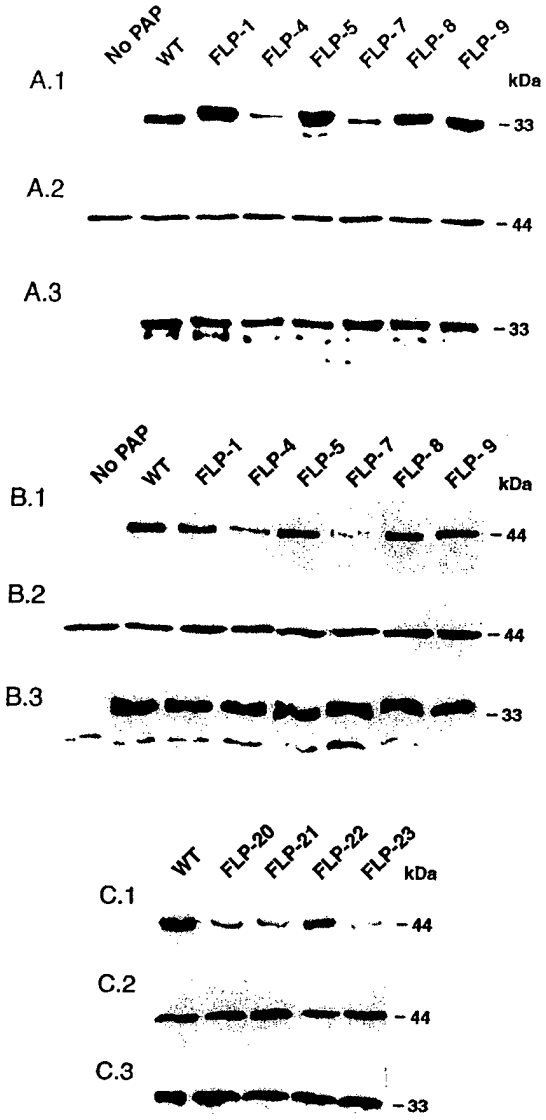

FIGURE 3: Association of wild-type and mutant PAP proteins with in vitro synthesized ribosomal protein L3. (A.1) Coimmunoprecipitated PAP revealed by immunoblotting using anti-PAP antibody. ^{35}S-Labeled L3 was incubated with wild-type and mutant PAP proteins and coimmunoprecipitated with protein A−Sepharose beads precoated with monoclonal antibody to L3. The PAP−L3 complexes were separated through SDS−12% PAGE, transferred to a PVDF membrane, and immunoblotted with a polyclonal anti-PAP antibody. (A.2) The blot was exposed to X-ray film, showing equal amounts of labeled L3 protein in each reaction. (A.3) A fraction (5 μL) of the reaction, prior to the coimmunoprecipitation, was removed from the reaction, separated through SDS−12% PAGE, transferred to a PVDF membrane, and immunoblotted with a polyclonal antibody to PAP. The results show that equal amounts of PAP were added to each reaction. (B.1 and C.1) Coimmunoprecipitated L3 revealed by immunoblotting using anti-L3 antibody. ^{35}S-Labeled L3 was incubated with wild-type and mutant PAP proteins and coimmunoprecipitated with protein A−Sepharose beads precoated with anti-PAP antibody. The PAP−L3 complexes were separated through SDS−12% PAGE, transferred to a PVDF membrane, and immunoblotted with a monoclonal anti-L3 antibody. (B.2 and C.2) A fraction (5 μL) of the reaction, prior to the coimmunoprecipitation, was removed from the reaction, separated through SDS−12% PAGE, dried, and autoradiographed. The results show that equal amounts of labeled L3 protein were added in each reaction. (B.3 and C.3) A fraction (5 μL) of the reaction, prior to the coimmunoprecipitation, was removed from the reaction, separated through SDS−12% PAGE, transferred to a PVDF membrane, and probed with polyclonal antibody to PAP. The results show that equal amounts of PAP were added to each reaction.

= 0.8 nM) was 3-fold lower than that of the wild type. The affinity of mutant FLP-8 (K_D = 0.9 nM), with alanine substitutions of residues ^{111}SR^{112} that are distant from the active center cleft, was only 3-fold lower than that of wild-type PAP (Table 1). Taken together, these results demonstrate that the active center cleft residues are critical for the ribosome binding of PAP.

Interaction of Wild-Type or Mutant Recombinant PAP Proteins with the Ribosome Protein L3. The ribosomal protein L3, a highly conserved protein located at the peptidyltransferase center of the ribosomes, plays a critical role in the binding of PAP to ribosomes and subsequent depurination of the SRL (*13*). Therefore, we next sought to determine if the active center cleft mutants FLP-4, FLP-7, FLP-20, FLP-21, FLP-22, and FLP-23, which exhibited poor binding to intact rabbit ribosomes, can bind L3 protein. To this end, we treated an in vitro synthesized yeast ribosomal protein L3 preparation with various recombinant PAP proteins, immunoprecipitated with a monoclonal anti-L3 antibody, and examined the L3 immune complexes for the presence of any coimmunoprecipitated PAP protein by immunoblotting with a polyclonal anti-PAP antibody. The L3 immune complexes contained relatively less FLP-4 or FLP-7 than other PAP proteins (Figure 3A.1). By comparison, FLP-1, FLP-5, FLP-8, and FLP-9 were coimmunoprecipitated as effectively as wild-type PAP. Controls confirmed that similar amounts of L3 (Figure 4A.2) and mutant PAP proteins (Figure 4A.3) were used in the respective incubations and immunoprecipitations. Similarly, the immune complexes of FLP-4 and FLP-7 contained much less L3 protein than the immune complexes of FLP-1, FLP-5, FLP-8, FLP-9 or wild-type PAP, when the recombinant PAP proteins were immunoprecipitated with the anti-PAP antibody and the coimmunoprecipitation of L3 protein was monitored by immunoblotting with the anti-L3 monoclonal antibody (Figure 3.B1−B3). The poor coimmunoprecipitation of mutant PAP proteins FLP-4 and FLP-7 with the in vitro synthesized yeast L3 protein indicates that the active center cleft residues ^{69}NN^{70} and ^{90}FND^{92} (but not the residues ^{28}KD^{29}, ^{71}LY^{72}, ^{111}SR^{112}, or ^{122}RY^{123} outside the active center cleft) play a pivotal role in L3 binding. The single amino acid substitution mutants FLP-20 (N69A), FLP-21 (F90A), FLP-23 (D92A), and, albeit to a lesser degree, FLP-22 (N91A) also showed reduced L3 binding, which provided further evidence that the active center cleft residues N69, F90, D92, and, to a lesser degree, N91 contribute to the ability of PAP to bind the L3 protein (Figure 3C.1−C.3).

In binding assays using a His-tagged recombinant wild-type PAP protein which was immobilized on the BIAcore sensor chip and surface plasmon resonance technology, which permits direct measurements of the association and disscoation kinetics of binding interactions, recombinant wild-type PAP exhibited high-affinity binding to L3 protein ($k_a = 5.2 \times 10^4$ M^{-1} s^{-1}, $k_d = 4.3 \times 10^{-4}$ s^{-1}, and K_D = 8.2 nM). This binding was blocked by treating the L3 protein with excess soluble recombinant wild-type PAP or excess native PAP, confirming the specificity of the binding interactions (Figure 4).

We next sought to compare the affinity of recombinant PAP proteins for the L3 protein by surface plasmon resonance. In the first series of experiments, we used MBP−L3 protein produced in *E. coli* (Figure 5.A1 and A2). The

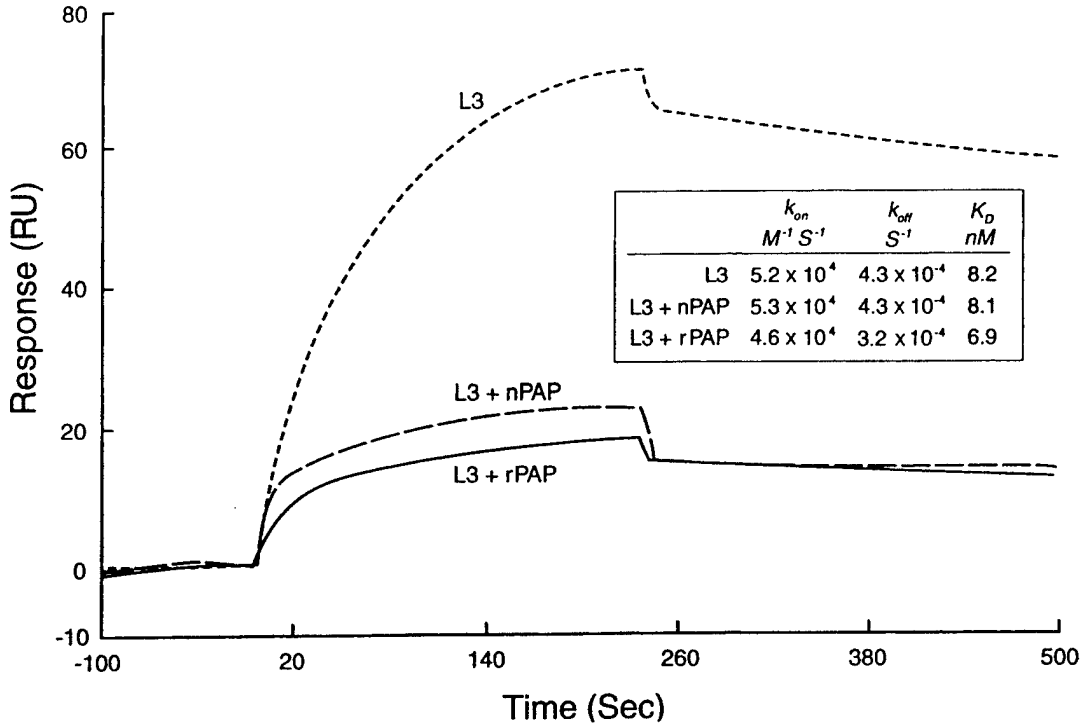

FIGURE 4: Binding specificity of L3 protein to immobilized recombinant wild-type PAP. 6×His−PAP was immobilized onto the NTA-modified surface at a level of 275 RU. A 30 mL solution (25 nM) of MBP−L3 fusion protein was preincubated without or with 250 nM native PAP or recombinant wild-type PAP at room temperature for 1 h and was then injected over immobilized 6×His−PAP at a flow rate of 8 μL/min. Between samples, the binding surface was regenerated by injecting 30 μL of regeneration buffer at a flow rate of 10 μL/min.

Table 2: Kinetic Rates and Dissociation Constants of the Binding Interactions between Recombinant PAP Proteins and Recombinant Yeast Ribosomal Protein L3 (MBP−L3)

mutants	original residue numbered	substituted residue	k_{on} (M^{-1} s^{-1})[a]	k_{off} (M^{-1} s^{-1})[b]	K_D (nM)[c]	K_D/K_D of wild-type PAP
wild type			$3.3 \pm 0.2 \times 10^4$	$8.6 \pm 0.5 \times 10^{-5}$	2.6 ± 0.2	1
FLP-1	^{28}KD^{29}	^{28}AA^{29}	$4.5 \pm 0.3 \times 10^4$	$2.2 \pm 0.1 \times 10^{-4}$	4.7 ± 0.3	1.7
FLP-4	^{69}NN^{70}	^{69}AA^{70}	$3.1 \pm 0.1 \times 10^4$	$4.2 \pm 0.3 \times 10^{-4}$	13.4 ± 0.9	5.2
FLP-5	^{71}LY^{72}	^{71}AA^{72}	$5.3 \pm 0.4 \times 10^4$	$7.9 \pm 0.4 \times 10^{-5}$	1.5 ± 0.1	0.6
FLP-7	^{90}FND^{92}	^{90}AAA^{92}	$2.1 \pm 0.2 \times 10^4$	$2.5 \pm 0.2 \times 10^{-4}$	11.9 ± 0.9	4.6
FLP-9	^{122}RY^{123}	^{122}AA^{123}	$3.7 \pm 0.2 \times 10^4$	$1.1 \pm 0.1 \times 10^{-4}$	3.0 ± 0.2	1.1
FLP-20	N69	A69	$3.4 \pm 0.2 \times 10^4$	$4.4 \pm 0.3 \times 10^{-4}$	12.9 ± 1.1	4.6
FLP-21	F90	A90	$1.7 \pm 0.1 \times 10^4$	$2.6 \pm 0.2 \times 10^{-4}$	15.7 ± 1.3	6.0
FLP-22	N91	A91	$1.4 \pm 0.1 \times 10^4$	$2.5 \pm 0.2 \times 10^{-4}$	17.8 ± 2.0	6.8
FLP-23	D92	A92	$2.5 \pm 0.2 \times 10^4$	$4.3 \pm 0.3 \times 10^{-4}$	17.2 ± 2.0	6.6

[a] k_{on} is the average and SD of measurements from the association phase from two cycles, where 50 nM/150 nM samples were injected. [b] k_{off} is the average and SD of measurements from the dissociation phase from two cycles, where 50 nM/150 nM samples were injected. [c] $K_D = k_{off}/k_{on}$.

MBP protein fused to the N-terminus of the yeast ribosomal protein L3 allowed the L3 protein to be captured in a unique homogeneous orientation on the BIAcore sensor chip. Figure 5.A3 shows a representative sensorgram that was used to generate the kinetic constants summarized in Table 2. The binding traces were analyzed assuming a single bimolecular binding equilibrium between PAP and L3 proteins. The active center cleft mutants FLP-4 and FLP-7 had slower on rates and faster off rates than the wild-type recombinant PAP protein (Table 2, Figure 5.A3). The affinities of FLP-4 (K_D = 13.4 nM) and FLP-7 (K_D = 11.9 nM) for MBP-L3 were approximately 5-fold lower than the affinity of wild-type PAP. The single amino acid substitution mutants FLP-20 (N69A), FLP-21 (F90A), FLP-23 (D92A), and FLP-22 (N91A) also showed a reduced affinity toward L3 binding. Although FLP-22 showed better binding to yeast L3 protein than FLP-20, FLP-21, and FLP-23 (see Figure 3), it did not exhibit a higher affinity than those other active cleft mutants toward the MBP-L3 protein (Table 2). Thus, the MBP tail might affect the binding interactions of L3 with PAP. Nevertheless, the binding affinities of all other recombinant PAP proteins for the MBP−L3 fusion protein were similar to that of wild-yype PAP (Table 2).

Virtually identical results were obtained in binding assays using a His-tagged recombinant L3 protein (6×His−L3) produced in the baculovirus expression system (Table 3, Figure 5.B1−B3). These findings extend the coimmunoprecipitation results and demonstrate the importance of the PAP active cleft residues for the binding interactions between PAP and the ribosomal protein L3. As shown in Figure 5.B4, the high-affinity L3 binding of the catalytic site mutants FLP-5 and FLP-9 confirmed that alanine substitution of the highly conserved catalytic site residues Tyr^{72} and Tyr^{123} does not affect the binding of PAP to the L3 protein, which is in agreement with the assumed role of these residues in binding of PAP to the SRL of rRNA (*20*−*22*).

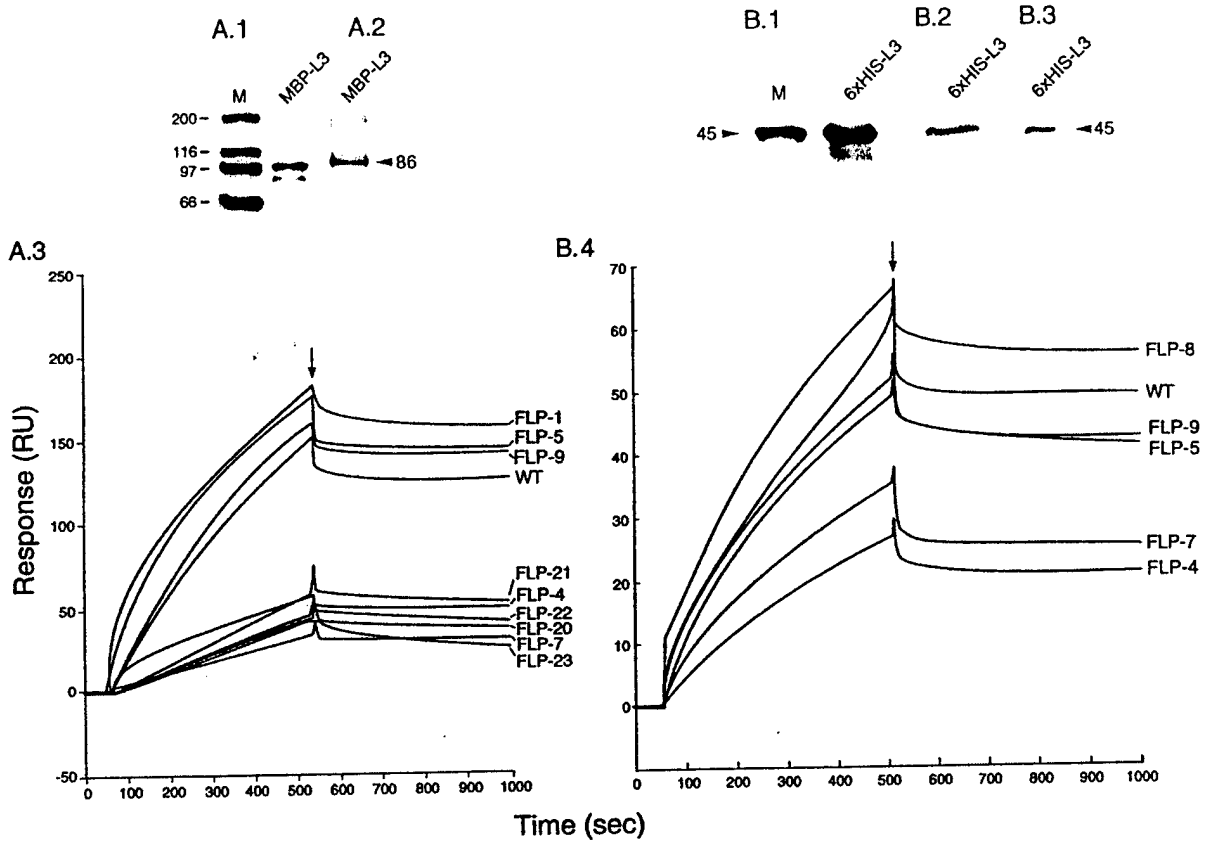

FIGURE 5: Binding of wild-type and mutant PAP proteins to ribosomal protein L3. (A.1) Coomassie Blue-stained SDS−10% PAGE of column-purified recombinant MBP−L3 fusion protein. (A.2) Western blot analysis of MBP−L3 fusion protein using anti-L3 antibody. The mass of the protein (in kDa) is shown on the right. M: molecular mass marker positions (in kDa). (A.3) Representative sensorgram showing the binding of wild-type and mutant PAP proteins to the MBP−L3 fusion protein captured by anti-MBP antibody that was immobilized on a CM5 sensor chip. Wild-type or mutant protein was injected onto the surface on which 1500 RU of the MBP−L3 fusion protein had been immobilized at a flow rate of 5 μL/min (40 μL total volume). The dissociation was started by injecting buffer lacking the sample as indicated by the arrow. (B.1) Coomassie Blue-stained SDS−10% PAGE of column-purified recombinant 6×His−L3 fusion protein. (B.2) Western blot analysis of 6×His−L3 fusion protein using anti-L3 antibody. (B.3) Western blot analysis of 6×His−L3 fusion protein using an anti-His antibody (Qiagen). The mass of the protein (in kDa) is shown on the right. M: molecular mass marker positions (in kDa). (B.4) Representative sensorgram showing the binding of wild-type and mutant PAP to a recombinant yeast ribosomal protein L3 (6×His−L3) biosensor surface.

Table 3: Kinetic Rate and Dissociation Constants of the Binding Interactions between Recombinant PAP Proteins and Recombinant Yeast Ribosomal Protein L3 (MBP−L3)

mutants	original residue numbered	substituted residue	k_{on} (M^{-1} s^{-1})[a]	k_{off} (M^{-1} s^{-1})[b]	K_D (nM)[c]	K_D/K_D of wild-type PAP
wild type			$4.4 \pm 0.4 \times 10^4$	$1.5 \pm 0.18 \times 10^{-4}$	3.5 ± 0.2	1.0
FLP-4	^{69}NN^{70}	^{69}AA^{70}	$4.2 \pm 0.3 \times 10^4$	$7.5 \pm 0.31 \times 10^{-4}$	18.1 ± 0.9	5.2
FLP-5	^{71}LY^{72}	^{71}AA^{72}	$5.0 \pm 0.5 \times 10^4$	$2.3 \pm 0.21 \times 10^{-4}$	4.6 ± 0.3	1.2
FLP-7	^{90}FND^{92}	^{90}AAA^{92}	$4.2 \pm 0.4 \times 10^4$	$5.7 \pm 0.38 \times 10^{-4}$	13.8 ± 0.6	4.0
FLP-8	^{111}SR^{112}	^{111}AA^{112}	$3.4 \pm 0.3 \times 10^4$	$1.2 \pm 0.09 \times 10^{-4}$	3.6 ± 0.3	1.0
FLP-9	^{122}RY^{123}	^{122}AA^{123}	$6.3 \pm 0.5 \times 10^4$	$2.5 \pm 0.17 \times 10^{-4}$	4.0 ± 0.3	1.2

[a] k_{on} is the average and SD of measurements from the association phase from two cycles, where 50 nM/150 nM samples were injected. [b] k_{off} is the average and SD of measurements from the dissociation phase from two cycles, where 50 nM/150 nM samples were injected. [c] $K_D = k_{off}/k_{on}$.

The recombinant PAP protein used in this study contains a 22 amino acid N-terminal signal peptide and a 29 amino acid C-terminal peptide (*15*, *18*). Our previous work demonstrated that the ribosome inhibitory activities of the native and recombinant wild-type protein are comparable (IC_{50} = 0.010 ± 0.004 versus 0.013 ± 0.005 mg/mL) (*18*). Furthermore, our present study shows that native PAP effectively blocks the binding of our recombinant PAP to the L3 protein. Nevertheless, our binding data obtained with the recombinant PAP protein might not accurately reflect the binding of the native protein to the ribosomes in vivo. We are currently trying to cocrystallize native PAP and L3 to decipher the exact structural basis for their interaction. Ultimately, cocrystallization of PAP and a large ribosomal subunit will be required to better understand the in vivo binding of PAP to ribosomes and ribosomal proteins such as L3.

In summary, we employed molecular modeling, structure-based protein design, and site-directed mutagenesis combined with standard immunoprecipitation assays and surface plasmon resonance technology to elucidate the putative role of the PAP active center cleft in the binding of PAP to the ribosomal protein L3, which has been previously shown to mediate the binding of PAP to ribosomes. Our findings provide experimental evidence that the active center cleft of

PAP is important for its binding to ribosomes via the L3 protein and therefore its access to the target α-sarcin/ricin loop of the large ribosomal RNA (rRNA) species in eukaryotic (28S rRNA) and prokaryotic (23S rRNA) ribosomes (*7*, *8*). The insights gained from this study also explain why and how the conserved charged and polar side chains located at the active center cleft of PAP that do not directly participate in the catalytic deadenylation of ribosomal RNA play a critical role in the catalytic removal of the adenine base from target rRNA substrates by affecting the binding interactions between PAP and ribosomes.

The ribosomal protein L3 is expected to bind to and may stabilize the rRNA conformation in which SRL can most effectively bind to and react with PAP. In our model, PAP mutations such as D92A would affect binding with SRL and may thus cause PAP to adopt an unusual binding mode with the tetraloop which consequently changes the docking position of L3. Additionally, L3, rRNA, and PAP are not three separated identities. They form an integrated complex sharing an overlapped binding region. Interaction between two componets of this complex would affect their interaction with the third component. Therefore, under physiologic conditions, L3 may have reduced binding affinity to the PAP mutants which have impaired binding with SRL. We postulate that the active center cleft mutants would have markedly reduced ability to interact with the L3 ribosomal protein under physiologic conditions because of their poor L3 binding as well as poor rRNA binding.

Our results showing the ability of PAP to bind purified L3 in the absence of other ribosomal components indicate that conformational changes of L3, if any should occur as a result of its incorporation into the ribosome, are not required for its interactions with PAP. Therefore, our model for L3–PAP interactions did not take into account any conformational changes which may occur when L3 is incorporated into the ribosome. The elucidation of the exact details of the physical interactions between L3 and PAP will require the cocrystallization of these two proteins and ideally the cocrystallization of a large ribosomal subunit and PAP.

ACKNOWLEDGMENT

We thank Tammy J. Denton, Dawn M. Dahlke, Michelle L. Henning, Rebecca S. Larue, Dina Clementson, Brad Nodland, and Andrea Dopkins for technical assistance.

REFERENCES

1. Irvin, J. D. (1995) Antiviral proteins from Phytolacca, *Antiviral Proteins in Higher Plants* (Chessin, M., DeBorde, D., and Zipf, A., Eds.) CRC Press, Boca Raton, FL.
2. Irvin, J. D. (1983) *Pharmacol. Ther. 21*, 371–387.
3. Irvin, J. D., and Uckun, F. M. (1992) *Pharmacol. Ther.* 55, 279–302.
4. Uckun, F. M. (1993) *Br. J. Haematol. 85*, 435–438.
5. Uckun, F. M., and Reaman, G. H. (1995) *Leuk. Lymphoma 18*, 195–201.
6. Myers, D. E., and Uckun, F. M. (1995) *Leuk. Lymphoma 18*, 119–122.
7. Endo, Y., Mitsui, K., Motizuki, M., and Tsurugi, K. (1987) *J. Biol. Chem. 262*, 5908–5912.
8. Endo, Y., and Tsurugi, K. (1988) *J. Biol. Chem. 263*, 8735–8739.
9. Obrig, T. G., Irvin, J. D., and Hardesty, B. (1973) *Arch. Biochem. Biophys. 155*, 278–289.
10. Gessner, S. L., and Irvin, J. D. (1980) *J. Biol. Chem. 255*, 3251–3253.
11. Montanaro, L., Sperti, S., Mattioli, A., Testoni, G., and Stirpe, F. (1975) *Biochem. J. 146*, 127–131.
12. Barbieri, L., Battelli, M. G., and Stirpe, F. (1993) *Biochim. Biophys. Acta 1154*, 237–282.
13. Hudak, K. A., Dinman, J. D., and Tumer, N. E. (1999) *J. Biol. Chem. 274*, 3859–3864.
14. Uchiumi, T., Sato, N., Wada, A., and Hachimori, A. (1999) *J. Biol. Chem. 274*, 681–686.
15. Rajamohan, F., Pugmire, M. J., Kurinov, I. V., and Uckun, F. M. (2000) *J. Biol. Chem. 275*, 3382–3390.
16. Ban, N., Nissen, P., Hansen, J., Moore, P. B., and Steitz, T. A. (2000) *Science 289*, 905–920.
17. Sack, J. S. (1988) *J. Mol. Graphics 6*, 244–249.
18. Rajamohan, F., Engstrom, C. R., Denton, T. J., Engen, L. A., Kourinov, I., and Uckun, F. M. (1999) *Protein Expression Purif. 16*, 359–368.
19. Boyd Hardesty, W. M., and Culp, W. (1979) *Methods Enzymol. 33*, 316–327.
20. Peltz, S. W., Hammell, A. B., Cui, Y., Yasenchak, J., Puljanowski, L., and Dinman, J. D. (1999) *Mol. Cell. Biol. 19*, 384–391.
21. Monzingo, A. F., Collins, E. J., Ernst, S. R., Irvin, J. D., and Robertus, J. D. (1993) *J. Mol. Biol. 233*, 705–715.
22. Poyet, J. L., Hoeveler, A., and Jongeneel, C. V. (1998) *Biochem. Biophys. Res. Commun. 253*, 582–587.
23. Nicholls, A., Sharp, K. A., and Honig, B. (1991) *Proteins 11*, 281–296.

BI002851P

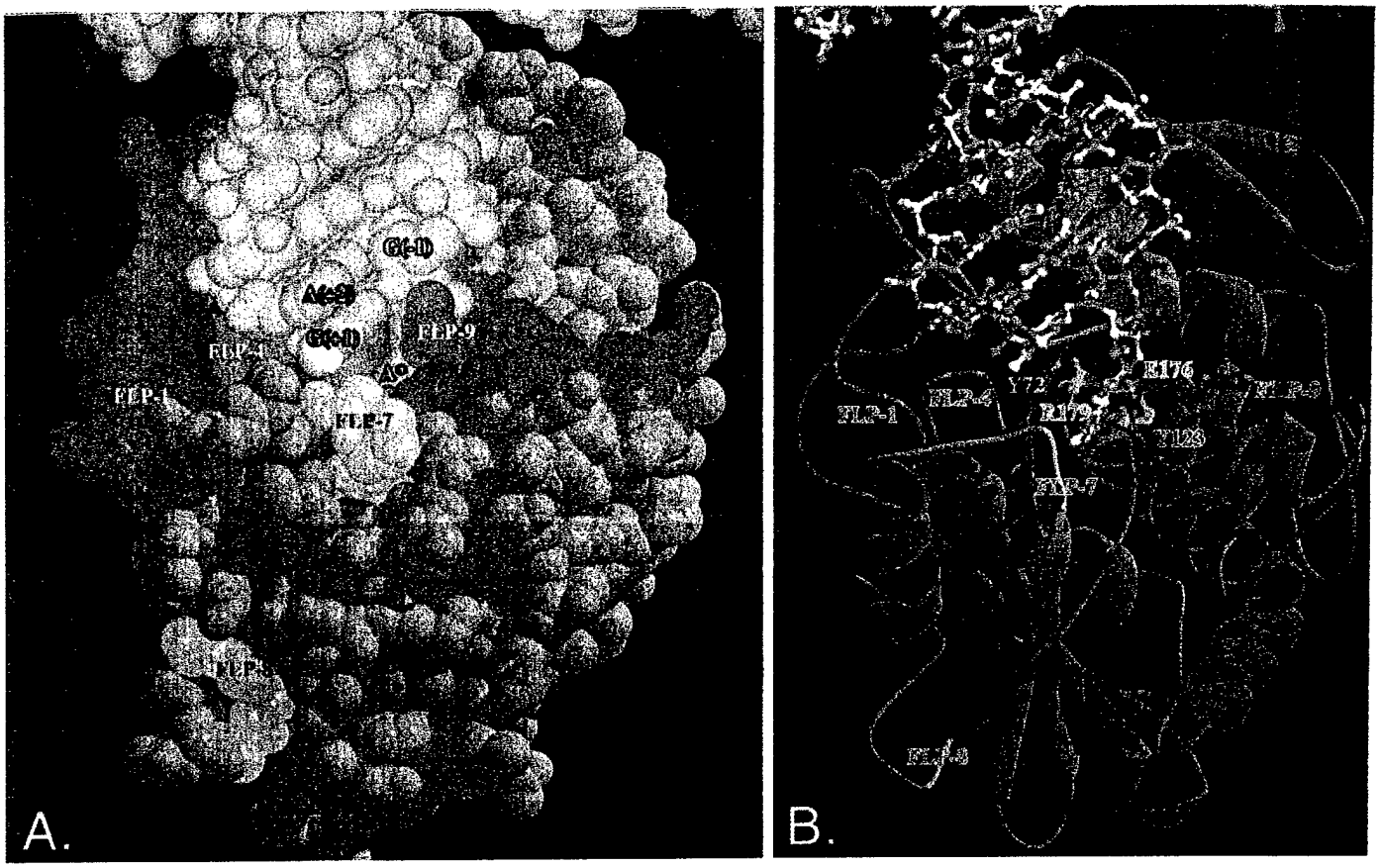

FIG. 1. **Molecular model of PAP-rRNA stem loop complex.** *A*, PAP molecule (*blue*) interacting with the SRL region of rRNA (*white*). The positions of the alanine-substituted residues of the recombinant PAP mutants FLP-1, FLP-4, FLP-7, FLP-8, and FLP-9 are indicated. The conformation of rRNA (*colored* in *white*; phosphate backbone in *yellow*) was adjusted around the adenine A^{2697} (A^{2660} in *E. coli*) of the GAGA tetraloop, and the rest of the PAP molecule remained unchanged. The adenosine was manually adjusted by a 38° degree out-flipping rotation at the C5′-position and a 5.4-Å translation of the adenine ring. There are no steric collisions between PAP and nearby ribosomal proteins. *B*, close-up view of PAP (*blue*) interacting with rRNA. The rRNA including the target tetraloop GAGA is shown in a *white ball-and-stick model* (phosphate groups in *yellow*). The active site residues of PAP including Tyr^{72}, Arg^{179}, Glu^{176}, and Tyr^{123}, which are shown as a *ball-and-stick model*, are critical in catalysis. The ribosomal proteins are not shown for clarity. This *figure* was prepared using MOLSCRIPT (27) and RASTER3D (28).

proteins were dissolved in HSEM buffer (10 mM HEPES, pH 8.0, 50 mM NaCl, 1 mM EDTA, 5 mM $MgCl_2$) to yield a final concentration of 5 μg/ml. In a kinetic study, 30-μl samples (150 nM) were injected at 25 °C at a flow rate of 8 μl/min onto the sensor chip surface on which the oligo has been immobilized or onto a control surface on which SA had been blocked with biotin, using HBS-EP as the running buffer. Between samples, the binding surfaces were regenerated by a 3-min injection of 2 M NaCl at a flow rate of 10 μl/min. Due to the large number of samples, the experiment was carried out twice on the same chip, and samples were injected in random order. To prepare the data for analysis, base lines were adjusted to zero for all curves, and injection start times were aligned. Background sensorgrams were then subtracted from the experimental sensorgrams to yield curves representing specific binding. The association and dissociation phases of the sensorgrams were fit simultaneously, assuming a simple bimolecular reaction model for interaction between soluble analyte and immobilized ligand, equivalent to the Langmuir isotherm for adsorption to a surface. The goodness of fit was assessed by inspecting the statistical value χ^2 and the residuals (observed − calculated). The χ^2 values were low (<2), and the residuals were randomly distributed about zero. The association and dissociation rate constants were calculated by nonlinear fitting of the primary sensorgram data using the BIAevaluation software (version 3.0), supplied with the instrument (BIAcore Inc.). Affinities were calculated from rate constants and from analysis of equilibrium binding.

RESULTS AND DISCUSSION

Molecular Model of PAP-Ribosome (Large Subunit) Complex and Structure-based Design of Recombinant PAP Proteins with Altered rRNA Binding Affinity—Our previous modeling studies (16) indicated that the active center cleft residues Asn^{69}, Asn^{70}, and Asp^{92} as well as the active site residue Arg^{122}, which are not directly involved in the catalytic depurination of rRNA, promote specific interactions with the phosphate backbone of the target α-sarcin/ricin stem loop of rRNA. Therefore, mutations of these residues were predicted to result in destabilization of interactions with rRNA. Our refined molecular model of the PAP-RNA stem loop complex is depicted in Fig. 1. According to this model, PAP residues 43, 67 (paired with 97), 69–70, 92, 206–210, 212–213, 217, 224–225, and 253–255 participate in its interaction with rRNA. The mutant PAP protein FLP-4 ($^{69}AA^{70}$) has been engineered by alanine substitution of the active center cleft residues Asn^{69} and Asn^{70}, which are located on an antiparallel β turn and interact via hydrogen bonds with the backbone of rRNA from the A^{+1} position to the A^{+3} position. FLP-7 ($^{90}AAA^{92}$) has been engineered by alanine substitution of the active center cleft residues 90–92 ($^{90}FND^{92}$), which are positioned on the C-terminal of the β_7 strand and are predicted to contribute to the binding of PAP to the tetraloop structure of RNA. Asp^{92} interacts with the base of G^{+1}. Phe^{90} has van der Waals interactions with four nearby hydrophobic residues. Thus, mutation of Phe^{90} is anticipated to affect the local conformation of the β_8 strand and the following loop region, which consists of residues 121–123 ($^{121}SRY^{123}$). The 121–123 loop interacts with the sugar, base, and phosphate groups of the targeted adenosine. Therefore, both FLP-4 and FLP-7 were predicted to have impaired binding to rRNA. The catalytic site mutant FLP-9 ($^{122}AA^{123}$) has alanine substitutions of Arg^{122} and Tyr^{123}. Arg^{122} interacts with the phosphate of the targeted adenosine, and the base ring of Tyr^{123} stacks

TABLE I
Sequence identity, adenine release, and substrate binding of recombinant wild-type and mutant PAP proteins

Mutant	Original residues	Substituted residues	Adenine released[a]	Maximum bound[b]	
				rRNA	Oligo
			pmol/μg RNA	*pmol*	
Wild type			396 ± 15	0.79 ± 0.03	1.2 ± 0.2
FLP-1	^{28}KD^{29}	^{28}AA^{29}	319 ± 14	0.81 ± 0.03	1.3 ± 0.2
FLP-4	^{69}NN^{70}	^{69}AA^{70}	132 ± 12	0.27 ± 0.02	0.53 ± 0.1
FLP-7	^{90}FND^{92}	^{90}AAA^{92}	19 ± 5	0.29 ± 0.02	0.38 ± 0.1
FLP-8	^{111}SR^{112}	^{111}AA^{112}	376 ± 11	0.75 ± 0.03	1.2 ± 0.1
FLP-9	^{122}RY^{123}	^{122}AA^{123}	12 ± 3	0.29 ± 0.02	0.47 ± 0.1
FLP-12	Arg^{179}	Ala^{179}	14 ± 7	0.28 ± 0.02	0.42 ± 0.1
FLP-13	Trp^{208}	Ala^{208}	4 ± 2	0.27 ± 0.02	0.48 ± 0.1

[a] The adenine released values were adopted from Rajamohan *et al.* (16) for comparison.
[b] The maximum level of binding (B_{max}) of ^{32}P-labeled 23 S/16 S rRNA and ^{32}P-labeled SR loop oligo (pmol/pmol of protein) were derived from fitting the data of Fig. 4, *A* and *C*, to a hyperbolic binding function (Graphpad Prism 2). Each value is the mean and S.D. of three experiments.

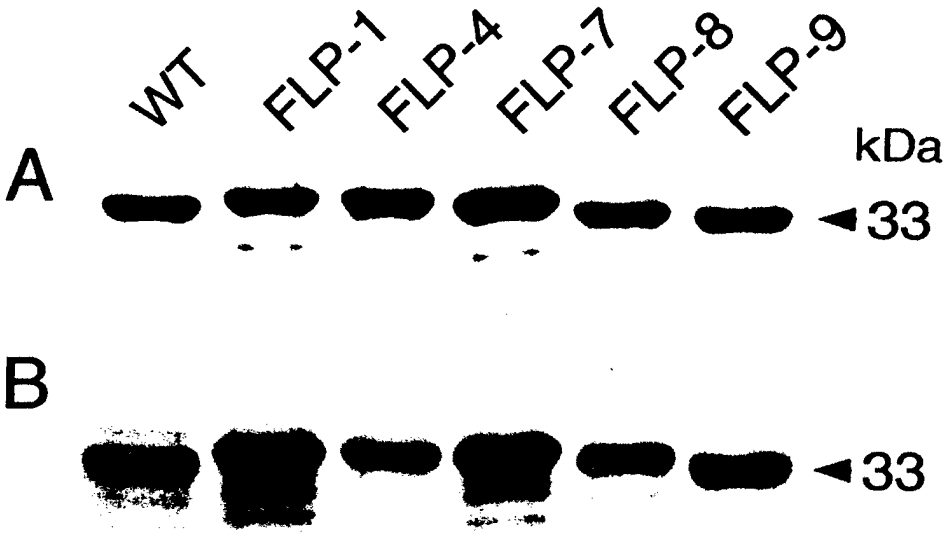

FIG. 2. **Coomassie Blue-stained SDS-12% polyacrylamide gel electrophoresis (*A*) and Western blot analysis (*B*) of wild-type and mutant recombinant PAP proteins.** Masses of the proteins (in kDa) are shown on the *right*. Each *lane* contained 5 μg of recombinant PAP protein. *WT*, wild type.

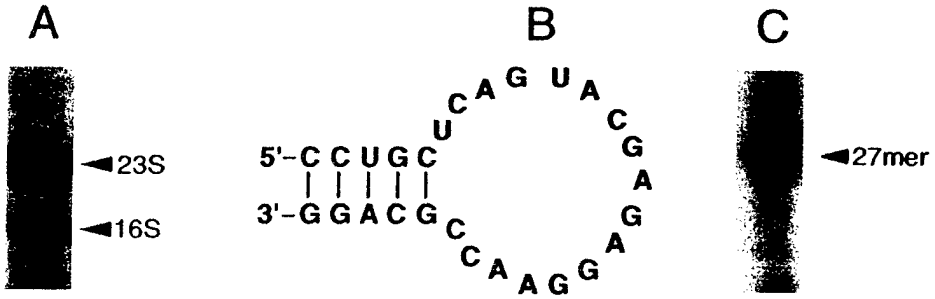

FIG. 3. **Substrate RNA targets.** *A*, 23 S/16 S naked rRNA from *E. coli* was 5′-end-labeled with ^{32}P, and 5 μl of the sample was separated by 7% polyacrylamide/urea gel, dried, and autoradiographed. The *arrow* indicates the position of 23 S and 16 S rRNA. *B*, sequence and putative secondary structure of the synthetic oligoribonucleotide (27-mer) used in this study that mimics the α-sarcin/ricin loop in the 28 S rRNA. *C*, 5 μl of the 5′-end-radiolabeled (^{32}P-labeled) oligo was separated by a 16% polyacrylamide/urea gel, dried, and autoradiographed. The *arrow* shows the position of the 27-mer.

with the targeted adenine base. Therefore, FLP-9 was predicted to have a poor binding affinity to rRNA and poor enzymatic activity. By contrast, the control PAP mutants FLP-1 (^{28}AA^{29}) and FLP-8 (^{111}AA^{112}) with mutations of residues ^{28}KD^{29} and ^{111}SR^{112} that are distant from the rRNA binding site were predicted to have a normal rRNA binding comparable with that of wild-type PAP. These predictions are in accord with the recently reported rRNA depurinating activities of FLP-1, FLP-4, FLP-7, FLP-8, FLP-9, FLP-12 (Ala^{179}), and FLP-13 (Ala^{208}) (16). The rRNA depurinating activities of the active center cleft mutants FLP-4 and FLP-7 as well as the catalytic site mutants, FLP-9, FLP-12, and FLP-13, were significantly lower than the activity of wild-type PAP. By comparison, the depurinating activities of FLP-1 and FLP-8 were comparable with that of wild-type PAP (Table I).

Impaired Binding Interactions of Recombinant PAP Active Center Cleft Mutants FLP-4 (^{69}AA^{70}) and FLP-7 (^{90}AAA^{92}) with E. coli 23 S/16 S rRNA—We next sought to more directly evaluate the predictions of our modeling studies regarding the role of the PAP active center cleft in rRNA binding by studying the binding interactions of recombinant PAP proteins with target RNAs (23 S rRNA and SR loop oligoribonucleotide). The recombinant PAP mutants with alanine substitutions were constructed using site-directed mutagenesis, as previously described (16). These mutant proteins were expressed in the *E. coli* strain, MV1190, as inclusion bodies, purified, solubilized,

refolded, and analyzed by SDS-polyacrylamide gel electrophoresis (Fig. 2*A*). Each of the mutant PAP proteins had an apparent molecular mass of 33 kDa, similar to that of the recombinant wild-type PAP (Fig. 2*A*). The refolded recombinant wild-type and mutant proteins were highly immunoreactive with the anti-PAP serum (Fig. 2*B*).

We first evaluated the saturation binding of radiolabeled 23 S/16 S rRNA (Fig. 3*A*) with increasing concentrations of recombinant wild-type or mutant PAP proteins with alanine substitutions in three independent experiments using standard filter binding assays. When increasing amounts of PAP proteins were reacted with 3.5 pmol of ^{32}P-labeled 23 S/16 S rRNA (specific activity 460 cpm/pmol), wild-type PAP showed concentration-dependent and saturable binding to the substrate RNA (23 S/16 S rRNA). As evidenced in Fig. 4*A* and Table I, the catalytic site mutants FLP-9(^{122}AA^{123}), FLP-12(A^{179}), and FLP-13(A^{208}) as well as the active center cleft mutants FLP-4 (^{69}AA^{70}) and FLP-7 (^{90}AAA^{92}) exhibited significantly impaired RNA binding ability when compared with wild-type PAP. By comparison, recombinant PAP mutants with alanine substitutions of residues ^{28}KD^{29} (FLP-1) and ^{111}SR^{112} (FLP-8) that are distant from the catalytic site and active center cleft were able to bind 23 S/16 S rRNA in amounts comparable with that of the wild-type PAP (Fig. 4*A*, Table I). Control protein BSA did not bind to ^{32}P-labeled 23 S/16 S rRNA even at the highest concentration.

Interaction of Recombinant PAP Mutants with α-Sarcin/Ricin Stem Loop of Eukaryotic 28 S rRNA—It is known that PAP catalytically removes a specific adenine from the highly conserved, surface-exposed, α-sarcin/ricin loop in the large rRNA of prokaryotic and eukaryotic ribosomes (3–6). Therefore, in our present study of RNA-PAP interactions, we used a 27-mer model RNA fragment corresponding to the conserved target α-sarcin/ricin stem loop (SR loop) of eukaryotic 28 S rRNA (Fig. 3*B*). Synthetic RNA fragments that mimic the local structures of rRNA have widely been employed to investigate RNA-protein interactions (24–26). The 5′-end of this oligoribonucleotide (Fig. 3*C*) was radiolabeled with ^{32}P (specific activity 140 cpm/pmol), and its interaction with increasing amounts of wild-type or mutant recombinant PAP proteins was investigated using filter binding assays. We first examined the binding of PAP (33 pmol) to ^{32}P-labeled SR loop oligo (50 pmol) in the absence as well as presence of increasing concentrations of unlabeled oligo. PAP exhibited significant binding to the oligo, and this binding was competitively blocked by the cold oligo in a concentration-dependent fashion, confirming the specificity of the binding interaction (Fig. 4*B*). Control protein BSA, however, exhibited very little binding, and its binding was not competitively blocked by the unlabeled oligo (Fig. 4*B*).

We next compared the binding of wild-type and mutant PAP proteins to the SR loop oligo. In accordance with the binding results obtained using naked 23 S/16 S rRNA, the active center cleft mutants, FLP-4 (^{69}AA^{70}) and FLP-7 (^{90}AAA^{92}), as well as the catalytic site mutants FLP-9 (^{122}AA^{123}), FLP-12 (Ala^{179}), and FLP-13 (Ala^{208}), exhibited significantly reduced binding to the stem loop RNA fragment (Table I, Fig. 4*C*). By comparison, the binding of recombinant PAP mutants FLP-1(^{28}AA^{29}) and FLP-8 (^{111}AA^{112}) to the SR loop RNA fragment is comparable with that of the wild-type PAP (Fig. 4*C*, Table I). BSA, which was included as a non-RNA-binding control protein, showed no binding to the SR loop oligo.

We next performed equilibrium binding studies to determine the maximum specific substrate (SR loop oligo) binding capacity (B_{max}) and apparent association constant (K_a) of the equilibrium binding to the stem loop RNA fragment for wild-type and the mutant recombinant PAP proteins. Recombinant PAP proteins (25 pmol) were incubated with increasing concentrations of the ^{32}P-labeled SR stem loop RNA fragment for 30 min at room temperature. All PAP proteins exhibited saturable

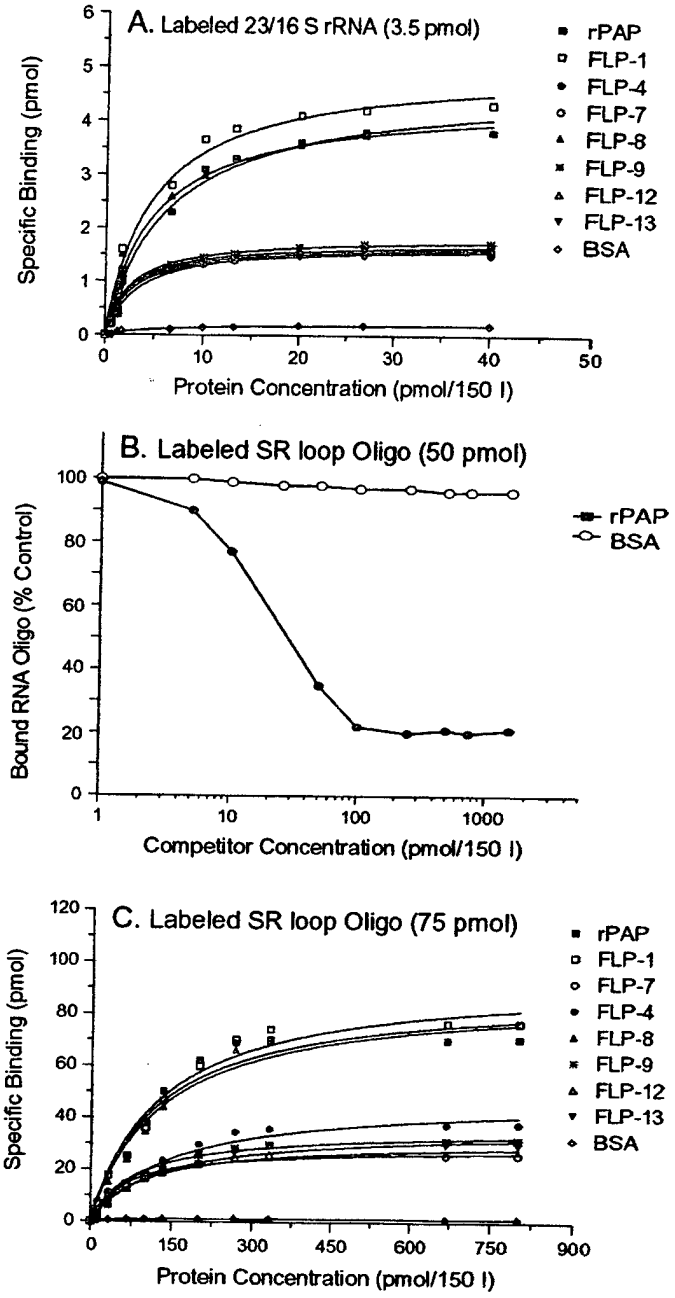

FIG. 4. **RNA binding of wild-type and mutant recombinant PAP proteins.** *A*, increasing concentrations of wild-type or mutant PAP proteins were incubated with ^{32}P-labeled 23 S/16 S rRNA from *E. coli* for 30 min at room temperature in a final volume of 150 μl. Each reaction mixture was applied to a nitrocellulose filter. Each value is the mean of at least three experiments. A background (50–70 cpm) determined by filtration of samples containing all the reagents except PAP was subtracted from each assay. *B*, 33 pmol of wild-type recombinant PAP protein or BSA, control protein, were incubated with 50 pmol of ^{32}P-labeled SR loop oligo (specific activity 140 cpm/pmol) and increasing concentrations (0–1500 pmol) of nonlabeled SR loop oligo as a competitor in 150 μl of binding buffer. Binding is expressed as the percentage of the amount bound upon incubation with the labeled SR loop oligo alone. The specific binding was 40 pmol for wild-type PAP and 0.2 pmol for BSA. *C*, increasing concentrations of wild-type or mutant PAP proteins were incubated with ^{32}P-labeled SR loop oligo for 30 min at room temperature in a final volume of 150 μl. Each reaction mixture was applied to a nitrocellulose filter. Each value is the mean of at least three experiments. A background (50–70 cpm) determined by filtration of samples containing all of the reagents except PAP was subtracted from each assay.

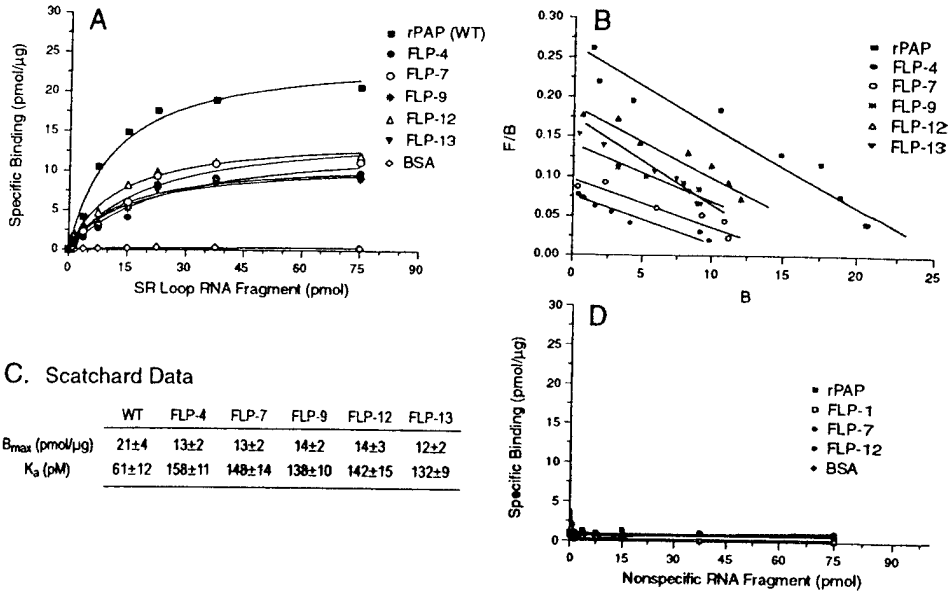

C. Scatchard Data

	WT	FLP-4	FLP-7	FLP-9	FLP-12	FLP-13
B_{max} (pmol/μg)	21±4	13±2	13±2	14±2	14±3	12±2
K_a (pM)	61±12	158±11	148±14	138±10	142±15	132±9

FIG. 5. **Binding of recombinant PAP proteins to radiolabeled oligoribonucleotide as a function of free ligand concentration.** *Panel A*, binding of PAP mutant proteins (25 pmol) with increasing concentrations of ^{32}P-labeled α-sarcin/ricin loop oligo. *Panel B*, equilibrium binding data from *A* was transformed and replotted in the Scatchard plot. Results are shown as number of oligonucleotide specifically bound to 1.0 μg of protein (*B*) and concentration (nM) of free radiolabeled oligonucleotide (*F*). *Panel C*, Scatchard data. *Panel D*, binding of recombinant PAP proteins (25 pmol) to ^{32}P-labeled control oligo. Data points represent mean values obtained from two independent experiments.

binding at increasing substrate oligoribonucleotide concentrations (Fig. 5*A*). For each recombinant PAP protein, the display of the equilibrium binding data in a Scatchard coordinate system yielded a straight line ($r = -0.99$) for binding measured over a concentration range of 0–22.5 pmol, supporting the notion that a single class of rRNA binding sites exists for PAP (Fig. 5*B*). The intercepts on the x axis (B_{max}) that correspond to the maximum loop RNA fragment binding capacity of the PAP proteins were 21 ± 4 pmol/μg for recombinant wild-type PAP, 13 ± 2 pmol/μg for FLP-4 (^{69}AA^{70}), 13 ± 2 pmol/μg for FLP-7 (^{90}AAA^{92}), 14 ± 2 pmol/μg for FLP-9 (^{122}AA^{123}), 14 ± 3 pmol/μg for FLP-12 (Ala^{179}), and 12 ± 2 pmol/μg for FLP-13 (Ala^{208}) (Fig. 5, *B* and *C*). These findings demonstrate that RNA binding capacity of PAP is markedly reduced by mutations involving its catalytic site or active center cleft. The estimated values of the apparent K_a as determined from the negative slope of the linear Scatchard plots were 61 ± 12 pM for the wild-type protein, 158 ± 11 pM for FLP-4, 148 ± 14 pM for FLP-7, 138 ± 10 pM for FLP-9, 142 ± 15 pM for FLP-12, and 132 ± 9 pM for FLP-13 (Fig. 5*C*). Thus, the K_a values of the mutant PAP proteins were higher than the K_a of the wild-type protein. Therefore, the reduced binding capacity of the mutant PAP proteins to the stem loop RNA fragment appears to be caused at least in part by an impairment in the association phase of the rRNA binding to the mutated binding region.

In order to further assess the binding specificity, we also used a ^{32}P-labeled control oligo (5′-CGCGCUUUUGCGCG-3′) that does not contain the required substrate tetraloop motif, GAGA, for PAP binding. Filter binding assays with this control oligo did not exhibit significant binding to either the wild-type or mutant PAP proteins (Fig. 5*D*). These experiments further confirm that PAP proteins specifically bind to their RNA substrates via the target tetraloop. Taken together, the presented results of the saturation and competition binding assays confirmed the predictions of our modeling studies (16) and provided the first direct biochemical evidence that, besides the catalytic site residues of PAP, the residues of the active center cleft located between the central and C-terminal domains of PAP also contribute to its binding to the target α-sarcin/ricin stem loop of eukaryotic 28 S rRNA.

Because of the inherent uncertainties associated with using radiolabeled substrates in binding assays, we next sought to compare the affinity of recombinant PAP proteins for the non-radiolabeled stem loop RNA fragment by surface plasmon resonance. The active center cleft mutants FLP-4 and FLP-7 as

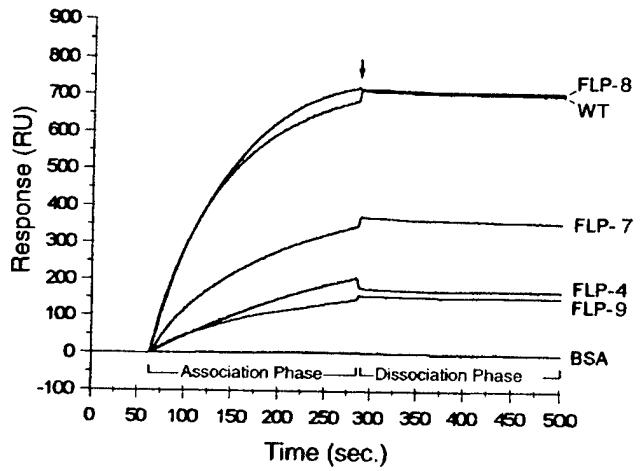

B

Mutants	k_{on} ($M^{-1}s^{-1}$)	k_{off} (s^{-1})	K_D (nM)
Wild-type	9.48×10^4	1.95×10^{-5}	0.2
FLP-4	5.65×10^4	5.73×10^{-5}	1.0
FLP-7	6.02×10^4	8.60×10^{-5}	1.4
FLP-8	9.95×10^4	1.74×10^{-5}	0.2
FLP-9	1.37×10^4	4.52×10^{-5}	3.3

k_{on} is the measurements from the association phase of Panel A

k_{off} is the measurements from the dissociation phase of Panel A

$K_D = k_{off}/k_{on}$

FIG. 6. **Binding of wild-type and mutant PAP proteins to a synthetic oligoribonucleotide (27-mer) that mimics the α-sarcin/ricin domain in 28 S rRNA.** *A*, a representative sensorgram showing the binding of wild-type (*WT*) and mutant PAP proteins to the 5′-biotin-labeled oligoribonucleotide immobilized, 70–100 response units (*RU*), on a SA sensor chip. 30 μl of each protein (150 nM) was injected at a flow rate of 8 μl/min. *B*, kinetic rates and dissociation constants of the binding interactions between recombinant PAP proteins and the 27-mer oligoribonucleotide.

well as the catalytic site mutant FLP-9 had much slower on-rates than the wild-type recombinant PAP protein (Fig. 6, *A* and *B*). All three mutant proteins also had faster off-rates, consistent with instability of their RNA binding (Fig. 6*B*). The affinities of FLP-4 (K_D = 1.0 nM), FLP-7 (K_D = 1.4 nM), and FLP-9 (K_D = 3.3 nM) were 5-, 7-, and 16-fold lower, respectively, than the affinity of the wild-type PAP (K_D = 0.2 nM) protein

THE JOURNAL OF BIOLOGICAL CHEMISTRY
Vol. 276, No. 26, Issue of June 29, pp. 24075–24081, 2001
Printed in U.S.A.

Binding Interactions between the Active Center Cleft of Recombinant Pokeweed Antiviral Protein and the α-Sarcin/Ricin Stem Loop of Ribosomal RNA*

Received for publication, December 18, 2000, and in revised form, April 17, 2001
Published, JBC Papers in Press, April 19, 2001, DOI 10.1074/jbc.M011406200

Francis Rajamohan‡§¶‖, Chen Mao, and Fatih M. Uckun‡¶‡‡**

*From the ‡Biotherapy Program, Parker Hughes Cancer Center, and the Departments of §Protein Engineering, **Structural Biology, and ¶Virology, Parker Hughes Institute, St. Paul, Minnesota 55113*

Pokeweed antiviral protein (PAP) is a ribosome-inactivating protein that catalytically cleaves a specific adenine base from the highly conserved α-sarcin/ricin loop of the large ribosomal RNA, thereby inhibiting protein synthesis at the elongation step. Recently, we discovered that alanine substitutions of the active center cleft residues significantly impair the depurinating and ribosome inhibitory activity of PAP. Here we employed site-directed mutagenesis combined with standard filter binding assays, equilibrium binding assays with Scatchard analyses, and surface plasmon resonance technology to elucidate the putative role of the PAP active center cleft in the binding of PAP to the α-sarcin/ricin stem loop of rRNA. Our findings presented herein provide experimental evidence that besides the catalytic site, the active center cleft also participates in the binding of PAP to the target tetraloop structure of rRNA. These results extend our recent modeling studies, which predicted that the residues of the active center cleft could, via electrostatic interactions, contribute to both the correct orientation and stable binding of the substrate RNA molecules in PAP active site pocket. The insights gained from this study also explain why and how the conserved charged and polar side chains located at the active center cleft of PAP and certain catalytic site residues, that do not directly participate in the catalytic deadenylation of ribosomal RNA, play a critical role in the catalytic removal of the adenine base from target rRNA substrates by affecting the binding interactions between PAP and rRNA.

Pokeweed antiviral protein (PAP)[1] is a 30-kDa ribosome-inactivating protein (RIP) isolated from the leaves of *Phytolacca americana* (pokeweed plant) (1, 2). PAP catalytically removes an adenine from the highly conserved, surface-exposed, α-sarcin/ricin loop in the large rRNA of prokaryotic and eukaryotic ribosomes (3–6). PAP-depurinated ribosomes cannot interact with elongation factors 1 and 2, leading to an irreversible inhibition of protein synthesis at the translocation step (5, 7–9). The therapeutic potential of PAP as a ribosome inhibitory anticancer agent has gained considerable interest in recent years due to the clinical use of native PAP as the active moiety of immunoconjugates against cancer (4).

The resolved three-dimensional x-ray structure of PAP revealed that the protein could be divided into three distinct domains: the N-terminal domain (residues 1–69, PAP numbering), the central domain (residues 70–179), and the C-terminal domain (residues 180–262) (10–13). The central domain accommodates all of the enzyme-active (catalytic) residues, Tyr^{72}, Tyr^{123}, Glu^{176}, and Arg^{179}, that are highly conserved among the RIPs. Based on structural and biochemical evaluation of several RIPs, it has been proposed that the amino acids Tyr^{72} and Tyr^{123} (PAP numbering) have the role of "sandwiching" the substrate adenine ring of rRNA in an energetically favorable stacking conformation, while Arg^{179} and Glu^{176} are directly engaged in the catalytic deadenylation of the α-sarcin/ricin loop (10, 14, 15). Alanine substitution by site-directed mutagenesis of the PAP active side residues Tyr^{72}, Tyr^{123}, Glu^{176}, and Arg^{179} that directly participate in the catalytic deadenylation of ribosomal RNA resulted in greater than 3 logs of loss in depurinating and ribosome inhibitory activity (16). Structural studies of PAP have also revealed a prominent cleft at the interface between the central and C-terminal domain that could accommodate substrate rRNA molecules (16). Our recent studies provided unprecedented and direct biochemical evidence that, besides the catalytic residues of PAP, the highly conserved, charged, and polar residues of the active center cleft of PAP are also critical for PAP-mediated depurination of rRNA (16). Alanine substitutions of these residues, especially $^{69}NN^{70}$ (191-fold loss of activity) and $^{90}FND^{92}$ (352-fold loss of activity), substantially impaired the catalytic removal of the adenine base from target rRNA substrates (16).

Our modeling studies aimed at understanding the molecular basis for the contribution of the active center cleft residues of PAP-mediated depurination of rRNA prompted the hypothesis that the residues of the active center cleft could, via electrostatic interactions, contribute to both the correct orientation and stable binding of the substrate RNA molecule in the active site pocket (16). The purpose of the present structure-function relationship study was to test this hypothesis by evaluating the ability of recombinant PAP molecules FLP-4 ($^{69}AA^{70}$) and FLP-7 ($^{90}AAA^{92}$) with mutated active center cleft residues to bind 23 S/16 S rRNA from *Escherichia coli* as well as a synthetic model oligoribonucleotide corresponding to the α-sarcin/ricin stem loop of 28 S rRNA from eukaryotic ribosomes. The binding affinities of the mutant PAP proteins for the synthetic oligoribonucleotide were calculated from rate constants and

* This work was supported in part by Defense Advanced Research Projects Agency Grant N65236-99-1-5422 (to F. M. U.). The costs of publication of this article were defrayed in part by the payment of page charges. This article must therefore be hereby marked "*advertisement*" in accordance with 18 U.S.C. Section 1734 solely to indicate this fact.

‖ To whom correspondence may be addressed: Parker Hughes Institute, 2657 Patton Rd., Roseville, MN 55113. Tel.: 651-628-9988; Fax: 651-697-1042; E-mail: frajamohan@ih.org.

‡‡ To whom correspondence may be addressed: Parker Hughes Institute, 2657 Patton Rd., Roseville, MN 55113. Tel.: 651-628-9988; Fax: 651-697-1042; E-mail: fatih_uckun@ih.org.

[1] The abbreviations used are: PAP, pokeweed antiviral protein; RIP, ribosome-inactivating protein; surface plasmon resonance; BSA, bovine serum albumin; HPLC, high pressure liquid chromatograph; oligo, oligonucleotide; SA, streptavidin.

analysis of binding using surface plasmon resonance (SPR) biosensor technology. Here, we present direct evidence that, compared with wild-type PAP, both FLP-4 and FLP-7 exhibit significantly impaired affinity for RNA substrates, providing a cogent explanation for their reduced depurinating activity. Similarly, FLP-9 (^{122}AA^{123}) with alanine substitutions expected to affect the orientation of the substrate adenine in the active site showed markedly reduced affinity for RNA targets. Catalytic site mutants FLP-12 (Ala^{179}) and FLP-13 (Ala^{208}), that were included as controls, also showed markedly reduced binding affinity for RNA substrates, consistent with the previously established importance of Arg^{179} and Trp^{208} residues in rRNA binding and depurination (10, 17, 18). By comparison, recombinant PAP mutants with alanine substitutions of residues ^{28}KD^{29} (FLP-1) and ^{111}SR^{112} (FLP-8) that are distant from the active site and active center cleft showed normal binding affinity to RNA substrates. The experimental findings presented herein are in accordance with the predictions of our recent modeling studies, which suggested that the active center cleft of PAP is important for binding to rRNA.

MATERIALS AND METHODS

Molecular Modeling—The molecular model of the PAP-ribosome (large subunit) complex was derived from the 2.4-Å crystal structure of the large ribosomal subunit from *Haloarcula marismortui* (Protein Data Bank access code 1FFK) (19) and the crystal structure of PAP-nucleotide complex (access code 1pag). This model represents a refinement of our recently published model of the PAP-rRNA stem loop complex (16). First, we superimposed the *H. marismortui* subunit ribosome structure with the stem loop structure in our previous PAP-RNA complex model. The conformation of rRNA was adjusted around the adenine A^{2697} (A^{2660} in *Escherichia coli*) of the GAGA tetraloop, and the rest of the PAP molecule remains unchanged. The adenosine was manually adjusted by a 38° degree out-flipping rotation at the C5′-position and a 5.4-Å translation of the adenine ring. The model was used to perform fixed docking using the *Docking* module in InsightII employing the CVFF (29). The parameters used in this docking included searching for five unique structures: 1000 minimization steps for each structure, energy range of 10.0 kcal/mol, maximum translation of the ligand of 3.0 Å, maximum rotation of the ligand of 10°, and an energy tolerance of 1500 kcal/mol. During the minimization steps of the docking procedure, only the tetraloop and the active site residue of PAP were allowed to be flexible, whereas the rest of rRNA and PAP remained fixed. The refined structure was then analyzed in CHAIN (20).

Construction of Mutants—Recombinant wild-type PAP construct (pBS-PAP) was obtained by subcloning the *PAP-I* gene encoding PAP amino acids 22–313 at the *Bam*HI and *Hin*dIII sites of the *E. coli* expression vector, pBluescript SK$^-$ (Stratagene, La Jolla, CA). PAP mutants were constructed using site-directed mutagenesis techniques as described previously (16). Unlike native PAP, which has 262 amino acids, recombinant PAP proteins have 292 amino acids. Therefore, they are larger than native PAP (33 *versus* 29 kDa) (16).

Expression and Purification of Mutants—Wild-type and mutant recombinant PAP proteins were expressed in *E. coli* MV1190 as inclusion bodies, isolated, solubilized, and refolded, as described previously (21). The refolded proteins were analyzed by SDS-12% polyacrylamide gel electrophoresis. Protein concentrations were determined from the gel using bovine serum albumin (BSA) as a standard.

Immunoblot Analysis of PAP Mutants—One μg of the protein samples was resolved on a SDS-12% polyacrylamide gel and transferred onto a polyvinylidene difluoride membrane (Roche Molecular Biochemicals) using the Bio-Rad transblot apparatus, as described previously (21). The membrane was immunoblotted using rabbit anti-PAP serum (1:2000 dilution) and horseradish peroxidase-conjugated goat anti-rabbit IgG (Sigma; 1:1000 dilution) as the primary and secondary antibodies, respectively. The blot was developed using 3,3′-diaminobenzidine (Sigma) as the colorimetric indicator for peroxidase activity.

Adenine Release Assays—The release of adenine from *E. coli* 23 S/16 S ribosomal RNA (Roche Molecular Biochemicals) was measured using HPLC (Hewlett Packard, Palo Alto, CA) equipped with a diode array detector, as described previously (16).

Preparation of Radiolabeled RNA Substrates—A 27-mer oligoribonucleotide (5′-CCUGCTCAGUACGAGAGGAACCGCAGG-3′), which contains the required substrate tetraloop motif, GAGA (α-sarcin/ricin loop), was synthesized on the 1-μmol scale and HPLC-purified by CyberSyn (Lenni, PA). The oligoribonucleotide (oligo) (5 μg) was labeled at the 5′-end using [γ-^{32}P]ATP and T4 polynucleotide kinase (Roche Molecular Biochemicals), and the unincorporated label was removed by Sephadex G-25 quick spin oligo columns (Roche Molecular Biochemicals) according to the manufacturer's instructions. As a control, we used a ^{32}P-labeled oligo (5′-CGCGCUUUUGCGCG-3′) that does not contain the substrate tetraloop motif GAGA. This radiolabeled control oligo was prepared using the procedures described above for the SR loop oligo.

The *E. coli* 23 S/16 S ribosomal RNA (50 μg) was alkaline-hydrolyzed by treating with 500 μl (final volume) of 100 mM $NaHCO_3$, pH 9.5, and incubated at 95 °C for 15 min. Following incubation on ice for an additional 10 min, the reaction was terminated by adding 50 μl of 7.5 M ammonium acetate, and the rRNA was recovered by extraction with phenol/chloroform (1:1) and precipitated with ethanol. The rRNA pellet was dissolved in the labeling reaction mixture containing 2.0 μl (100 mCi/ml) of [γ-^{32}P]ATP, 10 μl of 10× polynucleotide kinase buffer (0.1 M $MgCl_2$, 50 mM dithiothreitol, 50% glycerol, 0.5 M Tris, pH 9.5), 5 units of polynucleotide kinase, and the volume was adjusted to 40 μl with RNase-free water. After 30 min of incubation at 37 °C, the unincorporated label was removed by Sephadex G-50 quick spin RNA columns (Roche Molecular Biochemicals) per the supplier's instructions. The specific activities of the labeled oligoribonucleotide and rRNA were 0.73 and 0.9 μCi/μg, respectively. Typically, 45–55% of the [γ-^{32}P]ATP was incorporated into the labeled oligoribonucleotide.

Filter Binding Assays—For saturation binding assays, radiolabeled 23 S/16 S rRNA (3.5 pmol; specific activity 460 cpm/pmol), radiolabeled RNA SR loop oligo (75 pmol; specific activity 140 cpm/pmol), or radiolabeled control oligo (75 pmol; specific activity 172 cpm/pmol) were preincubated in separate tubes at 65 °C for 5 min in 50 μl of 350 mM KCl, 20 mM $MgCl_2$, 30 mM Tris-HCl, pH 7.5. Increasing amounts of recombinant wild-type or mutant PAP proteins were mixed with the preincubated radiolabeled probes, and the solution was adjusted to 150 μl with binding buffer (1 mM EDTA, 5% glycerol, 1 mM dithiothreitol, 3 mM $MgCl_2$, 0.01% BSA, and 10 mM HEPES, pH 8.0). The mixture was incubated for another 15 min at 30 °C and then placed on ice for 10 min. The reaction mixture was filtered through a nitrocellulose membrane (Millipore Corp.; type HA, 0.45-μM pore size, 25-mm diameter), and the membrane was washed three times with 1 ml of wash buffer (1 mM EDTA, 0.1% Tween 20, and 10 mM HEPES, pH 8.0) each time. The membrane was dried at room temperature and was counted for ^{32}P using a Beckman LS6000SC counter. The background binding determined by filtration in the absence of protein was subtracted from each assay. We also examined the nonspecific binding of radiolabeled 23 S/16 S rRNA and radiolabeled RNA SR loop oligo to BSA, which was included as a control protein.

Substrate specific binding of wild-type and mutant PAP proteins was determined by treating 25 pmol of protein samples with increasing concentrations of ^{32}P-labeled RNA SR loop oligo (specific activity 140 cpm/pmol) for 30 min at room temperature in a final volume of 150 μl with binding buffer. The reaction mixture was filtered through a nitrocellulose membrane, washed, and counted as described above. Scatchard plot (22) analysis of equilibrium binding data was performed as described previously (23). The association constant K_a was calculated from the slope of the line.

Competition binding was performed by incubating 33 pmol of wild-type PAP or BSA (control) proteins with 50 pmol of ^{32}P-labeled SR loop oligo and increasing concentrations (0–1500 pmol) of unlabeled SR loop oligo as competitor in 150 μl of binding buffer. The reaction mixture was incubated at room temperature for 1 h, and the unbound oligo was separated from the bound oligo by filtration and washing through a nitrocellulose membrane. The membrane was dried at room temperature, and the radioactivity in the membrane was measured as described before. Each experiment was repeated at least two times, and the average values were plotted using the CA-CRICKET Graph III application program.

SPR Analysis—A BIAcore 2000 SPR-based biosensor system (Amersham Pharmacia Biotech) was used to measure the kinetic parameters of the interaction between soluble mutant PAP proteins (analytes) and the immobilized RNA oligo (ligand). The oligo (27-mer) was synthesized, 5′-end-biotinylated, and HPLC-purified by CyberSyn (Lennin, PA). The 5′-end biotinylated oligo (40 μg/ml) was immobilized (streptavidin-biotin coupling) on the surface of the streptavidin (SA) sensor chips by injecting 30 μl of the oligo at a flow rate of 5 μl/min in HBS-EP buffer (0.1 M HEPES, pH 7.4, 0.15 M NaCl, 3 mM EDTA, and 0.005% polysorbate 20). Typically, the resonance unit value increase following this procedure was 70–100. The unoccupied SA surface was blocked by injecting 30 μl of 25 μg/ml biotin in HBS-EP buffer as above. All of the

(Fig. 6*B*). By comparison, the affinity of the recombinant PAP mutant FLP-8 with alanine substitution of residues ^{111}SR^{112} that are distant from the catalytic site and active center cleft for the stem loop RNA fragment was identical to that of the wild-type PAP (Fig. 6*B*).

In summary, we employed site-directed mutagenesis combined with standard filter binding assays, equilibrium binding assays with Scatchard analyses, and surface plasmon resonance technology to elucidate the putative role of the PAP active center cleft in the binding of PAP to the α-sarcin/ricin stem loop of rRNA. Our findings provide experimental evidence that besides the catalytic site the active center cleft also participates in the binding of PAP to the target tetraloop structure of rRNA. These results extend our recent modeling studies (16), which predicted that the residues of the active center cleft could, via electrostatic interactions, contribute to both the correct orientation and stable binding of the substrate RNA molecules in the PAP active site pocket. The insights gained from this study also explain why and how the conserved charged and polar side chains located at the active center cleft of PAP and certain catalytic site residues that do not directly participate in the catalytic deadenylation of ribosomal RNA play a critical role in the catalytic removal of the adenine base from target rRNA substrates by affecting the binding interactions between PAP and rRNA.

Control mutant proteins FLP-1 and FLP-8 exhibited similar rRNA binding as wild-type PAP protein. Furthermore, the expression, solubility, and yield of refolded wild-type and mutant proteins were comparable (see Fig. 2). Nevertheless, the presented findings should be interpreted with due caution because of the inherent shortcomings of the mutagenesis techniques, which may yield mutant proteins with a nonnative conformation, especially when the mutant proteins are insoluble and need to be renatured.

Acknowledgments—We thank Tammy J. Denton, Dawn M. Dahlke, Michelle L. Henning, Rebecca S. Larue, Dina Clementson, and Brad Nodland for technical assistance.

REFERENCES

1. Irvin, J. D. (1975) *Arch. Biochem. Biophys.* **169,** 522–528
2. Irvin, J. D., Kelly, T., and Robertus, J. D. (1980) *Arch. Biochem. Biophys.* **200,** 418–425
3. Hartley, M. R., Legname, G., Osborn, R., Chen, Z., and Lord, J. M. (1991) *FEBS Lett.* **290,** 65–68
4. Irvin, J. D., and Uckun, F. M. (1992) *Pharmacol. Ther.* **55,** 279–302
5. Dallal, J. A., and Irvin, J. D. (1978) *FEBS Lett.* **89,** 257–259
6. Endo, Y., and Tsurugi, K. (1988) *J. Biol. Chem.* **263,** 8735–8739
7. Obrig, T. G., Irvin, J. D., and Hardesty, B. (1973) *Arch. Biochem. Biophys.* **155,** 278–289
8. Gessner, S. L., and Irvin, J. D. (1980) *J. Biol. Chem.* **255,** 3251–3253
9. Montanaro, L., Sperti, S., Mattioli, A., Testoni, G., and Stirpe, F. (1975) *Biochem. J.* **146,** 127–131
10. Monzingo, A. F., Collins, E. J., Ernst, S. R., Irvin, J. D., and Robertus, J. D. (1993) *J. Mol. Biol.* **233,** 705–715
11. Kurinov, I. V., Myers, D. E., Irvin, J. D., and Uckun, F. M. (1999) *Protein Sci.* **8,** 1765–1772
12. Ago, H., Kataoka, J., Tsuge, H., Habuka, N., Inagaki, E., Noma, M., and Miyano, M. (1994) *Eur. J. Biochem.* **225,** 369–374
13. Bravi, G., Legname, G., and Chan, A. W. (1995) *J. Mol. Graph.* **13,** 83–88
14. Montfort, W., Villafranca, J. E., Monzingo, A. F., Ernst, S. R., Katzin, B., Rutenber, E., Xuong, N. H., Hamlin, R., and Robertus, J. D. (1987) *J. Biol. Chem.* **262,** 5398–5403
15. Kurinov, I. V., Rajamohan, F., Venkatachalam, T. K., and Uckun, F. M. (1999) *Protein Sci.* **8,** 2399–2405
16. Rajamohan, F., Pugmire, M. J., Kurinov, I. V., and Uckun, F. M. (2000) *J. Biol. Chem.* **275,** 3382–3390
17. Frankel, A., Welsh, P., Richardson, J., and Robertus, J. D. (1990) *Mol. Cell. Biol.* **10,** 6257–6263
18. Gu, Y-J., and Xia, Z-X. (2000) *Proteins* **39,** 37–46
19. Ban, N., Nissen, P., Hansen, J., Moore, P. B., Steitz, T. A. (2000) *Science* **289,** 905–920
20. Sack, J. S. (1988) *J. Mol. Graphics* **6,** 244–249
21. Rajamohan, F., Engstrom, C. R., Denton, T. J., Engen, L. A., Kourinov, I., Uckun, F. M. (1999) *Protein Expression Purif.* **16,** 359–368
22. Scatchard, G. (1949) *Ann. N. Y. Acad. Sci.* **51,** 660–672
23. Uckun, F. M., Gessner, T. G., Song, C. W., Myers, D. E., and Mufson, A. (1989) *Blood* **73,** 533–542
24. Munishkin, A., and Wool, I. G. (1997) *Proc. Natl. Acad. Sci. U. S. A.* **94,** 12280–12284
25. Ryan, P. C., and Draper, D. E. (1991) *Proc. Natl. Acad. Sci. U. S. A.* **88,** 6308–6312
26. Uchiumi, T., Wada, A., and Kominami, R. (1995) *J. Biol. Chem.* **270,** 29889–29893
27. Kraulis, P. J. (1991) *J. Appl. Crystallogr.* **24,** 946–950
28. Merritt, E. A., and Murphy, M. E. P. (1994) *Acta Crystallogr. Sec. D* **50,** 869–873
29. MSI (1991) *InsightII User Guide*, MSI, San Diego, CA

Protein Expression and Purification 18, 193–201 (2000)
doi:10.1006/prep.1999.1181, available online at http://www.idealibrary.com on IDEAL®

Expression of Biologically Active Recombinant Pokeweed Antiviral Protein in Methylotrophic Yeast *Pichia pastoris*

Francis Rajamohan,*,†,[1] Sekou O. Doumbia,† Cherri R. Engstrom,† Sharon L. Pendergras,‡ Daniell L. Maher,‡ and Fatih M. Uckun*,‡

Biotherapy Program, †Department of Protein Engineering, and ‡Department of Virology, Hughes Institute, Roseville, Minnesota 55113

Received September 24, 1999, and in revised form November 17, 1999

Pokeweed antiviral protein (PAP)-I from the spring leaves of *Phytolacca americana* is a naturally occurring RNA-depurinating enzyme with broad-spectrum antiviral activity. Interest in PAP is growing due to its use as a potential anti-HIV agent. However, the clinical use of native PAP is limited due to inherent difficulties in obtaining sufficient quantities of homogeneously pure active PAP without batch-to-batch variation from its natural resource. Here, we report the expression of mature PAP (residues 23 to 284) with a C-terminal hexahistidine tag in the methylotrophic yeast *Pichia pastoris*, as a secreted soluble protein. The final yield of the secreted PAP is greater than 10 mg/L culture in shaker flasks. The secreted recombinant protein is not toxic to the yeast cells and has an apparent molecular mass of 33-kDa on SDS–PAGE gels. The *in vitro* enzymatic activity and cellular anti-HIV activity of recombinant PAP were of the same magnitude as those of the native PAP purified from *P. americana*. To our knowledge, this is the first large-scale expression and purification of soluble and biologically active recombinant mature PAP from yeast. © 2000 Academic Press

Key Words: **pokeweed antiviral protein; ribosome depurination; anti-HIV; protein synthesis inhibition.**

Pokeweed antiviral protein (PAP)-I[2] is a 29-kDa naturally occurring RNA-depurinating enzyme isolated from the early spring leaves of the pokeweed plant, *Phytolacca americana* (1). PAP cleaves the N-glycosidic bond of a single adenine base from a highly conserved stem-loop (α-sarcin) sequence of the large ribosomal RNA (rRNA) species in prokaryotic (23S rRNA) and eukaryotic (28S rRNA) ribosomes (2,3). This catalytic depurination impairs the interaction of ribosomes with elongation factor 2–GTP complex, resulting in irreversible inhibition of protein synthesis at the translocation step (4–6). Hudak *et al.* (7) have shown that PAP binds to the yeast large ribosomal protein L3, suggesting that this ribosomal protein may provide a receptor site for PAP to depurinate the target adenine in its rRNA substrate. Recently, PAP has been shown to efficiently depurinate adenine-containing polynucleotides (8), single-stranded DNA (9), double-stranded DNA (10), and viral RNA (11), suggesting that the depurinating activity of PAP is not restricted to the α-sarcin loop of rRNA.

The full-length PAP gene codes for 313 amino acids (12). However, during posttranslational modification, 22 amino acids (signal peptide) from the N-terminus and 29 amino acids from the C-terminus are cleaved leaving a mature PAP of 262 amino acids with an apparent molecular mass of 29 kDa (13). The ability of PAP to irreversibly inhibit protein synthesis has gained considerable interest due to its therapeutic implications. PAP has been targeted to cancer cells using monoclonal antibodies (14,15). PAP-containing immunoconjugates against CD7 and CD19 surface antigens on leukemia cells have shown potent and selective antileukemic activity both *in vitro* and *in vivo* (15–17).

PAP has also been shown to effectively inhibit the replication of several plant and mammalian viruses, including cytomegalovirus (18), poliovirus (19), influenza virus (20), herpes simplex virus (21), and HIV (22). The molecular mechanism of the antiviral activity of PAP is under active investigation. We have previously reported that PAP inhibits HIV-1 replication in both T-cells and macrophages at concentrations that do

[1] To whom correspondence should be addressed at Hughes Institute, 2657 Patton Road, Roseville, MN 55113. Fax: (651) 628-9891. E-mail: frajamohan@ih.org.

[2] Abbreviations used: PAP, pokeweed antiviral protein; rRNA, ribosomal RNA; rPAP, recombinant PAP; HSA, human serum albumin; PVDF, polyvinylidene difluoride; PBMC, peripheral blood mononuclear cells.

1046-5928/00 $35.00

not inhibit the cellular protein synthesis (22). Notably, PAP immunoconjugates showed marked anti-HIV activity in an *in vivo* SCID mouse model of human AIDS at dose levels well tolerated by cynomolgus monkeys (23). A Phase I clinical study has been initiated to evaluate the anti-HIV efficacy and safety of our anti-CD7–PAP immunoconjugate in AIDS patients (24).

The therapeutic application of PAP both as an anticancer and as an antiviral agent would greatly benefit from a large-scale production of PAP by the methods of recombinant DNA technology. Expression of recombinant PAP in *Escherichia coli* (25) as well as *Saccharomyces cerevisiae* (26) resulted in low yield because of its toxicity to the host system. We therefore explored other expression systems for generating large quantities of PAP without killing the host system.

Several eukaryotic proteins with clinical and therapeutic values, such as angiostatin (27), endostatin (28), insulin (29), growth factors (30), single-chain antibody fragments (31,32), and human serum albumin (33), have been expressed in the methylotrophic yeast *Pichia pastoris*. *P. pastoris* combines the general feature of eukaryotic protein expression machinery with fast growth (34) and the requirement for inexpensive, noncomplex, and chemically defined growth media of bacteria. *P. pastoris* has been shown to be suitable for high-level expression of various heterologous proteins either intracellulary or in secreted form. Although *P. pastoris* secretes very low levels of endogenous proteins, it has the capacity to secrete grams per liter of foreign proteins (34). In addition, protein expression level in *P. pastoris* can be scaled up by 100-fold when the cells are grown in a fermentor (35,36). Expression of recombinant proteins in *P. pastoris* is based on the use of the alcohol oxidase gene, *AOX1* (34,37).

The purpose of the present study was to examine the ability of *P. pastoris* as an alternative expression system for recombinant PAP. Here, we report the expression of mature PAP (residues 23 to 284) in the *P. pastoris* expression system. The recombinant PAP (rPAP) was expressed and secreted as a soluble protein into the medium. The average yield of the secreted protein in the culture supernatant was 10–12mg/L. The *P. pastoris*-derived recombinant PAP was as active as native PAP isolated from the leaves of the pokeweed plant, *P. americana*, in protein synthesis inhibition assays as well as cellular HIV-1 replication inhibition assays.

MATERIALS AND METHODS

Yeast and Bacterial Strains

P. pastoris GS115 (*his4*) and SMD1168H (*pep4*) strains were used for yeast expression (Invitrogen, San Diego, CA). The bacterial strains used for DNA manipulation were *E. coli* DH5αF′ and INV$_{\alpha}$ F′(Invitrogen).

Reagents

Restriction enzymes were purchased from New England Biolabs, Inc. (Beverly, MA). Chemical reagents and goat anti-rabbit IgG and goat anti-mouse IgG (both conjugated to horseradish peroxidase) antibodies were obtained from Sigma Chemical Company (St. Louis, MO). Anti-*myc* antibody was obtained from Invitrogen and Ni^{2+}–NTA–AP conjugates were obtained from Qiagen (Santa Clarita, CA). The cell-free *in vitro* translation assay kit was purchased from Promega Company (Madison, WI). BCA protein assay reagents were from Pierce Inc. (Rockford, IL).

Media and Growth Conditions

P. pastoris strains were cultured on YPD complete medium (2% peptone, 1% yeast extract, 2% glucose). The His^+, $Mut^{+/-}$ transformants were selected in minimal media containing 1.34% yeast nitrogen base with ammonium, 0.04% biotin, and either 2% dextrose (MD) or 0.5% methanol (MM) as the carbon source. For semi-solid cultures, 15 g/L agar was added to the above media. All yeast cultures were maintained at 30°C. For protein production, selected (His^- Mut^-) transformed strains were cultured to an OD_{600} = 2–6 in BMGY medium (2% peptone, 1% yeast extract, 0.04% biotin, 13.4% yeast nitrogen base with ammonium sulfate, 0.1 M potassium phosphate, pH 6.0, and 1% glycerol). Cells were then collected by centrifugation (10,000 rpm for 10 min) and resuspended to an OD_{600} = 10–15 in BMMY (2% peptone, 1% yeast extract, 0.04% biotin, 13.4% yeast nitrogen base with ammonium sulfate, 0.1 M potassium phosphate, pH 6.0, and 0.5% methanol) medium. All bacterial clones were grown in low-salt LB medium (10 g tryptone, 5 g sodium chloride, and 5 g yeast extract/L).

Construction of Mature PAP Expression Vector

The mature PAP (residues 23 to 284) was amplified by PCR on a plasmid DNA template containing the complete sequence of PAP (PTF-200). The oligonucleotide PAP-C1(5′-GATGC**ATCGAT**GGTGAATACAAT-CATCTAC-3′) was designed to remove the signal sequence as well as to generate a *Cla*I restriction site. A second oligonucleotide, PAP-X1 (5′-CCCC**TCTA-GA**AGCAGTTGTCTGACAGCT-3′), was designed to generate a *Xba*I restriction site at the 3′ end of the mature PAP (residue 284). Both oligonucleotides were purchased from Biosynthesis Inc. (Lewisville, TX) and dissolved in nuclease-free water. The PCR reaction mixture consisted of 20 pmol of primers, 20 nmol of dNTPs (New England Biolabs), 2 ng of template DNA (PTF-200), PCR buffer (final composition is 10 mM Tris, pH 8.3, 15 mM KCl, 1.5 mM $MgCl_2$, 0.1% Triton X-100), 0.5 U of AmpliTaq (Perkin–Elmer), and dH_2O

to 100 μl. PCR amplification was carried out with a thermocycler (Ericomp Inc., San Diego, CA) using the following protocol: hot start at 94°C for 2 min; 30 cycles at 94°C for 1 min, 55°C for 1 min 30 sec, 72°C for 2 min; final extension at 72°C for 10 min; and ramping down to 4°C. The expected 800-bp PCR product was subsequently cloned into a pCR 2.1 vector (Invitrogen) and transformed into INVαF′ following the manufacturer's instructions (Invitrogen). Positive clones were analyzed by automated DNA sequencing and a mutation-free mature *PAP* gene was force-cloned (*Cla*I and *Xba*I sites) in frame with the α-mating factor (Mfα1) secretion sequence of the yeast shuttle expression vector, pPICZαC (Invitrogen). The Mfα1 secretion signal of the vector (pPICZαC) comprises 89 amino acids, with the Kex2 protease signal cleavage occurring between the 85th and 86th amino acid residues and the STE13 (a dipeptidyl aminopeptidase) cleavage occurring between the 87th and 88th residues. The vector pPICZαC also encodes the Zeocin (a water soluble copper-chelated glycopeptide isolated from *Streptomyces verticillus*) resistance gene *Sh ble* (from *Streptoalloteichus hindustanus bleomycin*) for antibiotic selection. The mature PAP was inserted in frame with the α-factor at the N-terminus and with the *myc*-epitope and the hexahistidine (His_6) gene at the C-terminus. Ten micrograms of the pPICZαC–rPAP construct (PSF-262) was linearized by digestion with the restriction enzyme *Pme*I, which cuts once in the 5′*AOX*1 region of the plasmid, and then purified.

Transformation of PAP into P. pastoris Genome

The novel yeast *P. pastoris* strain SMD1168H (His^+) was used instead of its parent SMD 1168 *(pep4 his4)* for expression, since endogenous production of histidine is preferred due to the rapid growth and high metabolic rate of *P. pastoris*. The yeast cells were transformed by electroporation with 10 μg of linearized pPICZαC–rPAP DNA, on a Bio-Rad gene-pulser apparatus (1.5 KV, 25 μF, 200 Ω) for 5 ms. Transformants were first selected by plating on YPD plates containing 100 μg/ml of Zeocin and then screened for insertion of the construct at the alcohol oxidase promoter (*AOX1*) site by PCR using 5′AOX1 and 3′AOX1 primers (Invitrogen). For phenotype determination, clones were replica-plated on both MD and MM plates using GS115/human serum albumin (HSA) as a Mut^- control and GS115/β-galactosidase as a Mut^- control. Zeocin selection was used during the expression of PAP in yeast cells due to the high percentage of revertants with the histidine selection. The morphology of the clones on the plates was compared to that of the positive control (His^- Mut^-/HSA) and the negative control (His^- Mut^-). One-hundred percent of the transformants tested were able to utilize methanol as carbon source, attesting to their Mut phenotype as expected. Since mature PAP constructs were linearized within its 5′AOX1 region and the yeast cells (SMD 1168H) have a native AOX1 gene, the generated transformants were able to efficiently metabolize methanol and grow at the rate of wild-type cells.

Expression and Purification of Mature PAP

Nine PCR-positive clones (Mut^-) were initially grown in 10 ml YPD medium at 30°C in a shaking (250 rpm) incubator to an OD_{600} of 2–6. Cells were then centrifuged, resuspended in buffered-methanol complex medium (BMMY) to an OD_{600} = 10–15, and continuously incubated for 3 days. In this expression system, methanol induces expression of the tightly regulated *AOX*1 gene which in turn drives the expression and secretion of mature PAP. Aliquots of the supernatant (1 ml) were taken daily and examined by SDS–12% PAGE for expression of rPAP. The yeast transformant with the highest rPAP expression was selected for large-scale expression. For large-scale expression, the clone was grown in 1 L of YPD medium in baffle flasks to an OD_{600} = 2–6. Subsequently cells were separated by centrifugation and resuspended in buffered methanol induction medium to an OD_{600} = 10–15 and incubation was continued. After 3 days, the cells were harvested by centrifugation (8000 rpm for 10 min).

The supernatant was concentrated 10-fold using an Amicon stirred cells concentrator and a 10,000 NMWL ultrafiltration membrane at 4°C. The concentrated culture medium was dialyzed overnight at 4°C against 50 mM sodium phosphate, 150 mM NaCl, pH 7.0, using a dialysis membrane with a molecular weight cutoff of 10,000. The sample was then centrifuged at 15,000 rpm for 15 min to sediment any particulate matter and filtered through a 0.2-μm filter prior to purification. One milliliter of the filtered sample was loaded into a HiTrap (5 ml) chelating FPLC column (Pharmacia) that had been charged with 0.1 M $NiSO_4$ and washed with buffer A (5 mM sodium phosphate, 50 mM NaCl, pH 7.0, 5% glycerol). The bound rPAP was eluted with buffer B (5 mM sodium phosphate, 50 mM NaCl, pH7.0, 5% glycerol, and 250 mM imidazole) using the following gradient: 0–10 min, 100% A; and 10–25 min linearly increased to 100% B and maintained at that level for 5 min at a flow rate of 1.5 ml/min. The peak fractions containing rPAP were pooled and dialyzed to remove the imidazole, as described above. Purified rPAP was analyzed by SDS–12% PAGE and assayed for biological activity. The total protein concentration was measured using the BCA (Pierce) method and BSA as a standard.

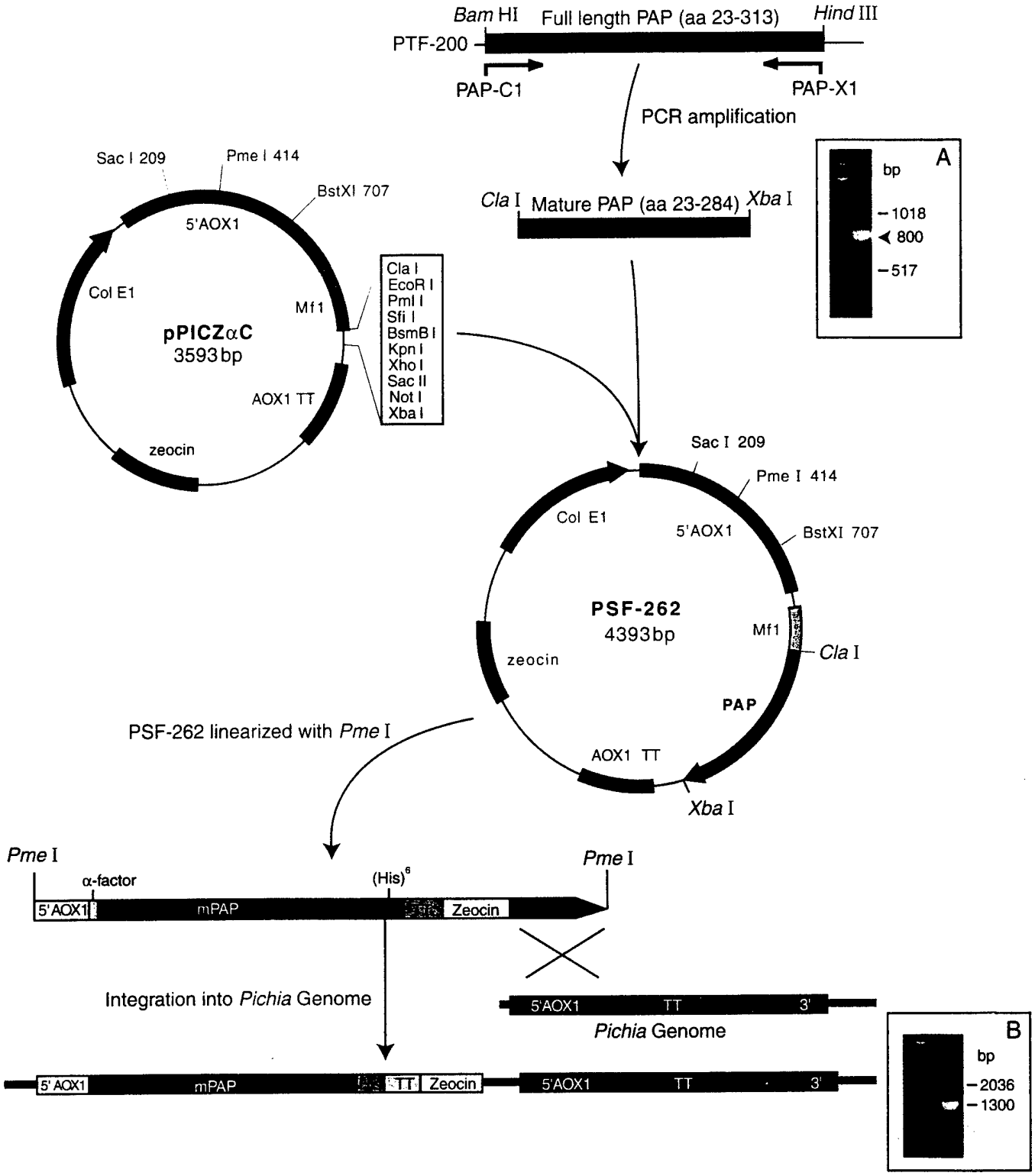

FIG. 1. Overview of the pPICZαC–PAP construction (PSF-232) and integration into *Pichia* genome. Expression is driven by the *AOX1* promoter induced by methanol. The Mfα1 directs secretion of the protein into the extracellular medium. *AOX1*TT, transcription termination, Mfα1, α-factor. (Inset A) PCR-amplified mature rPAP cDNA. Lane 1, marker (1-kb ladder); lane 2, PCR product. (Inset B) PCR analysis of recombinant *Pichia* genome for integration of PAP gene. Amplification of the PAP gene was carried out using 5′*AOX1* and 3′*AOX1* primer pairs (Invitrogen). A 10-μl sample from PCR was run on a 0.7% agarose gel. Lane 1, marker (1-kb ladder); lane 2, *Pichia* recombinant.

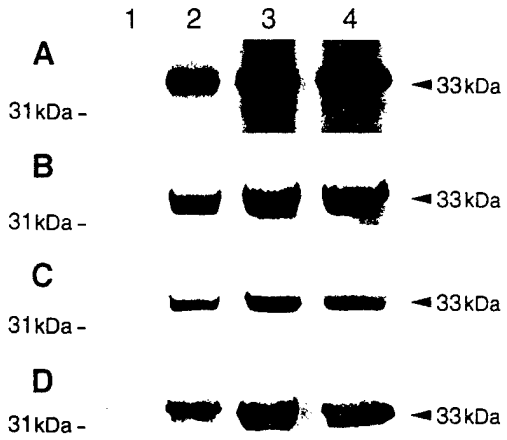

FIG. 2. (A) Coomassie blue-stained SDS–12% PAGE gel comparing the expression of three recombinant PAP clones of *P. pastoris* secreted into the medium. (B) Western blot analysis using anti-PAP serum. (C) Western blot analysis using anti-*myc* antibody. (D) Blotting of rPAP with Ni–NTA conjugated to alkaline phosphatase. Lane 1, uninduced culture medium; lane 2, induced culture medium of clone 1; lane 3, induced culture medium of clone 2; lane 4, induced culture medium of clone 3. Each lane contains 30 μl of the culture supernatant.

Immunoblot Analysis of PAP Protein

The protein samples were resolved on a SDS–12% PAGE gel and transferred onto a polyvinylidene difluoride (PVDF) membrane using the Bio-Rad trans-blot apparatus, as described (38). The PVDF membrane was blotted using rabbit anti-PAP serum, mouse anti-*myc* antibody, or anti-His antibody as primary antibodies and horseradish peroxidase-conjugated goat anti-rabbit IgG, horseradish peroxidase-conjugated goat anti-mouse IgG, or alkaline phosphatase-conjugated Ni–NTA as the corresponding secondary antibodies/reagent, respectively. The bound antibody was detected using the enhanced chemiluminescence detection kit (Amersham, Arlington Heights, IL) or a colorimetric indicator (3,3′-diaminobenzidine tablets, Sigma).

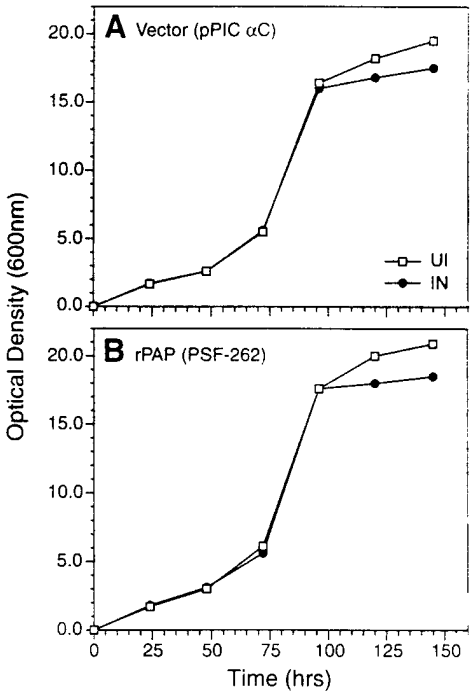

FIG. 3. Effect of mature PAP expression on the growth of yeast *P. pastoris*. UI, uninduced; IN, culture induced with methanol, as described under Materials and Methods.

TABLE 1

Purification and Yield of Recombinant Mature PAP from Yeast Medium

Steps	Total protein[a] (mg/L)	Percentage of total protein
Culture broth	205	100
After buffer exchange[b]	190	93
After concentration	175	85
FPLC fractions pool[c]	10	5

[a] Total protein measured using the Bradford assay with bovine serum albumin as the standard.

[b] Buffer exchange was performed by dialysis using 10K cutoff membrane (Pierce).

[c] FPLC column purification of rPAP was performed using $NiSO_4$ saturated HiTrap chelating column (Pharmacia), as described under Materials and Methods. The yield of FPLC fractions corresponds to the yield of rPAP.

Cell-Free Translation Assays

The inhibitory activity of rPAP on *in vitro* translation was examined as described previously (38). In brief, increasing concentrations of the FPLC-purified rPAP (0.01 to 5 ng/ml) were added to the translation mixture containing 10 μl of rabbit reticulocyte lysate (Promega), 0.5 μl of RNasin, 1.0 μl of 1 mM amino acids mixture (minus methionine), and 1.0 μl of [^{35}S]methionine (10 mCi/ml, Amersham). The final volume was adjusted to 19 μl with RNase free water. The reaction mixture was incubated for 15 min at room temperature. Protein translation was initiated by adding 100 ng (1 μl volume) of luciferase mRNA. After 2 h of incubation at 30°C, 10 μl of each reaction mixture was resolved by SDS–12% PAGE, dried, and autoradiographed. Alternatively, the incorporation of radioactive label into protein was determined by precipitating the synthesized luciferase protein (61-kDa) with 5% trichloroacetic acid according to the manufacturer's instructions (Promega). A minimum of 10 concentrations of rPAP was used for the calculation of the IC_{50} (50% inhibitory concentration) values. The average IC_{50} values (from precipitation assays) were calculated

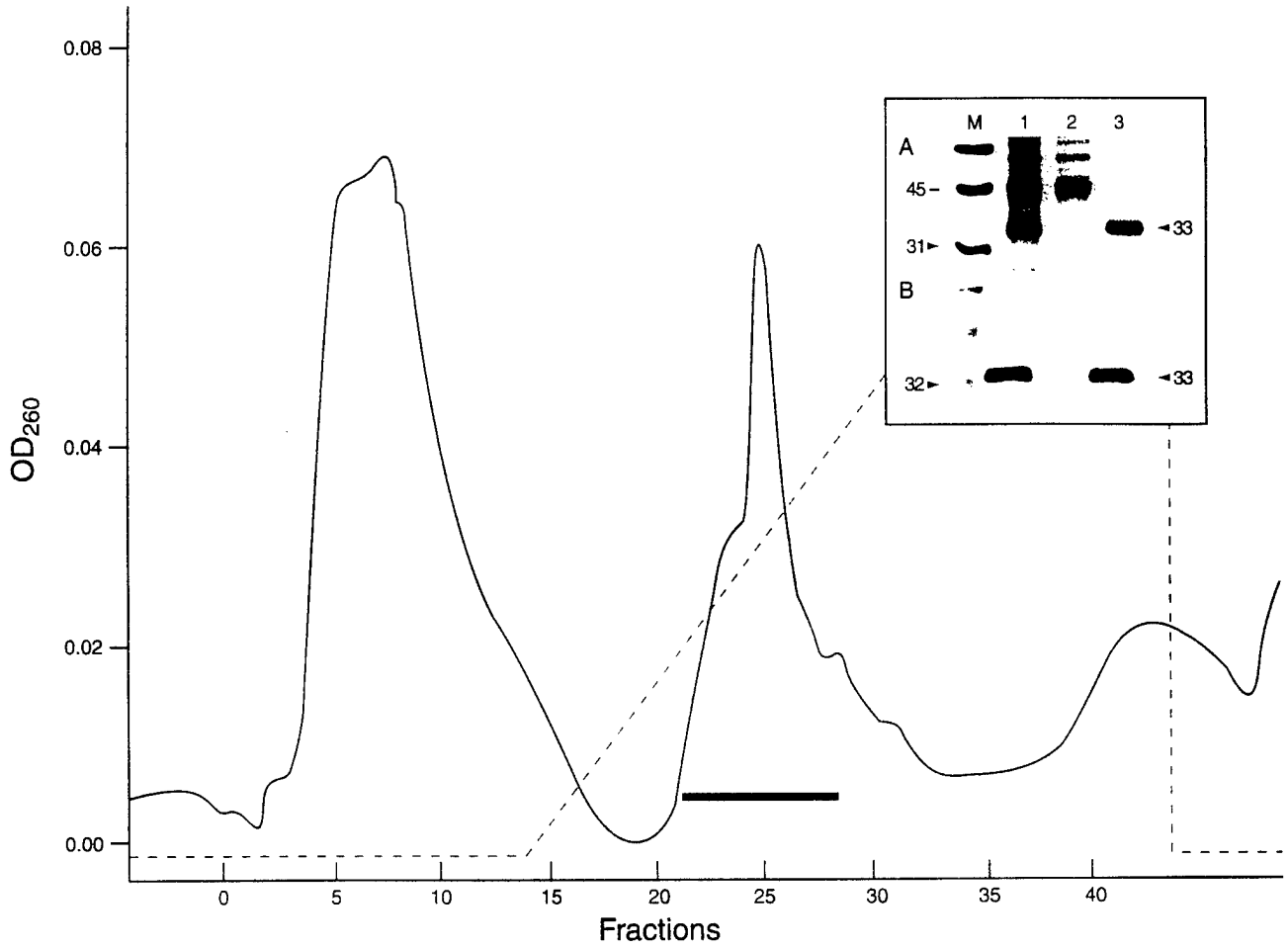

FIG. 4. One-step purification of rPAP using Ni–HiTrap-chelating FPLC column which was equilibrated with 5 mM sodium phosphate, 50 mM NaCl, pH 7.0, and 5% glycerol. rPAP was eluted with a linear gradient of buffer B (5 mM sodium phosphate, 50 mM NaCl, pH 7.0, 5% glycerol, 250 mM imidazole) at a flow rate of 1.5 ml/min (dotted line). The fractions containing the rPAP, as indicated by the black bar, were pooled, dialyzed and concentrated. (Inset A) Coomassie blue-stained SDS–12% PAGE of purified rPAP. Lane M, molecular mass marker positions; lane 1, culture supernatant; lane 2, flowthrough (fractions 5–15); lane 3, rPAP (fractions 23–28). (Inset B) Western blot analysis using anti-PAP serum.

by nonlinear regression analysis (Prism-2 GraphPad software, Santiago, CA) as the mean value from three independent experiments. The cpm values in control samples (all of the reagents added except for PAP) ranged from 3.7 to 4.5 $\times$ 10^7 cpm/ml and were used as 100% incorporation when determining the percentage of control protein synthesis values for PAP-treated samples.

In Vitro Assays of Anti-HIV-1 Activity

The anti-HIV-1 activity of rPAP was evaluated by determining its ability to inhibit the replication of the HIV-1 strain HTLV-IIIB in normal human peripheral blood mononuclear cells (PBMCs) from HIV-negative donors, as previously described (38). Percentage of viral inhibition was determined by comparing the HIV-1 p24 antigen production by the rPAP-treated infected cells with the p24 antigen production by untreated infected cells (i.e., virus controls). The IC_{50} values were calculated by nonlinear regression analysis (Prism-2 program) using the data from three independent experiments.

RESULTS AND DISCUSSION

We have cloned the *PAP* gene (Fig. 1, inset A) encoding amino acid residues 23 to 284 (mature PAP) into the yeast vector pPICZαC by fusing it to the prepro region of the α-factor mating secretion signal (Mfα1) derived from *S. cerevisiae* for expression in *P. pastoris* (Fig. 1). The Mfα1 prepro of the pPICZαC vector encodes an 89-amino-acid protein and is under the control of the *P. pastoris* alcohol oxidase promoter *AOX1*. The recombinant plasmid was linearized at *Pme*I site and transformed into *P. pastoris* for gene integration at

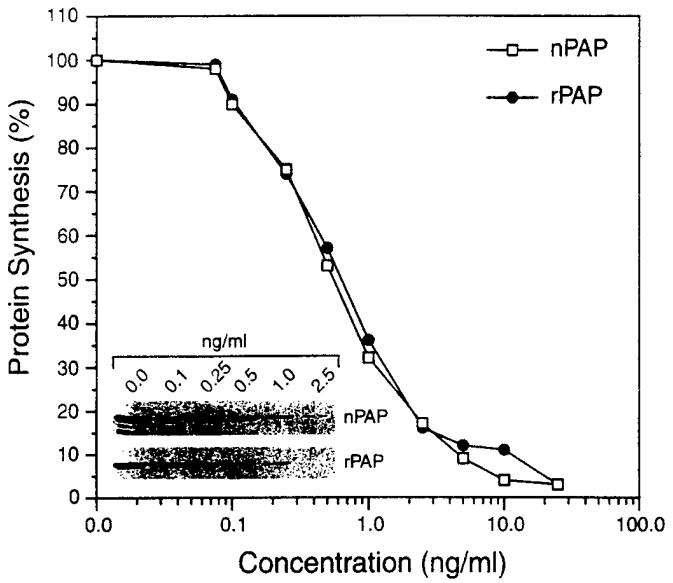

FIG. 5. Ribosome inhibitory activity of recombinant and native PAP in *in vitro* rabbit reticulocyte lysate system. Each value represents an average from three independent experiments. Protein synthesis was measured by [^{35}S]methionine incorporation and the amount of incorporation by the control samples containing all of the reagents except for PAP was assigned a value of 100%. (Inset) luciferase protein synthesized in the presence or absence of native (nPAP) and recombinant PAP (rPAP). Samples were resolved on SDS–10% PAGE and autoradiographed. Numbers at the top indicate the concentration of PAP.

AOX1 locus (Fig. 1). PCR analysis of the transformants confirmed the integration of the *PAP* gene into the *P. pastoris* genome (Fig. 1, inset B). Processing of the prepro–α-factor in this vector by proteolytic enzymes is expected to remove all but the last two amino acids of the prepro–α-factor. The C-terminus of PAP, however, is fused to a polyhistidine $(His)_6$-tag, which permits detection and single-step purification of the secreted PAP fusion protein by metal-affinity chromatography on a Ni^{2+}–HiTrap column (Pharmacia).

Nine (His^+, Mut^+) transformants were analyzed for their ability to secrete the recombinant PAP into the medium. Though all the transformants have expressed and secreted the rPAP into the culture medium, three transformants with highest expression levels were chosen for further assays. All three clones secreted a major soluble protein with an estimated molecular mass of 33 kDa (Fig. 2A), which was highly immunoreactive with the rabbit anti-PAP serum (Fig. 2B). The presence of the $(His)_6$-tag and *myc*-tag at the C-terminus of mature PAP was confirmed by blotting with a Ni^{2+}–NTA alkaline phosphatase conjugate (Fig. 2D) or an anti-*myc* antibody (Fig. 2C).

Since PAP inactivates both prokaryotic and eukaryotic ribosomes, we first examined the inhibitory effects of PAP on growth of *P. pastoris*. Cultures were initiated from plates and the yeast cell growth, with and without the presence of methanol (inducer) in the medium, was monitored by measuring A_{600}. As shown in Fig. 3, the expression of rPAP did not affect the growth of *P. pastoris* and the cells expressing either the PAP gene or the vector alone grew similarly in the liquid medium (Fig. 3). This lack of toxicity suggests that the rapid secretion of the mature rPAP into the culture medium likely prevents it from interacting with the yeast ribosomes. Secretion of a 33-kDa protein by yeast cells also shows that the α-mating factor signal sequence was processed efficiently by the dibasic specific protease Kex2p, since unprocessed proteins would have been 10 kDa larger.

In cultures of the *P. pastoris* transformants, rPAP production was detected in the medium 1 day after induction with methanol. The concentration of secreted rPAP continued to increase during the following 2 days of induction and resulted in the accumulation of 10 ± 2 mg (n = 3) of mature rPAP in each liter of culture medium by the third day (Table 1). The uninduced cultures did not express detectable levels of rPAP. The secreted rPAP was very stable under the described culture conditions, and no signs of degradation could be detected either by SDS–PAGE or Western blot analysis (Fig. 2). The soluble mature rPAP protein was purified from the culture broth by FPLC using Ni^{2+}–HiTrap metal-affinity column as described under Materials and Methods. Using this method we were able to purify 10 ± 2 mg/L of rPAP, which corresponds to approximately 5% of the total protein in the culture broth. The fractions containing rPAP were pooled, concentrated, and analyzed by SDS–12% PAGE (Fig. 4). The purified rPAP secreted by *P. pastoris* was virtually pure of contaminating proteins (Fig. 4, inset A).

In order to confirm that the secreted rPAP is correctly folded and possesses the expected enzymatic *N*-glycosidase activity, we next performed *in vitro* translation inhibition assays using the nuclease-treated rabbit reticulocyte lysate system. Luciferase mRNA was translated in the absence or presence of increasing concentrations of rPAP or native PAP (0.01 to 50 ng/

TABLE 2

Potency of Recombinant PAP in Inhibiting Protein Synthesis and HIV-1 Replication

	IC_{50} (ng/ml)	
Protein	Anti-ribosome[a]	Anti-HIV-1 (p24)[b]
rPAP	0.54 ± 0.2	89 ± 11
nPAP	0.52 ± 0.2	130 ± 18

[a] Anti-ribosome activity was measured from rabbit reticulocyte lysate *in vitro* translation assays.

[b] Anti-HIV-1 activity was determined from the HIV-1 replication assays using human PBMC infected with HTLV-IIIB.

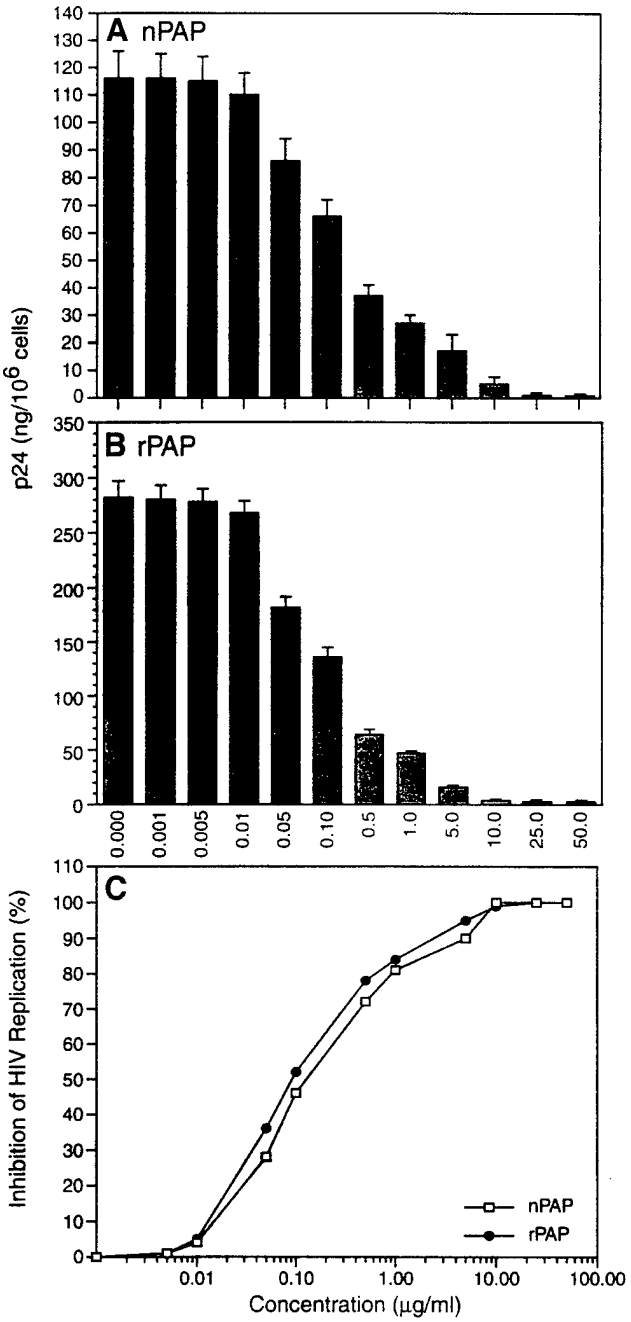

FIG. 6. Effect of rPAP on HIV-1 replication in human PBMC. (A) HIV-1 p24 antigen production in PBMC treated with native PAP. (B) HIV-1 p24 antigen production in rPAP-treated PBMC. (C) Inhibition of HIV-1 replication by native PAP (nPAP) versus recombinant PAP (rPAP). The viral replication was measured using the p24 core protein as a marker. The p24 value for untreated infected cells was used as 100% to determine the percentage inhibition of HIV-1 replication.

ml). Luciferase mRNA was selected because it encodes a monomeric protein of 61 kDa and yields a single major band upon SDS–PAGE (Fig. 5, inset). The ribosome inhibitory activity of rPAP was comparable to that of the native PAP. The IC_{50} values were 0.54 ± 0.2 and 0.52 ± 0.2 ng/ml for rPAP and native PAP, respectively (Table 2). We next compared the anti-HIV activity of rPAP to that of native PAP. As shown in Fig. 6, both rPAP and native PAP inhibited viral replication in HIV-1-infected human PBMC in a concentration-dependent fashion with IC_{50} values of 89 ± 11 and 130 ± 18 ng/ml, respectively (Table 2).

PAP has gained considerable interest in recent years due to its use as either a ribosome inhibitory anticancer agent or a broad-spectrum antiviral agent (18–22). Native PAP expressed in the *P. americana* plant is heterogeneous with several immunologically distinct isoforms which vary significantly in their catalytic and antiviral activities (1–3). The preclinical and clinical testing, however, requires large quantities of PAP purified to homogeneity. Therefore, large-scale production of homogeneous PAP by the methods of recombinant DNA technology would be greatly beneficial. Previous attempts on expression of PAP in *E. coli* (25), *S. cerevisiae* (26), and plants by several investigators have resulted in unacceptably low levels of yields (0.3 to 0.9 mg/L). Recently we have successfully expressed the full-length PAP (residues 23 to 313) in *E. coli* using an expression vector PQE-31(38). However, the expressed PAP sequestered as inactive inclusion bodies which needed further time-consuming solubilization and refolding steps (38). Our results presented herein illustrate that rPAP can be efficiently produced in the *P. pastoris* expression system. To our knowledge this is the first successful secretion of soluble and fully active mature rPAP using a yeast expression system. Our study represents a significant step toward improving and simplifying the production of recombinant pokeweed antiviral protein for advanced preclinical and potential clinical studies.

ACKNOWLEDGMENTS

The first two authors contributed equally to this work. This material is based in part upon work sponsored by the Defense Advanced Research Projects Agency under Grant N65236-99-1-5422 awarded to F.M.U. The content does not necessarily reflect the position or policy of the U.S. Government, and no official endorsement should be inferred.

REFERENCES

1. Irvin, J. D. (1975) Purification and partial characterization of the antiviral protein from *Phytolacca americana* which inhibits eukaryotic protein synthesis. *Arch. Biochem, Biophys.* **169,** 522–526.
2. Irvin, J. D. (1983) Pokeweed antiviral protein. *Pharmacol. Ther.* **21,** 371–381.
3. Irvin, J. D (1995) Antiviral proteins from *Phytolacca in* "Antiviral Proteins in Higher Plants" (Chessin, M., Deborde, D., and Zipf, A., Eds.), pp. 65–94. CRC Press. Boca Raton. FL.
4. Dallal, J. A., and Irvin, J. D. (1978) Enzymatic inactivation of eukaryotic ribosomes by the pokeweed antiviral protein. *FEBS Lett.* **89,** 257–259.
5. Gessner, S. L., and Irvin, J. D. (1980) Inhibition of elongation factor 2-dependent translocation by the pokeweed antiviral protein and ricin. *J. Biol. Chem.* **255,** 3251–3253.

6. Montanaro, L., Sperti, S., Mattioli, A. Testoni, G., and Stirpe, F. (1975) Inhibition by ricin of protein synthesis *in vitro:* Inhibition of the binding of elongation factor 2 and of adenosine diphosphate-ribosylated elongation factor 2 to ribosomes. *Biochem. J.* **146,** 127–131.
7. Hudak, K. A., Dinman, J. D., and Tumer, N. E. (1999) Pokeweed antiviral protein accesses ribosomes by binding to L3. *J. Biol. Chem.* **274,** 3859–3854.
8. Barbieri, L., Valbonesi, P., Bonora, E., Gorini, P., Bolognesi, A., and Stirpe, F. (1997) Polynucleotide:adenosine glycosidase activity of ribosome-inactivating proteins: Effects on DNA, RNA and poly(A). *Nucleic Acids Res.* **25,** 518–522.
9. Nicolas, E., Beggs, J. M., Haltiwanger, B. M., and Taraschi, T. F. (1998) A new class of DNA glycosylase/apyrimidinic lyases that act on specific adenines in single-stranded DNA. *J. Biol. Chem.* **273,** 17216–17220.
10. Wang, P., and Tumer, N. E. (1999) Pokeweed antiviral protein cleaves double-stranded supercoiled DNA using the same active site required to depurinate rRNA. *Nucleic Acids. Res.* **27,** 1900–1905.
11. Rajamohan, F., Venkatachalam, T. K., Irvin, J. D., and Uckun, F. M. (1999) Pokeweed antiviral protein isoforms PAP-I, PAP-II, PAP-III depurinate RNA of human immunodeficiency virus (HIV)-I. *Biochem. Biophys. Res. Commun.* **260,** 453–458.
12. Lin, Q., Chen, Z. C., Antoniw, J. F., and White, R. F. (1991) Isolation and characterization of a cDNA clone encoding the antiviral protein from *Phytolacca americana. Plant Mol. Biol.* **17,** 609–614.
13. Monzingo, A. F., Collins, E. J., Ernst, S. R., Irvin, J. D., and Robertus, J. D. (1993) The 2.5 Å structure of pokeweed antiviral protein. *J. Mol. Biol.* **233,** 705–715.
14. Irvin, J. D., and Uckun, F. M. (1993) Pokeweed antiviral protein: Ribosome inactivation and therapeutic applications. *Pharmacol. Ther.* **55,** 279–302.
15. Uckun, F. M., and Reaman, G. H. (1995) Immunotoxins for the treatment of leukemia and lymphoma. *Leukemia Lymphoma* **18,** 195–201.
16. Uckun, F. M. (1993) Immunotoxins for the treatment of leukemia. *Br. J. Hematol.* **85,** 435–438.
17. Gaynon, P. S., Bostrom, B., Reaman, G., Sather, H., Trigg, M. E., Tubergen, D. G., and Uckun, F. M. (1998) Childrens cancer group (CCG) initiatives in childhood acute lymphoblastic leukemia (ALL). *Int. J. Pediatr. Hematol. Oncol.* **5, 99–114.**
18. Gehrz, R. C., Wilson, C., Eckhardt, J., Myers, D., Irvin, J. D., and Uckun, F. M. (1991) Treatment of human cytomegalovirus (HCMV) with noval antiviral immunoconjugates *in* "Progress in Cytomegalovirus Research" (Landini, M., Ed.), pp. 353–356, Elsevier, Amsterdam.
19. Ussery, M. A., Irvin, J. D., and Hardesty, B. (1977) Inhibition of poliovirus replication by a plant antiviral peptide. *Ann. N. Y. Acad. Sci.* **284,** 431–440.
20. Tomlinson, J. A., Walker, V. M., Flewett, T. H., and Barclay, G. R. (1974) The inhibition of infection by cucumber mosaic virus and influenza virus by extracts from *Phyltolacca americana. J. Gen. Virol.* **22,** 225–232.
21. Aron, G. M., and Irvin, J. D. (1980) Inhibition of herpes simplex virus multiplication by the pokeweed antiviral protein. *Antimicrob. Agents Chemother.* **17,** 1302–1303.
22. Zarling, J. M., Moran, P. A.,Haffar, O., Sias, J., Richmann, D. D., Spina, C. A., Myers, D. E., Kuebelbeck, V., Ledbetter, J. A., and Uckun, F. M. (1990) Inhibition of HIV replication by pokeweed antiviral protein targeted to CD4$^+$ cells by monoclonal antibodies. *Nature* **347,** 92–95.
23. Uckun, F. M., Chelstrom, L. M., Tuel-Ahlgren, L., Irvin J. D., Chandan-Langlie, M., and Myers, D. E. (1998) TXU (Anti-CD7)-pokeweed antiviral protein as a potent inhibitor of human immunodeficiency virus. *Antimicrob.l Agents Chemother.* **42,** 383–388.
24. Uckun, F. M., Bellomy, K., O'Neill, K., Messinger, Y., Johnson, T., and Chen, C. L. (1999) Toxicity, Biological Activity, and Pharmacokinetics of TXU (anti-CD7)-Pokeweed antiviral protein in chimpanzees and adult patients infected with human immunodeficiency virus (HIV- 1). *J. Pharmacol. Exp. Ther.* **291,** 1301–1307.
25. Kataoka, J., Ago, H., Habuka, N., Furano, M., Masuta, C., Miyano, M., and Koiwai, A. (1990) Expression of a pokeweed antiviral protein in *Escherichia coli* and its characterization. *FEBS Lett.* **320,** 31–34.
26. Hur, Y., Hwang, D. K., Zoubenko, O., Coetzer, C., Uckun, F. M., and Tumer, N. E. (1995) Isolation and characterization of pokeweed antiviral mutation in *Saccharomyces cerevisiae:* Identification of residues important for toxicity. *Proc. Natl. Acad. Sci. USA* **92,** 8448–8452.
27. Sim, B. K., O' Reilly, M. S., Liang, H., Fortier, A. H.,, He, W., Madsen, J. W., Lapcevich, R., and Nacy, C. A. (1991) A recombinant human angiostatin protein inhibits experimental primary and metastatic cancer. *Cancer Res.* **57, 1329–1334.**
28. Boehm T., Pirie-Shepherd, S., Trinh, L. B., Shiloach, J., and Folkman, J. (1999) Disruption of the KEX1 gene in *Pichia pastoris* allows expression of full-length murine and human endostatin. *Yeast* **15,** 563–567.
29. Kjeldsen, T., Pettersen, A. F., and Hach, M. (1999) Secretory expression and characterization of insulin in *Pichia pastoris. Biotechnol. Appl. Biochem.* **29,** 79–86.
30. Mohanraj, D., Olson, T., and Ramakrishnan, S. (1995) Expression of biologically active human vascular endothelial growth factor in yeast. *Growth Factors* **12,** 17–27.
31. Eldin, P., Pauza, M. E., Hieda, Y., Lin, G. F., Murtaugh, M. P., Pentel, P. R., and Pennell, C. A. (1997) High-level secretion of two antibody single chain Fv fragments by *Pichia pastoris. J. Immunol. Methods* **21,** 67–75.
32. Luo, D., Mah, N., Krantz, M., Wilde, K., Wishart, D., Zhang, Y., and Jacobs, F. (1995) VL-linker-VH orientation-dependent expression of single chain Fv-containing an engineered disulfide-stabilized bond in the framework regions. *J. Biochem.* **118, 825–831.**
33. Kobayashi, K., Nakamura, N., Sumi, A., Ohmura, T., and Yokoyama, K. (1998) The development of recombinant human serum albumin. *Ther. Apher.* **2, 257–262.**
34. Cregg, J. M., and Higginns., D. R. (1995) Production of foreign proteins in the yeast *Pichia pastoris. Can. J. Bot.* **73**(Suppl. 1), S891–S987.
35. White, C. E., Hunter, M. J., Meininger, D. P., White, L. R., and Komives, E. A. (1995) Large scale, expression, purification and characterization of the smallest active fragment of thrombomodulin: The roles of the sixth domain and of methionine388. *Protein Eng.* **8,** 1177–1187.
36. Romanos, M. (1995) Advances in the use of *Pichia pastoris* for high-level expression. *Curr. Opin. Biotechnol.* **6,** 527–533.
37. Sreekrishna, K., Brankamp, R. G., Kropp, K. E., Blankenship, D. T., Tsay, J. T., Smith, P. L., Wierschke, J. D., Subramaniam, A., and Brikenberger, L. A. (1997) Strategies for optimal synthesis and secretion of heterologous proteins in the methylotrophic yeast *Pichia pastoris. Gene* **190,** 55–62.
38. Rajamohan, F., Engstrom, C. R., Denton, T. J., Engen, L. A., Kourinov, I., and Uckun, F. M. (1999) High-level expression and purification of biologically active recombinant pokeweed antiviral protein. *Protein Express. Purif.* **16,** 359–368.

THE JOURNAL OF BIOLOGICAL CHEMISTRY

Vol. 275, No. 5, Issue of February 4, pp. 3382–3390, 2000
Printed in U.S.A.

Modeling and Alanine Scanning Mutagenesis Studies of Recombinant Pokeweed Antiviral Protein*

(Received for publication, October 12, 1999)

Francis Rajamohan‡§¶, Matthew J. Pugmire‖, Igor V. Kurinov‡‖, and Fatih M. Uckun‡‡‡**

*From the ‡Biotherapy Program and the Departments of §Protein Engineering, ‖Structural Biology, **Biochemistry, and ‡‡Virology, Parker Hughes Institute, St. Paul, Minnesota 55113*

The *Phytolacca americana*-derived naturally occurring ribosome inhibitory protein pokeweed antiviral protein (PAP) is an *N*-glycosidase that catalytically removes a specific adenine residue from the stem loop of ribosomal RNA. We have employed molecular modeling studies using a novel model of PAP-RNA complexes and site-directed mutagenesis combined with bioassays to evaluate the importance of the residues at the catalytic site and a putative RNA binding active center cleft between the catalytic site and C-terminal domain for the enzymatic deadenylation of ribosomal RNA by PAP. As anticipated, alanine substitutions by site-directed mutagenesis of the PAP active site residues Tyr^{72}, Tyr^{123}, Glu^{176}, and Arg^{179} that directly participate in the catalytic deadenylation of RNA resulted in greater than 3 logs of loss in depurinating and ribosome inhibitory activity. Similarly, alanine substitution of the conserved active site residue Trp^{208}, which results in the loss of stabilizing hydrophobic interactions with the ribose as well as a hydrogen bond to the phosphate backbone of the RNA substrate, caused greater than 3 logs of loss in enzymatic activity. By comparison, alanine substitutions of residues $^{28}KD^{29}$, $^{80}FE^{81}$, $^{111}SR^{112}$, $^{166}FL^{167}$ that are distant from the active site did not significantly reduce the enzymatic activity of PAP. Our modeling studies predicted that the residues of the active center cleft could via electrostatic interactions contribute to both the correct orientation and stable binding of the substrate RNA molecule in the active site pocket. Notably, alanine substitutions of the highly conserved, charged, and polar residues of the active site cleft including $^{48}KY^{49}$, $^{67}RR^{68}$, $^{69}NN^{70}$, and $^{90}FND^{92}$ substantially reduced the depurinating and ribosome inhibitory activity of PAP. These results provide unprecedented evidence that besides the active site residues of PAP, the conserved, charged, and polar side chains located at its active center cleft also play a critical role in the PAP-mediated depurination of ribosomal RNA.

Pokeweed antiviral protein (PAP)[1] is a 29-kDa naturally occurring protein isolated from the leaves of the pokeweed plant, *Phytolacca americana* (1–3). PAP belongs to a family of plant ribosome-inactivating proteins (RIPs) that catalytically depurinate ribosomal RNA (3, 4). The enzymatic activity of PAP has been shown to be the specific cleavage of the glycosidic bond of a single adenine residue (A^{4324} of the tetraloop sequence GAGA) that is located in the highly conserved sarcin/ricin stem loop (4–7) and is found in both eukaryotic rRNA (28 S) and in prokaryotic rRNA (23 S). The ribosomes depurinated by PAP in this manner are unable to interact with elongation factors 1 and 2 (8, 9), and thus the protein synthesis is irreversibly inhibited at the translocation step (7, 8).

The x-ray structure of PAP has been determined previously and is composed of eight α helices and a β sheet consisting of six strands (15–17). The refined crystal structure of PAP suggests that the protein can be divided into three domains: the N-terminal domain (residues 1–69, PAP numbering), the central domain (residues 70–179), and the C-terminal domain (residues 180–262). All of the highly conserved catalytic site residues (Tyr^{72}, Tyr^{123}, Glu^{176}, and Arg^{179}) are located in the central domain. A deep cleft ("active center cleft") at the interface between the central and C-terminal domains forms the putative substrate-binding site (16).

Structural studies involving complexes of PAP with various ligands (adenine, formycin, and pteoric acid) have helped clarify the nature of the substrate binding site of PAP (15, 17) and provided valuable information concerning its substrate specificity. However, these studies have largely been limited to single nucleotides or nucleotide analogs in the active site, and details of how PAP binds a larger RNA fragment of the ribosome remain unknown. Recent modeling studies of another member of the RIP family (ricin) have also been useful in suggesting binding modes of RNA fragments in the active site (18). Based on structural, mutagenesis, and biochemical studies of several RIPs (ricin-A chain, trichosanthin, and momorcharin), it has been proposed that the amino acids Tyr^{72} and Tyr^{123} (PAP numbering) have the role of sandwiching the susceptible adenine ring of ribosomal RNA into the energetically favorable stacking conformation (19, 20). Subsequently, the side chain of Arg^{179} can protonate the N-3 atom of the adenine base, whereas Glu^{176} stabilizes a positive oxocarbonium transition state (15, 20). Huang *et al.* (21) have recently proposed that the N-7 atom of the adenine base can also be protonated by an acidic residue such as Asp^{92} (PAP numbering) in trichosanthin and momorcharin.

We have recently reported the expression of biologically active recombinant PAP in *Escherichia coli* (22). The biological activity of recombinant PAP was virtually identical to that of native PAP purified from the pokeweed plant (22). The availability of recombinant PAP provides a unique opportunity for structure-activity relationship (SAR) analyses. Furthermore, we have refined the x-ray structure of PAP (17) and established a novel model of the PAP-RNA complex using the coordinates of PAP (Protein Data Bank access code 1qcg), PAP complexed

* This work is based in part upon work sponsored by the Defense Advanced Research Projects Agency under Grant N65236-99-1-5422 (to F. M. U.). The costs of publication of this article were defrayed in part by the payment of page charges. This article must therefore be hereby marked "*advertisement*" in accordance with 18 U.S.C. Section 1734 solely to indicate this fact.

¶ To whom correspondence should be addressed: Parker Hughes Inst., 2657 Patton Rd., Roseville, MN 55113.

[1] The abbreviations used are: PAP, pokeweed antiviral protein; RIP, ribosome-inactivating protein; FMP, formycin 5′-monophosphate; PAGE, polyacrylamide gel electrophoresis; HPLC, high pressure liquid chromatography; SAR, structure-activity relationship.

with formycin 5'-monophosphate (Protein Data Bank access code 1pag), as well as the coordinates of the ribosomal RNA stem loop from the crystal structure of the 29-nucleotide RNA fragment (Protein Data Bank access code 430d) of rat 28 S ribosomal RNA, which contains the sarcin/ricin loop.

In the present SAR study, we employed molecular modeling studies using our model of PAP-RNA complexes and site-directed mutagenesis combined with bioassays to evaluate the importance of the residues at the catalytic site and a putative RNA binding active center cleft between the catalytic site and C-terminal domain for the enzymatic deadenylation of ribosomal RNA by PAP. As anticipated, alanine substitutions by site-directed mutagenesis of the PAP active site residues Tyr^{72}, Tyr^{123}, Glu^{176}, and Arg^{179} that directly participate in the catalytic deadenylation of ribosomal RNA resulted in greater than 3 logs of loss in depurinating and ribosome inhibitory activity. Similarly, alanine substitution of the conserved active site residue Trp^{208}, which results in the loss of stabilizing hydrophobic interactions with the ribose as well as a hydrogen bond to the phosphate backbone of the RNA substrate, caused greater than 3 logs of loss in enzymatic activity. By comparison, alanine substitutions of residues $^{28}KD^{29}$, $^{80}FE^{81}$, $^{111}SR^{112}$, and $^{166}FL^{167}$ that are distant from the active site did not significantly reduce the enzymatic activity of PAP. Our modeling studies predicted that the residues of the active center cleft could via electrostatic interactions contribute to both the correct orientation and stable binding of the substrate RNA molecule in the active site pocket. Notably, alanine substitutions of the highly conserved, charged, and polar residues of the active site cleft including $^{48}KY^{49}$, $^{67}RR^{68}$, $^{69}NN^{70}$, and $^{90}FND^{92}$ substantially reduced the depurinating and ribosome inhibitory activity of PAP. Our findings presented herein provide unprecedented experimental evidence that besides the catalytic site residues, the conserved charged and polar side chains located at the active site cleft of PAP also play a critical role in the catalytic removal of the adenine base from target ribosomal RNA substrates.

MATERIALS AND METHODS

Molecular Modeling—We first modeled the interaction of PAP with the single-stranded RNA heptamer GAGAGGA, which contains the target sequence for PAP. The initial position of GAGAGGA single-stranded RNA was built manually using RNA coordinates generated by InsightII (33). The position of the adenine base in PAP active site pocket (Protein Data Bank access code 1QCI) (17) was used as a guide to properly position the second adenine in the modeled RNA heptamer. Major steric collisions with PAP were removed by manually adjusting the torsion angles of the phosphate backbone. The RNA heptamer was roughly positioned within the long concave region on the surface of PAP. This general position of the RNA heptamer was used as a starting point for subsequent docking trials. We created a definitive binding set of PAP residues in the active site pocket to move as a 3.5 Å shell around the manually docked RNA substrate during energy minimization. The number of final docking positions was set to 10, although finally only 2–4 promising positions were identified. The calculations used a consistent valence force field in the Discovery program and a Monte Carlo strategy in the Affinity program. Each energy-minimized final docking position of the ligand was evaluated using the interactive score function in the Ludi module. During RNA docking four torsion angles in phosphate backbone near the bound alanine were freed to increase the volume of conformational search. The final binding position of the RNA heptamer was determined based on the evaluation of favorable binding interactions using the Ludi score function. Ludi score included the contribution of the loss of translational and rotational entropy of the RNA fragment, number, and quality of hydrogen bonds and contributions from ionic and lipophilic interactions to the binding energy.

We next modeled the interaction of PAP with a 29-nucleotide RNA fragment of rat 28 S rRNA. The initial position of the ribosomal RNA stem loop in the PAP active site was built manually. This was done using the coordinates of PAP (Protein Data Bank access code 1qcg) (17), PAP complexed with FMP (an adenosine analog, Protein Data Bank access code 1pag) (15) and the coordinates of the ribosomal RNA stem loop, which contains the sarcin/ricin loop, from the crystal structure of the 29-nucleotide RNA fragment (Protein Data Bank access code 430d) (23). To place the RNA fragment in the PAP active site, the nucleotide A15 (analogous to A4324 in eukaryotic rRNA) was first removed from the coordinates of the RNA fragment. Because FMP binds the PAP active site in a conformation thought to be similar to that of the targeted adenine of the rRNA fragment, this position was used as a guide to place the resulting 28-nucleotide RNA fragment (residues 1–14, 16–29). The possible positions of this RNA fragment in the PAP active site were manually explored by allowing only rigid body movements under the following constraints: the 5'-phosphate group of G^{16} should be within a bonding distance from the 3'-OH of FMP, and the 3'-OH of G^{14} should be within a bonding distance from the 5'-phosphate group of FMP. Under such constraints, there was only one general position of the RNA structure that avoided major steric interference with PAP. Once the RNA fragment was positioned, the coordinates of the A^{15} nucleotide were reinserted so that it matched the position of FMP. This general position of RNA in the active site of PAP was then used as a starting point for further modeling studies.

To refine this initial position and to explore other possible positions, the initial model was used to perform fixed docking using the *Docking* module in InsightII employing the CVFF forcefield (33). The parameters used in this docking included searching for five unique structures: 1000 minimization steps for each structure, energy range of 10.0 kcal/mol, maximum translation of the ligand of 3.0 Å, maximum rotation of the ligand of 10°, and an energy tolerance of 1500 kcal/mol. During the minimization steps of the docking procedure, only the stem loop residues 13–18 were allowed to be flexible, whereas the residues 1–12 and 19–29 were held fixed. In addition, several distance and torsion restraints were applied to the 13–18 GC base pair to maintain this interaction.

Bacterial Strains and Construction of Mutants—Recombinant wild-type PAP (phosphate-buffered saline-PAP) was obtained by subcloning the *PAP-I* gene (amino acids 22–313) into the pBluescript SK^- expression vector (22). Uracil-containing template of *PAP* was obtained by transforming *E. coli* CJ236 with the recombinant plasmid phosphate-buffered saline-PAP. The oligonucleotides used for site-directed mutagenesis were synthesized by Biosynthesis Inc. (Lewisville, TX). Site-directed mutagenesis procedure was as described in the manufacturer's manual (Mutagene M13 *in vitro* mutagenesis kit; Bio-Rad). DNA sequencing was carried out by the method of Sanger *et al.* (24) following the manufacturer's instructions (U. S. Biochemical Corp.). Fine chemicals and restriction enzymes were purchased from Roche Molecular Biochemicals.

Expression and Purification of Mutants—Wild-type and mutant recombinant(r) PAP proteins were expressed in *E. coli* MV1190 as inclusion bodies, isolated, solubilized, and refolded as described previously (22). The refolded proteins were analyzed by SDS-12% polyacrylamide gel electrophoresis (PAGE). Protein concentrations were determined from the gel using bovine serum albumin as a standard.

Immunoblot Analysis of rPAP Mutants—The protein samples were resolved on a SDS-12% PAGE and transferred onto a polyvinylidene difluoride membrane (Bio-Rad) using the Bio-Rad trans-blot apparatus, as described previously (22). The membrane was immunoblotted using rabbit anti-PAP serum (1:2000 dilution) and horseradish peroxidase-conjugated goat anti-rabbit IgG (Sigma) as the primary and secondary antibodies, respectively. The blot was developed using 3,3'-diaminobenzidine (Sigma) as the colorimetric indicator for peroxidase activity.

Aniline Cleavage Assays of Ribosomal RNA Depurination—5 μg of *E. coli* 16 S and 23 S rRNA (Roche Molecular Biochemicals) or 30 μg of total ribosome prepared from the rabbit reticulocyte-rich whole blood (25) were incubated with either 5 or 25 μg of wild-type or mutant rPAP proteins in 50 μl (final volume) of binding buffer (25 mM Tris·HCl, pH 7.8, 10 mM KCl, 5 mM $MgCl_2$, 2% glycerol) at 37 °C for 1 h. The RNA was extracted with phenol:chloroform (24:24), precipitated with ethanol, and treated with 20 μl of 1 M aniline acetate (pH 4.5) for 30 min on ice. The RNA was precipitated with ethanol, electrophoresed in a 6% urea/polyacrylamide gel, and stained with ethidium bromide as described previously (22).

Adenine Release Assays—The release of adenine from *E. coli* ribosomal RNA (Roche Molecular Biochemicals) was measured using HPLC (Hewlett Packard, Palo Alto, CA) equipped with a diode array detector and a ChemStation software program for data analysis (14). *E. coli* ribosomal RNA (2 μg) was incubated with 5.0 μM of wild-type or mutant rPAP proteins for 1 h at 37 °C in 50 μl of binding buffer (25 mM Tris·HCl, pH 7.8, 10 mM KCl, 5 mM $MgCl_2$, 2% glycerol). The reaction was stopped by adding 100 μl of HPLC running buffer (50 mM $NH_4C_2H_3O_2$, 5% methanol, pH 5.0), and 100 μl of the sample was

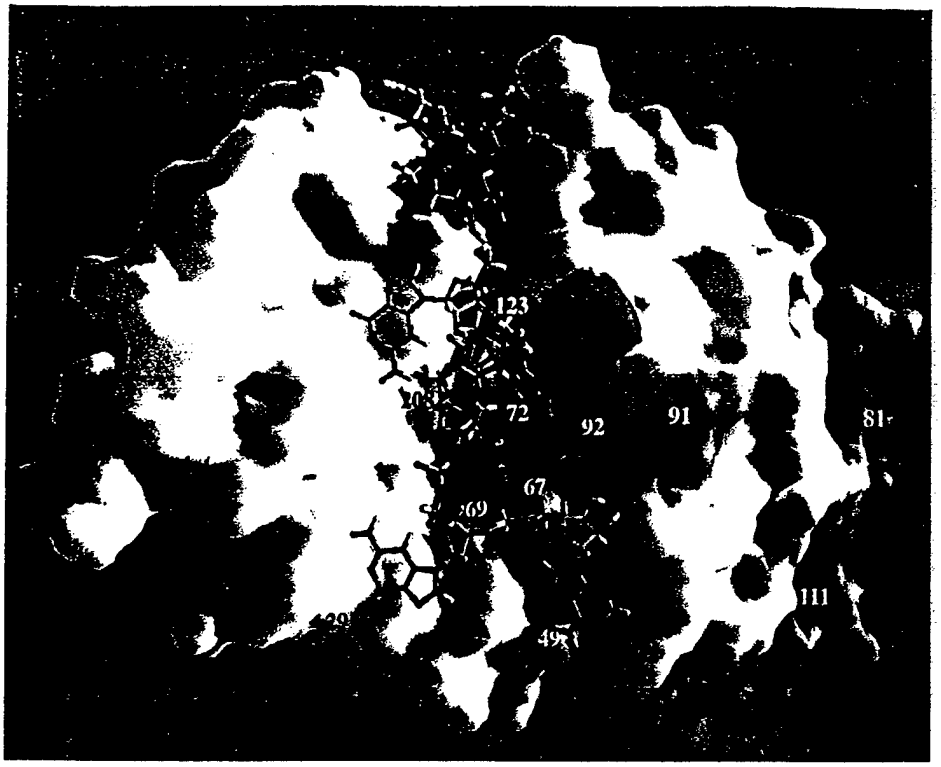

FIG. 1. **Putative substrate binding site of PAP.** The depicted ball-and-stick model represents an RNA heptamer (GAGAGGA) that was docked into the RNA binding site by computer simulation. The image was created using GRASP software (28). Alanine substitution of residues furthest from the catalytic site, at the catalytic active site, and at the active center cleft are differentially represented by *blue*, *red*, and *green*, respectively.

injected automatically into a reverse-phase Lichrospher 100RP-18E analytical column (Hawlett-Pakard, 5-mm particle size, 250 × 4 mm) that was equilibrated with HPLC running buffer. The detector wavelength was set at 260 nm, and the sample was eluted under isocratic conditions at a flow rate of 1.0 ml/min as described before (14). Controls included (*a*) samples containing untreated ribosomal RNA and (*b*) samples without ribosomal RNA. The adenine standard was purchased from Sigma. A calibration curve was generated to establish the linear relationship between the absolute peak area and the concentrations of adenine in the tested samples. Adenine at final concentrations of 0.1, 0.5, 1.0, 2.5, and 5.0 μM (5, 25, 50, 125, and 250 pmol/50 ml, respectively) was injected into the HPLC system for analysis, and the calibration curve was generated by plotting the absolute peak area against the concentrations of adenine as described previously (14). Unweighted linear regression analysis of the calibration curve was performed by using the CA-Cricket graph III computer program (Computer Association, Inc., Islandia, NY). Intra-assay and inter-assay accuracy and precisions were evaluated as described previously (14). Under the described chromatographic conditions, the retention time for adenine was 9.7 min, and adenine was eluted without an interference peak from the blank controls (data not shown). The lowest limit of detection for adenine was 2.5 pmol at a signal to noise ratio of ~3. The intra- and inter-assay coefficients of variation were less than 4%. The overall intra- and inter-assay accuracies of this method were 98.7 ± 1.7% (n = 6) and 95.7 ± 3.0% (n = 6), respectively.

Cell-free Translation Assays—Protein synthesis was assayed in a cell-free system using nuclease-treated rabbit reticulocyte lysates (Promega, Madison, WI) and luciferase mRNA, as described previously (22). In this assay, luciferase mRNA was translated in the presence or absence of increasing concentrations of wild-type or mutant rPAP proteins. Luciferase mRNA encodes for a monomeric protein of 61 kDa on SDS-PAGE. In brief, varying amounts (0.01–12,000 ng/ml) of wild-type or mutant rPAP proteins were added to the translation mixture (10 μl rabbit reticulocyte lysate; 0.5 μl of 1.0 mM methionine-free amino acids mixture; and 1.0 μl of [^{35}S]methionine, 10 mCi/ml) to a final volume of 19 μl and incubated for 15 min at room temperature. Protein synthesis was initiated by adding 0.12 μg of luciferase mRNA in a 1.0-μl volume, and the incubation was continued for 2 h at 30 °C. Translation was stopped by the addition of 5% trichloroacetic acid, and the precipitated polypeptides were collected on Whatman GF/C glass microfiber filters. The incorporation of ^{35}S was determined by counting the radioactivity on the filters using a liquid scintillation counter (Beckman LS 6000SC) as described previously (22). The IC_{50} (50% inhibitory concentration) values were calculated by nonlinear regression analysis (Prism-2 Graph Pad software, San Diego, CA) using the average values of three independent experiments. The cpm values in control sample with all the reagents added except the test sample ranged from 3 to 4 × 10^7 cpm/ml and were considered as 100% incorporation when determining the percentage of control protein synthesis values for samples treated with test materials.

RESULTS AND DISCUSSION

Modeling Studies of the Catalytic Active Site and RNA-binding Residues of PAP—Our first model of PAP-RNA heptamer complex (*i.e.* PAP-GAGAGGA complex) indicated that the target RNA heptamer can bind very strongly to PAP via multiple interactions along the concave cleft region (Fig. 1). The central adenine base is sandwiched between Tyr^{72} and Tyr^{123} as observed previously (15, 17) and forms four hydrogen bonds with active site residues (Val^{73}, Ser^{121}, and Arg^{179}). There are additional stabilizing electrostatic interactions between neighboring negatively charged phosphate groups and two clusters of positively charged interactions on the PAP surface formed by Arg^{179} and Lys^{210} from one side and by Arg^{122} and Arg^{135} from the other side of the active site. The two adjacent guanines (G^3 and G^5) of the bound adenine (A^4) do not have any specific interactions with PAP, whereas the other ribonucleotides interact with the active site cleft residues. These interactions help to properly position the adenine base in the PAP active site so that it can be cleaved with high efficiency.

Our second more advanced model of PAP-RNA complex involved an RNA stem loop fragment (29-nucleotide, 5′-GGGUGCUCAGUACGAGAGGAACCGCACCC-3′) docked into the active site of PAP as shown in Fig. 2. This orientation allows the purine ring of adenine, at the position that corresponds to 15 (A^{15}), of the stem loop to be sandwiched between the side chains of Tyr^{123} and Tyr^{72}, as observed crystallographically (15) for the adenine analog, FMP (formycin monophosphate). The crystallographic position of FMP shows that the N^6 of the adenine analog ring donating a hydrogen bond to the carbonyl oxygen of Val^{73}, whereas N^1 is accepting a hydrogen bond from the amide backbone of Val^{73}. Our model, however, positions A^{15} in a slightly different position and now has N^6 donating a hydrogen bond to the carbonyl oxygen of Ser^{121} and is slightly more distanced from the carbonyl oxygen of Val^{73}. In addition, the distance between N^1 and the amide

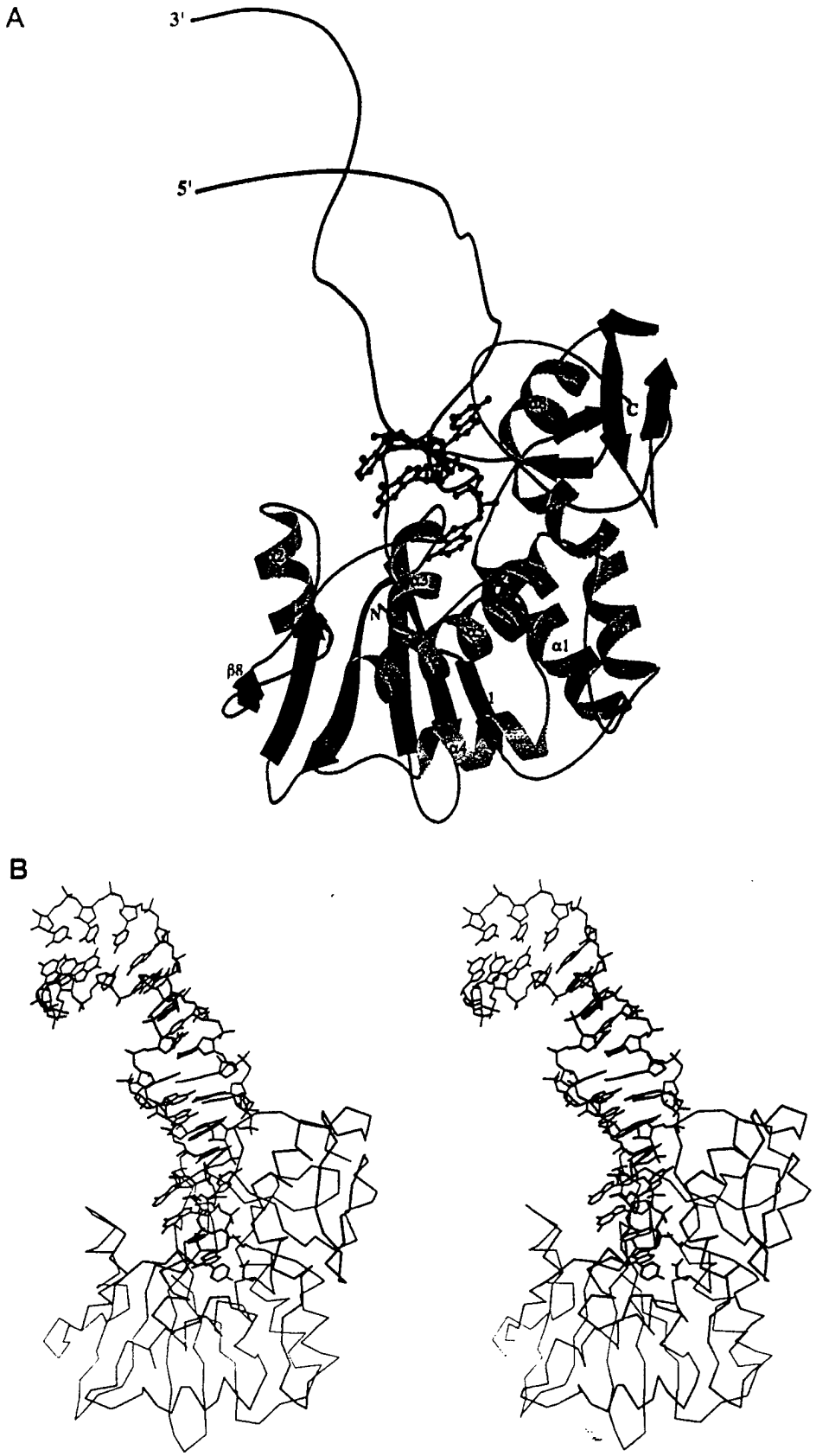

FIG. 2. **Molecular model of PAP-RNA stem loop complex.** *A*, the β strands of PAP are *blue* and are labeled *β1–β10*. The α helices are *yellow* and are labeled *α1–α8*. The phosphate backbone of the RNA fragment is *violet*, and the four nucleotides that make up the targeted tetra-loop (GAGA) of the conserved sarcin/ricin loop sequence are shown as ball-and-stick models. The structure of the 29-nucleotide ribosomal RNA fragment comes from the recently published crystal structure (Protein Data Bank access code 430d) and has the sequence 5′-GGGUGCUCAGUACGAGAGGAACCGC-ACCC-3′. This figure was produced with MOLSCRIPT (29) and RASTER3D (30). *B*, stereoview of the overall orientation for the modeled complex of PAP with 29-nucleotide RNA stem loop fragment. PAP is shown as a *red* Cα trace, where the active site residues Tyr^{72}, Tyr^{123}, Glu^{176}, and Arg^{179} are shown as *green* stick models. The 29-nucleotide RNA fragment is *gray*, with the four residues of the conserved tetra-loop (GAGA) in *blue*. The model shows the position of A^{15} in RNA buried in the active site of PAP and shows several of the residues of the stem loop in positions to interact with PAP. This figure was produced using MOLSCRIPT (29).

backbone of Val^{73} is also slightly out of range for a hydrogen bond to occur. The active site residue Glu^{176} is in a position similar to what has been observed experimentally, where the negatively charged chain is under the glycosidic bond of A^{15} and is proposed to stabilize the positive oxocarbonium ion that develops on the ribose group in the transition state (15, 26). Another active site residue Arg^{179} also shows a similar conformation where it is in a position to protonate N^3 of the adenine ring. Thus, the overall conformation of the PAP active site residues of our model is similar to those observed previously (18), as shown in Fig. 2.

The base stacking pattern of the model is also interesting to

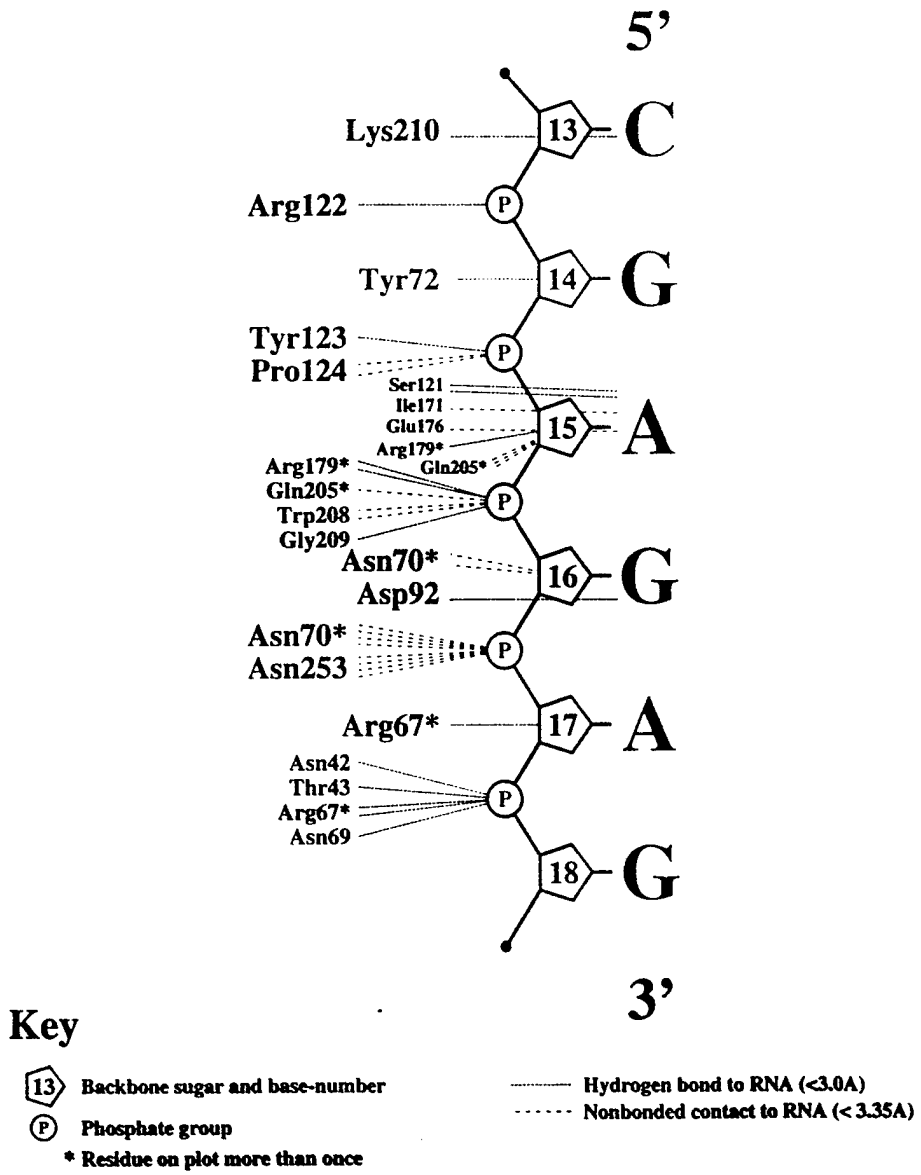

FIG. 3. **Schematic diagram of the interactions observed in the model between PAP and the 29-nucleotide stem loop RNA fragment.** This figure was produced using NUCPLOT (31).

note. As mentioned previously, A^{15} is sandwiched between two tyrosine residues, and G^{16} is stacked on top of Tyr^{72}. The modeled positions of A^{15} between the tyrosine residues (Tyr^{72} and Tyr^{123}) of PAP should allow A^{15} to be inserted into the active site of PAP and still maintain the favorable base stacking interactions that help stabilize the RNA structure. Several contacts are formed with the stem loop that appear to provide specificity for A^{15} and G^{16} of the stem loop. The majority of these contacts are formed with A^{15} and include hydrogen bonds with Ser^{121} and Arg^{179}. The Asp^{92} forms a hydrogen bonds with the amine and N^1 of the G^{16} base. There are several additional binding contacts are formed between the phosphate backbone and the positively charged residues Arg^{67}, Arg^{122}, Arg^{179}, and Lys^{210}, as well as several other polar residues such as Asn^{70} of the active site cleft. All of the contacts that are formed between PAP and the RNA fragment are shown schematically in Fig. 3.

Both models support the notion that the active site residues Tyr^{72}, Tyr^{123}, Glu^{176}, and Arg^{179} are directly responsible for the catalytic function of PAP. In addition, modeling studies with the RNA fragments uniquely indicate that several residues (Lys^{48}, Arg^{67}, Asn^{69}, Asn^{70}, Asp^{92}, Arg^{122}, and Lys^{210}) that are not directly involved in the catalytic depurination at the active site are forming specific interactions with the RNA substrate. The model of PAP complexed with the 29-nucleotide RNA stem loop fragment indicates that the positive charge of Arg^{67} should enable this residue to favorably interact with the negatively charged phosphate backbone of G^{18} in RNA, whereas Asn^{69} and Asn^{70} interact with the phosphate backbone of G^{18} and ribose of G^{16}, respectively (Fig. 3). According to our model, Asp^{92} interacts with the base of G^{16} and may therefore contribute to the binding of PAP to the tetra-loop structure of RNA (Fig. 3). Our model also suggests that the side chain of Trp^{208} can engage in a hydrophobic interaction with the ribose of G^{16} and the amide backbone of Trp^{208} can form hydrogen bonds with the phosphate backbone of G^{16}. Therefore, mutations involving Trp^{208} could result in local conformational change at the catalytic site of the PAP and disrupt these stabilizing interactions with G^{16}.

Our models indicate that the above interactions are important for binding, orientation, and stabilization of the RNA substrate, and their mutation could therefore lead to significant loss of catalytic activity. Obviously the removal of positively charged residues will diminish the strength of binding to the negatively charged phosphate backbone of RNA and subsequently reduce the activity PAP. Besides, Asn^{70} forms a hydrogen bond with the catalytic site residue Arg^{179}, and ala-

A **Conserved Active Site Residues**

Ricin-A	^{77}TNAYV^{81}....	^{121}GNYD^{124}....	^{176}SEAARFQ^{182}.... ^{210}SWG^{212}
PAP-S	^{69}NNLYV^{73}....	^{120}GLYP^{123}....	^{174}SEAARFK^{180}.... ^{206}NWG^{208}
PAP-II	^{66}GNLYL^{70}....	^{115}KSYK^{118}....	^{171}TEASRFK^{177}.... ^{205}NWD^{207}
PAP-I	^{69}NNLYV^{73}....	^{121}SRYP^{124}....	^{175}SEAARFK^{181}.... ^{207}TWG^{209}

B **Stereo view of PAP Active Site Residues**

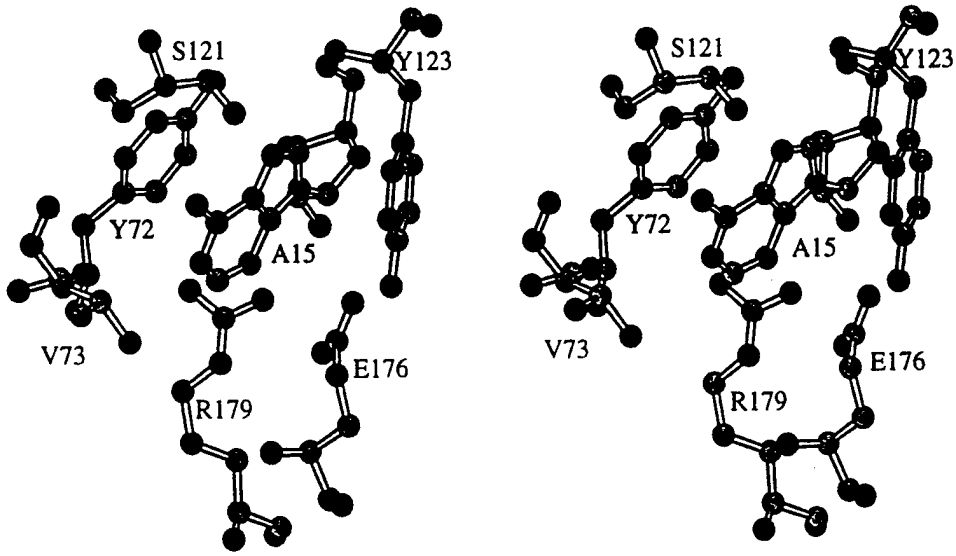

C **Residues Conserved Among PAP isoforms**

Ricin-A	^{32}LTTG^{35}...	^{55}QRFI^{58}...	^{74}LDVTNA^{79}...	^{87}G----N-SAYFFH-P^{95}... ^{112}--QN^{113}..... ^{166}RSFI^{169}
PAP-S	^{27}AKDP^{30}...	^{47}IKYL^{50}...	^{66}LRRNNL^{71}...	^{79}PYD-NKCRYHIFNDI^{92}... ^{102}NPRV^{105}..... ^{164}KFLL^{167}
PAP-II	^{25}VKDK^{28}...	^{45}PKYV^{48}...	^{63}IRRGNL^{68}...	^{76}IYNG-KCRYRIFKDS^{89}... ^{109}KSKP^{112}..... ^{161}EFLL^{164}
PAP-I	^{27}AKDP^{30}...	^{47}PKYV^{50}...	^{66}LRRNNL^{71}...	^{79}PFETNKCRYHIFNDI^{93}... ^{110}NSRV^{113}..... ^{165}EFLL^{168}

FIG. 4. Structural alignment of selected primary sequence of PAP-I with PAP-II, PAP-S and Ricin-A. Numbering is relative to the initiation codon. *A*, comparison of the residues that were conserved among the RIPs. *B*, stereoview of the active site residues along with the adenine residue (*A15*) of RNA. The PAP residues thought to be involved in the catalytic mechanism (*Y72*, *V73*, *Y123*, *E176*, and *R179*) are also shown. The figure was produced using MOLSCRIPT (29). *C*, comparison of the amino acids that are highly conserved among the PAP isoforms but not ricin-A chain. The conserved residues are in *bold type*. The residues that were mutated in this study are *underlined* in the PAP-I sequence.

nine mutation of this residue would therefore likely affect the enzymatic activity of PAP.

Construction and Expression of PAP Mutants—Recombinant PAP mutants with alanine substitutions of the conserved catalytic site and active center cleft residues were constructed using site-directed mutagenesis techniques. Alanine substitutions were considered because the replacement of side chains with alanine would be least disruptive to the overall structure (27). Also, alanine does not impose new hydrogen bonding, sterically bulky, or unusually hydrophobic side chains (27). An amino acid alignment of PAP residues, selected for mutagenesis, with those of PAP-II, PAP-S, and ricin-A chain is shown in Fig. 4. The active site residues selected for mutagenesis are highly conserved among the various RIPs identified to date (Fig. 4*A*). The residues outside the active site chosen for mutagenesis are highly conserved among the PAP isoforms, but they are different from those in ricin-A chain (Fig. 4*C*). The positions, chemical nature, and secondary structural elements of the amino acids substituted with alanine are indicated in Table I.

Thirteen point mutants of recombinant PAP (Table I), containing single, double, or triple alanine substitutions, were constructed and expressed in the *E. coli* strain, MV1190, as inclusion bodies. The inclusion bodies were purified, solubilized, refolded, and analyzed by SDS-PAGE (Fig. 5*A*). All of the mutant proteins were expressed in yields comparable to that of the wild-type PAP (Fig. 5*A*). The solubilized and refolded mutants displayed a 33-kDa major protein on SDS-PAGE, were highly reactive to the anti-PAP serum and were stable under our solubilization and refolding conditions (Fig. 5*B*).

Inhibition of Translation in the Rabbit Reticulocyte Lysate Assays—The mutants could be roughly categorized into three major groups. The first group includes PAP mutants with alanine substitutions distant from the catalytic active site (FLP-1/^{28}AA^{29}, FLP-6/^{80}AA^{81}, FLP-8/^{111}AA^{112}, and FLP-10/^{166}AA^{167}; colored *blue* in Fig. 1). Based on our modeling studies we did not expect these mutants to have substantially reduced activity. The experimentally determined IC_{50} values from cell-free translation assays confirmed that the ribosome inhibitory activity of FLP-1, FLP-6, FLP-8, and FLP-10 proteins (IC_{50} =

TABLE I

Sequence identity, secondary structural elements, and biological activity of wild-type and mutant PAP proteins

Secondary structure denotations are as follows: L, loop; α, α-helix.

Mutant	Original residue numbered	Substituted residue	Secondary structural element	Translation inhibition IC_{50}[a]	Mutant IC_{50} / Wild-type IC_{50}	Adenine released[b]
				ng/ml		*pmol/μg RNA*
Wild type				6.7 (4.6–6.9)	1	396 ± 15
FLP-1	^{28}KD^{29}	^{28}AA^{29}	L	5.9 (3.9–8.8)	1	319 ± 14
FLP-2	^{48}KY^{49}	^{48}AA^{49}	L	131 (105–162)	23	211 ± 10
FLP-3	^{67}RR^{68}	^{67}AA^{68}	L	189 (158–225)	33	132 ± 12
FLP-4	^{69}NN^{70}	^{69}AA^{70}	L	1086 (833–1416)	191	46 ± 5
FLP-5	^{71}LY^{72}	^{71}AA^{72}	L	>10,000	>1754	9 ± 2
FLP-6	^{80}FE^{81}	^{80}AA^{81}	L	49 (33–74)	9	235 ± 13
FLP-7	^{90}FND^{92}	^{90}AAA^{92}	L	2006 (1874–2258)	352	19 ± 5
FLP-8	^{111}SR^{112}	^{111}AA^{112}	L	6.7 (5.6–8.1)	1	376 ± 11
FLP-9	^{122}RY^{123}	^{122}AA^{123}	L	>10,000	>1754	12 ± 3
FLP-10	^{166}FL^{167}	^{166}AA^{167}	α_5	6.8 (5.8–7.8)	1	392 ± 15
FLP-11	Glu^{176}	Ala^{176}	α_5	>10,000	>1754	7 ± 2
FLP-12	Arg^{179}	Ala^{179}	α_5	2193 (1998–2210)	385	14 ± 7
FLP-13	Trp^{208}	Ala^{208}	α_7	>10,000	>1754	4 ± 2

[a] 95% confidence limits are given in parentheses.
[b] Each value is the mean ± S.D. of three experiments.

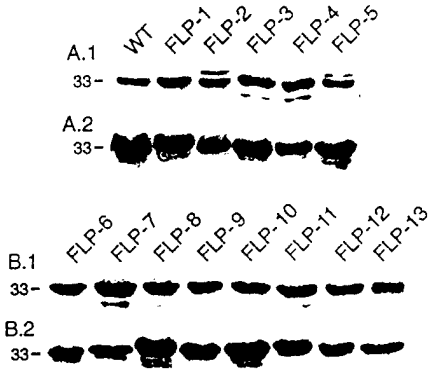

FIG. 5. **Coomassie Blue-stained SDS-12% PAGE (*A.1* and *B.1*) and Western blot analysis (*A.2* and *B.2*) of wild-type and mutant recombinant PAP Proteins.** Mass of the protein (in kDa) is shown on the *left*. Each *lane* contains 5–7 μg of recombinant PAP protein. *WT*, wild type.

5.9 ± 1.0, 49 ± 3.0, 6.7 ± 1.0, and 6.8 ± 0.9 ng/ml, respectively) were comparable with that of the wild type (IC_{50} = 5.7 ± 1.0 ng/ml; Fig. 6*A* and Table I). The data from adenine release assays and aniline cleavage assays were in accordance with the translation inhibition data.

The second group of PAP mutants include those with mutations at the catalytic active site (FLP-5/^{71}AA^{72}, FLP-9/^{122}AA^{123}, FLP-11/Ala^{176}, FLP-12/Ala^{179}, and FLP-13/Ala^{208}; colored *red* in Fig. 1). Alanine substitutions at these locations were expected to affect the orientation of the substrate adenine in the active site and subsequent enzymatic cleavage of the glycosidic bond. As predicted from our modeling studies, these mutants were enzymatically inactive (Fig. 6*B* and Table I). At a 5 μM concentration, wild-type PAP released 396 ± 15 pmol of adenine/μg of ribosomal RNA (Table I). By comparison, the catalytic site mutants, FLP-5, FLP-9, FLP-11, FLP-12, and FLP-13 released 9 ± 2, 12 ± 3, 7 ± 2, 14 ± 7, and 4 ± 2 pmol of adenine/μg of rRNA, respectively. Substitution of the catalytic active site residues ^{71}LY^{72} (FLP-5) and ^{122}RY^{123} (FLP-9), Glu^{176} (FLP-11) and Trp^{208} (FLP-13) have resulted in nearly complete loss (>1700-fold less active) of ribosomal depurination activity, as we expected. Arg^{179} (active site residue), however, apparently plays a less important role in catalytic deadenylation than the other active site residues (only 385-fold less active than the wild type).

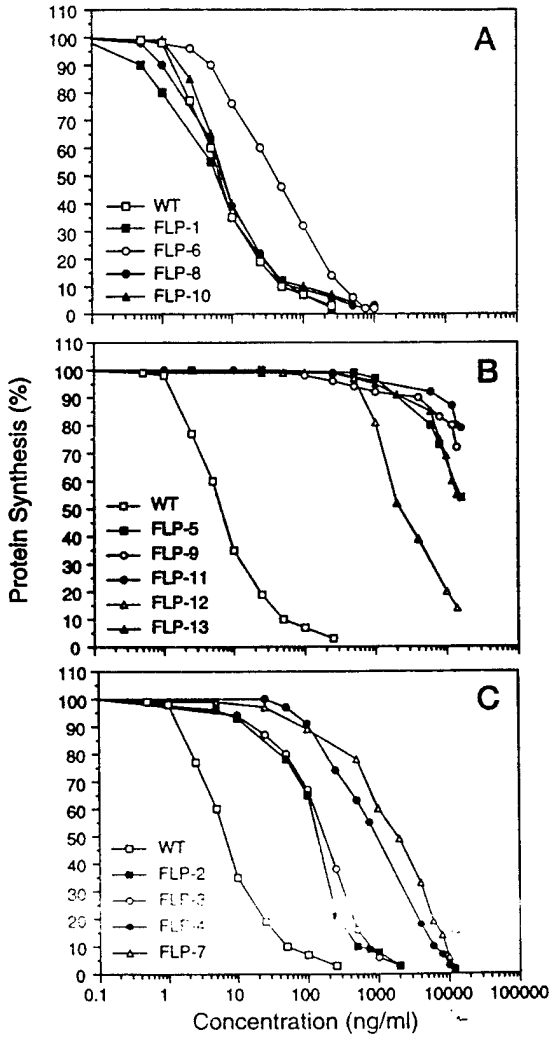

FIG. 6. **Ribosome inhibitory activity of wild-type and mutant recombinant PAP proteins in an *in vitro* rabbit reticulocyte lysate system.** Each value is an average from four independent experiments. Cell-free protein synthesis in the rabbit reticulocyte lysate system was measured by [^{35}S]methionine incorporation. Control samples treated with all the reagents except PAP were assigned a value of 100% incorporation. *A*, mutants furthest from the active site. *B*, mutants at the catalytic active site. *C*, mutants at the active center cleft.

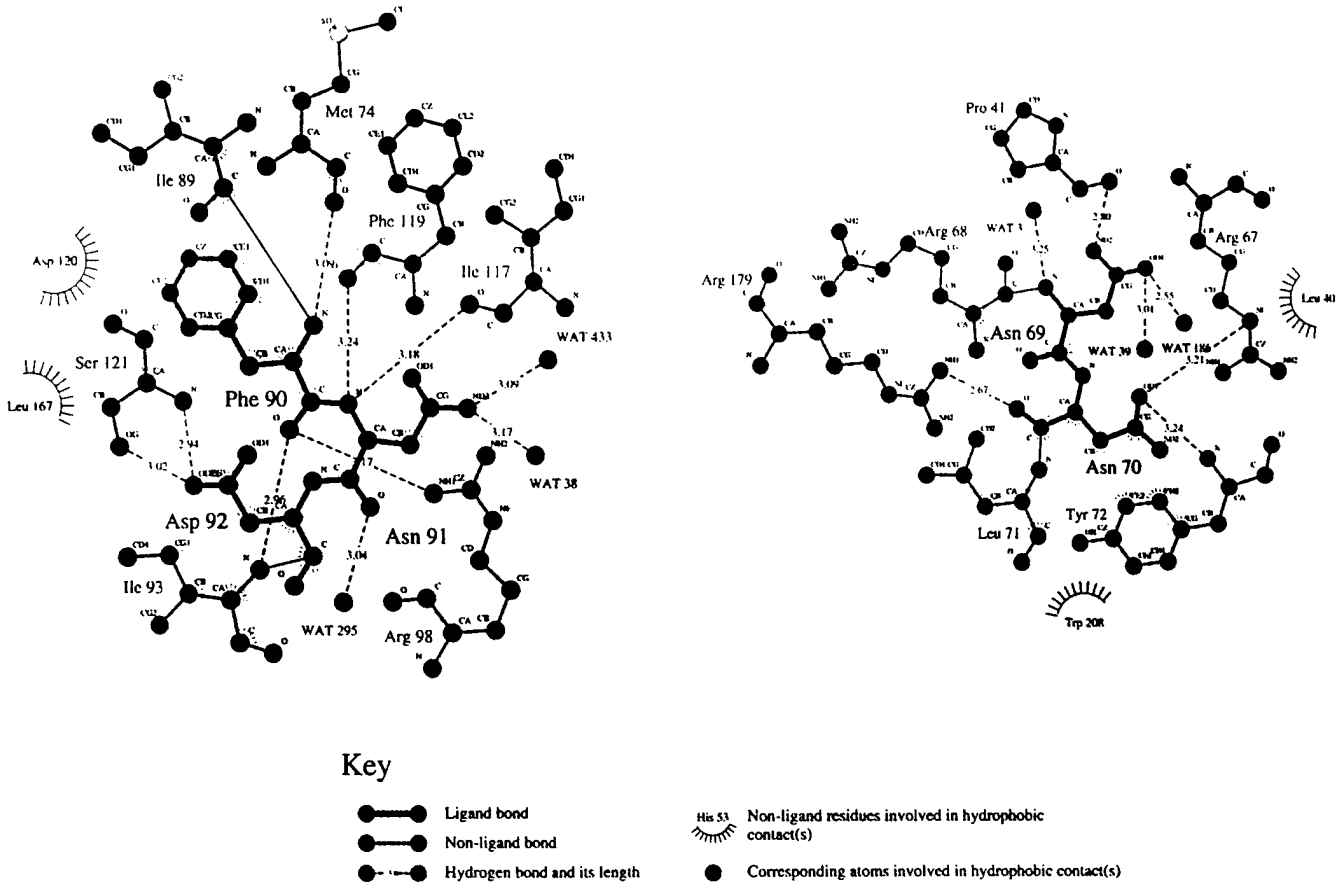

FIG. 7. **Details of interactions of PAP residues 69–70 (*A*) and 90–92 (*B*) with neighboring residues.** Most of the pictured hydrogen bonds are lost in alanine substitution. The figure was created using LIGPLOT (32).

The third group of PAP mutants included those with mutations in the active center cleft between the central and C-terminal domains, dominated by charged (Lys^{48}, Arg^{67}, Arg^{68}, and Asp^{92}) and polar (Asn^{69} and Asn^{70}) side chains forming contacts with the modeled RNA substrates, (FLP-2/^{48}AA^{49}, FLP-3/^{67}AA^{68}, FLP-4/^{69}AA^{70}, and FLP-7/^{90}AAA^{92}; colored *green* in Fig. 1). All of these mutated residues are involved in a complex network of interactions pivotal for the proper orientation of the substrate RNA. In addition, Asn^{70} (FLP-4) forms a hydrogen bond with the catalytic residue Arg^{179}, and alanine substitution might lead to a functionally unfavorable conformation of the Arg^{179} side chain (Fig. 7). Notably, mutations at the active center cleft have markedly diminished (23-, 33- 191-, and 352-fold less active, respectively) the enzymatic activity of PAP (Fig. 6*C* and Table I). As shown in Fig. 6, the inhibition curves shifted to the right, consistent with a significant decrease in enzymatic activity. The bioassays were carried out using at least four different preparations of wild-type and mutant rPAP and yielded comparable results. Substitution of ^{48}KY^{49} (FLP-2) at the far end of the cleft had a less pronounced effect on the catalytic activity (23-fold less active) than the substitution of the residues ^{67}RR^{68}, ^{69}NN^{70}, and ^{90}FND^{92} that are located closer to the catalytic site (Table I). The adenine release assays were also consistent with the protein synthesis inhibition assay results (Table I).

We next examined whether there was deadenylation of ribosomal RNA (rabbit) by the catalytic site mutants or active center cleft mutants. The rabbit rRNA depurination was determined by treating the ribosomes with wild-type or mutant proteins and subsequent purification of the rRNA and cleavage with aniline. Because aniline cleaves the sugar-phosphate backbone of RNA at depurination sites, the release of fragments from aniline-treated RNA is indicative of depurination. Our results indicated that neither the catalytic site mutants nor the active site cleft mutants have deadenylated the rRNA

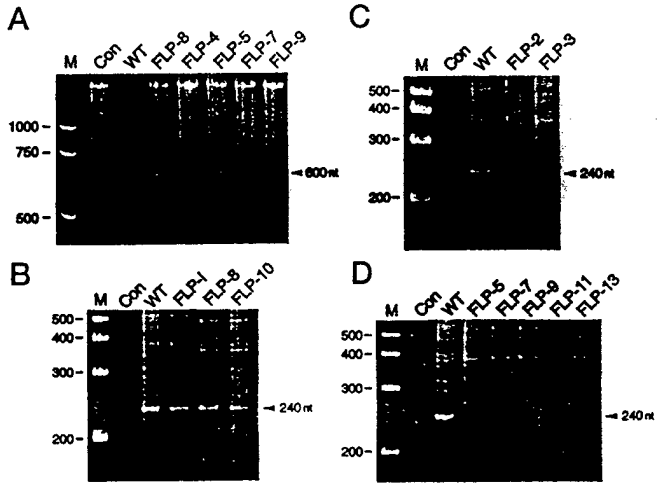

FIG. 8. ***In vitro* depurination of ribosomal RNA by wild-type and mutant recombinant PAP proteins.** *A*, total rRNA extracted from rPAP-treated rabbit ribosomes, treated with aniline, separated by 6% urea/polyacrylamide gel, and stained with ethidium bromide. The *arrow* shows the fragment split by aniline. *B–D*, 23 S and 16 S rRNA (5 μg) from *E. coli* was incubated with the test proteins (2.5 μg for *B* and 25 μg for *C* and *D*), treated with aniline, separated on a 6% urea/polyacrylamide gel, and stained with ethidium bromide. The *arrows* show the fragments split by aniline. *B*, mutants furthest from the active site. *C*, mutants that are less active. *D*, mutants with substantially reduced activity. *Con*, control ribosome incubated with bovine serum albumin, instead of PAP, and treated with aniline; *M*, molecular mass marker positions (in kDa); *WT*, wild type.

(Fig. 8A).

The ribosomal RNA depurination activity was also determined by treatment of *E. coli* 16 S and 23 S ribosomal RNA with wild-type and mutant proteins and subsequent cleavage of the treated RNA with aniline. Treatment of the naked rRNA (2 μg) with 2.5 μg of either the wild-type or the enzymatically active mutant proteins (FLP-1, FPL-8, and FLP-10) has released an RNA fragment of ≈240 nucleotides (Fig. 8*B*), whereas the less active mutants, FLP-2 and FLP-3, required a 10-fold higher amount of protein (25 μg) to release the 240-nucleotide RNA fragment (Fig. 8*C*). On the other hand, the mutants that substantially reduced the deadenylation activity (FLP-5, FLP-7, FLP-9, FLP-11, and FLP-13) did not release the fragment even at 25 μg/ml concentration of the mutant proteins (Fig. 8*D*). These results are in agreement with the data obtained from adenine release assays and protein synthesis inhibition assays.

In summary, we employed molecular modeling studies using our model of PAP-RNA complexes and site-directed mutagenesis combined with bioassays to evaluate the importance of the residues at the catalytic site and a putative RNA binding active center cleft between the catalytic site and C-terminal domain for the enzymatic deadenylation of ribosomal RNA by PAP. Our findings presented herein provide unprecedented experimental evidence that in addition to the catalytic site residues, the conserved charged and polar side chains located at the active site cleft of PAP also play a critical role in the catalytic removal of the adenine base from target ribosomal RNA substrates.

Acknowledgments—We thank Cherri R. Engstrom, Tammy J. Denton, Rebecca S. Larue, Dawn M. Dahlke, and Dina Clementson for technical assistance and Dr. Chen Mao for valuable discussion.

REFERENCES

1. Irvin, J. D. (1975) *Arch. Biochem. Biophys.* **169,** 522–526
2. Irvin, J. D. (1983) *Pharmacol Ther.* **21,** 371–387
3. Irvin, J. D., and Uckun, F. M. (1992) *Pharmacol Ther.* **55,** 279–302
4. Endo, Y., and Tsurugi, K. (1988) *J. Biol. Chem.* **263,** 8735–8739
5. Hartley, M. R., Legname, G., Osborn, R., Chen, Z., and Lord, J. M. (1991) *FEBS Lett.* **290,** 65–68
6. Endo, Y., Mitsui, K., Motizuki, M., and Tsurugi, K. (1987) *J. Biol. Chem.* **262,** 5908–5912
7. Dallal, J. A., and Irvin, J. D. (1978) *FEBS Lett.* **89,** 257–259
8. Gessner, S. L., and Irvin, J. D. (1980) *J. Biol. Chem.* **255,** 3251–3253
9. Montanaro, L., Sperti, S., Mattioli, A., Testoni, G., and Stirpe, F. (1975) *Biochem. J.* **146,** 127–131
10. Deleted in proof
11. Deleted in proof
12. Deleted in proof
13. Deleted in proof
14. Rajamohan, F., Engstrom, C. R., Denton, T. J., Engen, L. A., Kourinov, I., Uckun, F. M. (1999) *Protein Expression Purif.* **16,** 359–368
15. Monzingo, A. F., Collins, E. J., Ernst, S. R., Irvin, J. D., and Robertus, J. D. (1993) *J. Mol. Biol.* **233,** 705–715
16. Ago, H., Kataoka, J., Tsuge, H., Habuka, N., Inagaki, E., Noma, M., and Miyano, M. (1994) *Eur. J. Biochem.* **225,** 369–374
17. Kurinov, I. V., Myers, D. E., Irvin, J. D and Uckun, F. M. (1999) *Prot. Sci.* **8,** 1765–1772
18. Olson, M. A. (1997) *Proteins* **27,** 80–95
19. Bravi, G., Legname, G., and Chan, A. W. (1995) *J. Mol. Graph.* **13,** 83–88
20. Montfort, W., Villafranca, J. E., Monzingo, A. F., Ernst, S. R., Katzin, B., Rutenber, E., Xuong, N. H., Hamlin, R., and Robertus, J. D. (1987) *J. Biol. Chem.* **262,** 5398–5403
21. Huang, Q., Liu, S., Tang, Y., Jin, S., and Wang, Y. (1995) *Biochem. J.* **309,** 285–298
22. Correll, C. C., Munishkin, A., Chan, Y. L., Ren, Z., Wool, I. G., and Steitz, T. A. (1998) *Proc. Natl. Acad. Sci. U. S. A.* **95,** 13436–13441
23. Sanger, F., Nicklen, S., and Coulson, A. R. (1977) *Proc. Natl. Acad. Sci. U. S. A.* **74,** 5463- 5467
24. Boyd Hardesty, W. M., and Culp, W. (1979) *Methods Enzymol.* **33,** 316–327
25. Rajamohan, F., Venkatachalam, T. K., Irvin, J. D., and Uckun, F. M. (1999) *Biochem. Biophys. Res. Commun.* **260,** 453–458
26. Monzingo, A. F., and Robertus, J. D. (1992) *J. Mol. Biol.* **227,** 1136–1145
27. Wells, J. A. (1991) *Methods Enzymol.* **202,** 390–411
28. Nicholls, A., Sharp, K. A., and Honig, B. (1991) *Proteins* **11,** 281–296
29. Kraulis, P. J. (1991) *J. Appl. Cryst.* **24,** 946–950
30. Merritt, E. A., and Murphy, M. E. P. (1994) *Acta Cryst. D* **50,** 869–873
31. Luscombe, N. M., Laskowski, R. A., and Thornton, J. M. (1997) *Nucleic Acids Res.* **25,** 4940–4945
32. Wallace, A. C., Laskowski, R. A., and Thornton, J. M. (1995) *Protein Eng.* **8,** 127–134 3859–3864
33. InsightII User Guide (1991) Molecular Simulation, Inc. (MSI), San Diego, CA

Biochemical and Biophysical Research Communications 263, 419–424 (1999)
Article ID bbrc.1999.1335, available online at http://www.idealibrary.com on IDEAL®

Deguanylation of Human Immunodeficiency Virus (HIV-1) RNA by Recombinant Pokeweed Antiviral Protein

Francis Rajamohan,*,†,‡ Igor V. Kurinov,§ Taracad K. Venkatachalam,* and Fatih M. Uckun*,†,¶,[1]
*Biotherapy Program, †Department of Biochemistry, ‡Department of Protein Engineering, §Department of Structural Biology, and ¶Department of Virology, Hughes Institute, St. Paul, Minnesota 55113

Received August 9, 1999

Modeling studies, combined with the molecular docking of the trinucleotide GGG into the active site of the deadenylating RNA *N*-glycosidase pokeweed antiviral protein (PAP), indicated that a guanine base can fit into the active site pocket of PAP without disturbing its unique geometry and is sandwiched between residues Tyr[72] and Tyr[123] very much like an adenine base. The guanine base can form two specific hydrogen bonds with the active site residues Ser[121] and Val[73] and the attached negatively charged phosphate groups can entertain stabilizing electrostatic interactions with two clusters of positively charged patches on the PAP surface formed by Lys[210] and Arg[179] from one side and Arg[122] and Arg[135] from the other side of the active site. These observations prompted the hypothesis that the RNA depurinating activity of PAP may not be restricted to adenine residues and PAP should be capable of deguanylating ribosomal and viral RNA as well. This hypothesis was experimentally confirmed by direct demonstration that guanine base is released from both ribosomal and HIV-1 RNA after treatment with purified recombinant PAP using quantitative high performance liquid chromatography. Recombinant PAP released adenine and guanine residues at a 1:1 ratio from HIV-1 RNA and at an approximately 3:1 (adenine:guanine) ratio from *Escherichia coli* ribosomal RNA. At a concentration of 5 μM, recombinant PAP released 263 ± 10 pmol of adenine and 100 ± 11 pmol of guanine from 1 μg of *E. coli* ribosomal RNA (16S + 23S) within 4 h of treatment. By comparison, 138 ± 12 pmol of adenine and 143 ± 10 pmol of guanine were released from 1 μg of HIV-1 RNA under identical treatment conditions (5 μM recombinant PAP, 4 h treatment). The deguanylation of the ribosomal and viral RNA targets by recombinant PAP was concentration-dependent and is abolished by alanine substitutions of the catalytic active site residues Tyr[72] and Tyr[123]. To our knowledge, these findings provide the first evidence that PAP can deguanylate both ribosomal and viral RNA. © 1999 Academic Press

Key Words: **RNA; HIV; deguanylation; pokeweed antiviral protein.**

Pokeweed antiviral protein (PAP) is a naturally occurring single-chain ribosome-inactivating protein (RIP) isolated from the leaves of the pokeweed plant, *Phytolacca americana* (1, 2). PAP has been reported to act as a site-specific RNA *N*-glycosidase which catalytically removes a single adenine base from a highly conserved "α-sarcin/ricin (SR)" loop of the large ribosomal (r) RNA species in eukaryotic (28S rRNA) and prokaryotic (23S rRNA) ribosomes (3, 4). This catalytic depurination of the SR loop results in irreversible inhibition of protein synthesis at the translocation step by impairing both the elongation factor (EF)-1-dependent binding of aminoacyl-tRNA and the GTP-dependent binding of EF-2 to the affected ribosome (5). L3, a highly conserved ribosomal protein at the peptidyltransferase center, may provide a binding site for PAP, allowing depurination of the target adenine in its rRNA substrate (6). The X-ray crystallographic structure of PAP reveals a protein composed of eight alpha helices and a beta sheet consisting of six strands (7, 8). Sequence alignment of PAP with the A chain of ricin (RTA), a type-2 RIP, revealed considerable similarity and identified a number of highly conserved residues (active site residues). This highly comparable structural topology between PAP and ricin A-chain suggests a similar mechanism of rRNA depurination (1). However, PAP has recently been shown to efficiently depurinate adenine-containing polynucleotides (9), single-stranded DNA (10), viral RNAs (11) and double-stranded DNA (12), suggesting that the deadenylating activity of PAP is not restricted to the SR loop of rRNA.

Unlike ricin A chain, PAP exhibits a broad spectrum antiviral activity against plant and animal viruses, including poliovirus (13), herpes simplex virus (14), influenza virus (15), cytomegalovirus (16), and human

[1] To whom correspondence should be addressed at Hughes Institute, 2665 Long Lake Road, Roseville, MN 55113. Fax: (651) 697-1057. E-mail: fatih_uckun@ih.org.

0006-291X/99 $30.00

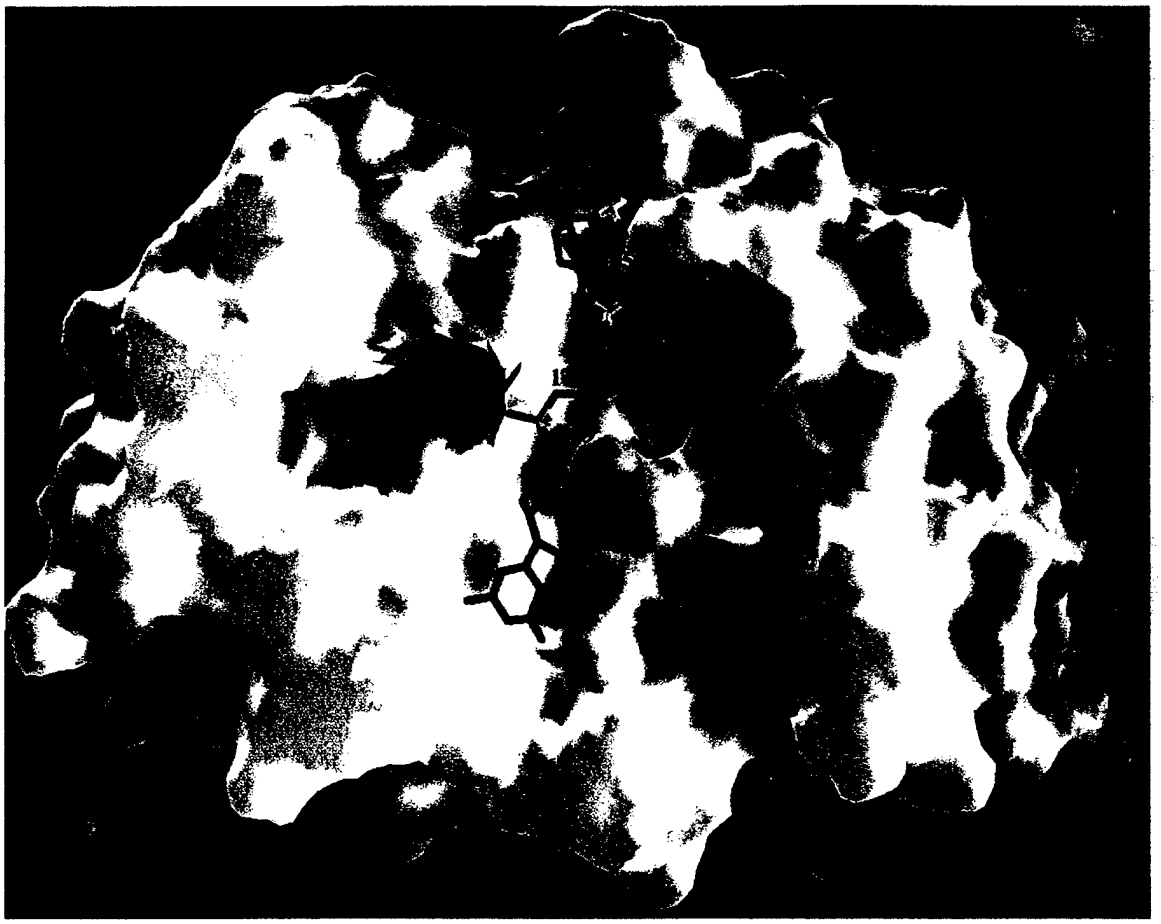

FIG. 1. Putative binding mode of GGG with PAP. The analysis of the crystal structure of PAP revealed an active site region located in the midsection of the long concave binding region. The stick molecular model represents a RNA trinucleotide GGG that was docked into the binding site by computer simulation. The figure was drawn using GRASP (25).

immunodeficiency virus (HIV)-1 (17). The molecular mechanism of the antiviral activity of PAP is under active investigation (18–20). PAP can effectively inhibit viral replication at concentrations which do not inhibit the protein synthesis of host cells (17, 21). PAP conjugates of monoclonal antibodies recognizing CD4, CD5 or CD7 antigens on the cell surface effectively inhibit HIV-1 replication in normal T-cells at noncytotoxic concentrations (17, 22). Thus, the antiviral activity of PAP, especially its anti-HIV activity, cannot be sufficiently explained by its RIP activity. Furthermore, three different PAP species from *Phytolacca americana* (PAP-I from spring leaves, PAP-II from early summer leaves, and PAP-III from late summer leaves) cause concentration-dependent depurination of genomic RNA purified from HIV-1 as well as tobacco mosaicvirus (TMV) RNA, and bacteriophage (MS 2) RNA (11). In contrast to the three PAP isoforms, the A chain of ricin (RTA) failed to cause detectable depurination of viral RNA, although it was almost as effective as PAP in inhibiting protein synthesis in cell-free translation assays. PAP-I, PAP-II, and PAP-III (but not RTA) inhibited the replication of HIV-1 in human peripheral blood mononuclear cells at nanomolar concentrations (11). These findings indicate that the highly conserved active site residues responsible for the depurination of rRNA by PAP or RTA are not sufficient for the recognition and depurination of viral RNA.

We now report the results of our modeling studies of PAP which uniquely indicated that the RNA depurinating activity of PAP may not be restricted to adenine residues and PAP should be capable of deguanylating ribosomal and viral RNA as well. This hypothesis was experimentally confirmed by direct demonstration of guanine base released from both ribosomal and HIV-1 RNA after treatment with purified recombinant PAP using quantitative high performance liquid chromatography. The deguanylation of ribosomal as well as viral RNA targets by recombinant PAP was concentration-dependent and is abolished by alanine substitutions of the catalytic active site residues Tyr^{72} and Tyr^{123}. To our knowledge, these findings provide the first evidence that PAP can deguanylate both ribosomal and viral RNA.

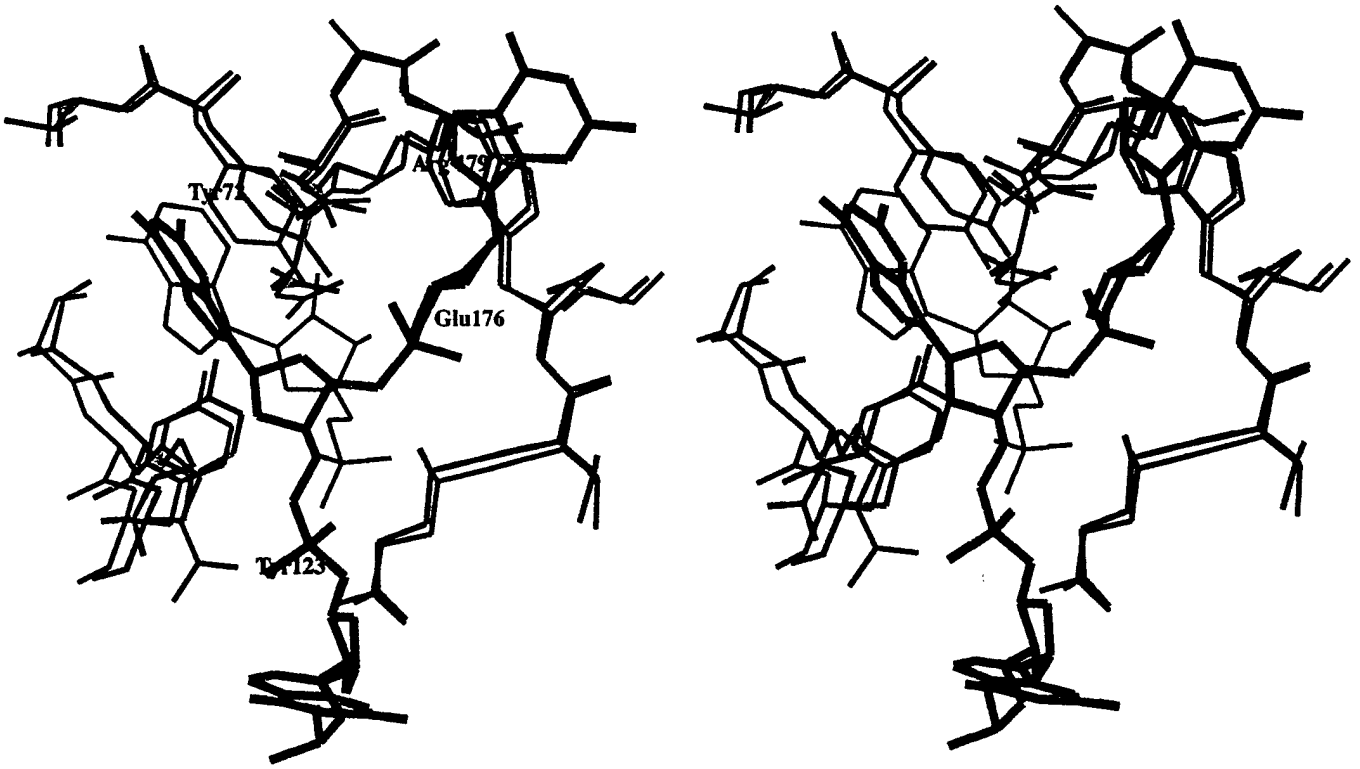

FIG. 2. Stereo view of the superimposition of computer-modeled PAP complex with GGG and X-ray structure of PAP complexed with formycin (7). Our modeled PAP complex is drawn in color with GGG in thicker lines. PAP complexed with formycin is drawn in black. Active site residues are labeled.

MATERIALS AND METHODS

Materials. Adenine and guanine were purchased from Sigma Chemical Co. (St. Louis, MO). *Escherichia coli* rRNA (16S and 23S ribosomal RNA) was purchased from Boehringer Mannheim (Indianapolis, IN). The HPLC-based guanine detection system consisted of a Hewlett Packard (HP) series 1100 (Hewlett Packard, Palo Alto, CA) in conjunction with a quaternary pump, an autosampler, an auto electronic degasser, an automatic thermostatic column compartment, diode array detector and a computer with a Chemstation software program for data analysis.

Modeling studies. The molecular docking of ligands and estimation of the interaction scores were performed using a *Fixed Docking* procedure in the *Affinity* program within the InsightII modeling software [InsightII User Guide, San Diego: MSI, 1996]. The position of the adenine base in the PAP active site (PDB access code 1QCI) was used as a guide to where the central guanine base of GGG should be placed (8). All major steric interference with protein was removed by manually adjusting the torsion angles of the phosphate backbone. Both end guaninosines were placed along the central part of the concave region of the PAP surface. This general position of GGG in the active site of PAP was then used for further modeling studies. We created a definitive binding set of PAP residues in the active site pocket to move as a 3.5 Å shell around the manually docked ligand during the energy minimization. The number of final docking positions was set to 10, although finally only 2–4 promising positions were identified. The calculations used a CVFF force-field in the *Discovery* program and a Monte Carlo strategy in the *Affinity* program. Each energy-minimized final docking position of the ligand was evaluated using the interactive score function in the *Ludi* module. Ludi score includes contribution of the loss of translational and rotational entropy of the fragment, number and quality of hydrogen bonds and contributions from ionic and lipophilic interactions to the binding energy.

Expression and purification of recombinant wildtype and mutant PAP. The expression vector for recombinant wild-type PAP (PBS-PAP) was obtained by subcloning the *PAP-I* gene (amino acids 22 to 313) into the pBluescript SK-expression vector (23). Uracil-containing template of the *PAP* gene was obtained by transforming *E. coli* CJ236 with the recombinant plasmid PBS-PAP. The oligonucleotides used for site-directed mutagenesis were synthesized by Biosynthesis Inc. (Lewisville, TX). Site-directed mutagenesis procedure for alanine substitutions of the catalytic active site residues Tyr^{72} ($^{71}LY^{72} \rightarrow {}^{71}AA^{72}$) and Tyr^{123} ($^{122}RY^{123} \rightarrow {}^{122}AA^{123}$) was as described in the manufacturer's manual (Mutagene M13 *In vitro* Mutagenesis Kit; Bio-Rad, Hercules, CA). DNA sequencing was carried out by the method of Sanger *et al.* (24) following the manufacturer's (U.S. Biochemical Corp. Cleveland, OH) instructions. Fine chemicals and restrictions enzymes were purchased from Roche Molecular Biochemicals (Indianapolis, IN). Wild-type and mutant PAP proteins were expressed in *E. coli* MV1190 as inclusion bodies, isolated, solubilized and refolded as described previously (23). The refolded proteins were analyzed by sodium dodecyl sulfate–12% polyacrylamide gel electrophoresis (SDS-12% PAGE). Protein concentrations were estimated from the gel using bovine serum albumin as a standard. The protein samples were resolved on a SDS-12% PAGE and transfered onto a polyvinylident difluoride membrane (Bio-Rad) using Bio-Rad trans-blot apperatus, as described previously (23). The membrane was immunoblotted using rabbit anti-PAP serum (1:2000 dilution) and horseradish peroxidase-conjugated goat anti-rabbit IgG (Sigma Chemical Co.) as the first and second antibodies, respectively. The blot was developed using 3,3′-diaminobenzidine (Sigma) as the colorimetric indicator for peroxidase activity. All mutant PAP proteins as well as wild-type PAP were immunoreactive with the

anti-PAP serum and were stable under our solubilization and refolding conditions. We have previously shown that the ribosome depurinating *in vitro* *N*-glycosidase activity (IC_{50} = 10 ± 4 ng/mL) and cellular anti-HIV activity of (IC_{50} = 500 ± 100 ng/mL) recombinant wild-type PAP are comparable to those of the native PAP (23). The active site mutants of PAP ($^{71}AA^{72}$ and $^{122}AA^{123}$) did not exhibit detectable *N*-glycosidase or anti-HIV activity even at concentrations as high as 10,000 ng/ml (data not shown).

Isolation of HIV-1 RNA. Human peripheral blood mononuclear cells (PBMCs) were obtained from HIV-1 negative donors and were infected (30 × 10^6 cells) with the HIV-1 strain $HTLV_{IIIB}$ at a multiplicity of infection (MOI) of 0.1, as previously described (11). The isolation of the total genomic RNA of HIV-1 was performed, as described previously (11). In brief, after 13 days of infection, 100 ml of the culture were removed and centrifuged at 10,000*g* for 5 min. The supernatant was filtered through a 0.22 μm filter, mixed with 50 ml of the virus precipitation buffer (30% PEG 8000, 0.4 M NaCl) and incubated for 3 h at 4°C. The sample was centrifuged at 15,000 rpm for 30 min and the pellet was resuspended in 4 ml of urea lysis buffer (7 M urea, 2% SDS, 0.35 M NaCl, 0.001 M EDTA, 0.01 M Tris, pH 8.0). The sample was diluted with 4 ml of RNase-free water, extracted with phenol:chloroform (24:24) and precipitated with ethanol. The RNA pellet was resuspended in 0.5 ml DNase digestion buffer (0.005 M $MgCl_2$, 0.01 M Tris, pH 7.4) and treated with 50 U of RNase-free DNase for 30 min at 37°C. The RNA was extracted with phenol:chloroform, precipitated with ethanol and resuspended in 500 μl RNase free water and stored at −20°C.

Depurination assays. Release of adenine/guanine from RNA substrates was determined using a reverse-phase Lichrospher 100, RP-18 analytical column (Hawlett-Pakard, 5 mm particle size, 250 × 4 mm). HPLC running buffer (50 mM $NH_4C_2H_3O_2$, 5% methanol, pH 5.0) was used as the mobile phase. The mobile phase was degassed automatically by the electronic degasser system. The column was equilibrated and eluted under isocratic conditions at a flow rate of 1.0 ml/min. RNA samples (2 μg) were incubated with increasing concentrations (1.0, 2.5, 5.0 and 10 μM) of recombinant PAP for 4 h at 37°C in 50 μl of binding buffer (25 mM Tris · HCl, pH 7.8, 10 mM KCl, 5 mM $MgCl_2$, 2% glycerol). The reaction was stopped by adding 100 μl of HPLC running buffer and 100 μl of the sample was injected automatically into the Lichrospher 100RP-18E column. The detector wavelength was set at 260 nm and the flow rate was maintained at 1 ml/min. Control samples containing untreated HIV-1 RNA (2 μg) and recombinant PAP (10 μM) without viral RNA were also analyzed. Calibration curves for adenine and guanine were generated to confirm the linear relationship between the absolute peak area and the quantities of adenine/guanine in the tested samples. Adenine/guanine (50 μl) at final concentration of 0.5, 1.0, 2.5, 5.0 and 10.0 μM (25, 50, 125, 250, and 500 pmol, respectively), was injected to HPLC system for analysis and the calibration curves were generated by plotting the absolute peak area (mAu) against the quantities of adenine/guanine. Unweighted linear regression analysis of the calibration curve was performed by using the CA-Cricket graph III computer program, version 1.1 (Computer Association, Inc., Islandia, NY). To evaluate the intra-assay accuracy and precision, the standard samples (0.5 and 2.5 μM) were prepared and analyzed as described previously (11). The inter-assay accuracy was calculated as the mean ratio of the calculated quantities over the known quantities from 3 independent experiments and the inter-assay precision was estimated by determining the mean coefficient of variation from 3 independent experiments.

Under the described chromatographic conditions, the retention times for guanine and adenine were 3.8 and 7.1 min, respectively. At this retention time, adenine and guanine were eluted without an interference peak from the blank control. The calibration curve for guanine was linear between 5 and 250 pmol and could be described by the regression equation: $Y = 2.407X + 1.518$ ($r = 0.999$), where Y is the amount of adenine recovered in pmol and X is the absolute peak area. The lowest limit of detection of guanine was 3.0 pmol at a signal to noise ratio of ≈3. The intra- and interassay coefficients of variation were less than 5% for both the adenine- and guanine-release assays. The overall intra- and interassay accuracies of this

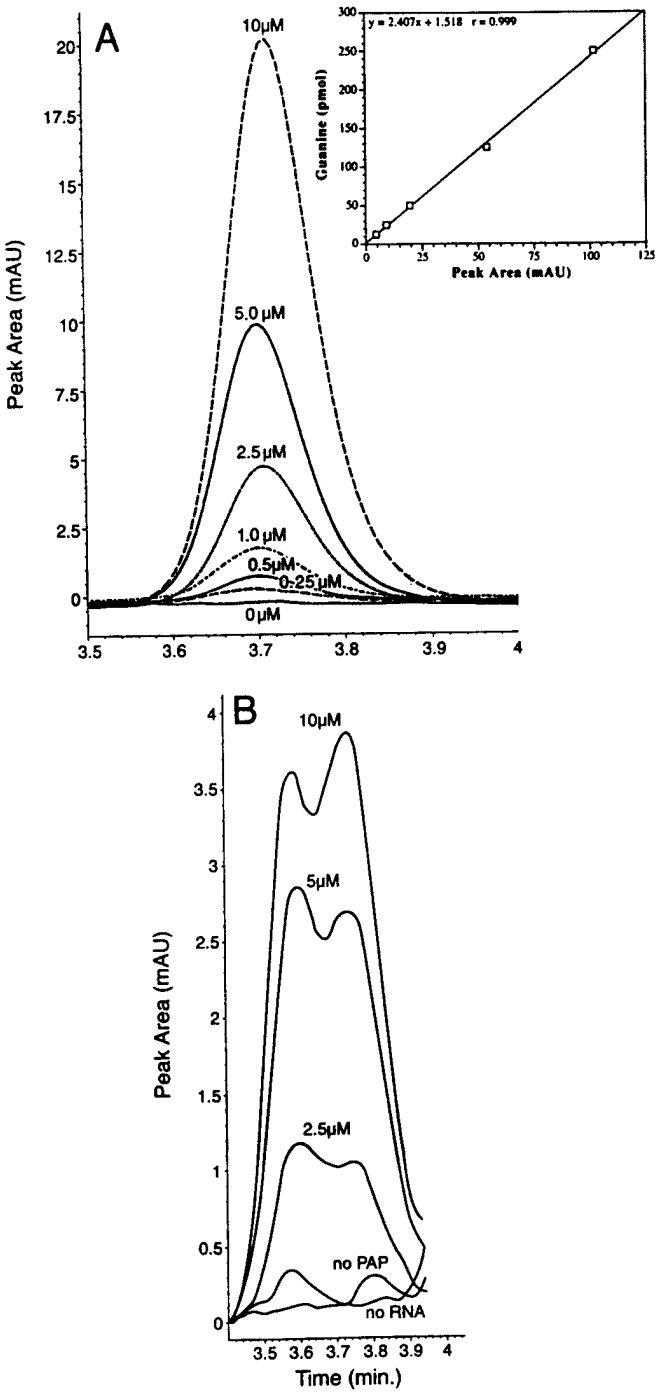

FIG. 3. HPLC-based detection of guanine released from HIV-1 RNA by recombinant PAP. (A) Chromatogram of guanine standard showing peak area and elution time. Inset: Standard curve of guanine standards. (B) Representative chromatogram of guanine release from HIV-1 RNA after treatment with increasing concentrations of recombinant PAP. Experimental conditions are described under Materials and Methods. No PAP, control sample contain untreated HIV-I RNA (2 μg). No RNA, control sample contain rPAP (10 μg) without HIV-I RNA.

method were 98.7 ± 1.7% (N = 3) and 95.7 ± 3.3% (N = 3), respectively for the adenine release assays, and 100.0 ± 2.8% (N = 3) and 100.0 ± 4.2% (N = 3), respectively for the guanine release assays.

RESULTS AND DISCUSSION

Modeling studies of a PAP-GGG complex. Computer modeling studies used an atomic model of PAP which closely corresponds to its refined X-ray structure (PDB code 1QCT), combined with the molecular docking of the trinucleotide GGG into the active site. Our model showed that the central guanine base can fit into the active site pocket of PAP without disturbing its unique geometry and is sandwiched between residues Tyr^{72} and Tyr^{123} very much like an adenine base (7, 8). The overall orientation of the docked GGG in the active site of PAP is shown in Fig. 1. In this conformation the guanine base has two hydrogen bonds with the active site residues Ser^{121} and Val^{73}. This mode of guanine base binding in the active site of PAP is energetically less favorable than the adenine base binding, where four hydrogen bonds were observed. There are additional stabilizing electrostatic interactions between the negatively charged phosphate groups and two clusters of positively charged patches on the PAP surface formed by Lys^{210} and Arg^{179} from one side and Arg^{122} and Arg^{135} from the other side of the active site. Two neighboring guanines close to the bound guanine do not have any strong and specific interactions with PAP. Many different conformations for first and third guanines were observed during computer simulation with nearly the same interaction energy. Our model demonstrated that the PAP has no selectivity towards the nucleotides close to the active site.

Figure 2 shows a superimposition of the modeled PAP complex with GGG and the X-ray structure of PAP with bound formycin. Glu^{176} and Arg^{179} are believed to be involved in the enzymatic cleavage of the bond between adenine base and sugar in adenine-containing oligonucleotides (7). The observed conformation of the active site residues Glu^{176} and Arg^{179} with nearly the same spatial position as in other PAP-ligand complexes may also be favorable for enzymatic cleavage of the C—N bond in guanine-containing oligonucleotides. It is conceivable that PAP could release a guanine base from the oligonucleotide targets with the help of Arg^{179} and Glu^{176} upon only a small structure rearrangement of nearby residues of the active site in the same manner it releases an adenine base. Taken together, these observations prompted the hypothesis that the RNA depurinating activity of PAP may not be restricted to adenine residues and PAP should be capable of deguanylating ribosomal and viral RNA as well.

Depurination of E. coli rRNA and HIV-1 RNA by recombinant PAP. We next sought to experimentally determine if PAP can deguanylate RNA targets as implicated by our modeling studies. To this end, we examined the depurination of ribosomal (*E. coli*) and viral (HIV-1) RNA by recombinant PAP using both adenine and guanine release assays (Fig. 3). Recombinant PAP released adenine and guanine residues at a 1:1 ratio from HIV-1 RNA and at an approximately 3:1 (adenine:guanine) ratio from *E. coli* ribosomal RNA. At a concentration of 5 μM, recombinant PAP released 263 ± 10 pmol of adenine and 100 ± 11 pmol of guanine from 1 μg of *E. coli* ribosomal RNA (16S + 23S) within 4 h of treatment (Fig. 4, Table 1). By comparison, 138 ± 12 pmol of adenine and 143 ± 10 pmol of guanine were released from 1 μg of HIV-1 RNA under identical treatment conditions (5 μM recombinant PAP, 4 h treatment) (Fig. 4, Table 1). The deguanyla-

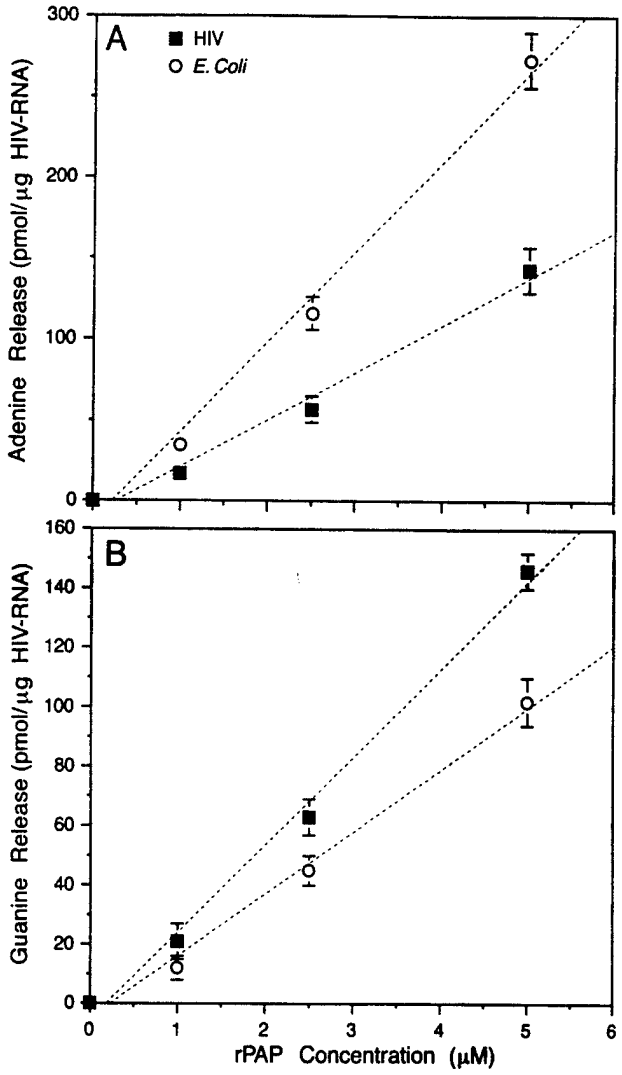

FIG. 4. Concentration-dependent depurination of *E. coli* rRNA and HIV-1 RNA by recombinant PAP. (A) Adenine release after treatment with recombinant PAP. (B) Guanine release after treatment with recombinant PAP. Values were calculated using the standard curve for adenine and guanine. Lines represent the linear regression using data points at the exponential phase. The experimental conditions are as described under Materials and Methods.

TABLE 1

Depurination of *E. coli* rRNA and HIV-1 RNA by Recombinant PAP

Protein	RNA	Purines released (pmol/μg RNA)[a] Adenine	Guanine
rPAP, WT	*E. coli*	263 ± 10	100 ± 11
	HIV-I	138 ± 12	143 ± 10
rPAP, ^{71}AA^{72}	*E. coli*	9 ± 2	6 ± 1
	HIV-I	UD[b]	UD
rPAP, ^{122}AA^{123}	*E. coli*	10 ± 2	5 ± 1
	HIV-I	UD	UD

[a] The values were calculated from the linear regression analysis of the dose-dependent depurination curves (Figs. 4A and B) for a rPAP concentration of 5 μM. Each value is the mean ± SD of three experiments.

[b] UD, undetectable.

tion of the ribosomal and viral RNA targets by recombinant PAP was concentration-dependent and is nearly abolished by alanine substitutions of the catalytic active site residues Tyr^{72} or Tyr^{123} (Table 1).

To our knowledge, these findings provide the first evidence that PAP can deguanylate both ribosomal and viral RNA. Our modeling studies of PAP complex with GGG had indicated that the guanine base interactions in the active site and phosphate backbone are the main contributors to the binding of GGG fragment by PAP. The model of PAP-GGG complex does not show any base specific contacts for end-points guanine bases with PAP residues, thereby providing PAP with a flexibility for depurinating multiple purine-containing oligonucleotide substrates without a limiting selectivity towards the closest nucleotide residues. While extending our recent structural and biochemical studies of PAP (8, 11), the present study prompts the hypothesis that the potent anti-HIV activity of PAP may in part be due to the previously unknown deguanylating activity of PAP on viral RNA.

ACKNOWLEDGMENTS

The authors thank D. M. Dahlke and K. Chang for their technical assistance. This material is based in part upon work sponsored by the Defense Advanced Research Projects Agency under Grant N65236-99-1-5422 awarded to F.M.U. The content does not necessarily reflect the position or policy of the U.S. Government, and no official endorsement should be inferred.

REFERENCES

1. Irvin, J. D. (1995) Antiviral Proteins from Phytolacca, CRC Press, Boca Raton.
2. Irvin, J. D. (1983) *Pharmacol. Ther.* **21,** 371–387.
3. Endo, Y., Mitsui, K., Motizuki, M., and Tsurugi, K. (1987) *J. Biol. Chem.* **262,** 5908–5912.
4. Endo, Y., and Tsurugi, K. (1988) *J. Biol. Chem.* **263,** 8735–8739.
5. Irvin, J. D., and Uckun, F. M. (1992) *Pharmacol. Ther.* **55,** 279–302.
6. Hudak, K. A., Dinman, J. D., and Tumer, N. E. (1999) *J. Biol. Chem.* **274,** 3859–3864.
7. Monzingo, A. F., Collins, E. J., Ernst, S. R., Irvin, J. D., and Robertus, J. D. (1993) *J. Mol. Biol.* **233,** 705–715.
8. Kurinov, I. V., Myers, D. E., Irvin, J. D., and Uckun, F. M. (1999) *Prot. Sci.* **8** (in press).
9. Barbieri, L., Valbonesi, P., Bonora, E., Gorini, P., Bolognesi, A., and Stirpe, F. (1997) *Nucleic Acids Res.* **25,** 518–522.
10. Nicolas, E., Beggs, J. M., Haltiwanger, B. M., and Taraschi, T. F. (1998) *J. Biol. Chem.* **273,** 17216–17220.
11. Rajamohan, F., Venkatachalam, T. K., Irvin, J. D., and Uckun, F. M. (1999) *Biochem. Biophys. Res. Commun.* **260,** 453–458.
12. Wang, P., and Tumer, N. E. (1999) *Nucleic Acids Res.* **27,** 1900–1905.
13. Ussery, M. A., Irvin, J. D., and Hardesty, B. (1977) *Ann. N.Y. Acad. Sci.* **284,** 431–440.
14. Aron, G. M., and Irvin, J. D. (1980) *Antimicrob. Agents Chemother.* **17,** 1032–1033.
15. Tomlinson, J. A., Walker, V. M., Flewett, T. H., and Barclay, G. R. (1974) *J. Gen. Virol.* **22,** 225–232.
16. Gehrz, R. C., Wilson, C., Eckhardt, J., Myers, D., Irvin, J. D., and Uckun, F. M. (1991) *in* Progress in Cytomegalovirus Research (Landini, M. P., Ed.), pp. 353–356, Elsevier.
17. Zarling, J. M., Moran, P. A., Haffar, O., Sias, J., Richman, D. D., Spina, C. A., Myers, D. E., Kuebelbeck, V., Ledbetter, J. A., and Uckun, F. M. (1990) *Nature* **347,** 92–95.
18. Chaddock, J. A., Monzingo, A. F., Robertus, J. D., Lord, J. M., and Roberts, L. M. (1996) *Eur. J. Biochem.* **235,** 159–166.
19. Bonness, M. S., Ready, M. P., Irvin, J. D., and Mabry, T. J. (1994) *Plant J.* **5,** 173–183.
20. Tumer, N. E., Parikh, B. A., Li, P., and Dinman, J. D. (1998) *J. Virol.* **72,** 1036–1042.
21. Teltow, G. J., Irvin, J. D., and Aron, G. M. (1983) *Antimicrob. Agents Chemother.* **23,** 390–396.
22. Zarling, J. M., Moran, P. A., Haffar, O., Diegel, M., Myers, D. E., Kuelbeck, V., Ledbetter, J. A., and Uckun, F. M. (1991) *Int. J. Immunopharmacol.* **13,** 63–68.
23. Rajamohan, F., Engstrom, C. R., Denton, T. J., Engen, L. A., Kourinov, I., Uckun, F. M. (1999) *Protein Express. Purif.* **16,** 359–368.
24. Sanger, F., Nicklen, S., and Coulson, A. R. (1977) *Proc. Natl. Acad. Sci. USA* **74,** 5463–5467.
25. Nicholls, A., Sharp, K. A., and Honig, B. (1991) *Proteins* **11,** 281–296.

Protein Expression and Purification 16, 359–368 (1999)
Article ID prep.1999.1084. available online at http://www.idealibrary.com on IDEAL®

High-Level Expression and Purification of Biologically Active Recombinant Pokeweed Antiviral Protein

Francis Rajamohan,*,†,[1] Cherri R. Engstrom,†,‡ Tammy J. Denton,*,† Lisa A. Engen,*,† Igor Kourinov,* and Fatih M. Uckun*,§

*Biotherapy Program, †Department of Protein Engineering, ‡Department of Biochemistry, and §Department of Virology, Hughes Institute, St. Paul, Minnesota 55113

Received March 8, 1999

Pokeweed antiviral protein (PAP) from the leaves of the pokeweed plant, *Phytolacca americana*, is a naturally occurring single-chain ribosome-inactivating protein, which catalytically inactivates both prokaryotic and eukaryotic ribosomes. The therapeutic potential of PAP has gained considerable interest in recent years due to the clinical use of native PAP as the active moiety of immunoconjugates against cancer and AIDS. The clinical use of native PAP is limited due to inherent difficulties in obtaining sufficient quantities of a homogenously pure and active PAP preparation with minimal batch to batch variability from its natural source. Previous methods for expression of recombinant PAP in yeast, transgenic plants and *Escherichia coli* have resulted in either unacceptably low yields or were too toxic to the host system. Here, we report a successful strategy which allows high level expression of PAP as inclusion bodies in *E. coli*. Purification of refolded recombinant protein from solubilized inclusion bodies by size-exclusion chromatography yielded biologically active recombinant PAP (final yield: 10 to 12 mg/L). The ribosome depurinating *in vitro* N-glycosidase activity and cellular anti-HIV activity of recombinant PAP were comparable to those of the native PAP. This expression and purification system makes it possible to obtain sufficient quantities of biologically active and homogenous recombinant PAP sufficient to carry out advanced clinical trials. To our knowledge, this is the first large-scale expression and purification of biologically active recombinant PAP from *E. coli*. © 1999 Academic Press

Pokeweed antiviral protein (PAP) is a 29-kDa ribosome-inactivating protein isolated from the spring leaves of the pokeweed plant, *Phytolacca americana* (1). The primary structure of PAP is composed of 313 amino acids (2). During posttranslational modification, 22 amino acids (leader sequence) from the N-terminal end and 29 amino acids from the C-terminal end of PAP are cleaved leaving a mature protein of 262 amino acids with a final molecular weight of approximately 29 kDa (3). The X-ray crystallographic structure of PAP reveals a protein composed of eight α helices and a β sheet consisting of six strands (3).

PAP is a site-specific RNA *N*-glycosidase that enzymatically removes a single adenine base (A4324) from a highly conserved, surface exposed "α-sarcin" loop of the large rRNA species in eukaryotic (28S rRNA) and prokaryotic (23S rRNA) ribosomes (4, 5). This catalytic depurination of the α-sarcin loop, which is positioned in immediate vicinity of the peptidyltransferase center within the 50S subunit of *Escherichia coli* ribosomes, impairs the interactions between ribosomes and elongation factor 2 (EF-2), resulting in irreversible inhibition of protein synthesis at the EF-2-mediated translocation step (6–8). Recent evidence indicates that L3, a large ribosomal subunit protein in the peptidyltransferase center, may provide a receptor site for PAP, allowing depurination of the target adenine in its rRNA substrate (9). Because of its ability to irreversibly inhibit protein synthesis, PAP has been targeted to cancer cells using monoclonal antibodies (10,11). PAP-containing immunoconjugates against CD7 and CD19 surface antigens on leukemia cells have shown potent and selective antileukemic activity both *in vitro* and *in vivo* (11,12). These biotherapeutic agents resulted in long-term survival of SCID mice challenged with an otherwise invariably fatal number of human leukemia cells at dose levels nontoxic to mice or cynomolgus monkeys, and their efficacy is currently being evaluated in clinical trials of the Children's Cancer Group (13).

[1] To whom correspondence should be addressed at Hughes Institute, 2657 Patton Road, Roseville, MN 55113. Fax: (651) 628-9891.

1046-5928/99 $30.00

PAP has also been shown to effectively inhibit the replication of several plant and animal viruses including poliovirus (14), herpes simplex virus (15), cytomegalovirus (16), influenza virus (17), and human immunodeficiency virus (HIV)-1 (18). In our first study on the anti-HIV activity of PAP, we found that PAP conjugated to monoclonal antibodies recognizing CD4, CD5, or CD7 antigens effectively inhibited HIV-1 replication in normal $CD4^+$ T-cells infected with a laboratory strain of HIV-1, as well as in activated T-cells from asymptomatic HIV-1-seropositive donors (18,19). Production of p24 and p55 gag proteins as well as gp160 env protein in $CD4^+$ T-cells was inhibited by PAP immunoconjugates at picomolar concentrations that did not affect (a) *in vitro* hematopoietic colony formation by normal bone marrow progenitor cells or (b) proliferation and CD4 antigen-linked transmembrane signaling of T-cells (18). Notably, HIV-1 protein synthesis in infected T-cells was at least 3 log more sensitive to PAP immunoconjugates than was protein synthesis necessary for T-cell function or survival (18). In a subsequent study, we found that (a) clinical HIV-1 isolates are >4 log more sensitive to PAP immunoconjugates than to zidovudine, and (b) replication of zidovudine-resistant HIV-1 isolates in T-cells is effectively inhibited by picomolar concentrations of PAP immunoconjugates that are not toxic to lymphohematopoietic cells including the normal bone marrow progenitor cell pop ulations CFU-GM, BFU-E, and CFU-GEMM; B-lymphocyte precursors/B-cells; or T-lymphocyte precursors/T-cells (18–20). Notably, PAP immunoconjugates showed marked anti-HIV activity in an *in vivo* SCID mouse model of human AIDS at dose levels well tolerated by cynomolgus monkeys (19). A Phase I clinical study has been initiated to evaluate the safety and anti-HIV activity of our anti-CD7 PAP immunoconjugate in AIDS patients. The molecular mechanism of the antiviral activity of PAP is under active investigation. Besides its ability to inhibit viral protein synthesis, PAP is also capable of directly depurinating viral RNA (21). Furthermore, PAP also displays viral RNA-specific effects *in vivo* and has been shown to inhibit ribosomal frameshifting and retrotransposition, a molecular mechanism used by many RNA viruses to produce Gag–Pol fusion proteins (22).

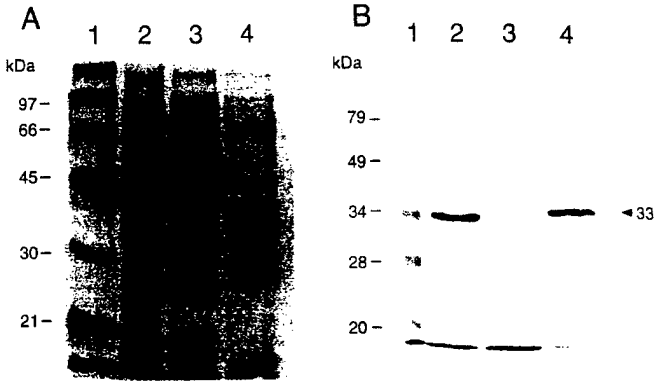

FIG. 2. (A) Coomassie blue-stained SDS–12% PAGE gel comparing the expression of recombinant PAP in soluble and insoluble fractions of *E. coli* cell lysate. (B) Western blot analysis of the *E. coli* fractions using anti-PAP antibody. Lane 1, molecular mass marker positions; lane 2, total cell lysate; lane 3, soluble fraction; lane 4, insoluble fraction. Each lane contained 5.0 μg of protein.

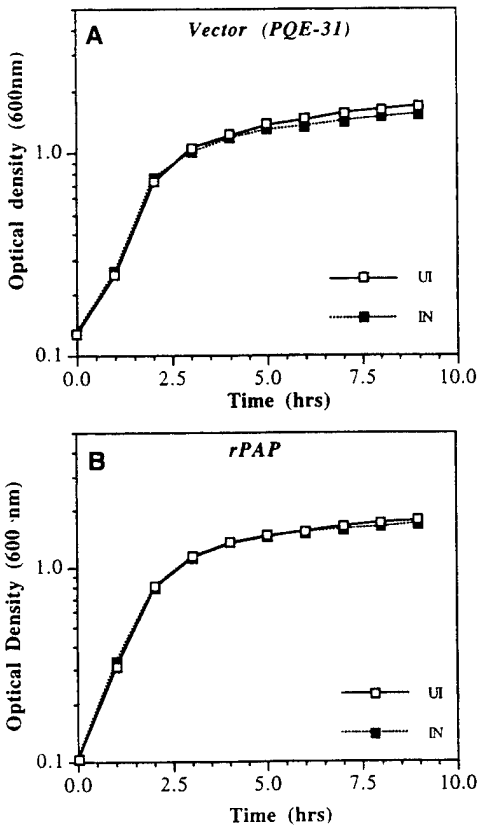

FIG. 1. Effect of PAP expression on the growth of *E. coli*. UI, uninduced; IN, culture induced with 1 mM IPTG as described under Materials and Methods.

The therapeutic applications of PAP both as an antiviral and as an anticancer agent would greatly benefit from a large-scale production of PAP by the methods of recombinant DNA technology. Several investigators have attempted to express the full-length or N-terminal truncated PAP gene in *E. coli*. However, either the expression levels of PAP in those experiments were too low or the produced recombinant PAP was too toxic to the host system (23,24). Here, we report the first successful expression of the *PAP* gene, devoid of the N-terminal signal peptide (residues 1 to 22), in *E. coli* under a phage T5 promoter and an inducible *lac* operator. The recombinant PAP, which accumulated in bacterial cytoplasm in the form of inclusion bodies, was solubilized and refolded *in vitro*. The biological activi-

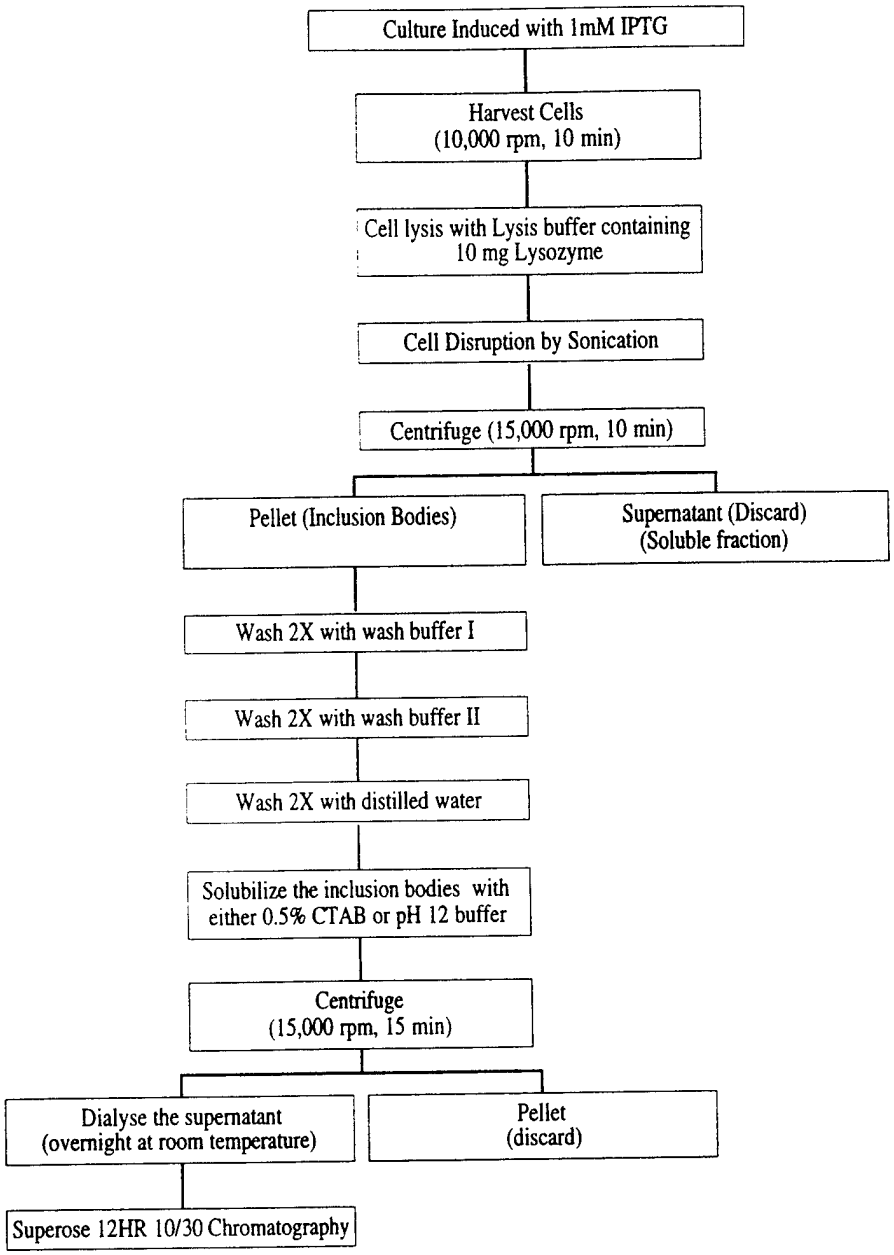

FIG. 3. Schematic flow chart for the purification of recombinant PAP from *E. coli* MV1190.

ities (i.e., rRNA-specific *N*-glycosidase and cellular anti-HIV activities) of the purified recombinant PAP were comparable to those of the native PAP purified from the spring leaves of *P. americana*. This expression and purification system, which is amenable to further scale-up, should provide sufficient amounts of biologically active and homogenously pure recombinant PAP for clinical use.

MATERIALS AND METHODS

Construction of full-length PAP in PQE-31. The isolation and sequencing of the PAP gene was previously reported (25). The *PAP* gene was cloned into the *E. coli* expression vector, PQE-31 (Qiagen, Santa Clarita, CA), as follows: The *PAP* gene was amplified by polymerase chain reaction (PCR) using the following primers PAP-Bam (5′CGCGGATCCAGTGAATACAATCATCTACA-ATGTTGGAAGTACC3′), which introduces a *Bam*HI site at the N-terminus, and PAP-H3 (5′GCCTCTTATT-TAAGCTTTATAATATAGTTGGAG3′), which introduces a *Hin*dIII site at the C-terminus. The gel-purified PCR product (930 bp) was digested with *Bam*HI and *Hin*d-III restriction enzymes and subcloned into the PQE-31 vector (Qiagen) treated with the corresponding enzymes.

TABLE 1

Yield of Recombinant PAP at Different Stages of Purification

Fraction	Protein (mg/L)	Percentage of total protein
Total cell lysate	210 ± 9	100
Inclusion bodies	52 ± 5	25
CTAB solubilized	31 ± 2	15
pH solubilized	33 ± 2	16
After refolding	17 ± 3	8
After gel filtration	10 ± 2	5

Note. The values given are means and SEM of six experiments.

PQE-31 vector contains a powerful phage T5 promoter (recognized by *E. coli* RNA polymerase) and a synthetic ribosome-binding site. Expression is controlled through a double *lac* operator system and is induced by addition of IPTG. The final construct that encodes the full-length PAP (amino acids 22 to 313) in PQE-31 is referred to as PQE-FLP. Oligonucleotides (25–30 nucleotides long) with *Bam*HI and *Hin*dIII linkers were synthesized by Biosynthesis Inc (Lewisville, TX).

Expression and purification of PAP inclusion bodies. The *E. coli* strain, MV1190, was transformed with plasmid PQE-FLP and the transformants were selected on LB (Luria-Bertain) agar plates containing ampicillin (100 μg/ml). An Erlenmeyer flask containing 500 ml LB broth supplemented with 100 μg/ml ampicillin was inoculated with an overnight culture (5 ml) of PQE-FLP-transformed MV1190 and cultured under vigorous shaking at 37°C. Expression of recombinant PAP was induced by adding 1 mM isopropylthiogalactoside (IPTG) when the cells reached an optical density of 0.6 to 0.8 at 600 nm and the incubation was continued for an additional 4 h. Cells were harvested by centrifugation (10,000 rpm for 10 min) and resuspended in 25 ml lysis buffer (50 mM Tris, pH 8.0, 50 mM EDTA, 15% sucrose) containing 10 mg lysozyme (50,000 U/mg, Sigma Chemical Co., St Louis, MO). The cell suspension was incubated for 2 h at 37°C with gentle shaking and then sonicated with a Branson ultrasonic disintegrator (VWR Scientific Products, Chicago, IL) for 2–4 min. The cell lysate was centrifuged at 15,000 rpm for 15 min and the pellet containing the inclusion bodies was washed two times with 50 ml of wash buffer I (0.5 M NaCl, 2% Triton X-100), two times with wash buffer II (0.5 M NaCl), and two times with distilled water. The pelleted PAP inclusion bodies were resuspended in 10 ml of sterile distilled water and stored at 4°C until further use.

Solubilization of PAP-containing E. coli inclusion bodies. The inclusion bodies were centrifuged at 15,000 rpm for 10 min. The pellet was solubilized in 10 ml of 50 mM Tris–HCl (pH 8.0) containing an appropriate concentration (0.1 to 5%) of detergents at room temperature overnight. The insoluble material was removed by centrifugation and the supernatant was dialyzed overnight at room temperature against 10 mM Tris buffer (pH 8.0). After dialysis, the samples were centrifuged at 15,000 rpm for 15 min to remove the precipitate, if any, and were analyzed on a SDS–12% polyacrylamide gel electrophoresis (PAGE). For pH solubilization, the inclusion bodies were suspended in 5 mM K_2HPO_4, pH 12, to a final volume of 8 ml and incubated at room temperature with shaking for 10 min. The insoluble proteins were removed by centrifugation at 15,000 rpm for 5 min. The soluble fraction of recombinant (r)PAP was renatured by adding 20% glycerol (final concentration) and dialyzing very slowly in 4 L of 5 mM K_2HPO_4, pH 8, overnight. The dialyzed samples were loaded onto a gel filtration column (Superose 12 HR 10/30, Pharmacia) and equilibrated with 20 mM citric acid, pH 6.0, at a flow rate of 0.3 ml/min. Fractions of 1.0 ml in volume were collected and analyzed on a SDS–12% PAGE. Protein concentrations were determined using the BCA assay system (Pierce, Rockford, IL) with bovine serum albumin as a standard.

Immunoblot analysis of PAP proteins. The protein samples were resolved on a SDS–12% PAGE and transferred onto a polyvinylidene difluoride membrane using the Bio-Rad trans-blot apparatus, as described (26). The membrane was immunoblotted using rabbit anti-PAP antibody (1:2000 dilution) and horseradish

TABLE 2

Comparison of the Solubility (%) of Recombinant PAP Inclusion Bodies in Different Detergents

Solubilizing agent	Detergent concentrations (%) 0.5	1.0	2.5	5.0
Nonionic				
Triton X-100	0[a]	0	0	0
Tween 20	0	0	0	0
n-Octyl-glucopyranoside	<10	<10	<10	<10
n-Octyl-thioglucopyranoside	0	<10	<10	<10
Big CHAP	<10	<10	<10	<10
NP-40	0	0	0	0
Chaps	0	0	0	0
Zwitterionic				
Zwittergent 3-10	<10	<10	<10	<10
Ionic				
Cetyltrimethylammonium bromide (CTAB)	90	90	90	>95
BATC	30	50	60	60
Lauroylsarcosine	20	50	90	>95
pH	9	10	11	12
pH solubilization (5 mM K_2HPO_4)	0	15	50	>95

[a] Numbers indicate the percentage of solubility.

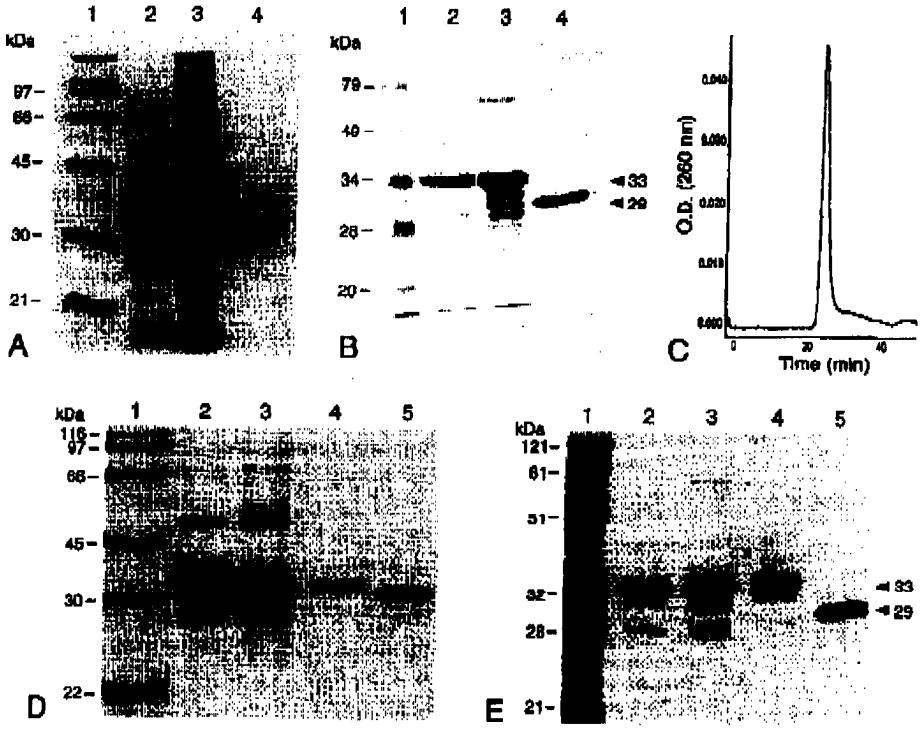

FIG. 4. Solubilization and purification of recombinant PAP (rPAP). (A) Coomassie blue-stained SDS–12% PAGE gel comparing the yield of pH solubilized rPAP. (B) Western blot analysis of the pH solubilized samples using anti-PAP antibody. Lane 1, molecular mass marker positions; lane 2, inclusion bodies; lane 3, inclusion bodies solubilized with pH 12 buffer; lane 4 native PAP purified from pokeweed spring leaves. (C) Purification of rPAP using Superose 12 HR10/30 column which was equilibrated with 20 mM citric acid, pH 6.0, at a flow rate of 0.3 ml/min. (D) Coomassie blue-stained SDS–12% PAGE gel comparing the yield of 0.5% CTAB solubilized and purified rPAP. (E) Western blot analysis of the CTAB solubilized samples using anti-PAP antibody. Lane 1, molecular mass marker positions; lane 2, inclusion bodies; lane 3, inclusion bodies solubilized with 0.5% CTAB; lane 4, Superose 12 HR10/30 column purified sample (peak fraction from C); lane 5, nPAP purified from pokeweed spring leaves. Each lane contained 5.0 μg of protein.

peroxidase-conjugated goat anti-rabbit IgG (Sigma Chemical Co.) as the first and second antibodies, respectively. 3,3′-Diaminobenzidine was used as the colorimetric indicator for peroxidase activity (Sigma Chemical Co.).

Cell-free translation assays. Varying amounts (0.01 to 100 ng/ml) of recombinant (pH solubilized) or native (n) PAP were added to the translation mixture containing: 10 μl of rabbit reticulocyte lysate (Promega, Madison, WI), 0.5 μl of RNasin, 1.0 μl of 1 mM amino acids mixture (minus methionine), and 1.0 μl of [^{35}S]methionine (10 mCi/ml, Amersham, Arlington Heights, IL). The final volume was adjusted to 19 μl with RNase-free water. The reaction mixture was incubated for 15 min at room temperature. Protein translation was initiated by adding 1.0 μl of 1:8 diluted luciferase mRNA (0.12 μg). After 2 h of incubation at 30°C, 10 μl of each reaction mixture was resolved by SDS–PAGE on a 10% SDS gel, dried, and autoradiographed. Alternatively, the incorporation of radioactive label into protein was determined by precipitating the synthesized luciferase protein (61 kDa) with 5% trichloroacetic acid according to the manufacturer's instructions (Promega). A minimum of ten concentrations of rPAP or nPAP were used for the calculation of the IC_{50} (50% inhibitory concentration) values. The IC_{50} values (from precipitation assays) were calculated by nonlinear regression analysis (Prism-2 GraphPad Software, San Diego, CA) using the average value of three independent experiments. The cpm values in control samples with all the reagents added except PAP ranged from 3.5 to 4.0 × 10^7 cpm/ml and were used as 100% incorporation when determining the percentage of control protein synthesis values for PAP-treated samples.

In vitro assays of anti-HIV-1 activity. The anti-HIV-1 activities of nPAP and rPAP (pH solubilized) were evaluated by determining their ability to inhibit the replication of the HIV-1 strain HTLV-IIIB in normal human peripheral blood mononuclear cells from HIV-negative donors, as previously described (20). Per-

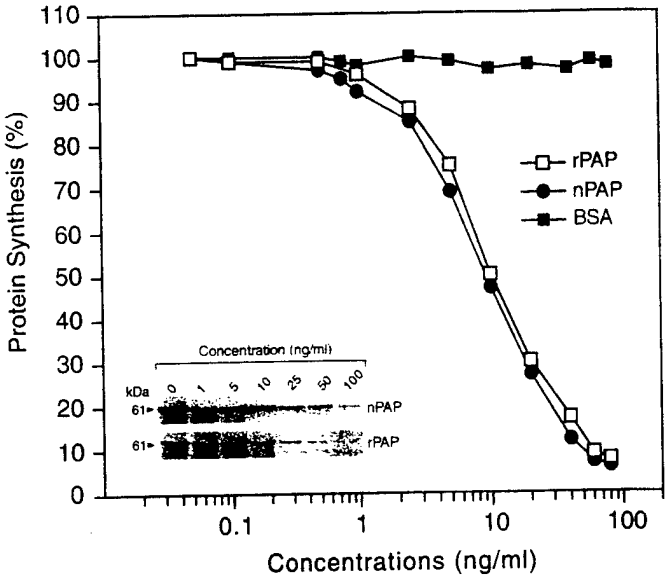

FIG. 5. Ribosome inhibitory activity of recombinant and native PAP in *in vitro* rabbit reticulocyte lysate system. Each value is an average of three experiments. Protein synthesis was measured by [^{35}S]methionine incorporation and the sample with all the reagents except PAP was assigned a value of 100% incorporation. (Inset) luciferase protein synthesized in the presence or absence of native (nPAP) and recombinant PAP (rPAP). Samples were resolved on SDS–10% PAGE and autoradiographed. Numbers at the top indicate the concentrations of PAP.

centage of viral inhibition was calculated by comparing the mean p24 antigen/reverse transcriptase (RT) assay values for the test substance-treated infected cells with the p24/RT values for untreated infected cells (i.e., virus controls). The IC_{50} values were calculated by nonlinear regression analysis (Prism-2 program) using the data from three independent experiments.

Ribosomal RNA depurination assay. Ten micrograms of *E. coli* 16S and 23S ribosomal RNA (Boehringer Mannheim, Indianapolis, IN) was incubated with increasing concentrations (0.5 to 5 μg) of either rPAP (pH solubilized) or nPAP in 50 μl (final volume) of binding buffer (25 mM Hepes, pH 7.8, 50 mM KCl, 1.5 mM $MgCl_2$, 5% glycerol) at 30°C for 30 min. The reaction was stopped by the addition of SDS (0.1%). The RNA was extracted with phenol:chloroform (24:24), precipitated with ethanol, and treated with 20 μl of 1 M anilin acetate (pH 4.5) for 30 min on ice. The RNA was precipitated with ethanol, electrophoresed in a 4% urea/polyacrylamide gel, and stained with ethidium bromide as previously described (9).

RESULTS

Expression of Recombinant PAP in E. coli

The *PAP* gene encoding amino acids 23 to 313 (pre-PAP) was cloned into PQE-31 vector (PQE-FLP) and expressed in *E. coli* MV1190 in the presence of IPTG. Since PAP inactivates prokaryotic and eukaryotic ribosomes, we first examined the inhibitory effects of PAP on the growth of *E. coli.* Cultures were initiated from overnight precultures and the growth, with and without the presence of IPTG in the medium, was monitored by measuring at A_{600}. In our experiments, the expression of PAP did not appear to have any effect on the growth of *E. coli,* since the cells expressing either the *PAP* gene or the vector alone grew similarly in the liquid medium (Fig. 1). The soluble and insoluble fractions of total *E. coli* cell lysate were separated by centrifugation and resolved by SDS–PAGE to determine the nature of PAP expression in *E. coli* (Fig. 2A). Western blot analysis using anti-PAP antibody revealed that the PAP was located largely in the insoluble fraction, suggesting that the PAP is aggregated as insoluble inclusion bodies in the cytoplasm (Fig. 2B). The overall purification scheme of inclusion bodies is presented in Fig. 3. The inclusion body fraction, containing mainly the recombinant PAP (25–27% of total protein), was isolated and used for further solubilization. The yield of recombinant PAP at various steps of purification from *E. coli* is presented in Table 1.

Solubilization, Renaturation, and Purification of Recombinant PAP

Solubilization of the PAP inclusion bodies was initially attempted using nonionic, zwitterionic, and ionic detergents. The results presented in Table 2 indicate that the PAP inclusion bodies were not soluble in nonionic detergents such as Tween 20, Triton X-100, Chaps, and NP-40 and poorly soluble (<10%) in *n*-octyl-glucopyranoside, Big CHAP, and Zwittergent 3-10, at concentrations up to 5%. In contrast, the ionic detergents CTAB and lauroylsarcosine solubilized the PAP inclusion bodies efficiently (Table 2). Over 90% of PAP inclusion body proteins were solubilized and re-

TABLE 3

Potency of Native and Recombinant PAP in Inhibiting Protein Synthesis and HIV-1 Replication

	IC_{50} (μg/ml)		
Protein	Anti-ribosome[a]	Anti-HIV (p24)[b]	Anti-HIV (RT)[c]
nPAP	0.010 ± 0.004	0.4 ± 0.1	0.5 ± 0.2
rPAP	0.013 ± 0.005	0.5 ± 0.1	0.4 ± 0.2

[a] Anti-ribosome activity was measured by rabbit reticulocyte lysate *in vitro* translation assays.

[b] Anti-HIV activity was determined from p24 viral core protein assays.

[c] Anti-HIV activity was determined from reverse transcriptase (RT) activity.

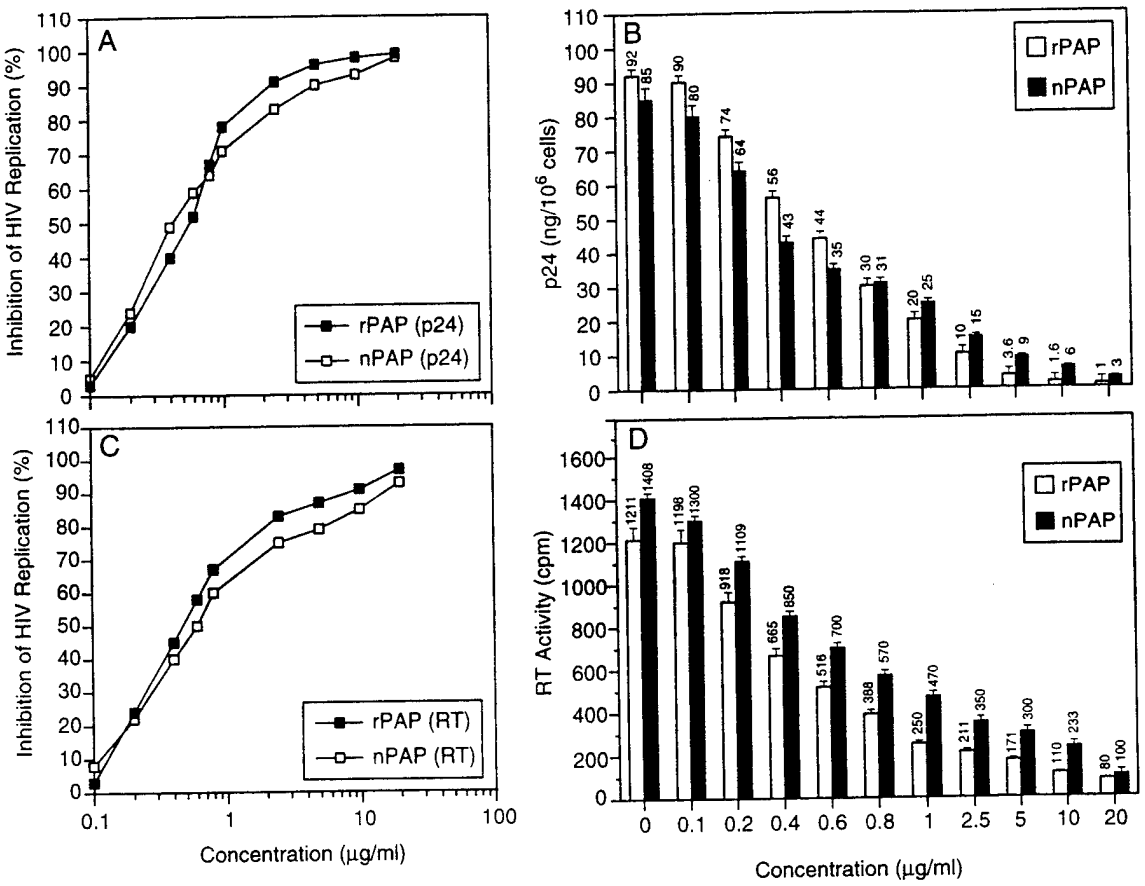

FIG. 6. (A) Inhibition of HTLV-IIIB (HIV-1) replication by native (nPAP) and recombinant PAP (rPAP). The percentage of inhibition was measured using HIV-1 mediated production of p24 core protein as a marker. The p24 value for untreated infected cells was considered as 100% infection. Each value is an average of three experiments. (B) Mean values of concentration-dependent inhibition of p24 production in PBMC infected with HIV-I. (C) Effect of nPAP and rPAP on HIV-I replication as determined by viral-reverse transcriptase activity as a marker. Percentage of viral inhibition is calculated by comparing cpm from PAP-treated infected cells with cpm values from untreated infected cells (virus control, 100% infection) and untreated noninfected cells (cells control). Each value is an average of three experiments. (D) Mean values of dose-dependent inhibition of HIV-RT activity. The RT activity was measured by radioenzyme assay and the resulting signals were detected by scintillation counter and recorded as counts per minute (cpm). Results were normalized to values obtained for control cultures without PAP.

covered by CTAB at concentrations as low as 0.5%, while 2.5% of lauroylsarcosine was required to solubilize >90% of the PAP inclusion body proteins (Table 2). The solubilization of inclusion bodies was also achieved using 5 mM K_2HPO_4 buffer, pH 12, without any detergents (Table 2). Refolding of the soluble PAP was achieved by diluting the sample with glycerol (20% final concentration) and subsequently dialyzing in pH 8 buffer. SDS–PAGE analysis of inclusion bodies and solubilized fractions revealed the presence of a major protein with the estimated molecular mass of 33 kDa (Figs. 4A and 4D). The PAP constituted approximately 33% of the solubilized inclusion body proteins, as determined by integrated density measurements. The Western blot analysis showed that the 33 kDa protein is highly reactive with the anti-PAP antibody and is very stable under our solubilization conditions (Figs. 4B and 4E). The solubilized recombinant PAP was purified using Superose 12 HR 10/30 gel filtration column (Fig. 4C). Recombinant PAP eluted as a single peak at 25 min. Fractions containing PAP were identified by SDS–PAGE/Western blot analysis, pooled, and concentrated (Fig. 4C, lane 4). The final yield of the recombinant PAP was estimated as 10-12 mg/L culture, which corresponds to approximately 5% of the total *E. coli* cellular protein (Table 1).

Biological Activity of rPAP

In order to compare the enzymatic *N*-glycosidase activities of nPAP and rPAP, we have performed *in vitro* translation assays using the nuclease-treated rabbit reticulocyte lysate system (Promega). In this assay, luciferase mRNA was translated in the absence or presence of increasing concentrations of PAP (0.01 to 100 ng/ml). Luciferase mRNA was selected since it

encodes a monomeric protein of 61 kDa and yields a single major band upon SDS–PAGE (Fig. 5, inset) analysis. The average incorporation of ^{35}S without PAP was 3.5 to 4.0 $\times$ 10^3 cpm/ml. As shown in Fig. 5, the inhibition curve was linear in the range of 2.0 to 20 ng/ml for both nPAP and rPAP. The IC_{50} values for nPAP and rPAP were 10 $\pm$ 2 and 13 $\pm$ 2 ng/ml, respectively (Table 3). Thus, the enzymatic activity of nPAP was virtually identical to that of the rPAP.

We next compared the anti-HIV activity of rPAP to that of nPAP. As shown in Figs. 6A and 6C, both nPAP and rPAP inhibited viral replication in HIV-1-infected human peripheral blood mononuclear cells (PBMC) in a concentration-dependent fashion with IC_{50} values of 0.4 $\pm$ 0.1 and 0.5 $\pm$ 0.1 μg/ml, respectively, for p24 viral antigen production and IC_{50} values of 0.5 $\pm$ 0.2 and 0.4 $\pm$ 0.1 μg/ml, respectively for RT activity (Table 3). The mean p24 and RT values of HIV-infected PBMC measured after treatment with increasing concentrations of nPAP and rPAP are represented in Figs. 6B and 6D.

RNA Depurination Activity of rPAP

To determine if depurination of the rRNA can be detected, *E. coli* 16S and 23S rRNA was incubated with increasing concentrations of nPAP and rPAP, treated with aniline, and analyzed by electrophoresis before and after anilin treatment, as shown in Figs. 7A and 7B. An RNA fragment of ≈240 nt was released when treated with either nPAP or rPAP, whereas aniline treatment of rRNA in the absence of PAP failed to generate this fragment.

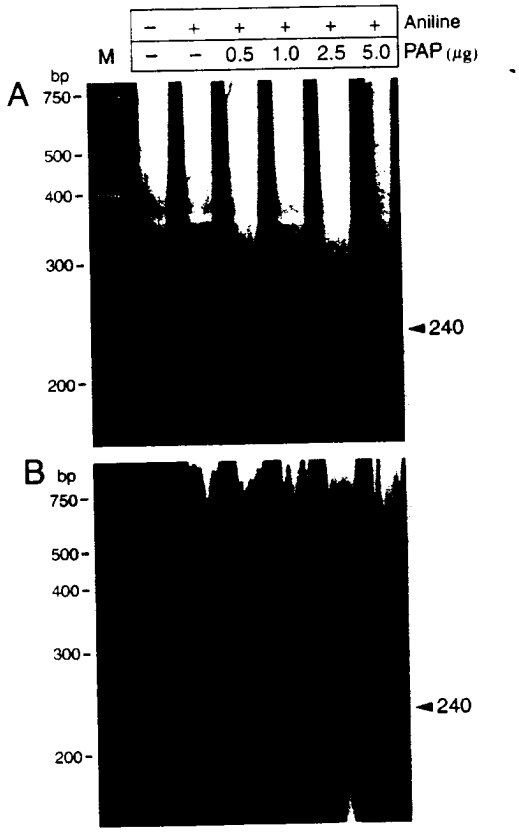

FIG. 7. Dose-dependent depurination of *E. coli* 23S and 16S ribosomal RNA *in vitro*. The rRNA (10 μg) was incubated with rPAP, treated with aniline, separated on a 4% urea/polyacrylamide gel, and stained with ethidium bromide. The arrow shows the fragment split by anilin and plus and minus denote the presence and absence of anilin/PAP (μg) treatment, respectively. M, molecular mass marker positions. (A) rRNA treated with rPAP. (B) rRNA treated with nPAP.

DISCUSSION

In recent years, there has been a growing interest in using PAP as either a ribosome inhibitory anticancer agent or a broad-spectrum antiviral agent (11, 19). However, extensive preclinical and clinical studies require large amounts of PAP purified to its homogeneity. Native PAP expressed in plants is mostly heterogeneous, since plants produce a number of immunologically distinct isoforms of PAP which vary in their catalytic activity (1). In addition, the isolated geographic distribution of pokeweed plants and seasonal variations in expression of PAP prompted us to explore an *E. coli* expression system for the large-scale production of PAP.

This study reports the successful expression, solubilization, and purification of functionally active rPAP from *E. coli*. Unlike the ricin A-chain, PAP efficiently inactivates both prokaryotic and eukaryotic ribosomes. Due to this activity, the wild-type PAP gene had not been successfully expressed in *E. coli*. Previous attempts to express the PAP gene in *E. coli* and yeast systems have been largely unsuccessful due to very low yield (0.3 to 0.9 mg/L) and PAP's ribosome inhibitory activity against the host (23,25,27). We have cloned the *PAP* gene, encoding amino acid residues 23–313, into an expression vector, PQE-31 (Qiagen), under a phage T5 promotor and an inducible *lac* operator and expressed in *E. coli* MV1190. Western blot analysis using anti-PAP antibody showed that PAP is located in the insoluble fraction of the cell lysate, suggesting that the overexpression of PAP has led to rapid aggregation of the protein (Fig. 2). Analysis of the inclusion bodies, enriched in PAP, exhibited a 33 kDa major protein which was highly reactive with anti-PAP antibodies (Fig. 4). The rPAP is approximately 4 kDa larger than the nPAP purified from plants (29 kDa), since the rPAP contains an additional 13 amino acids at the N-terminal end (His-tag) and 29 amino acids (from PAP) at the C-terminal end. The X-ray crystallographic analysis of PAP showed that the mature PAP is 29 amino acids shorter at its C-terminal end than the sequence predicted from the cDNA (2, 3), suggesting that the nPAP undergoes further processing at its C-terminus. The rPAP expressed in *E. coli* appears to be full length,

residues 23 to 313, suggesting that *E. coli* is lacking the enzyme which is responsible for C-terminus processing of PAP in plants. Although, the native PAP depurinates 23S rRNA of *E. coli* and inhibits bacterial protein synthesis and growth (28), the recombinant PAP permits the growth of *E. coli* (Fig. 1). We propose that the rapid accumulation of PAP into inclusion bodies likely prevents it from interacting with the host *E. coli* ribosomes.

In order to maximize the recovery of PAP, we attempted to solubilize the inclusion bodies using a variety of detergents. We found that the ionic detergents lauroylsarcosine and CTAB solubilized >90% of the PAP inclusion bodies at concentrations ranging from 0.5 to 5.0%, whereas the nonionic detergents solubilized <10% at these concentrations (Table 2). We also discovered that the inclusion bodies could be efficiently solubilized at pH 12. Recombinant PAP contained in the solubilized inclusion bodies was successfully renatured by slowly dialyzing at pH 8.0 buffer in the presence of glycerol and then purified by gel filtration. In contrast to the previously reported low yields (0.3 to 0.9 mg/L) in *E. coli*, yeast, and transgenic plants (23,25,27), our *E. coli* expression system allows us to routinely generate 10 to 12 mg/L of recombinant PAP and is amenable for large-scale production. The ribosome inhibitory activity of recombinant PAP expressed in *E. coli* was confirmed using a rabbit reticulocyte lysate *in vitro* translation system. Our results also show that the rPAP releases a 240-nt RNA fragment from anilin-treated *E. coli* 23S rRNA similar to that of the nPAP (Fig. 7). We have also documented the anti-HIV activity of the rPAP usir g human PBMCs infected with HIV-1. To our knowledge this is the first successful expression and solubilization of functionally active rPAP from inclusion bodies using an *E. coli* expression system. Our study represents a significant step toward improving the utility of PAP in treating human diseases.

ACKNOWLEDGMENTS

This material is based in part upon work sponsored by the Defense Advanced Research Projects Agency under Grant N65236-99-1-5422. The content does not necessarily reflect the position or policy of the U.S. Government, and no official endorsement should be inferred.

REFERENCES

1. Irvin, J. D. (1995) Antiviral proteins from Phytolacca *in* "Antiviral Proteins in Higher Plants" (Chessin, M., DeBorde, D., and Zipf, A., Eds.), pp. 65–94, CRC Press, Boca Raton, FL.
2. Lin, Q., Chen, Z. C., Antoniw, J. F., and White, R. F. (1991) Isolation and characterization of a cDNA clone encoding the anti-viral protein from Phytolacca americana. *Plant Mol. Biol.* **17,** 609–614.
3. Monzingo, A. F., Collins, E. J., Ernst, S. R., Irvin, J. D., and Robertus, J. D. (1993) The 2.5 Å structure of pokeweed antiviral protein. *J. Mol. Biol.* **233,** 705–715.
4. Endo, Y., Mitsui, K., Motizuki, M., and Tsurugi, K. (1987) The mechanism of action of ricin and related toxic lectins on eukaryotic ribosomes: The site and the characteristics of the modification in 28 S ribosomal RNA caused by the toxins. *J. Biol. Chem.* **262,** 5908–5912.
5. Endo, Y., Tsurugi, K., and Lambert, J. M. (1988) The site of action of six different ribosome-inactivating proteins from plants on eukaryotic ribosomes: The RNA N-glycosidase activity of the proteins. *Biochem. Biophys. Res. Commun.* **150,** 1032–1036.
6. Dallal, J. A., and Irvin, J. D. (1978) Enzymatic inactivation of eukaryotic ribosomes by the pokeweed antiviral protein. *FEBS Lett.* **89,** 257–259.
7. Gessner, S. L., and Irvin, J. D. (1980) Inhibition of elongation factor 2-dependent translocation by the pokeweed antiviral protein and ricin. *J. Biol. Chem.* **255,** 3251–3253.
8. Montanaro, L., Sperti, S., Mattioli, A., Testoni, G., and Stirpe, F. (1975) Inhibition by ricin of protein synthesis *in vitro:* Inhibition of the binding of elongation factor 2 and of adenosine diphosphate-ribosylated elongation factor 2 to ribosomes. *Biochem. J.* **146,** 127–131.
9. Hudak, K. A., Dinman, J. D., and Tumer, N. E. (1999) Pokeweed antiviral protein access ribosome by binding to L3. *J. Biol. Chem.* **274,** 3859–3864.
10. Irvin, J. D., and Uckun, F. M. (1992) Pokeweed antiviral protein: Ribosome inactivation and therapeutic applications. *Pharmacol Ther.* **55,** 279–302.
11. Uckun, F. M., and Reaman, G. H. (1995) Immunotoxins for treatment of leukemia and lymphoma. *Leukemia Lymphoma* **18,** 195–201.
12. Uckun, F. M. (1993) Immunotoxins for the treatment of leukemia. *Br. J. Haematol.* **85,** 435–438.
13. Gaynon, P. S, Bostrom, B., Reaman, G., Sather, H., Trigg, M. E., Tubergen, D. G., and Uckun, F. M. (1998) Childrens cancer group (CCG) initiatives in childhood acute lymphoblastic leukemia (ALL). *Int. J. Pediatr. Hematol. Oncol.* **5,** 99–114.
14. Ussery, M. A., Irvin, J. D., andHardesty, B. (1977) Inhibition of poliovirus replication by a plant antiviral peptide. *Ann. N. Y. Acad. Sci.* **284,** 431–440.
15. Aron, G. M., and Irvin, J. D. (1980) Inhibition of herpes simplex virus multiplication by the pokeweed antiviral protein. *Antimicrob. Agents Chemother.* **17,** 1032–1033.
16. Gehrz, R. C., Wilson, C., Eckhardt, J., Myers, D., Irvin, J. D., and Uckun, F. M. (1991) Treatment of human cytomegalovirus (HCMV) with noval antiviral immunoconjugates *in* "Progress in Cytomegalovirus Research" (Landini, M. P., Ed.), pp. 353–356, Elsevier, Amsterdam.
17. Tomlinson, J. A., Walker, V. M., Flewett, T. H., and Barclay, G. R. (1974) The inhibition of infection by cucumber mosaic virus and influenza virus by extracts from Phytolacca americana. *J. Gen. Virol.* **22,** 225–232.
18. Zarling, J. M., Moran, P. A., Haffar, O., Sias, J., Richman, D. D., Spina, C. A., Myers, D. E., Kuebelbeck, V., Ledbetter, J. A., and Uckun, F. M. (1990) Inhibition of HIV replication by pokeweed antiviral protein targeted to CD4+ cells by monoclonal antibodies. *Nature* **347,** 92–95.
19. Zarling, J. M., Moran, P. A., Haffar, O., Diegel, M., Myers, D. E., Kuelbeck, V. Ledbetter, J. A., and Uckun, F. M. (1991) Inhibition of HIV-1 replication in seropositive patients' CD4+ T-cells by pokeweed antiviral protein-monoclonal antibody conjugates. *Int. J. Immunopharmacol.* **13,** 63–68.

20. Uckun, F. M., Chelstrom, L. M., Tuel-Ahlgren, L., Dibirdik, I., Irvin, J. D., Langlie, M. C., and Myers, D. E. (1998) TXU (anti-CD7)-pokeweed antiviral protein as a potent inhibitor of human immunodeficiency virus. *Antimicrob. Agents Chemother.* **42,** 383–388.
21. Barbieri, L., Valbonesi, P., Bonora, E., Gorini, P., Bolognesi, A., and Stirpe, F. (1997) Polynucleotide:adenosine glycosidase activity of ribosome-inactivating proteins: Effect on DNA, RNA and poly(A). *Nucleic Acids Res.* **25,** 518–522.
22. Tumer, N. E., Parikh, B. A., Li, P., and Dinman, J. D. (1998) Pokeweed antiviral protein specifically inhibits Ty1-directed +1 ribosomal frameshifting and retrotransposition in *Saccharomyces cerevisiae. J. Virol.* **72,** 1036–1042.
23. Kataoka, J., Ago, H., Habuka, N., Furuno, M., Masuta, C., Miyano, M., and Koiwai, A. (1993) Expression of a pokeweed antiviral protein in *Escherichia coli* and its characterization. *FEBS Lett.* **320,** 31–34.
24. Kataoka, J., Habuka, N., Masuta, C., Miyano, M., and Koiwai, A. (1992) Isolation and analysis of a genomic clone encoding a pokeweed antiviral protein. *Plant Mol. Biol.* **20,** 879–886.
25. Hur, Y., Hwang, D. J., Zoubenko, O., Coetzer, C., Uckun, F. M., and Tumer, N. E. (1995) Isolation and characterization of pokeweed antiviral protein mutations in *Saccharomyces cerevisiae:* Identification of residues important for toxicity. *Proc. Natl. Acad. Sci. USA* **92,** 8448–8452.
26. Towbin, H., Staehelin, T., and Gordon, J. (1979) Electroporetic transfer of proteins from polyacrylamide gels to nitrocellulose sheets: Procedure and some applications. *Proc. Natl. Acad. Sci. USA* **76,** 4350–4354.
27. Xu, J., Kaloyanova, D., Ivanov, I. G., and AbouHaidar, M. G. (1998) The low expression level of pokeweed antiviral protein (PAP) gene in *Escherichia coli* by the inducible lac promoter is due to inefficient transcription and translation and not to the toxicity of the PAP. *Arch. Biochem. Biophys.* **351** 82–88.
28. Hartley, M. R., Legname, G., Osborn, R., Chen, Z., and Lord J. M. (1991) Single-chain ribosome inactivating proteins from plants depurinate *Escherichia coli* 23S ribosomal RNA. *FEBS Lett.* **290,** 65–68.

Reprinted from BIOCHEMICAL AND BIOPHYSICAL RESEARCH COMMUNICATIONS, Volume 260, No. 2, July 5, 1999

Biochemical and Biophysical Research Communications **260,** 453–458 (1999)
Article ID bbrc.1999.0922, available online at http://www.idealibrary.com on IDEAL®

Pokeweed Antiviral Protein Isoforms PAP-I, PAP-II, and PAP-III Depurinate RNA of Human Immunodeficiency Virus (HIV)-1[1]

Francis Rajamohan,*,† Taracad K. Venkatachalam,* James D. Irvin,‡ and Fatih M. Uckun*,§,[2]
**Biotherapy Program, †Department of Protein Engineering, and §Department of Virology, Hughes Institute, St. Paul, Minnesota; and ‡Department of Chemistry, Southwest Texas State University, San Marcos, Texas*

Received June 2, 1999

Pokeweed antiviral protein (PAP) is a naturally occurring broad-spectrum antiviral agent with potent anti-human immunodeficiency virus (HIV)-1 activity by an as yet undeciphered molecular mechanism. In the present study, we sought to determine if PAP is capable of recognizing and depurinating viral RNA. Depurination of viral RNA was monitored by directly measuring the amount of the adenine base released from the viral RNA species using quantitative high-performance liquid chromatography. Our findings presented herein provide direct evidence that three different PAP isoforms from *Phytolacca americana* (PAP-I from spring leaves, PAP-II from early summer leaves, and PAP-III from late summer leaves) cause concentration-dependent depurination of genomic RNA (63 to 400 pmols of adenine released per μg of RNA) purified from human immunodeficiency virus type-I (HIV-I), plant virus (tobacco mosaic virus (TMV), and bacteriophage (MS 2). In contrast to the three PAP isoforms, ricin A chain (RTA) failed to cause detectable depurination of viral RNA even at 5 μM, although it was as effective as PAP in inhibiting protein synthesis in cell-free translation assays. PAP-I, PAP-II, and PAP-III (but not RTA) inhibited the replication of HIV-1 in human peripheral blood mononuclear cells with IC_{50} values of 17 nM, 25 nM, and 16 nM, respectively. These findings indicate that the highly conserved active site residues responsible for the depurination of rRNA by PAP or RTA are not sufficient for the recognition and depurination of viral RNA. Our study prompts the hypothesis that the potent antiviral activity of PAP may in part be due to its unique ability to extensively depurinate viral RNA, including HIV-1 RNA. © 1999 Academic Press

Pokeweed antiviral protein (PAP) is a single-chain ribosome-inactivating protein (RIP) isolated from the leaves of the pokeweed plant, *Phytolacca americana* (1). PAP is a site-specific RNA N-glycosidase which catalytically removes a single adenine base from a highly conserved "α-sarcin/ricin (SR)" loop of the large rRNA species in eukaryotic (28S rRNA) and prokaryotic (23S rRNA) ribosomes (1, 2). This depurination of the SR loop results in irreversible inhibition of protein synthesis at the translocation step by impairing both the elongation factor (EF)-1-dependent binding of aminoacyl-tRNA and the GTP-dependent binding of EF-2 to the affected ribosome (1). Recent evidence indicates that L3, a highly conserved ribosomal protein at the peptidyltransferase center, may provide a binding site for PAP, allowing depurination of the target adenine in its rRNA substrate (3).

The X-ray crystallographic structure of PAP reveals a protein composed of eight alpha helices and a beta sheet consisting of six strands (4, 5). The protein is homologous with the A chain of ricin (RTA), a type-2 RIP, and exhibits a very similar folding pattern. This highly comparable structural topology between PAP and ricin A-chain suggests a similar mechanism of rRNA depurination. PAP-I, PAP-II, and PAP-III are different isoforms of PAP isolated from the spring leaves, early summer leaves and late summer leaves of the pokeweed plant (1). The putative active site residues participating in the rRNA depurination are highly conserved among the different PAP isoforms.

PAP exhibits a broad spectrum antiviral activity against plant and animal viruses, including poliovirus (6), herpes simplex virus (7), influenza virus (8), cytomegalovirus (9), and human immunodeficiency virus (HIV)-1 (10). PAP can effectively inhibit viral replication at concentrations which do not inhibit the protein synthesis of host cells (1, 10, 11). PAP conjugates of monoclonal antibodies recognizing CD4, CD5 or CD7 antigens on the cell surface effectively inhibit HIV-1

[1] This material is based in part upon work sponsored by the Defense Advanced Research Projects Agency under Grant N65236-99-1-5422 awarded to F.M.U. The content does not necessarily reflect the position or policy of the U.S. Government, and no official endorsement should be inferred.
[2] To whom correspondence should be addressed at Hughes Institute, 2665 Long Lake Road, Roseville, MN 55113. Fax: (651) 697-1042. E-mail: fatihuckun@ih.org.

0006-291X/99 $30.00

replication in normal T-cells at noncytotoxic concentrations (10, 11). Thus, the antiviral activity of PAP, especially its anti-HIV activity, cannot be sufficiently explained by its RIP activity.

Recently, PAP has been shown to efficiently depurinate adenine-containing polynucleotides (12), single-stranded DNA (13), and double-stranded DNA (14), suggesting that the deadenylating activity of PAP is not restricted to the SR loop of rRNA. In the present study, we sought to determine if PAP is capable of recognizing and depurinating HIV-1 RNA. Our findings presented herein provide direct evidence that three different PAP species from *Phytolacca americana* (PAP-I from spring leaves, PAP-II from early summer leaves, and PAP-III from late summer leaves) cause concentration-dependent depurination of genomic RNA purified from HIV-1 as well as TMV RNA, and bacteriophage MS 2 RNA. PAP-II and PAP-III were more effective than PAP-I in depurinating viral RNA, even though all three PAP species were equipotent in depurinating non-viral mouse RNA and inhibiting protein synthesis in cell-free translation assays using the rabbit reticulocyte lysate system. In contrast to the three PAP isoforms, RTA failed to cause detectable depurination of viral RNA, although it was almost as effective as PAP in inhibiting protein synthesis in cell-free translation assays. PAP-I, PAP-II, and PAP-III (but not RTA) inhibited the replication of HIV-1 in human peripheral blood mononuclear cells at nanomolar concentrations. These findings indicate that the highly conserved active site residues responsible for the depurination of rRNA by PAP or RTA are not sufficient for the recognition and depurination of viral RNA. Our study prompts the hypothesis that the potent antiviral activity of PAP may at least in part be due the unique ability of PAP to extensively depurinate viral RNA, including HIV-1 RNA.

MATERIALS AND METHODS

Materials. The PAP isoforms (PAP-I, PAP-II, and PAP-III) were purified from the spring, early summer and late summer leaves of *Phytolacca americana*, as described previously (15, 16). RTA and chemicals were purchased from Sigma (St. Louis, MI). PAP-I, PAP-II and PAP-III were purified from the spring, early summer and late summer leaves, respectively, of the pokeweed plant. Since PAP-II and PAP-III are separated as distinct peaks in ion-exchange column chromatography under identical conditions, they are considered different isoforms. SDS–PAGE analysis showed that the the approximate molecular mass of PAP-I, PAP-II and PAP-III are 29, 30, and 30 kDa, respectively (Figure 1A). PAP-III is a new isoform purified from the late summer leaves of *Phytolacca americana* and its first (N-terminal) 38 residues are identical to PAP-II. Genomic RNA from TMV and bacteriophage MS2 were purchased from Roche Molecular Biochemicals (Indianapolis, IN).

Isolation of HIV-I RNA. Human peripheral blood mononuclear cells (PBMCs) were obtained from HIV-1 negative donors and were infected (30×10^6 cells) with the HIV-1 strain HTLV-IIIB at a multiplicity of infection (MOI) of 0.1, as previously described. After 13 days, 40 mL of the culture were removed and centrifuged at

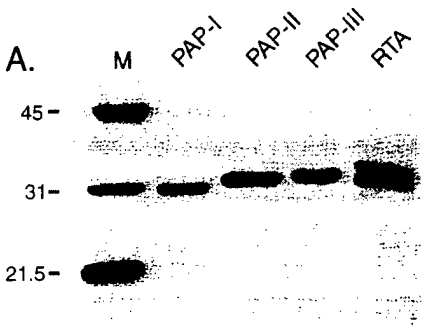

B.

RIP	IC_{50} (nM) [1]RIP Activity	[2]anti-HIV Activity
PAP-I	0.003 ± 0.0002	14 ± 2.1
PAP-II	0.004± 0.0002	26 ± 2.5
PAP-III	0.003 ± 0.0002	17 ± 2.0
RTA	0.006 ± 0.0003	>300

[1]anti-ribosome activity was measured from rabbit reticulocyte lysate *in vitro* translation assays. Each value is the mean ± SD of three experiments.

[2]anti-HIV activity was determined from HIV p24 viral core protein assays. Each value is the mean ± SD of three indepentdent experiments.

FIG. 1. Chemical and biological characteristics of pokeweed antiviral proteins. [A] Coomassie blue-stained SDS-12% PAGE gel comparing the molecular mass of the PAP isoforms and RTA. M, molecular mass marker. Masses of the protein markers (in kilodaltons) are shown on the left. [B] The RIP activity was measured in 3 independent experiments using rabbit reticulocyte lysate-based *in vitro* translation assays. The anti-HIV activity was measured using PBMC and the HIV-1 strain HTLVIIIB, as described in Materials and Methods.

10,000 × g for 5 min. The supernatant was filtered through a 0.22 μm filter, mixed with 20 mL of the virus precipitation buffer (30% PEG 8000, 0.4 M NaCl) and incubated for 3 h at 4°C. The sample was centrifuged at 15,000 rpm for 30 min and the pellet was resuspended in 2 ml of Urea lysis buffer (7 M Urea, 2% SDS, 0.35 M NaCl, 0.001 M EDTA, 0.01 M Tris, pH 8.0). The sample was diluted with 4 mL of RNase free water, extracted with phenol:chloroform (24:24) and precipitated with ethanol. The RNA pellet was resuspended in 0.5 ml DNase digestion buffer (0.005 M $MgCl_2$, 0.01 M Tris, pH 7.4) and treated with 50 U of RNase free DNase for 30 min at 37°C. The RNA was extracted with phenol:chloroform, precipitated with ethanol and resuspended in 400 μl RNase free water and stored at −20°C.

Adenine release assays. The HPLC (Hewlett Packard, Palo Alto, CA)-based adenine detection system consisted of a Hewlett Packard (HP) series 1100 in conjunction with a quaternary pump, an auosampler, an auto electronic degasser, an automatic thermostatic column compartment, diode array detector and a computer with a Chemstation software program for data analysis. Release of adenine from RNA substrates was determined using a reverse-phase Lichrospher 100, RP-18 analytical column (Hewlett Packard, 5 μm particle size, 250 × 4 mm). The HPLC running buffer (50 mM $NH_4C_2H_3O_2$, 5% Methanol, pH 5.0) was used as the mobile phase. The mobile phase was degassed automatically by the electronic degasser system. The column was equilibrated and eluted under isocratic conditions at a flow rate of 1.0 ml/min.

Viral RNA samples (2 μg) were incubated with increasing concentrations (0.25, 0.5, 1.0, 2.5 and 5.0 μM) of PAP (PAP-I, PAP-II, PAP-III) or RTA for 1 h at 37°C in 50 μl of binding buffer (25 mM

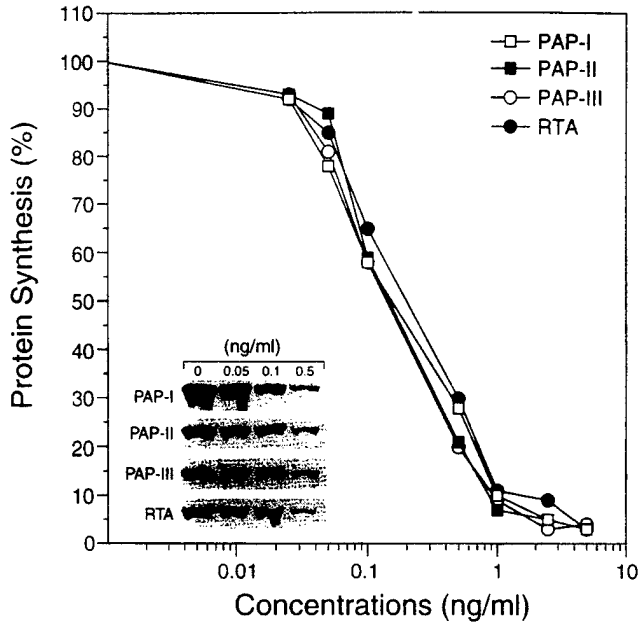

FIG. 2. RIP activity of pokeweed antiviral proteins. Dose-dependent inhibition of protein synthesis in the rabbit reticulocyte lysate system. Each data point represents an average from three experiments. Protein synthesis was measured by ^{35}S-methionine incorporation and the control sample with all the reagents except RIP was assigned a reference value of 100%. Inset: A representative experiment showing reduced synthesis of ^{35}S-labeled luciferase protein (61-kDa) in the presence of RIPs. Samples were resolved on SDS-10% PAGE and autoradiographed. Numbers at the top indicate the concentrations of RIPs.

Tris. HCl, pH 7.8, 10 mM KCl, 5 mM $MgCl_2$, 2% Glycerol). The reaction was stopped by adding 100 μl of HPLC running buffer and 100 μl of the sample was injected automatically into the Lichrospher 100RP-18E column. The detector wavelength was set at 260 nm and the flow rate was maintained at 1 ml/min. Controls included samples containing (a) untreated viral RNA, and (b) RIP (PAP isomers or RTA) without viral RNA.

Calibration curve. The adenine standard was obtained from Sigma Chemicals. A calibration curve was generated to confirm the linear relationship between the absolute peak area and the quantities of adenine in the tested samples. Adenine at final concentration of 0.1 μM (=5 pmols/50 μl), 0.5 μM (=25 pmols/50 μl), 1.0 μM (=50 pmols/50 μl), 2.5 μM (=125 pmols/50 μl) 5.0 μM (=250 pmols/50 μl) was injected into the HPLC system for analysis and the calibration curves were generated by plotting the absolute peak area against the quantities of adenine. Unweighted linear regression analysis of the calibration curve was performed by using the CA-Cricket graph III computer program, version 1.1 (Computer Association, Inc., Islandia, NY).

Intraassay and interassay accuracy and precision. To evaluate the intra-assay accuracy and precision, standard samples containing 0.5 μM or 2.5 μM adenine were prepared and analyzed within a single day and the quantities were calculated using the calibration curve as described above. The ratio of the calculated quantities over the known quantities spiked was calculated to evaluate the intra-assay precision. The inter-assay accuracy was calculated as the ratio of the calculated quantities over the known quantities using data from 3 independent experiments. The inter-assay precision was estimated by determining the coefficient of variation from 3 independent experiments.

Cell-free translation assays of RIP activity. The RIP activity of PAP isoforms (PAP-I, PAP-II and PAP-III) and RTA was measured using a cell-free *in vitro* protein synthesis inhibition assay, as described previously (17). In brief, varying amounts (0.01 to 5 ng/ml) of the RIPs were added to the "translation mixture" containing 10 μl of rabbit reticulocyte lysate (Promega), 0.5 μl of 1 mM methionine-free amino acids mixture and 1.0 μl of ^{35}S-methionine (10 mCi/ml, Amersham, Arlington Heights, IL). An appropriate amount of RNase free water was added to keep the final volume of the reaction mixture fixed at 19 μl and the reaction mixture was pre-incubated at room temperature for 15 min. Protein translation was initiated by adding

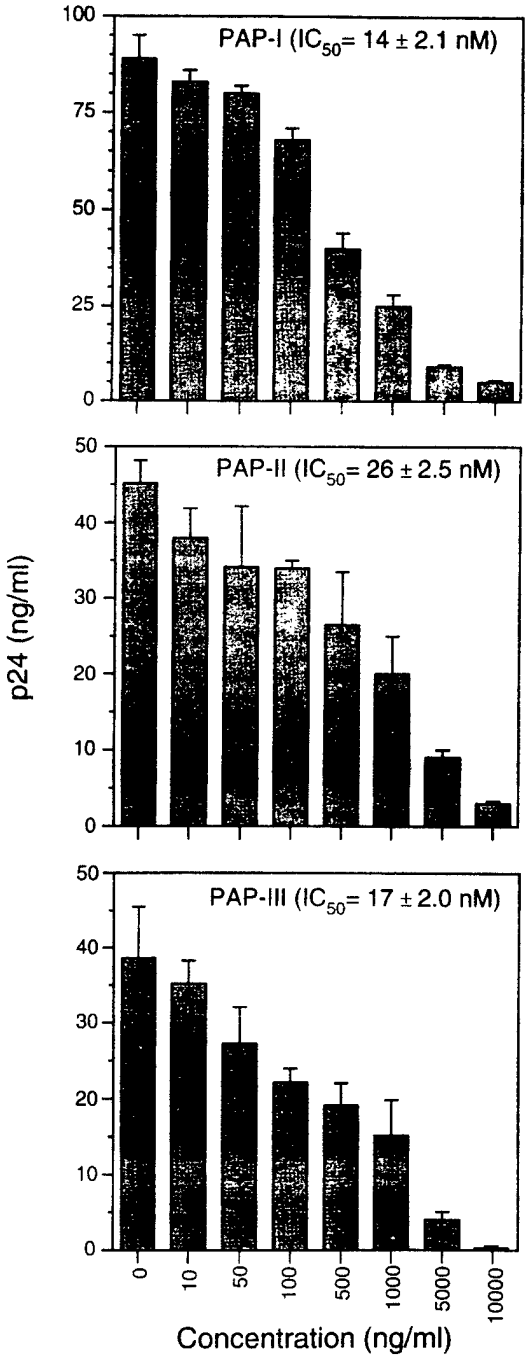

FIG. 3. Anti-HIV activity of pokeweed antiviral proteins. PBMCs were infected with the HIV-1 strain HTLVIIIB and cultured for 10 days in the presence or absence of PAP isomers. HIV-1 replication in PBMC was measured using p24 ELISA.

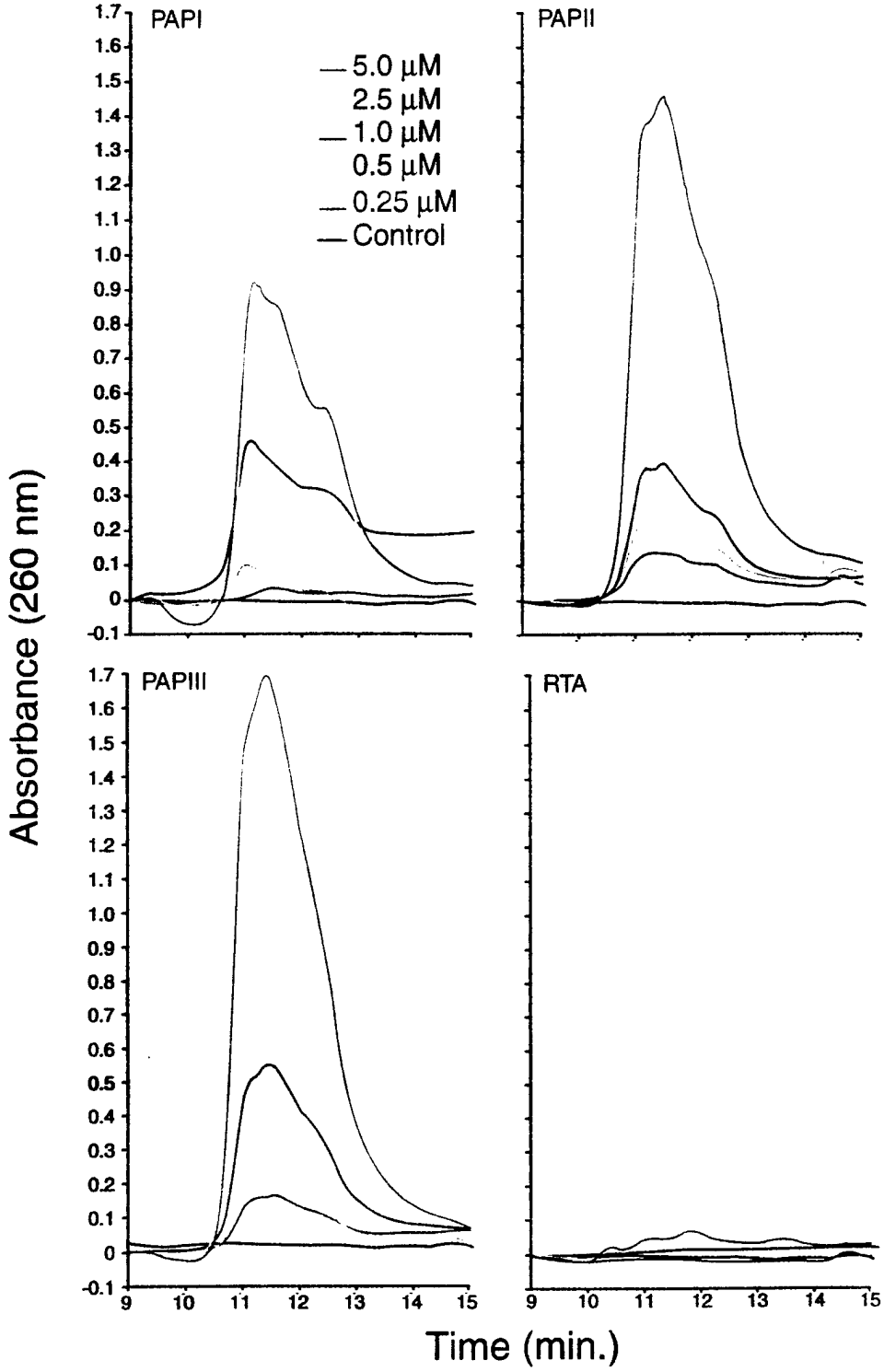

FIG. 4. Deadenylation of HIV-1 RNA by pokeweed antiviral proteins. Two μg of HIV-1 RNA was incubated with varying concentrations (0.25 to 5.0 μM) of RIPs for 1 h at 37°C in 50 μl of binding buffer. The reaction was stopped by adding 100 μl of HPLC running buffer and 100 μl of the sample was injected in to the column as described in Materials and Methods. Control samples of HIV-1 RNA were treated with PBS instead of RIPs.

0.12 μg luciferase mRNA in a 1.0 μl volume and continued the incubation at 30°C for 2 h. Translation was stopped by the addition of 5% trichloroacetic acid. The precipitated polypeptides were collected on Whatman GF/C glass microfiber filters and counted in a Beckman liquid scintillation counter as described previously (17). The IC_{50} values were calculated by non-linear regression analysis (Prism-2 graph pad software, San Diego, CA) using the pooled data from three independent experiments.

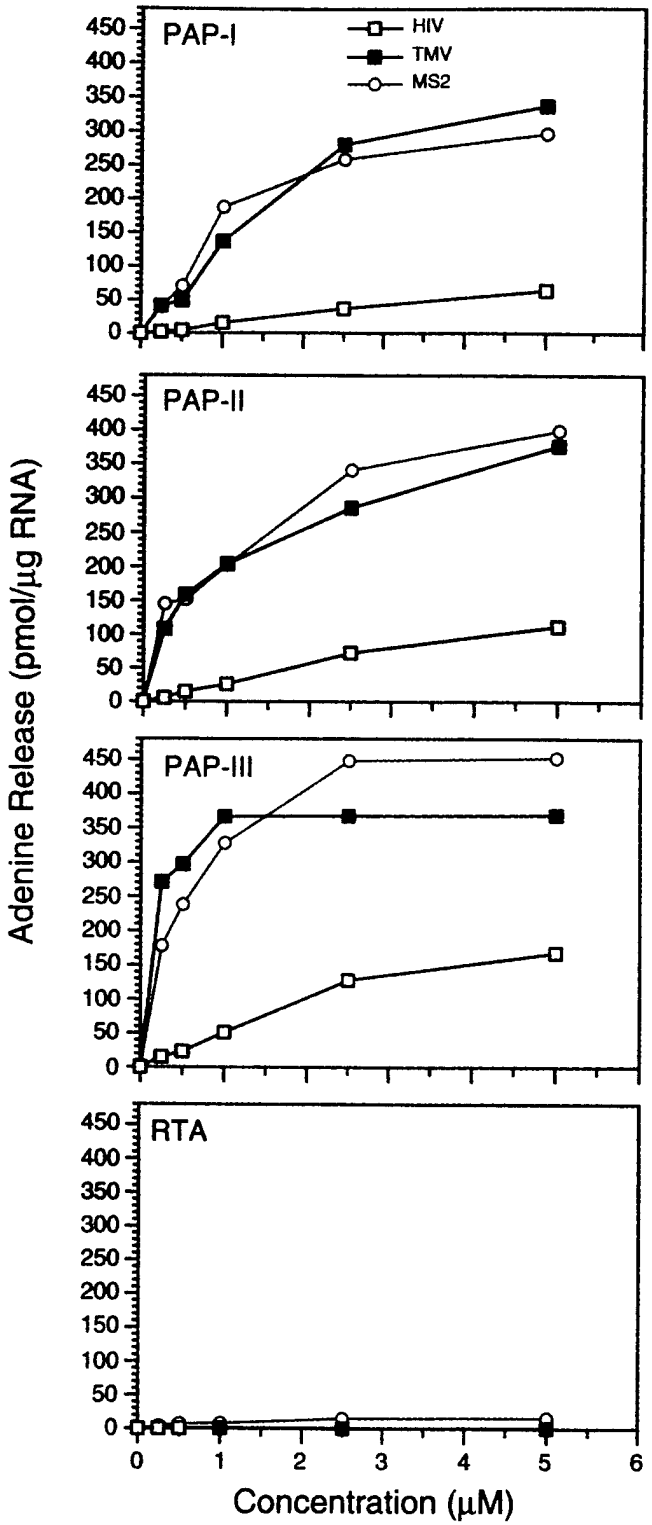

FIG. 5. Deadenylation of viral RNA by pokeweed antiviral proteins. Adenine release assays were performed as described in Materials and Methods. Each value is an average from three independent experiments.

Cellular assays of anti-HIV activity. The *in vitro* anti-HIV-I activities of PAP-I, PAP-II, PAP-III and RTA were evaluated by determining their ability to inhibit the replication, as measured by production of p24 antigen, of the HIV-I strain HTLV-IIIB in Ficoll-Hypaque separated normal human peripheral blood mononuclear cells (PBMCs) from HIV-seronegative donors, as previously described (11, 18). Controls included uninfected, untreated PBMCs for determining the background value for the p24 ELISA and infected, untreated PBMCs for comparison with infected, PAP/RTA-treated PBMCs. Percent inhibition of HIV-1 replication was calculated by comparing the background-subtracted p24 antigen values for the test substance-treated infected cells with the background-subtracted p24 antigen values for untreated infected cells. The mean (± SEM) IC_{50} values were calculated by non-linear regression analysis (Prism-2).

RESULTS AND DISCUSSION

RIP activity of PAP-I, PAP-II, PAP-III, and RTA. To compare the rRNA depurinating activity of our test RIPs (PAP-I, PAP-II, PAP-III and RTA), we have performed *in vitro* translation inhibition assays using luciferase mRNA as the template. Our results showed identical dose-response curves for all the test RIPs (IC_{50} values: 3 ± 0.2, 4 ± 0.2, 3 ± 0.2 and 6 ± 0.3 pM for PAP-I, PAP-II, PAP-III and RTA, respectively (Figure 1B, Figure 2). These data indicate that the rRNA depurination activities of PAP isomers and RTA are similar despite the differences of their primary amino acid sequences.

Anti-HIV activity of PAP-I, PAP-II, and PAP-III. PAP-I, PAP-II, and PAP-III effectively inhibited the replication of HIV-1 in human peripheral blood mononuclear cells with IC_{50} values of 14 ± 2.1 nM, 26 ± 2.5 nM, and 17 ± 2.0 nM, respectively (Figure 1B, Figure 3). The anti-HIV activity of PAP isomers cannot be exaplained only by their RIP activity since RTA with virtually identical potency as a rRNA-depurinating RIP did not show any detectable anti-HIV activity under identical experimental conditions (Figure 1B).

Depurination of HIV-1 RNA by PAP-I, PAP-II, and PAP-III. Aniline cleavage assays showed fragmentation of viral RNA from HIV-1, TMV, and MS2 after treatment with PAP-I, PAP-II, or PAP-III, but not with RTA (data not shown). Since aniline cleaves the sugar-phosphate backbone of RNA at depurination sites, these results strongly indicated that all three PAP isomers are capable of depurinating viral RNA. We next examined PAP-I, PAP-II, PAP-III and RTA for depurinating activity against genomic RNA purified from HIV-1 using adenine release assays. Genomic viral RNAs from TMV and MS2 were also included as controls. The depurinating activity of test RIPs was determined by measuring the amount of adenine released from the substrate viral RNA using a quantitative HPLC method, as described in Materials and Methods. Under the described chromatographic conditions, the retention time for adenine was 11.4 minutes. At this retention time, adenine was eluted without an interference peak from the blank control (Figure 4). The calibration curve for adenine was linear between 5 pmols–250 pmols and could be described by the

regression equation: $Y = 1.324X - 0.393$ ($r > 0.999$), where Y is the amount of adenine recovered in pmols and X is the absolute peak area. The lowest limit of detection of adenine was 2.5 pmol at a signal to noise ratio of Å3.

The intra- and inter-assay coefficients of variation were less than 5%. The overall intra- and inter-assay accuracies of this method were 98.7 ± 1.7% (N = 3) and 95.7 ± 3.3% (N = 3), respectively. All three isoforms of PAP (but not RTA) caused concentration-dependent depurination from HIV-1 RNA as well as control viral RNAs (TMV and MS2) (Figure 5). The order of deadenylation efficiency of viral RNA by PAP isoforms was PAP-III > PAP-II > PAP-I (Figure 5). At a 5 μM concentration, PAP-III released 168 ± 20, 452 ± 28, and 369 ± 13 pmols of adenine, respectively, from one μg of RNA from HIV-1, MS2, and TMV. By comparison, PAP-I released 63 ± 7, 292 ± 20, and 335 ± 15 pmols of adenine from one μg of RNA from HIV-1, MS2, and TMV, respectively. Thus, PAP-III and PAP-II were more effective than PAP-I in depurinating viral RNA, even though all three PAP species were equally potent in inhibiting protein synthesis in cell-free translation assays using the rabbit reticulocyte lysate system (Figure 1B, Figure 2). Furthermore, in contrast to the three PAP isoforms, RTA failed to cause detectable depurination of viral RNA even at 5 μM (Figure 5), although it was almost as effective as PAP in inhibiting protein synthesis in cell-free translation assays with an IC_{50} value of 6 pM (Figure 1B). These findings indicate that the highly conserved active site residues responsible for the depurination of rRNA by PAP or RTA are not sufficient for the recognition and depurination of viral RNA.

Our study prompts the hypothesis that the potent antiviral activity of PAP may in part be due to the unique ability of PAP to extensively depurinate viral RNA, including HIV-1 RNA. Until recently the rRNA was the only known substrate for RIPs. We report here a dose-dependent release of adenine from plant and human viral genomic RNAs by PAP isoforms (PAP-I, PAP-II, PAP-III). The fragments released from PAP and aniline treated viral RNAs was unique to each viral RNA (data not shown). The PAP isoforms showed higher depurinating activity on RNA from bacteriophage and TMV than on HIV RNA suggesting a preference for substrate. The elucidation of the determinants of PAP to interact with and depurinate viral RNA may provide the basis for the design of novel and effective antiviral treatment programs using PAP.

REFERENCES

1. Irvin, J. D., and Uckun, F. M. (1992) *Pharmacol. Ther.* **55,** 279–302.
2. Endo, Y., and Tsurugi, K. (1988) *J. Biol. Chem.* **263**(18), 8735–8739.
3. Hudak, K. A., Dinman, J. D., and Tumer, N. E. (1999) *J. Biol. Chem.* **274,** 3859–3864.
4. Monzingo, A. F., Collins, E. J., Ernst, S. R., Irvin, J. D., and Robertus, J. D. (1993) *J. Mol. Biol.* **233,** 705–715.
5. Kurinov, I. V., Myers, D. E., Irvin, J. D., and Uckun, F. M. (1999) *Protein Sci.*, in press.
6. Ussery, M. A., Irvin, J. D., and Hardesty, B. (1977) *Ann. NY Acad. Sci.* **284,** 431–440.
7. Aron, G. M., and Irvin, J. D. (1980) *Antimicrob. Agents Chemother.* **17,** 1032–1033.
8. Tomlinson, J. A., Walker, V. M., Flewett, T. H., and Barclay, G. R. (1974) *J. Gen. Virol.* **22,** 225–232.
9. Gehrz, R. C., Wilson, C., Eckhardt, J., Myers, D., Irvin, J. D., and Uckun, F. M. (1991) Progress in Cytomegalovirus Research (Landinin, M. P., Ed.), Elsevier Science Publishers, BV.
10. Zarling, J. M., Moran, P. A., Haffar, O., Sias, J., Richman, D. D., Spina, C. A., Myers, D. E., Kuebelbeck, V., Ledbetter, J. A., and Uckun, F. M. (1990) *Nature* **347,** 92–95.
11. Uckun, F. M., Chelstrom, L. M., Tuel-Ahlgren, L., Dibirdik, I., Irvin, J. D., Langlie, M. C., and Myers, D. E. (1998) *Antimicrob. Agents Chemother.* **42,** 383–388.
12. Barbieri, L., Valbonesi, P., Bonora, E., Gorini, P., Bolognesi, A., and Stirpe, F. (1997) *Nucleic Acids Res.* **25,** 518–522.
13. Nicolas, E., Beggs, J. M., Haltiwanger, B. M., and Taraschi, T. F. (1998) *J. Biol. Chem.* **273,** 17216–17220.
14. Wang, P., and Tumer, N. E. (1999) *Nucleic Acids Res.* **27,** 1900–1905.
15. Myers, D. E., Irvin, J. D., Smith, R. S., Kuebelbeck, V. M., and Uckun, F. M. (1991) *J. Immunol. Methods* **136,** 221–238.
16. Irvin, J. D. (1975) *Arch. Biochem. Biophys.* **169,** 522–526.
17. Rajamohan, F., Engstrom, C. R., Denton, T. J., Engen, L. A., Kourinov, I., and Uckun, F. M. (1999) *Protein Expression Purif.*, in press.

Biochemical and Biophysical Research Communications 275, 549–552 (2000)
doi:10.1006/bbrc.2000.3329, available online at http://www.idealibrary.com on IDEAL®

X-Ray Crystallographic Analysis of Pokeweed Antiviral Protein-II after Reductive Methylation of Lysine Residues

I. V. Kurinov,*[,1] C. Mao,* J. D. Irvin,† and F. M. Uckun*

*Department of Structural Biology, Department of Virology, and Department of Biotherapy, Parker Hughes Institute, Roseville, Minnesota 55113; and †Department of Chemistry, SouthWest Texas State University, San Marcos, Texas 78666

Received June 26, 2000

Pokeweed antiviral protein II (PAP-II) is a naturally occurring protein isolated from early summer leaves of the pokeweed plant (*Phytolacca americana*). PAP-II belongs to a family of ribosome-inactivating proteins which catalytically deadenylate ribosomal and viral RNA. The chemical modification of PAP-II by reductive methylation of its lysine residues significantly improved the crystal quality for X-ray diffraction studies. Hexagonal crystals of the modified PAP-II, with unit cell parameters a = b = 92.51 Å, c = 79.05 Å, were obtained using 1.8 M Na/K phosphate as the precipitant. These crystals contained one enzyme molecule per asymmetric unit and diffracted up to 2.4 Å, when exposed to a synchroton source. © 2000 Academic Press

Key Words: **pokeweed antiviral protein; reductive methylation; crystallization; X-ray diffraction.**

Pokeweed antiviral protein (PAP-I) is a 29-kDa naturally occurring protein isolated from the spring leaves of pokeweed plant (1, 2). PAP belongs to a family of ribosome-inactivating proteins (RIPs) which catalytically remove a single adenine base from the highly conserved α-sarcin/ricin loop of ribosomal RNA (2, 3). The ribosomes depurinated by PAP in this manner are unable to interact with the elongation factors (EF)-1 and EF-2 and thus the protein synthesis is irreversibly inhibited at the translocation step (4, 5). PAP has been shown to effectively depurinate adenine-containing polynucleotides (6), single-stranded DNA (7), double-stranded DNA (8) and viral RNA (9, 10), suggesting that the depurinating activity of PAP-I is not limited to the α-sarcin loop of rRNA. Recently it was found that PAP-I can deguanylate both ribosomal and viral RNA (10, 11). Studies also indicated that PAP-I effectively inhibits intracellular replication of several animal viruses, including HIV (12–15). The molecular mechanism of the antiviral activity of PAP-I is under active investigation (16–20). The therapeutic potential of PAP has gained considerable interest in recent years due to the clinical use of native PAP as the active moiety of immunoconjugates against cancer and AIDS (21).

Besides PAP-I, PAP-II and PAP-III (from summer leaves), as well as PAP-S (from seeds), were isolated from the pokeweed plant (22, 23). These molecules share distinct but homologous primary structure. The putative active site residues participating in the rRNA depurination are highly conserved among the different PAP species. Furthermore, all three PAP species cause concentration-dependent depurination of viral RNA (9). PAP-I, PAP-II, and PAP-III inhibited the replication of HIV in human peripheral blood mononuclear cells with IC_{50} values of 17, 25, and 16 nM, respectively.

We have determined the X-ray crystal structure of PAP-I with a 1.9 Å resolution and established a model as a guide for construction of superior PAP-I mutants. However, our efforts to crystallize PAP-II have not been successful. Here we report the successful crystallization of PAP-II after reductive methylation of its lysine residues. The structural comparison of PAP-II and PAP-I will likely provide further insights into the structure-activity relationship, affecting their ribosome inactivating and antiviral properties.

MATERIALS AND METHODS

Purification and crystallization. PAP-II was extracted from early summer leaves of *Phytolacca americana* and purified to homogeneity as previously described (22, 23). Just before the crystallization setup PAP-II was repurified on a MonoS cation-exchange column (Pharmacia Biotech), eluted using 500 mM NaCl in 25 mM citric buffer pH 6, and filtered through a 0.1-μm filter to remove possible aggregates.

Crystallization of native PAP-II. Crystallization conditions were screened with the hanging-drop vapor-diffusion method at three different temperatures (4°C, 20°C and 37°C), initially using commercially available crystallization kits (Hampton Research). Very small and poorly shaped microcrystals were found with PEG 8000 as a

[1] To whom correspondence should be addressed at Parker Hughes Institute, 2665 Long Lake Road, Roseville, MN 55113. Fax: (651) 697-1057. E-mail: igor@ih.org.

0006-291X/00 $35.00

precipitant and using extremely high protein concentrations of up to 140 mg/ml. All attempts to grow larger and better crystals failed without significant improvement of crystal quality despite many trials with a large variety of crystallization conditions.

Chemical modification of PAP-II. Because of the poor quality of PAP-II crystals, the protein was subjected to reductive methylation of lysine residues to decrease its solubility and enhance its surface hydrophobicity, using the protocol published in (24). The protein solution (~10 mg/ml) was dialyzed against 0.2 M sodium borate, pH 8.5, 60 μl of formaldehyde (1 M) was added to 2 ml of the protein solution. Subsequently, 6 μl of sodium borohydrate (1 M) was added with rapid mixing, followed by addition of another 4 μl sodium borohydrate after 10 min. This modification reaction was repeated six times at 30 min intervals, during which the reaction solution was left on ice. The protein was finally precipitated using ammonium sulfate. However, the protein failed to form a pellet upon repeated centrifugation, so the suspension was dialyzed back into solution against water. The resolubilized protein was concentrated and desalted by passing through a G-25 column previously equilibrated with water. The modified protein was then applied to cation-exchange column chromatography and was eluted as a single peak at a lower NaCl concentration than unmodified wild-type PAP-II.

Crystallization of reductively methylated PAP-II. The crystallization of modified PAP-II proved much easier when compared with to our year-long efforts to crystallize wild-type PAP-II protein. The crystals grew as a cluster of thin rods (Fig. 1) from 1.8 M Na/K phosphate solution (pH 7.2) at room temperature and ~36 mg/ml protein solution. These crystals appeared after approximately one week and grew to maximum dimensions of approximately 0.1 mm × 0.2 mm × 0.5 mm. For cryo-temperature data collection, the crystals were subjected to flash cooling in liquid nitrogen after a short (less than 5 sec) soaking in 30% PEG300 solution.

Data collection and processing. Initial X-ray diffraction data was collected using the R-AXIS IY imaging plate detector mounted on an RUH3R Rigaku rotating anode X-ray generator with a double mirror system operating at 50 kV and 100 mA. The crystal-to-detector distance was 150 mm and the crystal in two different orientations was rotated around the spindle axis with images collected over 1.5° to a resolution of 2.8 Å. X-ray data set was collected at low temperatures (~100K) to improve the diffraction quality and decrease the radiation decay.

A full data set was collected at the Cornell High Energy Synchrotron Source (CHESS), using the MacCHESS facility with the crystallographic setup and accompanying support on beamline F-2. Quantum-4 CCD area detector systems was used to collect data extending to 2.4 Å resolution at low temperature. The X-stream system from MSC was used for all low-temperature studies.

The diffraction data were evaluated using the HKL package (DENZO and SCALEPACK (25)). The real resolution of the data, used for structure refinement, was estimated by taking into consideration the completeness of the last resolution shell, I/σ ratio and R-merge values. The crystal structure was determined by molecular replacement using the known structure of wild type PAP-I. All structure refinement calculations were done using X-PLOR (version 3.8×) (26). As a guide to the quality of the structure, the values of the free R-factor were monitored during the course of the crystallographic refinement.

RESULTS AND DISCUSSION

Chemical modification of proteins has promoted the biochemical and structural characterization of proteins. The chemical labeling of a class of amino acids did not require considerable prior knowledge of the protein's structure and function in order to perform a meaningful experiment that can be readily interpreted. Reductive methylation of lysine ϵ-groups in proteins was shown to be accompanied by minimal changes in the gross physical properties (27). As it was reported in a few publications (24, 28), reductive methylation of lysine residues offers the opportunity to change the surface properties of a target protein and can potentially improve its crystallization properties. It was possible to grow crystals of myosin subfragment I (24), that has resisted crystallization for years. Besides, it was found that lysine modification with 2,4,6-trinitrobenzene sulfonyl chloride only slightly reduced the ability of PAP-I to inactivate ribosomes and had no detectable effect on its antiviral activity (29).

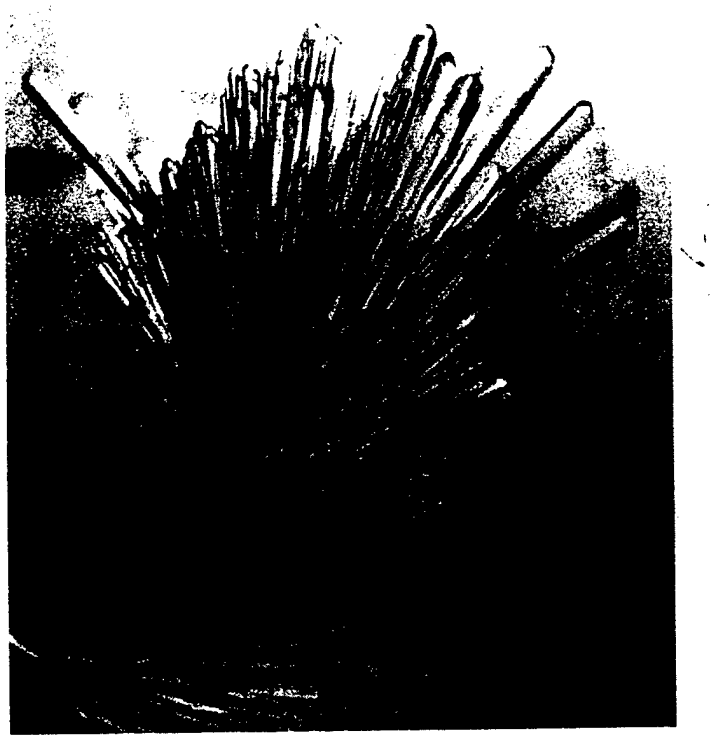

FIG. 1. The cluster of methylated PAP-II crystals. The dimension of the largest crystal are approximately 0.1 × 0.2 × 0.5 mm.

The cation-exchange HPLC profiles show that the methylated PAP-II peak shifted to lower retention time as compared with native PAP-II. However, the reverse phase HPLC profile showed that the methylated PAP-II shifted to longer retention times than unreacted PAP-II (Fig. 2). These results indicate that the reductive methylation of PAP-II reduced the apparent surface charge and increased the hydrophobicity of the protein.

The crystals of wild type PAP-II were very difficult to grow and crystallization conditions were not reproducible. The small and poorly shaped crystals diffracted

only to 4 Å resolution on a rotating anode X-ray generator operated at 50 kV and 100 mA and the crystals showed high mosaicity. On the other hand, crystals of reductively methylated PAP-II were easily grown, they diffracted up to 2.8 Å resolution under the same experimental conditions and up to 2.4 Å resolution using the synchrotron beamline at CHESS. According to the results deduced from DENZO indexing program, the crystals of PAP-II belong to the primitive hexagonal lattice. The calculations of merging R-factors for various crystal symmetries led to the assignment of P321 group. Examination of the systematic absences allowed the identification of the space group $P3_121$ or $P3_221$ and the unit cell parameters a = b = 92.51 Å, c = 79.05 Å, $\alpha = \beta = 90°$ and $\gamma = 120°$. A solvent content of 63% and an acceptable crystal packing density V_m of 3.15 Å^3/Da were calculated using the Matthews method (30), assuming the PAP-II crystals to contain one molecule per asymmetric unit. A total of 13727 unique reflections were collected at CHESS, which represent a completeness of 98.8% at 2.5 Å resolution. Full data statistics is shown in Table 1. The data was first processed in P321 group because of the ambiguous threefold axis.

We attempted structure solution using the molecular replacement method implemented in the program AMORE (31, 32) by employing our wild-type PAP-I model (PDB access code 1QCG) (33) as a search model. PAP-I and PAP-II share only 42% of identical residues, although there are many highly conserved residues and all ribosome inactivating proteins with known structure possess a very similar folding pattern and structure. No insertions or deletions were made in the search model. The molecular replacement calculations were performed using data in the resolution range 20–4 Å. Rotational function searches were carried out with an integration radius of 25 Å. Although a prominent pear was found, all peaks of the rotational function search were used in the subsequent translation function search in a two possible space groups $P3_221$ and $P3_121$, followed by rigid-body refinement. The space group $P3_121$ was eliminated after several attempts revealed that it was impossible to have a reasonable packing in a unit cell. The most promising solution has an outstanding correlation peak and the lowest R-factor. The solution was examined graphically and the crystal packing for this solution is good. Model rebuilding and structure refinement are under way.

X-ray crystallographic three-dimensional structure of PAP-II may help us elucidate the structural differences among different PAP species and help us understand the substrate specificity and stereoselectivity of these enzymes. Structural information from these proteins may also facilitate design and engineering of new enzymes with pre-determined properties in the area of clinical interest.

TABLE 1

Details of Data Collection

	PAP-II crystal (in-house RAXIS-IY)	PAP-II crystal CHESS data
Unit cell parameters		
(a)	93.75	92.51
(b)	93.75	92.51
(c)	79.69	79.05
α	90.0	90.0
β	90.0	90.0
γ	120.0	120.0
$I/\sigma(I)$	12.4	13.6
Number of unique reflections	8626	13727
Redundancy	5.9	4.76
Resolution limit for refinement (Å)	2.9	2.5
R-merge (%)[a]	12.4	9.5
R-merge (%) in last resolution shell	23.9	17.1
Completeness (%)	92.9	98.8
Completeness (%) in last resolution shell	97.8	97.7

Note. The last shell is the 2.5–2.59 Å resolution bin for synchrotron data and 2.9–3.0 Å for in house data collection.

[a] R-merge (%) = $(\Sigma|I_i - \langle I\rangle|/\Sigma I_i) \times 100$, where I_i is an individual intensity observation, $\langle I\rangle$ is the mean intensity for that reflection and the summation is over all reflections.

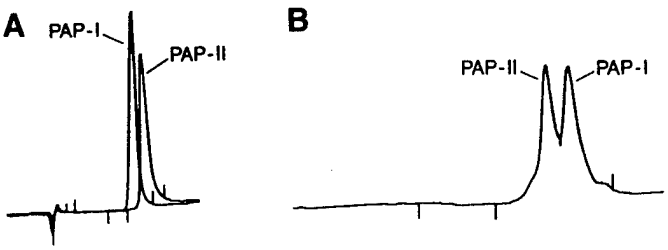

FIG. 2. The comparison of the elution profile of methylated PAP-II with native PAP. (A) Reversed-phase HPLC overlay. Native and methylated PAP-II were injected onto Beckman 4.6 × 250-mm octylsilane column equilibrated with 45% acetonitrile/0.1% TFA in water. The protein was eluted with a linear 45–60% acetonitrile gradient at 1.0 ml/min. The protein was detected by absorbance at 230 nm. (B) Cation-exchange HPLC. The mixture of native and methylated PAP-II were injected onto a BioRad 7.5 × 75-mm TSK-SP5 ion-exchange column equilibrated with 20 mM potassium phosphate, pH 6.5. The protein was eluted with a linear 0–500 mM NaCl gradient at 1 ml/min.

ACKNOWLEDGMENTS

This material is based in part upon work sponsored by the Defense Advanced Research Projects Agency under Grant N65236-99-1-5422 awarded to F.M.U. The content does not necessarily reflect the position or policy of the U.S. Government, and no official endorsement should be inferred. This work is based in part upon research conducted at the Cornell High Energy Synchrotron Source (CHESS), which is supported by the National Science Foundation under award DMR-9311772, using the Macromolecular Diffraction at CHESS fa-

cility, which is supported by award RR-01646 from the National Institutes of Health. Assistance during data collection at the CHESS synchrotron was provided by MacCHESS staff Drs. Marian Szebenyi and Mike Cook.

REFERENCES

1. Irvin, J. D. (1983) Pokeweed antiviral protein. *Pharmacol. Ther.* **21,** 371–387.
2. Barbieri, L., Batelli, M. G., and Stirpe, F. (1993) Ribosome-inactivating proteins from plants. *Biochem. Biophys. Acta* **1154,** 237–282.
3. Endo, Y., Tsurugi, K., and Lambert, J. M. (1988) The site of action of six different ribosome-inactivating proteins from plants on eukaryotic ribosomes: The RNA N-glycosidase activity of the proteins. *Biochem. Biophys. Res. Commun.* **150**(3), 1032–1036.
4. Dallal, J. A., and Irvin, J. D. (1978) Enzymatic inactivation of eukaryotic ribosomes by the pokeweed antiviral protein. *FEBS Lett.* **89,** 257–259.
5. Gessner, S. L., and Irvin, J. D. (1980) Inhibition of elongation factor 2-dependent translocation by the pokeweed antiviral protein and ricin. *J. Biol. Chem.* **255**(8), 3251–3253.
6. Barbieri, L., Valbonesi, P., Bonora, E., Gorini, P., Bolognesi, A., and Stirpe, F. (1997) Polynucleotide:adenosine glycosidase activity of ribosome-inactivating proteins: Effect on DNA, RNA and poly(A). *Nucleic Acids Res.* **25,** 518–522.
7. Nicolas, E., Beggs, J. M., Haltiwanger, B. M., and Taraschi, T. F. (1988) A new class of DNA glycosylase/apurinic/apyrimidinic lyases that act on specific adenines in single-stranded DNA. *J. Biol. Chem.* **273,** 17216–17220.
8. Wang, P., and Tumer, N. E. (1999) Pokeweed antiviral protein cleaves double-stranded supercoiled DNA using the same active site required to depurinate rRNA. *Nucleic Acids Res.* **27,** 1900–1905.
9. Rajamohan, F., Venkatachalam, T. K., Irvin, J. D., and Uckun, F. M. (1999) Pokeweed antiviral protein isoforms PAP-I, PAP-II, and PAP-III depurinate RNA of human immunodeficiency virus (HIV)-1. *Biochem. Biophys. Res. Commun.* **260,** 453–458.
10. Rajamohan, F., Kurinov, I. V., Venkatachlam, T. K., and Uckun, F. M. (1999) Deguanilation of human immunodeficiency virus (HIV-1) RNA by recombinant pokeweed antiviral protein. *Biochem. Biophys. Res. Commun.* **263,** 419–424.
11. Kurinov, I. V., Rajamohan, F., Venkatachlam, T. K., and Uckun, F. M. (1999) X-ray crystallographic analysis of the structural basis for the interaction of pokeweed antiviral protein with guanine residues of ribosomal RNA. *Protein Sci.* **8,** 2399–2405.
12. Aron, G. M., and Irvin, J. D. (1980) Inhibition of herpes simplex virus multiplication by the pokeweed antiviral protein. *Antimicrob. Agents Chemother.* **17,** 1032–1033.
13. Tomlinson, J. A., Walker, V. M., Flewett, T. H., and Barclay, G. R. (1974) The inhibition of infection by cucumber mosaic virus and influenza virus by extracts from *Phytolacca americana*. *J. Gen. Virol.* **22,** 225–232.
14. Gehrz, R. C., Wilson, C., Eckhardt, J., Myers, D., Irvin, J. D., and Uckun, F. M. (1991) Treatment of human cytomegalovirus (HCMV) with noval antiviral immunoconjugates. *In* Progress in Cytomegalovirus Research (Landini, M. P., Ed.), pp. 353–356, Elsevier, New York.
15. Zarling, J. M., Moran, P. A., Haffar, O., Sias, J., Richman, D. D., Spina, C. A., Myers, D. E., Kuebelbeck, V., Ledbetter, J. A., and Uckun, F. M. (1990) Inhibition of HIV replication by pokeweed antiviral protein targeted to CD4+ cells by monoclonal antibodies. *Nature* **347**(6288), 92–95.
16. Bonness, M. S., Ready, M. P., Irvin, J. D., and Mabry, T. J. (1994) Pokeweed antiviral protein inactivates pokeweed ribosomes; implications for the antiviral mechanism. *Plant J.* **5**(2), 173–183.
17. Chaddock, J. A., Lord, J. M., Hartley, M. R., and Roberts, L. M. (1994) Pokeweed antiviral protein (PAP) mutations which permit *E. coli* growth do not eliminate catalytic activity towards prokaryotic ribosomes. *Nucleic Acids Res.* **22**(9), 1536–1540.
18. Hur, Y., Hwang, D. J., Zoubenko, O., Coetzer, C., Uckun, F. M., and Tumer, N. E. (1995) Isolation and characterization of pokeweed antiviral protein mutations in *Saccharomyces cerevisiae:* Identification of residues important for toxicity. *Proc. Natl. Acad. Sci. USA* **92**(18), 8448–8452.
19. Tumer, N. E., Hwang, D. J., and Bonness, M. (1997) C-terminal deletion mutant of pokeweed antiviral protein inhibits viral infection but does not depurinate host ribosomes. *Proc. Natl. Acad. Sci. USA* **94**(8), 3866–3871.
20. Tumer, N. E., Parikh, B. A., Li, P., and Dinman, J. D. (1998) The pokeweed antiviral protein specifically inhibits Ty1-directed + 1 ribosomal frameshifting and retrotransposition in Saccharomyces cerevisiae. *J. Virol.* **72,** 1036–1042.
21. Irvin, J. D., and Uckun, F. M. (1992) Pokeweed antiviral protein: Ribosome inactivation and therapeutic applications. *Pharmacol. Ther.* **55**(3), 279–302.
22. Irvin, J. D., Kelly, T., and Robertus, J. D. (1980) Purification and properties of a second antiviral protein from *Phytolacca americana* which inactivates eukaryotic ribosomes. *Arch. Biochem. Biophys.* **200**(2), 418–425.
23. Myers, D. E., Irvin, J. D., Smith, R. S., Kuebelbeck, V. M., and Uckun, F. M. (1991) Production of a pokeweed antiviral protein (PAP)-containing immunotoxin, B43-PAP, directed against the CD19 human B lineage lymphoid differentiation antigen in highly purified form for human clinical trials. *J. Immunol. Methods* **136,** 221–237.
24. Rypniewski, W. R., Holden, H. M., and Rayment, I. (1993) Structural consequences of reductive methylation of lysine residues in hen egg white lysozyme: An X-ray analysis at 1.8 Å resolution. *Biochemistry* **32,** 9851–9858.
25. Otwinnowski, Z., and Minor, W. (1998) Processing of X-ray diffraction data collected in oscillation mode. *Methods Enzymol.* **276,** 307–325.
26. Brunger, A. T. (1992) X-PLOR (version 3.1) Manual, Yale Univ. Press, New Haven, CT.
27. Means, G. E., and Feeney, R. E. (1968) Reductive alkylation of amino groups in proteins. *Biochemistry* **7**(6), 2192–2201.
28. Kobayashi, M., Kubota, M., and Matsuura, Y. (1999) Crystallization and improvement of crystal quality for x-ray diffraction of maltooligosyl trehalose synthase by reductive methylation of lysine residues. *Acta Crystallogr. D Biol. Crystallogr.* **55**(Pt 4), 931–933.
29. Irvin, J. D., and Aron, G. M. (1982) Chemical modifications of pokeweed antiviral protein: effects upon ribosome inactivation, antiviral activity and cytotoxicity. *FEBS Lett.* **148**(1), 127–130.
30. Matthews, B. W. (1968) Solvent content of protein crystals. *J. Mol. Biol.* **33**(2), 491–497.
31. Collaborative Computational Project, Number 4 (1994) The CCP4 Suite: Programs for Protein Crystallography. *Acta Cryst.* **D50,** 760–776.
32. Navaza, J., and Saludjan, P. (1997) AMoRe: An automated molecular replacement program package. *Methods Enzymol.* **276,** 581–593.
33. Kurinov, I. V., Myers, D. E., Irvin, J. D., and Uckun, F. M. (1999) X-ray crystallographic analysis of the structural basis for the interactions of pokeweed antiviral protein with its active site inhibitor and ribosomal RNA substrate analogs. *Protein Sci.* **8,** 1765–1772.

Protein Science (1999), 8:1765–1772. Cambridge University Press. Printed in the USA.

X-ray crystallographic analysis of the structural basis for the interactions of pokeweed antiviral protein with its active site inhibitor and ribosomal RNA substrate analogs

I.V. KURINOV,[1] D.E. MYERS,[1] J.D. IRVIN,[2] AND F.M. UCKUN[1]

[1]Hughes Institute, 2665 Long Lake Road, Roseville, Minnesota 55113
[2]SouthWest Texas State University, 601 University Drive, San Marcos, Texas 78666

(RECEIVED March 3, 1999; ACCEPTED May 14, 1999)

Abstract

The pokeweed antiviral protein (PAP) belongs to a family of ribosome-inactivating proteins (RIP), which depurinate ribosomal RNA through their site-specific N-glycosidase activity. We report low temperature, three-dimensional structures of PAP co-crystallized with adenyl-guanosine (ApG) and adenyl-cytosine-cytosine (ApCpC). Crystal structures of 2.0–2.1 Å resolution revealed that both ApG or ApCpC nucleotides are cleaved by PAP, leaving only the adenine base clearly visible in the active site pocket of PAP. ApCpC does not resemble any known natural substrate for any ribosome-inactivating proteins and its cleavage by PAP provides unprecedented evidence for a broad spectrum N-glycosidase activity of PAP toward adenine-containing single stranded RNA. We also report the analysis of a 2.1 Å crystal structure of PAP complexed with the RIP inhibitor pteoric acid. The pterin ring is strongly bound in the active site, forming four hydrogen bonds with active site residues and one hydrogen bond with the coordinated water molecule. The second 180° rotation conformation of pterin ring can form only three hydrogen bonds in the active site and is less energetically favorable. The benzoate moiety is parallel to the protein surface of PAP and forms only one hydrogen bond with the guanido group of Arg135.

Keywords: active site interactions; ribosome inactivating proteins; RNA substrate analogs; X-ray crystallography

Pokeweed antiviral protein (PAP) from the leaves of the pokeweed plant, *Phytolacca americana*, is a naturally occurring 29 kDa single chain ribosome inactivating protein (RIP), which catalytically inactivates both prokaryotic and eukaryotic ribosomes. The therapeutic potential of PAP has gained considerable interest in recent years due to the clinical use of native PAP as the active moiety of immunoconjugates against cancer and AIDS (Irvin & Uckun, 1992).

PAP is a site-specific RNA N-glycosidase that enzymatically removes a single adenine base (A4324) from a highly conserved, surface exposed "α-sarcin" loop of the large rRNA species in eukaryotic (28S rRNA) and prokaryotic (23S rRNA) ribosomes (Irvin, 1983; Endo et al., 1988). This catalytic depurination of the α-sarcin loop, which is positioned in immediate vicinity of the peptidyltransferase center within the 50 S subunit of *Escherichia coli* ribosomes, impairs the interactions between ribosomes and elongation factor 2 (EF–2), resulting in irreversible inhibition of protein synthesis at the EF–2 mediated translocation step (Dallal & Irvin, 1978; Gessner & Irvin, 1980).

PAP has also been shown to effectively inhibit the replication of several plant and animal viruses including poliovirus, herpes simplex virus, cytomegalovirus, influenza virus, and human immunodeficiency virus (HIV)-1 (Zarling et al., 1990; Irvin & Uckun, 1992). The molecular mechanism of the antiviral activity of PAP is under active investigation (Bonness et al., 1994; Chaddock et al., 1994, 1996; Hur et al., 1995; Tumer et al., 1997, 1998; Xu et al., 1998). Besides its ability to inhibit viral protein synthesis, PAP is also capable of directly depurinating viral RNA (Barbieri et al., 1997). Furthermore, PAP also displays viral RNA-specific effects in vivo and has been shown to inhibit ribosomal frameshifting and retrotransposition, a molecular mechanism used by many RNA viruses to produce Gag-Pol fusion proteins (Tumer et al., 1998).

Wild-type PAP was crystallized and its structure refined to a 2.5 Å resolution at room temperature (Monzingo et al., 1993). To date, no structural information has been reported regarding the interaction of PAP with its natural substrates. A working hypothesis regarding the structural basis for the N-glycosidase activity of PAP was proposed based on the structural similarities of the active sites of PAP and a more extensively analyzed RIP, ricin A-chain (Katzin et al., 1991; Kim & Robertus, 1992; Monzingo & Robertus, 1992). This hypothesis was predicated upon the supposition that PAP and ricin A-chain are identical in their enzymatic activity and provides no explanation for the more broad-spectrum N-glycosidase activity of PAP (Hartley et al., 1991; Barbieri et al., 1993; Marchant & Hartley, 1995).

Reprint requests to: F.M. Uckun, Hughes Institute, 2665 Long Lake Road, Roseville, Minnesota 55113; e-mail: fatih_uckun@ih.org.

In this paper, we report a low temperature X-ray structure analysis and supporting modeling studies of the interactions of PAP with nucleotide analogs of its natural rRNA substrate. In particular, the dinucleotide adenyl(3′–5′)guanosine (ApG) and trinucleotide adenyl-cytosine-cytosine (ApCpC) were co-crystallized with PAP and computer modeling studies were performed to elucidate the structural basis of the interactions between PAP and its ligands. The low temperature X-ray data extended to a 1.9 Å resolution allowing a more detailed interpretation of the enzyme-substrate complexes. It was observed that PAP had cleaved both ApG and ApCpC, and only adenine base was visible in the active site pocket. The cleavage of ApCpC, which does not resemble any known natural substrate (GAGAG motif in a RNA stem-loop (Endo et al., 1988; Marchant & Hartley, 1995; Chen et al., 1998)) for any RIP, provides experimental evidence for a broad spectrum N-glycosidase activity of PAP toward any adenine containing single-stranded RNA. To better understand the interaction of the PAP active site with adenine containing oligonucleotides, we also performed a co-crystallization with pteoric acid (PTA), which is a weak inhibitor of ricin (Yan et al., 1997).

Results and discussion

PAP crystals belong to the triclinic space group with two molecules in the unit cell. There are no large conformational differences between the two PAP molecules of the asymmetric unit because of noncrystallographic symmetry restraints imposed during the crystallographic structure refinement. The root-mean-square deviation (RMSD) was 0.07 Å for the main-chain and 0.16 Å for side-chain atoms between two PAP monomers. Overall conformation and mode of interaction of all studied ligands were the same in two monomers. For the purpose of structural comparison, the average values of the two models will be used for subsequent analysis.

Analogous to other RIPs (ricin A-chain, trichosantin, momordin), PAP has a well-defined secondary structure: eight α-helices and a β-sheet composed of six strands. Comparison of our room temperature PAP structure at the resolution 2.0 Å with the published PAP structure at resolution 2.5 Å (Monzingo et al., 1993) shows better stereochemistry with RMSDs of 0.008 Å for bond lengths and 1.6° for angles, as compared to 0.027 Å and 3.4°, respectively, for 1PAF structure. A direct comparison of our structure with the published structure (Protein Data Bank (PDB) code 1PAF) did not show a significant discrepancy for backbone conformation and RMSD for the main-chain atoms was only 0.34 Å. Only a few atoms differ more than 0.9–1.0 Å. The comparison of the residues in the active site region showed even less discrepancy with RMSD of 0.24 Å.

Low temperature studies

In an attempt to prolong the crystal life and improve the resolution limits, we performed a low temperature study of PAP crystals. This is especially important for a triclinic unit cell. The first noticeable effect of lowering temperature was a decrease of unit cell parameters. The relative volume reduction caused by the lowering of temperature was approximately 2.4% and the corresponding actual volume change was 3,060 Å^3 per unit cell. The observed unit cell volume change was smaller than that reported for RNAse (4.7%) (Tilton et al., 1992) or myoglobin (5%) (Frauenfelder et al., 1987). The thermal expansion of the protein can also be parameterized in terms of the radius of gyration. Since the radius of gyration is proportional to the moment of inertia, it gives a rough estimation of protein volume. The radius of gyration calculated for all non-hydrogen atoms of PAP decreased by about 1.9% (this corresponds to a 5.7% decrease of the volume of the appropriate ellipsoid). A similar behavior was observed for the accessible surface area of PAP. A 3.2% decrease in the accessible surface area shows that the roughness of the PAP surface does not increase with freezing and reflects the overall shrinkage of protein. A direct comparison of low temperature (LT) and room temperature (RT) structures shows no significant structural differences except for the usual thermal expansion of the protein substance. Two monomers in the unit cell changed their relative position upon freezing—the relative sliding and pivoting of the monomers occurred to form a more dense packing at low temperature. After rigid-body rotation and translation (which are different for two monomers), both backbones were nearly identical (Fig. 1), which could be a consequence of abundant secondary structure elements. RMSD for the main-chain atoms was 0.30 Å and none of the main-chain atoms, except C- and N-terminus, had deviations more than 1 Å. A comparison between LT and RT structures is even smaller when comparing a secondary structure elements or active site region of the protein. No large conformational reorientations of side chains were observed; only some large and/or disordered side chains became more ordered at LT. We were unable to identify any definitive alternate conformations in PAP at LT. A lower overall B-factor and a smaller range in B-factor profile were observed for the LT structures. Although the temperature factor plotted against the residue number (Fig. 2) showed a similar pattern for LT and RT structures, there were many indications of a nonuniform decrease of the B-factor upon crystal freezing.

PAP interactions with substrate analogs

The structural element of rRNA targeted by PAP (Hartley et al., 1991; Barbieri et al., 1993) is a very conserved stem-loop structure containing the GAGAG motif (the cleaved adenine is underlined). Therefore, we co-crystallized PAP with adenyl-guanosine to elucidate the interactions of PAP with its rRNA substrates. Crystals of PAP-ApG complex have the same space group and very similar unit cell parameters (see Table 1). The initial $2F_o - F_c$ electron density map for PAP complexed with ApG showed continuous density in the active site pocket, which slightly protruded along the protein surface from the PAP active site. This density was initially fitted with ApG having the best and energetically favorable conformation from our modeling studies (see Materials and methods). Initially all atoms of ApG were assigned B-factors of 20 Å^2, close to mean value for the active site residues. The next round of structure refinement (slow cooling annealing, positional, and individual B-factor refinement) lead to an increase of the B-factor for guanosine group up to 40 Å^2 and the B-factor for the adenosine group to ~25 Å^2. The uneven distribution of B-factor on phosphate backbone excluded a consideration of static disorder for the guanosine group. The omit electron density maps showed continuous electron density covering only the adenine group and half of the sugar; the rest of the molecule is covered by separate peaks, more similar to water peaks (Fig. 3). So, we assumed that ApG was cleaved by PAP during the rather long crystallization setup and only the adenine moiety was left bound in the active site pocket. This hypothesis was clearly confirmed by the next round of structure refinement where we retained only the adenine base and in-

Fig. 1. A Cα traces of PAP A-monomers at RT and LT following superimposition of their respective main-chain coordinates. The trace of the RT PAP structure is drawn with thicker line. Comparison of B-monomers shows a similar pattern.

cluded water molecules in the distinctive peaks shown on the previous electron omit map density in place of guanidine and the phosphate linker. Although the resulting difference in *R*-free factor is not substantial (<0.3%), the final omit electron density map clearly covered only the adenine base in the active site and surrounding water molecules without any ambiguity.

Figure 4 shows the binding site region of the omit map for the PAP-adenine complex. The mode of adenine interaction with PAP

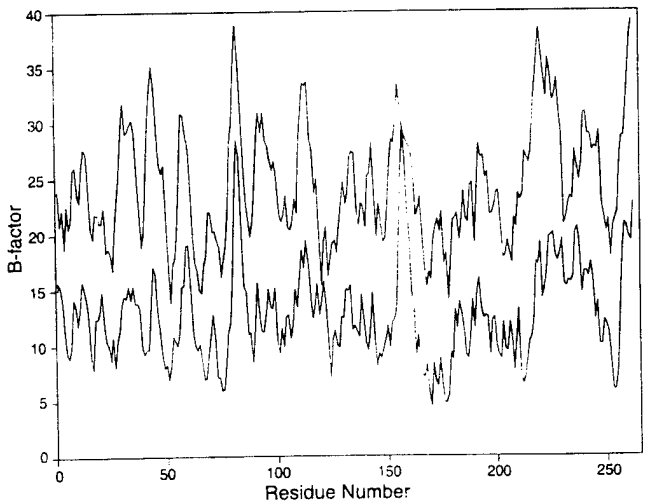

Fig. 2. Main-chain atoms averaged *B*-factor dependence on the residue number for ligand-free PAP structure at RT (upper line) and LT (lower line).

active site residues is essentially identical to that seen previously in ricin complexed with ApG (Monzingo & Robertus, 1992). The adenine ring is sandwiched between tyrosines 72 and 123. N6 of adenine donates a hydrogen bond to the carbonyl oxygen of Val73 (distance 3.4 Å), N1 receives a hydrogen bond from the amino nitrogen of Val73 (distance 2.9 Å). Arg179 can donate a hydrogen bond to N3 (distance 2.6 Å) and N7 is hydrogen bonded to the carbonyl oxygen of Ser121 (2.7 Å). The only noticeable difference between this complex and the complex of PAP with formycin (Monzingo et al., 1993) is the orientation of Tyr72. Tyr72 in the PAP-adenine complex does not appear to have altered its torsion angle χ_1 upon ligand binding as was observed in the PAP-formycin complex. Orientation of the Tyr72 in the PAP-adenine complex remains the same as in ligand-free form of PAP.

The absence of an electron density for the guanosine ring suggests that the enzyme remains active during the crystallization setup. Our study of the PAP-ApG complex follows the earlier study of a PAP complex with formycin-monophosphate (Monzingo et al., 1993). Formycin-monophosphate could not be cleaved by PAP because of the C-C bond between pyrazolepyrimidine and ribose sugar. Ricin A-chain is a more extensively studied RIP and its complexes with adenosine-monophosphate (Weston et al., 1994) and ApG (Monzingo & Robertus, 1992) were described. It was shown that adenosine-monophosphate is cleaved by ricin A-chain (only adenine was seen in the active site). The overall orientation of the dinucleotide ApG with adenine bound in the active site is definitively the same in the ApG-ricin complex and PAP. However, small differences in surface topology near the active site pocket may account for different rates of ApG depurination by PAP and ricin (ApG is not considered as a substrate for ricin in kinetics studies by (Chen et al., 1998)).

Table 1. *Details of data collection and refinement*

	Wild-type PAP RT	Wild-type PAP LT	PAP-ApG complex	PAP-ApCpC complex	PAP-PTA complex
Unit (*a*)	49.47	48.68	48.48	48.64	48.19
Cell (*b*)	49.47	49.09	49.03	49.08	48.50
Å (*c*)	64.77	64.56	63.87	64.39	63.92
α	68.73	67.95	68.79	68.75	68.85
β	81.12	82.90	81.05	82.55	81.78
γ	64.13	65.37	63.88	64.87	64.62
Unit cell volume ($Å^3$)	132,920	129,860	127,080	129,620	128,480
R-merge (%)	4.8	5.9	6.0	6.6	6.9
Resolution limit for refinement	2.0	2.1	2.0	2.1	2.1
Completeness of data used for refinement (%)	91.0	87.0	89.4	87.9	85.3
R-factor (%)	19.9	20.8	23.0	24.5	23.0
Number of water molecules	478	479	448	414	541
Protein *B*-factor (A^2)	23.9	13.3	19.9	20.1	16.2

Taking into consideration the broad specificity of PAP toward ribosomes from different sources and its very high affinity to the adenine base, we tried to explore the binding and interaction of PAP with the tri-nucleotide ApCpC. ApCpC is not known to be a natural substrate for PAP or RIPs, so we expected the PAP–ApCpC complex would at least help to characterize the interaction with phosphate backbone.

ApCpC was co-crystallized with PAP in the same manner as ApG with the same space group and unit cell parameters. However, the examination of the omit map density in the active site pocket again showed the presence of only an adenine base, without any indications of an electron density corresponding to two cytidines. This very unusual result supports the notion that PAP has a high affinity toward adenine-containing oligonucleotides without a high degree of selectivity toward the closest nucleotide residues in the sequence.

PAP complex with pteroic acid (PTA)

To further study the interaction of PAP with ligands, we co-crystallized PAP with pteoric acid. PTA was already shown to be a weak inhibitor of ricin A-chain and X-ray studies demonstrated the putative structure of PTA bound to ricin (Yan et al., 1997). Because there are no known natural inhibitors of PAP, and it is shown that ricin A-chain and PAP share the same active site structure, we decided to use PTA as a possible ligand for PAP. Our

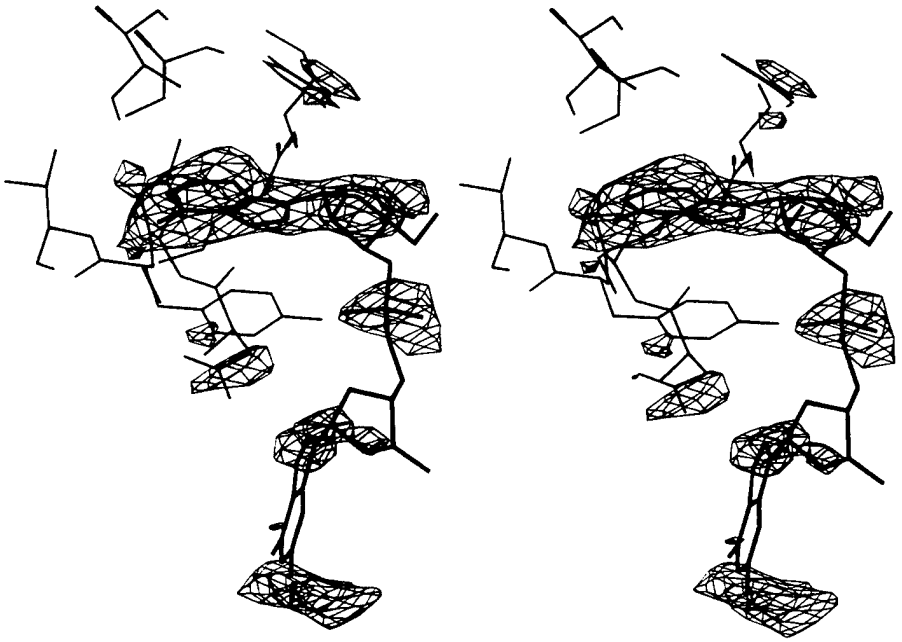

Fig. 3. Omit electron density map ($F_o - F_c$) for PAP-ApG complex at LT. ApG was omitted for map calculations. Model for ApG is drawn in bold. The map is contoured at 1.5σ.

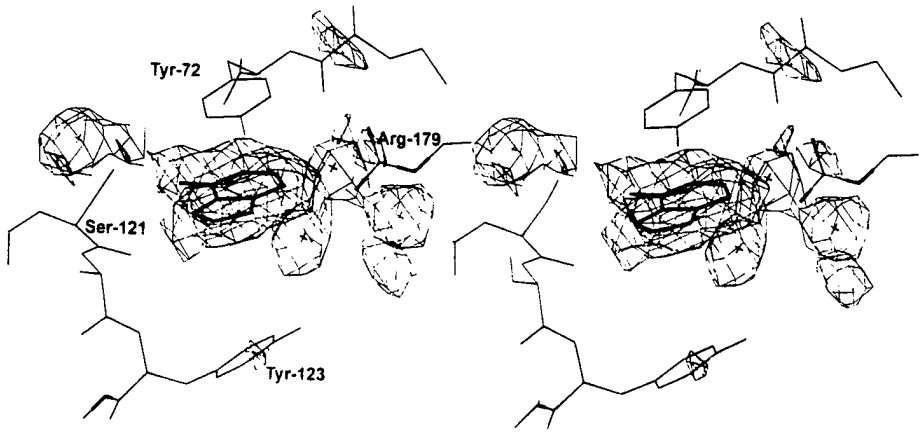

Fig. 4. Omit electron density map ($F_o - F_c$) for PAP-adenine complex at low temperature. Adenine base was omitted for map calculations. The map is contoured at 2σ.

preliminary kinetics data had revealed a decrease of ribosome depurination in the presence of PTA (F. Rajamohan & F.M. Uckun, unpubl. results).

Crystals of PAP complexed with PTA remained isomorphous to ligand-free PAP (see Table 1). Initially PTA was manually docked into the active site pocket in the conformation derived from our computer simulation results. After a crystallographic refinement, the omit electron density map clearly showed a continuous electron density covering the whole PTA molecule. The same orientation of bound PTA was observed in two PAP monomers. Although our modeling studies did not show the preferred orientation of PTA complexed with PAP, the initial electron density was sufficient to properly position the PTA benzoic acid outside the active site pocket. After the second cycle of refinement, the ambiguity concerning the orientation of the main ring in the active site pocket persisted. Therefore, two more cycles of refinement were performed with two different orientation of the pterin ring (180° flipping). The precision of the electron density maps was not enough to discriminate between the two conformations (Fig. 5). However, the mode of interaction of two conformation differ considerably, and we assume that only one of the conformations has the best pattern of hydrogen bonding of pterin ring with the active site residues. The best orientation of the pterin ring reveals four hydrogen bonds to protein atoms (backbone N of Val73, two bonds with Oγ of Ser121 and Oγ of Ser175), and one bond is mediated by strongly bound water molecule, WAT133 (details are displayed on Fig. 6). The second orientation of pterin ring can form only three hydrogen bonds, which are less optimal than those formed in the first orientation. The second orientation of pterin ring inside the PAP active site corresponds to the conformation observed in PTA-ricin complex (Yan et al., 1997), and its interactions with active site residues are similar to those of adenine. We observed a rotation of Tyr72 ring to accommodate pterin ring in the active site.

The benzoate moiety of PTA lies parallel to the protein surface, and its carboxyl oxygen is linked to the guanido group of Arg135. It is apparent that the benzoate group of PTA does not significantly

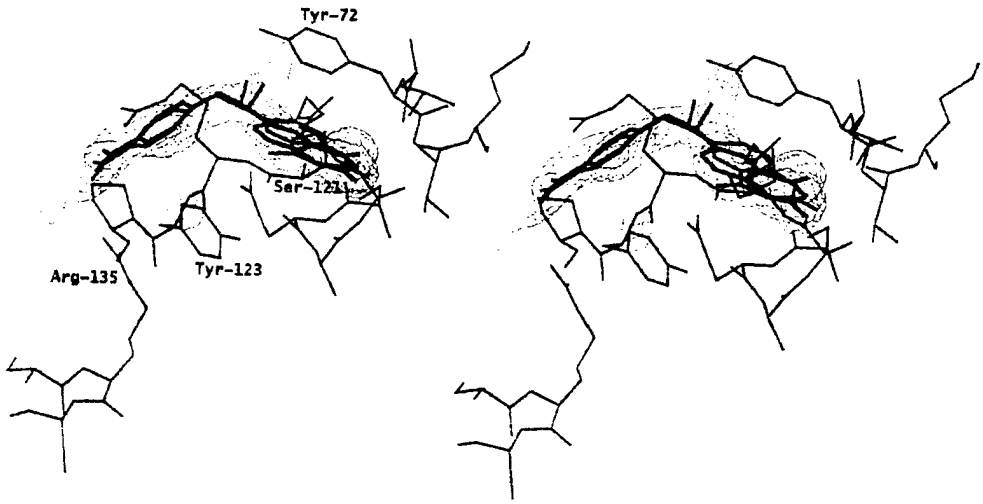

Fig. 5. Omit electron density map ($F_o - F_c$) for PAP-pteoric acid complex at low temperature. PTA was omitted for map calculations. The map is contoured at 2σ. Two different conformations (180° rotation) of pterin ring (shown in blue and red) are superimposed on the figure. The conformation having the more favorable interaction profile is shown in blue.

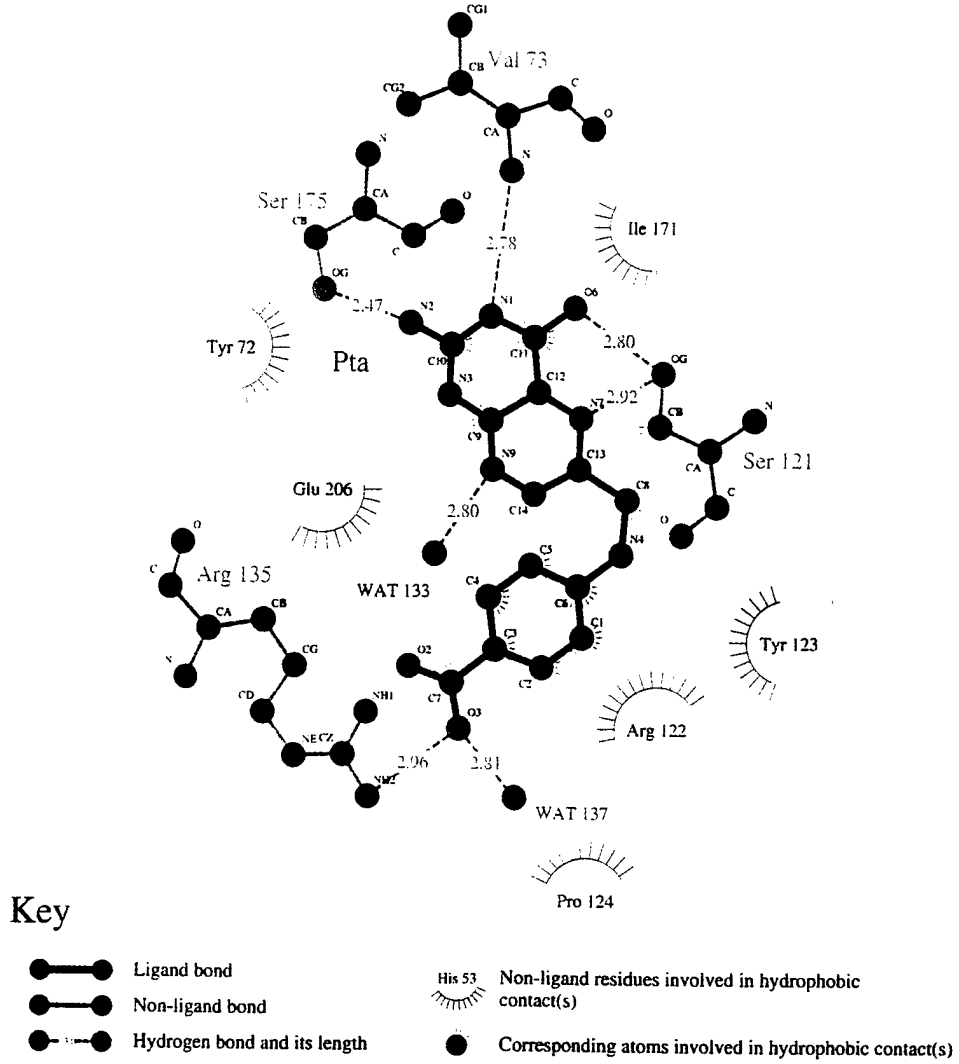

Fig. 6. Details of interaction of pteroic acid with active site residues of PAP. The figure was drawn using LIGPLOT (Wallace et al., 1995).

contribute to the binding of PTA to PAP. The overall orientation of the benzoate group is clearly different from its orientation in the ricin-PTA complex (Yan et al., 1997; Fig. 7). The benzoate ring of PTA is bent around Tyr80 of ricin (Tyr72 of PAP) and its carboxyl oxygen is near Asn78 (Asn70 of PAP). Although Asn78 of ricin and Asn70 of PAP occupy the same position, PTA complexed with PAP cannot assume the same orientation as PTA complexed with ricin because of the different orientation of the tyrosine ring. Side-chain Tyr72 of PAP has more restricted conformational freedom because of the neighboring Ser121. The ricin residue, which correspond to Ser121 of PAP, is Gly121, which has no interactions with the tyrosine ring. Because of the flexible links between pterin and benzoate rings, the latter can adopt a conformation toward Arg135, which is located on the opposite side of the active site from Asn70. In fact, the benzoate rings complexed with both ricin and PAP appear to be bound in a long concave region, which may accommodate a single strand of a natural RNA substrate.

An experimentally obtained three-dimensional structure of PAP complexed with a larger substrate analogue consisting of a stem-loop structure would be likely to provide valuable information about the details of mechanism of PAP enzymatic activity.

Materials and methods

Protein purification and crystallization

PAP was extracted from spring leaves of pokeweed and purified to homogeneity as previously described (Myers et al., 1991). Just before the crystallization setup PAP was repurified on a MonoS cation-exchange column (Pharmacia Biotech, Piscataway, New Jersey) and filtered through 0.22 μm filter. ApG, ApCpC, and pteoric acid were purchased from Sigma (St. Louis, Missouri) and were used without additional modifications.

PAP crystals were obtained from a concentrated PAP preparation (15–20 mg/mL) by the vapor diffusion method within 2–3 weeks using "hanging drop" experiments with 16–18% PEG 4000 and 0.1 M $CaCl_2$ (50 mM Tris-HCl buffer pH = 8) at room temperature. Crystals of PAP-ApG and PAP-ApCpC complexes were grown in the above solution with the addition of 5 mM ApG or ApCpC. PAP-PTA crystals were grown from same solution but saturated with PTA; otherwise the crystallization conditions were identical. Unit cell parameters, details of data collection, and refinement are presented in Table 1. To prolong the crystal lifetime and increase

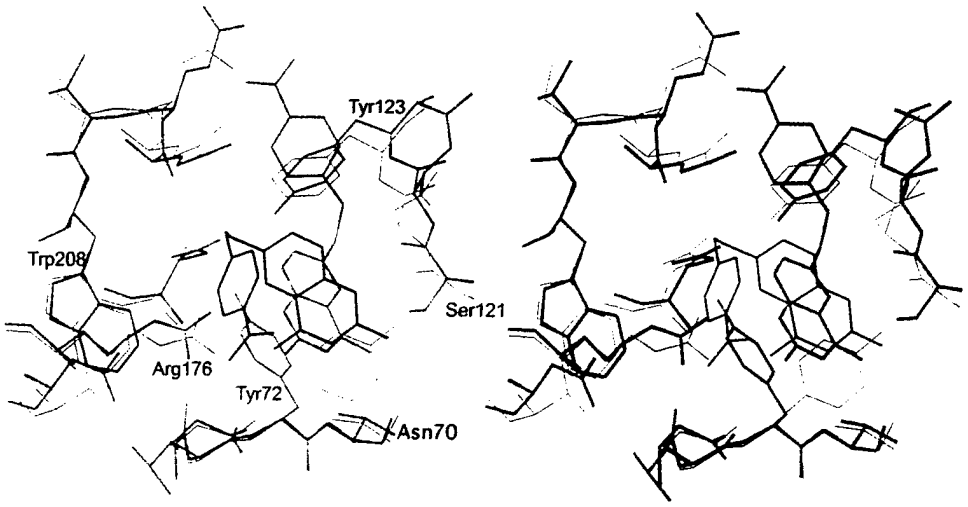

Fig. 7. Stereo view of the superimposition of PAP and ricin (Yan et al., 1997) active site residues with bound PTA. Ricin atoms are shown in thin lines; PTA is black. PAP with bound PTA is drawn in thick lines.

the resolution limits, low temperature studies were done using a 25% PEG4000 solution as a cryoprotectant, and the protein crystal was flash-frozen under a liquid nitrogen stream. Upon freezing, PAP crystals usually exhibited a mosaicity increase of 0.2–0.5°. Low temperature studies (~100 K) were done using the X-stream system from MSC (Woodlands, Texas). Diffraction data were collected on a Rigaku RaxisIY imaging plate. The X-ray source was a copper Rigaku RU300H generator with a double mirror system operating at 50 kV and 100 mA. The crystal-to-detector distance was 150 mm, and the crystal (in one or two different orientations) was rotated around the spindle axis with images collected over 1.5° to a resolution of 1.9–2.0 Å. Data were evaluated using the bioTex processing software (MSC) or HKL package (DENZO and SCALEPACK (Otwinowski & Minor, 1998)). The completeness of data sets at low temperature was over 85% when the completeness of the data set in the last resolution shell was 70–80%. The real resolution of the data, used for structure refinement, was estimated to be 2.0–2.1 Å (see Table 1) taking into consideration the completeness of the last resolution shell, I/σ ratio and R-merge values.

Model refinement

The atomic coordinates of the refined PAP (PDB access code 1PAF) were used for the initial crystallographic phasing and refinement of the new PAP structure. All calculations were done using X-PLOR (version 3.1) (Brünger, 1992). All data with $I/\sigma > 2$ and a low-resolution limit of 8 Å were used for structure refinement. Nonpolar hydrogens were implicitly included in their associated heavy atoms. There were two PAP monomers per unit cell, and they are approximately related by a twofold symmetry nearly coincident with the crystallographic a-axis. During the crystallographic refinement we imposed noncrystallographic symmetry (NCS) restraints on the atom position and B-factors of two monomers, including ligand models. At the early stage of the crystallographic refinement, strong NCS restraints were imposed to keep the structure of two molecules close and not to increase the free R-factor. As the refinement progressed, the values of the effective energy constant for the positional restraints between two monomers were relaxed from 300 to 60 kcal/mol/Å^2 for the main-chain atoms and 30 kcal/mol/Å^2 for the side-chain atoms. Complete removal of NCS restraints led to a small increase of R-free factor.

A few cycles of slow-cooling annealing (3,500 → 100 K), positional and restrained isotropic temperature factor refinements were followed by visual inspection of electron density maps, including omit maps, coupled with a manual model building (when necessary) using the graphics program CHAIN (Sack, 1988). A ligand-free PAP structure at room temperature (RT) was used as a starting point for the refinement of every PAP structure at low temperature (LT). Strong stereochemical restraints were imposed during the crystallographic refinement and all final PAP structures possessed a similarly good stereochemistry with an RMSD of ~0.008 Å for bond lengths and ~1.4° for angles. The RMSD between two molecules before and after the final round of refinement was 0.06 Å. The quality of the stereochemistry of the final protein structure was assessed with the PROCHECK package (Laskowski et al., 1993). The Ramachandran plot shows no residues in disallowed regions (data not shown).

All procedures during crystal growing, data collection and processing as well as structure refinement were identical for all studied complexes, which simplified the comparison of the final structures and eliminated some of the systematic errors. As a better guide to the quality of the structure, the values of the free R-factor were monitored during the course of the crystallographic refinement. The final value of free R-factors did not exceed the overall R-factor by more than 7%.

The refined coordinates of wild-type PAP at low temperature and PAP complexes with adenine and pteoric acid have been deposited in the PDB (access codes 1QCG, 1QCI, and 1QCJ, respectively).

Ligand docking modeling

The molecular docking of ligands and estimation of the interaction scores were done using a *Fixed Docking* procedure in the *Affinity*

program within the InsightII modeling software (InsightII User Guide, 1996). We created a definitive binding set of PAP residues in the active site pocket to move as a 3.5 Å shell around the manually docked ligand during the energy minimization. The number of final docking positions was set to 20, although finally only 3–5 promising positions were identified. The calculations used a CVFF force-field in the *Discovery* program and a Monte Carlo strategy in the *Affinity* program. Each energy-minimized final docking position of the ligand was evaluated using the interactive score function in the *Ludi* module. Ludi score includes contribution of the loss of translational and rotational entropy of the fragment, number and quality of hydrogen bonds, and contributions from ionic and lipophilic interactions to the binding energy.

Acknowledgments

This material is based in part upon work sponsored by the Defense Advanced Research Projects Agency under Grant N65236-99-1-5422. The content does not necessarily reflect the position or policy of the U.S. Government, and no official endorsement should be inferred.

References

Barbieri L, Batelli MG, Stirpe F. 1993. Ribosome-inactivating proteins from plants. *Biochem Biophys Acta 1154*:237–282.

Barbieri L, Valbonesi P, Bonora E, Gorini P, Bolognesi A, Stirpe F. 1997. Polynucleotide: Adenosine glycosidase activity of ribosome-inactivating proteins: Effect on DNA, RNA and poly(A). *Nucl Acids Res 25*:518–522.

Bonness MS, Ready MP, Irvin JD, Mabry TJ. 1994. Pokeweed antiviral protein inactivates pokeweed ribosomes: Implications for the antiviral mechanism. *Plant J 5*(2):173–183.

Brünger AT. 1992. *X-PLOR (version 3.1). A system for X-ray crystallography and NMR*. New Haven, Connecticut: Yale University Press. 405 pp.

Chaddock JA, Lord JM, Hartley MR, Roberts LM. 1994. Pokeweed antiviral protein (PAP) mutations which permit *E. coli* growth do not eliminate catalytic activity towards prokaryotic ribosomes. *Nucl Acids Res 22*(9):1536–1540.

Chaddock JA, Monzingo AF, Robertus JD, Lord JM, Roberts LM. 1996. Major structural differences between pokeweed antiviral protein and ricin A-chain do not account for their differing ribosome specificity. *Eur J Biochem 235*(1–2):159–166.

Chen XY, Link TM, Schramm VL. 1998. Ricin A-chain: Kinetics, mechanism and RNA stem-loop inhibitors. *Biochemistry 37*(33):11605–11613.

Dallal JA, Irvin JD. 1978. Enzymatic inactivation of eukaryotic ribosomes by the pokeweed antiviral protein. *FEBS Lett 89*:257–259.

Endo Y, Tsurugi K, Lambert JM. 1988. The site of action of six different ribosome-inactivating proteins from plants on eukaryotic ribosomes: The RNA N-glycosidase activity of the proteins. *Biochem Biophys Res Commun 150*(3):1032–1036.

Frauenfelder H, Hartmann H, Karplus M, Kuntz ID Jr, Kuriyan J, Parak F, Petsko GA, Ringe D, Tilton RF Jr, Connolly ML, Max N. 1987. Thermal expansion of a protein. *Biochemistry 26*(1):254–261.

Gessner SL, Irvin JD. 1980. Inhibition of elongation factor 2-dependent translocation by the pokeweed antiviral protein and ricin. *J Biol Chem 255*:3251–3253.

Hartley MR, Legname G, Osborn R, Chen Z, Lord JM. 1991. Single-chain ribosome inactivating proteins from plants depurinate *Escherichia coli* 23S ribosomal RNA. *FEBS Lett 290*(1–2):65–68.

Hur Y, Hwang DJ, Zoubenko O, Coetzer C, Uckun FM, Tumer NE. 1995. Isolation and characterization of pokeweed antiviral protein mutations in *Saccharomyces cerevisiae*: Identification of residues important for toxicity. *Proc Natl Acad Sci USA 92*(18):8448–8452.

InsightII User Guide. 1996. San Diego, California: MSI.

Irvin JD. 1983. Pokeweed antiviral protein. *Pharmacol Ther 21*:371–387.

Irvin JD, Uckun FM. 1992. Pokeweed antiviral protein: Ribosome inactivation and therapeutic applications. *Pharmacol Ther 55*(3):279–302.

Katzin BJ, Collins EJ, Robertus JD. 1991. Structure of ricin A-chain at 2.5 Å. *Proteins 10*(3):251–259.

Kim Y, Robertus JD. 1992. Analysis of several key active site residues of ricin A chain by mutagenesis and X-ray crystallography. *Protein Eng 5*(8):775–779.

Laskowski RA, MacArthur MW, Moss DS, Thornton JM. 1993. PROCHECK: A program to check the stereochemical quality of protein structures. *J Appl Crystallogr 26*:283–291.

Marchant A, Hartley MR. 1995. The action of pokeweed antiviral protein and ricin A-chain on mutants in the alpha-sarcin loop of *Escherichia coli* 23S ribosomal RNA. *J Mol Biol 254*(5):848–855.

Monzingo AF, Collins EJ, Ernst SR, Irvin JD, Robertus JD. 1993. The 2.5 Å structure of pokeweed antiviral protein. *J Mol Biol 233*(4):705–715.

Monzingo AF, Robertus JD. 1992. X-ray analysis of substrate analogs in the ricin A-chain active site. *J Mol Biol 227*(4):1136–1145.

Myers DE, Irvin JD, Smith RS, Kuebelbeck VM, Uckun FM. 1991. Production of a pokeweed antiviral protein (PAP)-containing immunotoxin, B43-PAP, directed against the CD19 human B lineage lymphoid differentiation antigen in highly purified form for human clinical trials. *J Immun Methods 136*:221–237.

Otwinowski Z, Minor W. 1998. Processing of X-ray diffraction data collected in oscillation mode. *Methods Enzymol 276*:307–325.

Sack JS. 1988. CHAIN: A crystallographic modeling program. *J Mol Graph 6*:224–225.

Tilton RF Jr, Dewan JC, Petsko GA. 1992. Effects of temperature on protein structure and dynamics: X-ray crystallographic studies of the protein ribonuclease-A at nine different temperatures from 98 to 320 K. *Biochemistry 31*(9):2469–2481.

Tumer NE, Hwang DJ, Bonness M. 1997. C-terminal deletion mutant of pokeweed antiviral protein inhibits viral infection but does not depurinate host ribosomes. *Proc Natl Acad Sci USA 94*(8):3866–3871.

Tumer NE, Parikh BA, Li P, Dinman JD. 1998. The pokeweed antiviral protein specifically inhibits Ty1-directed +1 ribosomal frameshifting and retrotransposition in *Saccharomyces cerevisiae*. *J Virol 72*(2):1036–1042.

Wallace AC, Laskowski RA, Thornton JM. 1995. LIGPLOT: A program to generate schematic diagrams of protein-ligand interactions. *Protein Eng 8*(2):127–134.

Weston SA, Tucker AD, Thatcher DR, Derbyshire DJ, Pauptit RA. 1994. X-ray structure of recombinant ricin A-chain at 1.8 Å resolution. *J Mol Biol 244*(4):410–422.

Xu J, Meng AX, Hefferon KL, Ivanov IG, Abouhaidar MG. 1998. Effect of N-terminal deletions on the activity of pokeweed antiviral protein expressed in *E. coli*. *Biochimie 80*(12):1069–1076.

Yan X, Hollis T, Svinth M, Day P, Monzingo AF, Milne GW, Robertus JD. 1997. Structure-based identification of a ricin inhibitor. *J Mol Biol 266*(5):1043–1049.

Zarling JM, Moran PA, Haffar O, Sias J, Richman DD, Spina CA, Myers DE, Kuebelbeck V, Ledbetter JA, Uckun FM. 1990. Inhibition of HIV replication by pokeweed antiviral protein targeted to CD 4+ cells by monoclonal antibodies. *Nature 347*(6288):92–95.

STRUCTURE-BASED DESIGN AND ENGINEERING OF A NONTOXIC RECOMBINANT POKEWEED ANTIVIRAL PROTEIN WITH POTENT ANTI-HIV ACTIVITY

Fatih M. Uckun‡†*, Francis Rajamohan‡§, Sharon Pendergrass†, Zahide Ozer§, Barbara Waurzyniak‡, Chen Mao§

From the ‡Biotherapy Program, Parker Hughes Cancer Center and the Departments of §Protein Engineering, and †Virology, Parker Hughes Institute, St. Paul, Minnesota 55113

Running title: Rationally Engineered Antiviral Protein

*To whom correspondence should be addressed: Parker Hughes Institute, 2657 Patton Rd., Roseville, MN 55113. Phone: (651) 796-5450; Fax: (651) 796-5493; Email: fatih_uckun@ih.org

This work was supported by the Defense Advanced Research Projects Agency under Grant N65236-99-1-5422 (awarded to F.M.U.).

ABSTRACT

A molecular model of pokeweed antiviral protein (PAP)-RNA interactions was used to rationally engineer FLP-102(^{151}AA^{152}) and FLP-105(^{191}AA^{192}) as nontoxic PAP proteins with potent anti-HIV activity. FLP-102 and FLP-105 have been produced in E. coli and tested both *in vitro* as well as *in vivo*. These proteins depurinate HIV-1 RNA much better than ribosomal RNA and are more potent anti-HIV agents than native PAP or recombinant wildtype PAP. They are substantially less toxic than wildtype PAP and exhibit potent *in vivo* activity against genotypically and phenotypically NRTI-resistant HIV-1 in a surrogate Hu-PBL-SCID mouse model of human AIDS. Rationally engineered nontoxic recombinant PAP proteins such as FLP-102 may provide the basis for effective salvage therapies for patients harboring highly drug resistant strains of HIV-1. The documented in vitro potency of FLP-102, its in vivo antiretroviral activity in HIV-infected Hu-PBL SCID mice, and its favorable toxicity profile warrant the further development of this promising new biotherapeutic agent.

INTRODUCTION

Pokeweed antiviral protein (PAP) is a 29-kDa naturally occurring antiviral agent that can be isolated from the leaves of the pokeweed plant, *Phytolacca americana* (1,2). PAP has a unique ability to depurinate HIV-1 RNA (3,4). PAP exhibits potent antiviral activity against NRTI-resistant primary clinical HIV-1 isolates (5). Both ZDV-sensitive and ZDV-resistant clinical HIV-1 isolates were found to be > 4 log more sensitive to PAP than to ZDV (5). We have cloned the gene for PAP and established procedures for large scale production and purification of the cloned recombinant pokeweed antiviral protein (6,7). We have tested recombinant PAP against a broad panel of viruses *in vitro* and documented that it is as active as native pokeweed antiviral protein against both DNA and RNA viruses (6,7). We were also able to determine the X-ray crystal structure of pokeweed antiviral protein at 2.1A resolution (8,9).

More recently, we have used a molecular model of PAP-HIV RNA interactions (10-12) for the rational design of PAP mutants with potent anti-HIV activity. In the present study, two such recombinant PAP proteins, FLP-102(^{151}AA^{152}) and FLP-105(^{191}AA^{192}) have been engineered, produced, and tested both *in vitro* as well as *in vivo*. These proteins depurinate HIV-1 RNA much better than ribosomal RNA and are more potent anti-HIV agents than native PAP or recombinant wild-type PAP. Our preliminary studies indicate that these proteins are substantially less toxic than wild-type PAP and exhibit potent in vivo activity against a genotypically and phenotypically NRTI-resistant clinical HIV-1 isolate in a surrogate Hu-PBL-SCID mouse model of human AIDS. We hypothesize that FLP-102, because of its potent anti-HIV activity and lack of systemic toxicity, may provide the basis for effective salvage therapies for patients harboring highly drug resistant strains of HIV-1.

MATERIALS AND METHODS

Engineering of Recombinant PAP Proteins. Molecular modeling studies for the rational design of recombinant PAP proteins were performed as previously described in detail (10-12). Recombinant wild-type PAP (PBS-PAP) was obtained by subcloning the *PAP-I* gene (amino acids 22 to 313) into the pBluescript SK- expression vector (6). An uracil-containing template of *PAP* was obtained by transforming *E. coli* CJ236 with the recombinant plasmid PBS-PAP. The oligonucleotides used for site-directed mutagenesis were synthesized on the 200 nmol scale and HPLC purified by Biosynthesis Inc. (Lewisville, TX). Site-directed mutagenesis procedure was performed as described in the manufacturer's manual using the Mutagene M13 *In vitro* Mutagenesis Kit (Bio-Rad, Hercules, CA). DNA sequencing was carried out by the method of Sangers *et al* (13), following the manufacturer's instructions (U.S. Biochemical Corp. Cleveland, OH). Fine chemicals and restriction enzymes were purchased from Roche Molecular Biochemicals (Indianapolis, IN).

Expression and Purification of Recombinant PAP Proteins. Wild-type and mutant PAP proteins were expressed in *E. coli* MV1190 as inclusion bodies and were isolated, solubilized and refolded as described previously (6). The refolded proteins were analyzed by sodium dodecyl sulfate-12% polyacrylamide gel electrophoresis (SDS-12% PAGE). Protein concentrations were quantitated from the gel using bovine serum albumin as a standard.

Immunoblot analysis of PAP mutants. Protein samples were resolved on a SDS-12% PAGE and transfered onto a polyvinylidene difluoride membrane (Bio-Rad) using Bio-Rad trans-blot apperatus, as described previously (6). The membrane was immunoblotted using a rabbit anti-PAP serum (1:2000 dilution) and a horseradish peroxidase- conjugated goat anti-rabbit IgG (Sigma Chemical Co., St. Louis, MO) as the primary and secondary antibodies, respectively. The blot was developed using 3, 3'-diaminobenzidine (Sigma) as the colorimetric indicator for peroxidase activity.

Aniline Cleavage Assays of Ribosomal RNA Depurination. Five micrograms of *E. coli* 23S and 16S rRNA (Roche Molecular Biochemicals) was incubated with increasing amounts of wild-type or mutant PAP protein in 50 µl (final volume) of binding buffer (25 mM Tris.HCl, pH 7.8, 10 mM KCl, 5 mM $MgCl_2$, 2% glycerol) at 37°C for 1 h. The rRNA was extracted with phenol:chloroform (24:24), precipitated with ethanol and treated with 20 µl of 1M aniline acetate (pH 4.5) for 30 min on ice. The rRNA was precipitated with ethanol, electrophoresed in a 6% urea/polyacrylamide gel, and stained with ethidium bromide as described previously (10).

HPLC-Based RNA Depurination Assays. The release of adenine/guanine from *E. coli* 23S+16S rRNA (Roche Molecular Biochemicals) and HIV-1 RNA (ABI Biotechnologies, Columbia, MD) was measured using an HPLC system (Hewlett Packard, Palo Alto, CA), equipped with a diode array detector and a ChemStation software program for data analysis as described previously (3,4). Briefly, 2 µg of the RNA substrate was incubated with 2.5 µM of wild-type or mutant PAP proteins for 1 h at 37°C in 50 µl of binding buffer (25 mM Tris.HCl, pH 7.8, 10 mM KCl, 5 mM $MgCl_2$, 2% glycerol). The reaction was stopped by adding 100 µl of HPLC running buffer (50 mM $NH_4C_2H_3O_2$, 5% methanol, pH 5.0) and 100 µl of the sample was injected automatically into a reverse-phase Lichrospher 100RP-18E analytical column (Hawlett-Pakard, 5 mm particle size, 250 x 4 mm) that was equilibrated with HPLC running buffer as described previously (3,4). Controls included samples containing (a) untreated rRNA, and (b) test samples without rRNA. A calibration curve was generated to establish the linear relationship between the absolute peak area and the quantities of adenine/guanine (Sigma) as described previously (3,4). Unweighted linear regression analysis of the calibration curve was performed using the CA-Cricket graph III computer program (Computer Association, Inc., Islandia, NY). Intra-assay and inter-assay accuracy and precisions were evaluated as described previously (11). Under the described chromatographic conditions, the retension times for adenine and guanine residues were 11.5 min and 5.7 min, respectively, and they were eluted without an interference peak from the blank controls. The lowest limit of detection of adenine was 2.5 pmol at a signal to noise ratio of $\approx$ 3. The average peak area obtained for 50 and 250 pmol/50µl of

adenine standard was 29 ± 1 and 143 ± 7 mAU, respectively. The average peak area obtained for 50 and 250 pmol/50µl of guanine standard was 31 ± 2 and 156 ± 8 mAU, respectively. The intra- and inter-assay coefficients of variation were less than 4%. The overall intra- and inter-assay accuracies of this method were 98.7 ± 1.7 % (N=5) and 95.7 ± 3.0 % (N=5), respectively.

Cell-free Translation Assays. Protein synthesis was assayed in a cell-free system using nuclease-treated rabbit reticulocyte lysates (Promega, Madison, WI) and luciferase mRNA, as described previously (6,10). The IC_{50} (50% inhibitory concentration) values were calculated by nonlinear regression analysis (Prism-2 Graph Pad software, San Diego, CA) using the average values of three independent experiments. The cpm values in control sample with all the reagents added except the test sample ranged from 3 to 4 x 10^7 cpm/ml and were considered as 100% incorporation when determining the % control protein synthesis values for samples treated with test materials.

Ribosome Binding Assays. Ribosomes were isolated from rabbit recticulocyte rich whole blood (Pel-Freez Biologicals, Rogers, AR) as described previously (12). Total ribosomes (30 µg) were incubated with 5 µg of wild-type or mutant PAP proteins to a final volume of 100 µl in binding buffer and incubated at room temperature for 1 h. After incubation, ribosomes were pelleted by centrifugation at 300,000 X g for 30 min at 4°C. The pellets were washed two times with solution D (10 mM Tris-HCl, pH 7.5, 1 mM KCl, 0.1 M $MgCl_2$) and resuspended in 20 µl of PBS (137 mM NaCl, 2.7 mM KCl, 10 mM Na_2HP0_4, 1 mM KH_2PO_4, pH 7.4). The protein samples were resolved on a SDS-12% PAGE gel and transferred onto a polyvinylidene difluoride membrane (Bio-Rad) using the Bio-Rad trans-blot apparatus, as described previously (6,10). The membrane was immunoblotted using a rabbit anti-PAP serum (1:2000 dilution) and horseradish peroxidase- conjugated goat anti-rabbit IgG (Sigma Chemical) as the primary and secondary antibodies, respectively.

L3 Binding Assays - A plasmid containing the cDNA (pJD166.trp) that encodes the wildtype *Saccharomycis cerevisiae* ribosomal protein L3 was a kind gift from Dr. Jonathan D. Dinman, University of Medicine and Dentistry of New Jersey, NJ. Radiolabeled L3 protein was synthesized by a linked transcription-translation system (TNT T3-coupled Reticulocyte Lysate System, Promega) (12) according to the manufacturer's instructions (Promega). The translation products were resolved on a SDS-10% PAGE gel, which was dried and autoradiographed. The mouse anti-L3 monoclonal antibody was a kind gift from Dr. Jonathan R. Warner, Department of Cell Biology, Albert Einstein College of Medicine, Bronx, NY. The *in vitro* synthesized L3 protein (8 X 10^4 cpm) was incubated with 1 µg of wild-type or mutant PAP proteins in 50 µl (final volume) of binding buffer (10 mM K_2HPO_4, 5 mM NaCl, pH 8.0) at 30 °C for 30 min. The PAP-L3 complex was co-immunoprecipitated by adding 5 µl of the mouse anti-L3 monoclonal antibody (1:500 dilution) (12). After 60 min of incubation at 30 °C, the PAP-L3-antibody complex was precipitated by adding 50 µl of protein A-sepharose beads that had been pretreated with rabbit anti-mouse IgG (20 µl/ml beads) and continued the incubation for another 1 h at 4 °C. The beads were washed three times with phosphate-buffered saline containing 0.1% Triton X-100 and the proteins were eluted from the Sepharose beads with SDS sample buffer. The proteins were separated through SDS-12% PAGE, transferred to a PVDF membrane, and probed with the polyclonal rabbit anti-PAP antibody (1:2000 dilution) and horseradish peroxidase conjugated goat anti-rabbit IgG (1:1000 dilution) as the primary and secondary antibodies, respectively. The blot was developed using 3, 3'-diaminobenzidine (Sigma) as the colorimetric indicator for peroxidase activity. The dried membrane was also exposed to autoradiography to estimate the amounts of L3 protein.

BALB/c Mice- All Balb/c mice used in this study were obtained from the specific pathologen free (SPF) breeding facilities of Taconic (Germantown, NY) at five weeks of age. All husbandary and experimental contact made with the female Balb/c mice were performed in a controlled environment (12-h light/12-h dark photoperiod, 22±1°C, 60±10% relative humidity), which is fully accredited by the USDA (United States Department of Agriculture). All mice were housed in microisolator cages (Lab Products, Inc., Maywood, NY) containing autoclaved bedding. The mice were allowed free access to autoclaved pellet food and tap water throughout the

experiments. Animal studies were approved by Parker Hughes Institute Animal Care and Use Committee and all animal care procedures conformed to the Guide for the Care and Use of Laboratory Animals (National Research Council, National Academy Press, Washington DC 1996).

Toxicity Studies in Mice- The toxicity profile of PAP proteins in Balb/c mice was examined, as previously reported for other new agents (14,15). Female Balb/c mice were injected intravenously with bolus doses of native or recombinant PAP proteins in HEPES buffer at the 2.5, 3.75, 5, 6.25 and 7.5 mg/kg dose levels and were monitored daily for lethargy, cleanliness and morbidity. Control mice were treated with PAP-free HEPES buffer. At the time of death, necropsies were performed and the toxic effects of PAP proteins were assessed. For histopathologic studies, tissues were fixed in 10% neutral buffered formalin, dehydrated, and embedded in paraffin by routine methods. Glass slides with affixed 6 micron tissue sections were prepared and stained with Hemotoxylin and Eosin (H&E). No sedation or anesthesia were used throughout the experiments. Mice were monitored daily for mortality for determination of the day 30 LD_{50} values. Animals were electively sacrificed on day 30 to determine the toxicity of STAMP by examining their blood chemistry profiles and blood counts. Blood was collected by intracardiac puncture following anesthesia with ketamine:xylazine and immediately heparinized. The blood chemistry profiles were examined using a Synchron CX5CE Chemical Analyzer (Beckman Instruments, Inc., Fullerton, CA). Blood counts (red blood cells [RBC], white blood cells [WBC] and platelets (Plt]) were determined using a HESKA Vet ABC-Diff Hematology Analyzer (HESKA Corporation, Fort Collins, CO). Absolute neutrophil counts (ANC) and absolute lymphocyte counts (ALC) were calculated from WBC values after determining the percentages of neutrophils and lymphocytes by a manual differential count.

SCID mouse model of human AIDS- All CB-17 SCID mice used in the present study were purchased from Taconic Labs (Germantown, NY) at 6-8 weeks of age and maintained in the Level 3 (BL-3) Containment Facility for Preclinical Research of the Parker Hughes Institute. All husbandry and experimental contact made with the mice maintained specific-pathogen-free conditions. The mice were housed in Micro-Isolator cages containing autoclaved food, water, and bedding. Trimethoprim-sulfamethoxazole (Bactrim) was added to the drinking water of the SCID mice three times a week. Human peripheral blood lymphocyte-SCID (Hu-PBL-SCID) mice were

generated by reconstituting SCID mice by intraperitoneal injection of $10x10^6$ PBMC from seronegative volunteer donors, as previously reported (16). Two weeks after inoculation of the cells, mice were anesthetized with Isoflurane and then challenged by intraperitoneal injection of $1x10^5$ median tissue culture infectious doses ($TCID_{50}$) of cell-free BR/92/019, a genotypically and phenotypically NRTI-resistant HIV-1 isolate. SCID mice were infected with BR/92/019 in the BL-3 containment facility, and all manipulations were performed in a biosafety cabinet. PAP proteins were administered by intraperitoneal injections. Throughout the experimental period, mice were monitored daily for overall health and survival. Two weeks after infection, Hu-PBL-SCID mice were electively killed, and their peritoneal lavage cells as well as spleen cells were examined for evidence of infection by an HIV-1 co-culture assay (5) and determination of the viral RNA load by RT PCR using the Organon Teknika's® Nuclisens™ HIV-1 QT assay kit. Extraction of RNA was done with silica (50 µL) utilizing standard Boom technology and the NucliSens™ Extractor. Standard amplification (NASBA - nucleic acid sequence-based amplification) and detection assay was performed according to the manufacturer's recommendations. Detection was based on electrochemiluminescent (ECL) labels that emit light due to chemical reactions occurring on the surface of an electrode. Differences in the proportional response rate in different drug treatment groups were analyzed using a Chi-Squared test of independence. To compare the HIV burden of SCID mice with PCR evidence of HIV infection, a logistic regression was fitted to obtain the dose level at which the mean HIV burden in the tested tissues was reduced by 50% (95% confidence intervals). For histopathologic studies, tissues were fixed in 10% neutral buffered formalin, dehydrated, and embedded in paraffin by routine methods. Glass slides with affixed 6-µm tissue sections were prepared, stained with hematoxylin-eosin, and submitted to the veterinary pathologist for examination in a blinded fashion.

RESULTS AND DISCUSSION

Structure-Based Design and Engineering of Nontoxic PAP Proteins with Potent Anti-HIV Activity.

Our molecular modeling studies indicated that ribosomal RNA and HIV-1 RNA adopt distinctly different binding modes in their interactions with PAP. In a systematic search for specific mutations that might result in selective enhancement of the anti-HIV activity of PAP, we noticed that the residue I152 on the opposite side of the active site is buried (**Figure 1**). Residues K151 and I152 are located on helix α4 which is followed by a loop and helix α5. The side chain of I152 is mostly buried in hydrophobic contact (~3-4Å) with those of F158 (from the loop), T162 and F166 (helix α5), and Y76 from the middle β strand. In contrast, the side chain of K151 is mostly exposed and may form a hydrogen bond with N148 from the same helix. Residue 152 is approximately 20 Å from the catalytic residue R179 and situated on the opposite side of the PAP active site. It is known that alanine substitution of hydrophobic residues on an alpha helix would generally not disrupt a helical conformation (16). In many cases, a large-to-small mutation such as I152A may, in fact, be structurally favored for a helical conformation (17). However, in light of multiple van der Waals contacts between I152 and surrounding residues, I152A mutation could potentially create a cavity in an otherwise tightly packed hydrophobic region. The bulky isoleucine side chain within the core of the protein confers greater hydrophobic stabilization than is the case for the smaller alanine side chain. The Ile-->Ala substitution that can create a large cavity would be especially destabilizing because it would result in a loss of both hydrophobic and van der Waals interactions. Consequently, the surrounding residues would relax and reduce the volume of the putative cavity. Such mutations may cause local conformational instability and lead to a significant conformational change (18). The side chain of the residue could rotate into a radically different orientation and permit repacking of the core as exemplified in the S117 mutation observed in T4 lysozyme. Such repacking is associated with adjustments of both the main chain and side chains. The backbone of a protein that contains mutated residues could deviate from the natural conformation. Such conformational changes could reach and affect the dynamic behavior of the catalytic residues that are farther than 25 Å away, as previously shown for the G93A mutation in SOD (19, 20). We and other groups have long recognized the dramatic effect that this kind of mutation may affect the enzyme activity (not substrate binding) and have been actively pursuing the concept in our protein engineering.

We have previously modeled the complex structure of PAP with ribosome, based on the crystal structures of PAP and ribosome, and the complex structure of PAP with an HIV viral RNA substrate. The proposed structural model is in good agreement with our mutation studies of residues involved in the active site and the extended substrate-binding site (10). Based on our modeling analyses, we have recognized that the binding mode of ribosome is distinctly different from that of viral RNA as shown in Figure 1. Our modeling studies indicated that a substitution of this isoleucine with a smaller residue such as alanine (I152A) would likely create a cavity causing a repacking of the core and considerable conformational changes of the active site that would be selectively unfavorable for PAP-mediated depurination of ribosomal RNA, but possibly would not affect the catalytic depurination of HIV-1 RNA.

A double mutation of both I152 and K151 residues was predicted to result in a more substantial loss of ribosome inhibitory activity than single mutations involving only one of these two residues. Residues F191 and N192 are located in a more flexible environment on the C-terminal end of helix 6 approximately 20 Å away from the catalytic residue R179 (**Figure 1**). Similar to the binding environment of I152, the side chain of F191 is buried and is in hydrophobic contact with the side chains of I142, I13, Y16 and the hydrophobic portion of K188, all of which are situated on nearby helices. The side chain of N192 is mostly exposed and shows no significant contact with nearby residues. Substitutions of these residues with alanine or glycine were postulated to cause conformational changes in the active site leading to a moderately reduced activity towards ribosomal RNA (but not HIV-1 RNA) substrates, albeit to a much lesser degree than the I152A mutation. However, none of the K151, I152, F191, or N192 mutations would cause an impairment in the ability of the respective PAP proteins to bind ribosomes or the ribosomal protein L3 which interacts with the partially exposed half of the active site cleft (**Figure 1**).

The recombinant PAP mutants with alanine substitutions of I152, K151, and F191, and glycine substitution of N192 were constructed using site-directed mutagenesis, as previously described (10). The mutant proteins FLP-100 (K151A), FLP-101(I152A), FLP-102 (K151A,I152A), FLP-103(F191A), FLP-104(N192G), and FLP-105(F191A,N192G) were expressed in the *E. coli* strain, MV1190, as inclusion bodies, purified, solubilized, refolded and analyzed by SDS-PAGE (Figure 2A). Each of the mutant PAP proteins had an apparent

molecular mass of 33 kDa similar to that of the recombinant wild-type PAP (**Figure 2A**). The refolded recombinant wild-type and mutant proteins were highly immunoreactive with the anti-PAP serum (**Figure 2B**).

The IC_{50} value of recombinant wild-type PAP in cell free translation inhibition assays was 3 ng/mL (**Figure 3, Table 1**). By comparison, the IC_{50} values for the double substitution mutants FLP-102 and FLP-105 were 994 ng/ml and 105 ng/ml, respectively. Thus, FLP-102 was 331-fold less toxic than wild type PAP and FLP-105 was 35-fold less toxic than wild type PAP (Figure 3, Table 1). The corresponding single residue mutants FLP-100 (K151A), FLP-101 (I152A), FLP-103 (F191A) and FLP-104 (N192G) also were less toxic than the wild type PAP (**Figure 3, Table 1**). As shown in **Table 1**, most of the 331-fold activity loss for FLP-102 could be attributed to the I152A mutation since the single residue substitution mutant FLP-101(I152A) was 206-fold less toxic but the single residue substitution mutant FLP-100 only 49-fold less toxic than wildtype PAP . In light of moderate changes in PAP activity as a result of the F191A and N192G mutations, the level of conformational change probably is less profound than that caused by I152A. Nevertheless, the F191A mutation probably adopts the same mechanism as proposed for the I152A mutation (leading to reduced activity), but with less impact.

Compared with the K151A and I152A mutations in FLP-102, the F191A and N192G mutations in FLP-105 had a lesser effect on PAP activity against the ribosomal and viral RNA substrates. Both N192G and F191A resulted in moderate reduction in ribosomal deactivation activity and slightly improved activity against HIV RNA substrate. This is consistent with the observation that N192 and F191 are located in more flexible environment than I152 is in. In light of moderate changes in PAP activity as a result of these two mutations, the level of conformational change probably is less profound than that caused by I152A. Nevertheless, the F191A mutation probably adopts the same mechanism as proposed for the I152A mutation (leading to reduced activity), but with less impact.

The ability of FLP-102 and FLP-105 proteins to depurinate rRNA in rabbit ribosomes was also evaluated by treating the ribosomes with the PAP proteins, subsequent purification of rRNA, and cleavage with aniline. Aniline cleaves the sugar-phosphate backbone of rRNA at PAP depurination sites. Therefore, the release of fragments from aniline-treated rRNA is an indicator of PAP-mediated rRNA depurination. As shown in **Figure 4**, aniline treatment resulted in the release of a 600 nt RNA fragment from rRNA of rabbit ribosomes pretreated

with the recombinant wild-type PAP. In contrast, aniline treatment failed to cause the release of the 600 nt RNA fragment from rRNA isolated from ribosomes treated with the mutant PAP proteins FLP-102 or FLP-105. These findings are consistent with the markedly reduced ribosome inhibitory activities of these recombinant PAP proteins in *in vitro* translation assays (**Figure 3**). In accord with the predictions of our modeling studies, the reduced ribosome inhibitory activity of FLP-102 or FLP-105 was not due to reduced binding to ribosome, the ribosomal protein L3, which serves as a docking site for PAP, or the SR-loop (**Figure 5**).

We next compared the ability of the mutant PAP proteins FLP-102 and FLP-105 to depurinate ribosomal RNA versus HIV-1 RNA to that of recombinant wildtype PAP using HPLC-based quantitative adenine release assays.While recombinant wild-type PAP depurinated ribosomal RNA more efficiently than HIV-1 RNA, both FLP-102 and FLP-105 were more efficient in depurinating HIV-1 RNA and their activity against HIV-1 RNA was superior to that of wild type PAP (**Table 2**). FLP-102 exhibited the most promising selective anti-HIV activity: Whereas the adenine release from E.coli ribosomal RNA wildtype PAP protein was 76±4 pmols/μg RNA/μmols protein, FLP-102 protein was 10-fold less active and released only 7±2 pmols adenine/μg RNA/μmols protein ($P<0.05$, Table 2, **Figure 6**). However, FLP-102 was more potent in deadenylating HIV-1 RNA than wildtype PAP: Whereas wildtype PAP released 36±3 pmols adenine/μg RNA/μmols protein, FLP-102 released 100±7 pmols adenine/μm RNA/μmols protein ($P<0.05$) (**Table 2, Figure 6**). Similar results were obtained in guanine release assays (**Table 2**).

We next examined in 6 independent experiments each performed in triplicate the ability of FLP-102 and FLP-105 to inhibit the replication of the HIV-1 strain HTLVIIIB in human peripheral blood mononuclear cells (**Table 2**). Both proteins inhibited the HIV-1 replication in a concentration dependent fashion with IC_{50} values of 0.2±0.0 μg/mL for FLP-102 and 0.7±0.2 μg/mL for FLP-105. By comparison, the wildtype protein FLP-WT was less active than either protein and inhibited the HIV-1 replication with an IC_{50} value of 2.9±1.3 μg/mL (Table 2, $P<0.001$).

In Vivo Anti-HIV Activity of FLP-102 and FLP-105.

FLP-102 and FLP-105 were nontoxic to BALB/c mice even at a 150 μg/mouse (~7.5 mg/kg) dose level, whereas wild type native PAP was exhibited toxicity at a 50 μg/mouse dose level and was invariably fatal at ≥125

μg/mouse dose level (Figure 7, Table 3). Control mice (n=10) were treated with i.p. injections of the PAP-free vehicle solution. All 49 FLP-102 -treated mice and all 50 FLP-105-treated mice remained healthy throughout the 30 day observation period with no evidence of morbidity. Blood tests done on day 30 did not suggest any significant systemic toxicity. In particular, even at the highest cumulative dose level of 150 μg/mouse, neither FLP-102 nor FLP-105 caused (a) anemia, neutropenia, or lymphopenia suggestive of hematologic toxicity, (b) elevations of BUN and creatinine or electrolyte disturbances suggestive of renal toxicity, (c) elevations of AST, ALT, Alk. Ptase, LDH, or bilirubin suggestive of hepatotoxicity, or (d) elevation of amylase suggestive of pancreas toxicity (**Table 3**).

We next sought to determine if FLP-102 and FLP-105 exhibit any *in vivo* anti-HIV activity in the Hu-PBL-SCID mouse model of human AIDS. Control mice were treated either with vehicle alone (negative control treatment) or with AZT+3TC (positive control treatment). FLP-102 and FLP-105 were used at the daily nontoxic dose levels of 20-40 μg/mouse (2-4 mg/kg), 5 days/week x 2weeks, administered by i.p bolus injections. AZT/3TC combination was used at a dose level of 8mg zidovudine/AZT+4 mg lamivudine/3TC, administered via gavage twice daily for 5 days/weekx 2 weeks. All mice were reconstituted with $10x10^6$ PBMC and infected with $1x10^5$ $TCID_{50}$ of the genotypically and phenotypically NRTI-resistant HIV-1 isolate BR/92/019 two weeks after reconstitution. Treatments were started immediately after the inoculation of the HIV-1 isolate. Spleen specimens from 9 of 10 (90%) vehicle-treated control mice were HIV-1 PCR-positive with an HIV RNA burden of 3.9±0.3 logs, whereas spleen specimens from only 3 of 10 (30%) AZT/3TC-treated mice were HIV-1 PCR-positive with an HIV RNA burden of 3.2±0.3 logs (**Table 4**). By comparison, spleens from only 2 of 10 (20%) FLP-102 treated mice (average HIV RNA burden = 2.9 logs) and 3 of 10 (30%) FLP-105-treated mice (average HIV RNA burden = 3.2±0.3 logs) were HIV-1 PCR-positive. Thus, both FLP-102 and FLP-105 were at least as effective as the in preventing the in vivo HIV-1 replication in the spleen of Hu-PBL-SCID mice. Peritoneal lavage specimens from 7 of 8 vehicle-treated control mice and 6 of 10 AZT/3TC-treated mice were HIV-1 PCR-positive. In contrast, none of peritoneal lavage specimens from 9 FLP-102 treated mice and the peritoneal lavage specimens from only 3 of the 9 FLP-105-treated mice showed PCR evidence of HIV-1 infection (**Table 4**). The in vivo anti-HIV activity of the mutant PAP proteins was further confirmed by HIV-11 cultures of spleen specimens. Whereas 9 of 10 spleen specimens and 9 of 10 spleen + lavage (mixed) specimens from vehicle-treated control

mice were HIV-1 culture-positive, only 2 of 10 spleen specimens and 3 of 10 spleen + lavage specimens from FLP-102-treated mice were HIV-1 culture-positive. By comparison, 3 of 10 spleen specimens and 5 of 10 spleen + lavage specimens from FLP-105-treated mice were HIV-1 culture-positive. Thus both PAP mutants were at least as effective as the AZT/3TC combination and FLP-102 was the most active PAP protein in preventing the HIV-1 replication in Hu-PBL-SCID mice.

Combination antiretroviral therapy has become the standard of care for patients with HIV infection in the United States (21-27). Anti-retroviral treatment regimens employing combinations of drugs from at least two of the three classes of antiretroviral therapy, namely nucleoside analog RT inhibitors (NRTI), non-nucleoside analog RT inhibitors (NNRTI), and protease inhibitors, exhibit a potent and sustained antiviral effect and confer consistent long-term viral suppression in patients with HIV infection (21-27). However, the individual components of these combination regimens can select for drug-resistant viruses and the emergence of antiviral drug resistance limits their clinical benefit (28-36). This resistance is a consequence of the high mutation rate and fast replication of HIV and the selective effect of these drugs, which favors emergence of mutations that can establish clinical drug resistance. Recent results indicate that failure of the highly active antiretroviral therapy (HAART), which typically includes at least 2 NRTI and a protease inhibitor or a NNRTI, results from the multiplicity of mutations that confer genotypic resistance to almost all available antiretroviral drugs (28-36). In these patients, genotypic resistance tests confirm the lack of alternative salvage therapy strategies based on the currently available antiretroviral drugs (28-36). Patients failing on HAART constitute a reservoir of multidrug resistant HIV that may limit treatment options in the future. The frequency of genotypic and phenotypic drug-resistant HIV is increasing among therapy-naive HIV-infected seroconverters (28-36). Thus, the transmission of drug-resistant HIV is a serious problem that merits further attention by public health officials as well as virologists and clinicians. Therefore, there is an urgent need for new anti-HIV agents capable of inhibiting the replication of drug-resistant HIV. Rationally engineered nontoxic recombinant PAP proteins such as FLP-102 may provide the basis for effective salvage therapies for patients harboring highly drug resistant strains of HIV-1. The documented in vitro potency of FLP-102, its in vivo antiretroviral activity in HIV-infected Hu-PBL SCID mice, and its favorable toxicity profile warrant the further development of this promising new biotherapeutic agent.

REFERENCES

1. Irvin JD and Uckun (1992) Pokeweed antiviral protein: ribosome inactivation and therapeutic applications. *Pharmacol Ther* 55:279-302.

2. Zarling JM, Moran PA, Haffar O, Sias J, Richman DD, Spina CA, Myers DE, Kuebelbeck V, Ledbetter JA, and Uckun FM (1990) Inhibition of HIV replication by pokeweed antiviral protein targeted to $CD4^+$ cells by monoclonal antibodies. *Nature* 347:92-95.

3. Rajamohan F, Kurinov I, Venkatachalam T, Uckun FM. Deguanylation of Human Immunodeficiency Virus (HIV-1) RNA by Recombinant Pokeweed Antiviral Protein. *Biochemical and Biophysical Research Communications*, 263(2): 419-424, 1999.

4. Rajamohan F, Venkatachalam TK, Irvin JD, Uckun FM. Pokeweed antiviral protein isoforms PAP-I, PAP-II, and PAP-III Depurinate RNA of Human Immunodeficiency Virus (HIV-1). *BBRC*, 260(2): 453-458 , 1999.

5. Erice A, Balfour HH Jr, Myers DE, Leske VL, Sannerud KJ, Kuebelbeck V, Irvin JD and Uckun FM (1993) Anti-human immunodeficiency virus type 1 activity of an anti-CD4 immunoconjugate containing pokeweed antiviral protein. *Antimicrob Agents Chemother* 37:835-838.

6. Rajamohan F, Engstrom CR, Denton TJ, Engen LA, Kourinov I, Uckun FM. High Level Expression and Purification of Biologically Active Recombinant Pokeweed Antiviral Protein. *Protein Expression and Purification*, 16(2): 359-368, 1999.

7. Rajamohan F, Doumbia S, Engstrom C, Pendergrass S, Maher D, Uckun FM. Expression of Biologically Active Recombinant Pokeweed Antiviral Protein in Methylotrophic Yeast Pichia pastoris. *Protein Expression and Purification*, 18(2):193-201, 2000.

8. Kurinov I, Rajamohan F, Venkatachalam T, Uckun FM. X-ray Crystallographic Analysis of the Structural Basis for the interaction of Pokeweed Antiviral Protein with Guanine Residues of Ribosomal RNA. *Protein Science*, 8(11): 2399-2405, 1999

9. Kurinov IV, Myers DE, Irvin JD, Uckun FM. X-ray Crystallographic Analysis of the Structural Basis for the Interactions of Pokeweed Antiviral Protein with its Active Site Inhibitor and Ribosomal RNA Substrate Analogs. *Protein Science*, 8(9): 1765-1772, 1999.

10. Rajamohan F, Pugmire M, Kurinov I, Uckun FM. Modeling and Alanine-Scanning Mutagenesis Studies of Recombinant Pokeweed Antiviral Protein. *Journal of Biological Chemistry*, 275(5):3382-3390, 2000.

11. Rajamohan, F., Mao, C., Uckun FM. Binding interactions between the active center cleft of recombinant pokeweed antiviral protein and the α-sarcin/ricin stem loop of ribosomal RNA. *Journal of Biological Chemistry*, 276(26): 24075-81, 2001.

12. Rajamohan, F., Ozer, Z., Mao, C., Uckun FM. Active center cleft residues of pokeweed antiviral protein mediate its high affinity binding to the ribosomal protein L3. *Biochemistry*, 40:9104-14, 2001.

13. Sanger, F., Nicklen, S., and Coulson, A. R. (1977) *Proc Natl Acad Sci U S A* 74(12), 5463-7

14. Uckun F. M., Narla R., Zeren T., Yanishevski Y., Myers D. E., Waurzyniak B., Ek O., Schneider E., Messinger Y., Chelstrom L. M., Gunther R., Evans W. (1998): In vivo toxicity, pharmacokinetics, and anti-cancer activity of genistein conjugated to human epidermal growth factor. Clin. Cancer Res. 4, 1125-1134.

15. Uckun FM, Chelstrom LM, Tuel-Ahlgren L, Dibirdik I, Irvin JD, Langlie, MC, Myers, DE (1998) TXU (anti-CD7)-pokeweed antiviral protein as a potent inhibitor of human immunodeficiency virus. *Antimicrob Agents Chemother apy* 42:383-388.

16. Bell JA, Becktel WJ, Sauer U, Baase WA, Matthews BW. Biochemistry 1992 Apr 14;31(14):3590-6

17. Zhang XJ, Baase WA, Matthews BW. Protein Sci 1992 Jun;1(6):761-76.

18. Matthews BW. Adv Protein Chem 1995; 46:249-78.

19. Yim HS, Kang JH, Chock PB, Stadtman ER, Yim MB. J Biol. Chem. 1997 Apr 4; 272(14):8861-3

20. Liu R. et al. Radiation Research, 151, 133-141, 1999.

21. Gottlieb MS. 2001. AIDS--past and future. N Engl J Med 344(23):1788-91

22. Sepkowitz KA. 2001. AIDS--the first 20 years. N Engl J Med 344(23):1764-72

23. Freedberg KA, Losina E, Weinstein MC, Paltiel AD, Cohen CJ, Seage GR, Craven DE, Zhang H, Kimmel AD, Goldie SJ. 2001. The cost effectiveness of combination antiretroviral therapy for HIV disease. N Engl J Med 344(11):824-31.

24. Richman DD. 2001. HIV chemotherapy. Nature 410:995-1001.

25. Shafer RW, Vuitton DA. 1999. Highly active antiretroviral therapy (HAART) for the treatment of infection with human immunodeficiency virus type 1. Biomed Pharmacother 53(2):73-86

26. Starr SE, Fletcher CV, Spector SA, Yong FH, Fenton T, Brundage RC, Manion D, Ruiz N, Gersten M, Becker M, McNamara J, Mofenson LM, Purdue L, Siminski S, Graham B, Kornhauser DM, Fiske W, Vincent C, Lischner HW, Dankner WM, Flynn PM. 1999. Combination therapy with efavirenz, nelfinavir, and nucleoside reverse-transcriptase inhibitors in children infected with human immunodeficiency virus type 1. Pediatric AIDS Clinical Trials Group 382 Team. N Engl J Med 341(25):1874-81.

27. Rey D, Schmitt MP, Partisani M, Hess-Kempf G, Krantz V, de Mautort E, Bernard-Henry C, Priester M, Cheneau C, Lang JM. 2001. Efavirenz as a substitute for protease inhibitors in HIV-1-infected patients with undetectable plasma viral load on HAART: a median follow-up of 64 weeks. J Acquir Immune Defic Syndr 27(5):459-62.

28. Ross L, Scarsella A, Raffanti S, Henry K, Becker S, Fisher R, Liao Q, Hirani A, Graham N, St Clair M, Hernandez J. 2001. Thymidine analog and multinucleoside resistance mutations are associated with decreased phenotypic susceptibility to stavudine in hiv type 1 isolated from zidovudine-naive patients experiencing viremia on stavudine-containing regimens. AIDS Res Hum Retroviruses 17(12):1107-15

29. Picard V, Angelini E, Maillard A, Race E, Clavel F, Chene G, Ferchal F, Molina JM. 2001. Comparison of Genotypic and Phenotypic Resistance Patterns of Human Immunodeficiency Virus Type 1 Isolates from Patients Treated with Stavudine and Didanosine or Zidovudine and Lamivudine. J Infect Dis 184(6):781-4

30. Suzuki K, Kaufmann GR, Mukaide M, Cunningham P, Harris C, Leas L, Kondo M, Imai M, Pett SL, Finlayson R, Zaunders J, Kelleher A, Cooper DA. 2001. Novel deletion of HIV type 1 reverse transcriptase residue 69 conferring selective high-level resistance to nevirapine. AIDS Res Hum Retroviruses 17(13):1293-6

31. Izopet J, Bicart-See A, Pasquier C, Sandres K, Bonnet E, Marchou B, Puel J, Massip P. 1999. Mutations conferring resistance to zidovudine diminish the antiviral effect of stavudine plus didanosine. J Med Virol 59(4):507-11

32. Venturi G, Romano L, Catucci M, Riccio ML, De Milito A, Gonnelli A, Rubino M, Valensin PE, Zazzi M. 1999. Genotypic resistance to zidovudine as a predictor of failure of subsequent therapy with human immunodeficiency virus type-1 nucleoside reverse-transcriptase inhibitors. Eur J Clin Microbiol Infect Dis 18(4):274-82

33. Kuritzkes DR, Sevin A, Young B, Bakhtiari M, Wu H, St Clair M, Connick E, Landay A, Spritzler J, Kessler H, Lederman MM. 2000. Effect of zidovudine resistance mutations on virologic response to treatment with zidovudine-lamivudine-ritonavir: genotypic analysis of human immunodeficiency virus type 1 isolates from AIDS clinical trials group protocol 315.ACTG Protocol 315 Team. J Infect Dis 181(2):491-7

34. O'Brien WA. 2000. Resistance against reverse transcriptase inhibitors. Clin Infect Dis 30 Suppl 2:S185-92

35. Pillay D, Taylor S, Richman DD. 2000. Incidence and impact of resistance against approved antiretroviral drugs. Rev Med Virol 10(4):231-53

36. Briones C, Soriano V, Gonzalez-Lahoz J. 2000. Prevalence of drug-resistant HIV-1 genotypes in heavily pre-treated patients on current virological failure. AIDS 14(11):1659-60

FIGURE LEGENDS

Figure 1. Molecular Model of PAP-RNA Interactions. *Ribbon and space-filling representation of PAP (blue) complex models with ribosomal RNA (left, in white) and viral RNA (right, in white) molecules.* Residues I152 and K151 (green) as shown in stick model are mutated in FLP-102. Residues F191 and N192 (red) as shown in stick model are mutated in FLP-105. These residues are located on the opposite side of the PAP active site and the mutation of these residues is not predicted to affect the binding of ribosomal RNA or HIV-1 viral RNA substrates. However, residue I152 is buried and the large-to-small mutation of Ile->Ala would presumably create a cavity and would permit repacking of the core; it thus can lead to considerable conformational changes of catalytic residues and differentially affect the activity of PAP against the ribosome substrate and the viral RNA.

Figure 2. Coomassie Blue-stained SDS-12% PAGE (A) and Western blot analysis (B) wild-type and mutant recombinant PAP proteins. Each lane contained 5 μg of recombinant PAP protein. WT, wild-type.

Figure 3. Ribosome inhibitory activity of PAP wild-type and mutants in *in vitro* rabbit reticulocyte lysate system. Each value is an average value obtained in three independent experiments. Protein synthesis was measured by [^{35}S] methionine incorporation and the samples with all the reagents except PAP was assigned a value of 100% incorporation. **(A)** FLP-102 and single residue mutants FLP-100 and FLP-101. **(B)** FLP-105 and single residue mutants FLP-103 and FLP-104.

Figure 4. *In vitro* depurination of ribosomal RNA by wild-type and mutant recombinant PAP proteins. E. coli 23S+16S rRNA was treated with increasing amounts of PAP, treated with aniline, separated by 6% urea/polyacrylamide gel, and stained with ethidium bromide. The arrow indicates the fragment split by aniline.

Figure 5. (A) Association of PAP mutants with ribosomes isolated from rabbit reticulocyte enriched blood. (A.1) Total ribosomal protein (5 μg) was incubated with 1 μg of PAP and the ribosome-PAP complexes were isolated by ultracentrifugation. The ribosome-PAP complexes were separated through SDS-12% PAGE, electroblotted onto a polyvinylidene difluoride (PVDF) membrane, and immunoblotted with a polyclonal antibody to PAP. (A.2) A fraction (5 μl) of the reaction mixture, prior to the separation of PAP-ribosome complex, was removed separated through SDS-12% PAGE, transferred to PVDF membrane, and immunoblotted with a polyclonal antibody to PAP. The results show that equal amounts of PAP proteins were added to the reaction mixture. **(B) Association of wild-type and mutant PAP proteins with *in vitro* synthesized ribosomal protein L3.** (B.1) Co-immunoprecipitated PAP revealed by immunoblotting using anti-PAP antibody. ^{35}S-labeled L3 was incubated with wild-type and mutant PAP proteins and co-immunoprecipitated with protein A-Sepharose beads pre-coated with monoclonal antibody to L3. The PAP-L3 complexes were separated through SDS-12% PAGE, transferred to a PVDF membrane, and immunoblotted with a polyclonal anti-PAP antibody. (B.2) The blot was exposed to X-ray film, showing equal amounts of labeled L3 protein in each reaction. (B.3) A fraction (5 μl) of the reaction, prior to the co-immunoprecipitation, was removed from the reaction, separated through SDS-12% PAGE, transferred to a PVDF membrane, and immunoblotted with a polyclonal antibody to PAP. The results show that equal amounts of PAP were added to each reaction.

Figure 6. Depurination of *E. coli* and HIV-1 RNA by wild-type and mutant PAP proteins. Two μg of *E. coli* rRNA and HIV-1 RNA was incubated with 2.5 μM of wild-type and mutant PAP proteins for 1 h at 37°C in 50 μl of binding buffer. The reaction was stopped by adding 100 μl ofHPLC running buffer and 100 μl of the sample was injected in to the column as described in Materials and Methods. Control samples of RNA were treated with PBS instead of PAP. ***Inset:*** Standard curve of adenine and guanine standards.

Figure 7. Mouse Toxicity of FLP-102 and FLP-105. BALB/c mice were treated with single i.p. bolus injections of either the mutant recombinant PAP proteins FLP-102 and FLP-105 or the native PAP protein at the indicated dose levels. Survival curves of mice treated at specific dose levels of the specified PAP proteins are

depicted. None of the 99 mice treated with FLP-102 or FLP-105 at dose levels ranging from 50 μg/mouse to 150 μg/mouse became sick or died within the 30 day observation period.